Molecular insights into *PCARE*-associated retinal disease

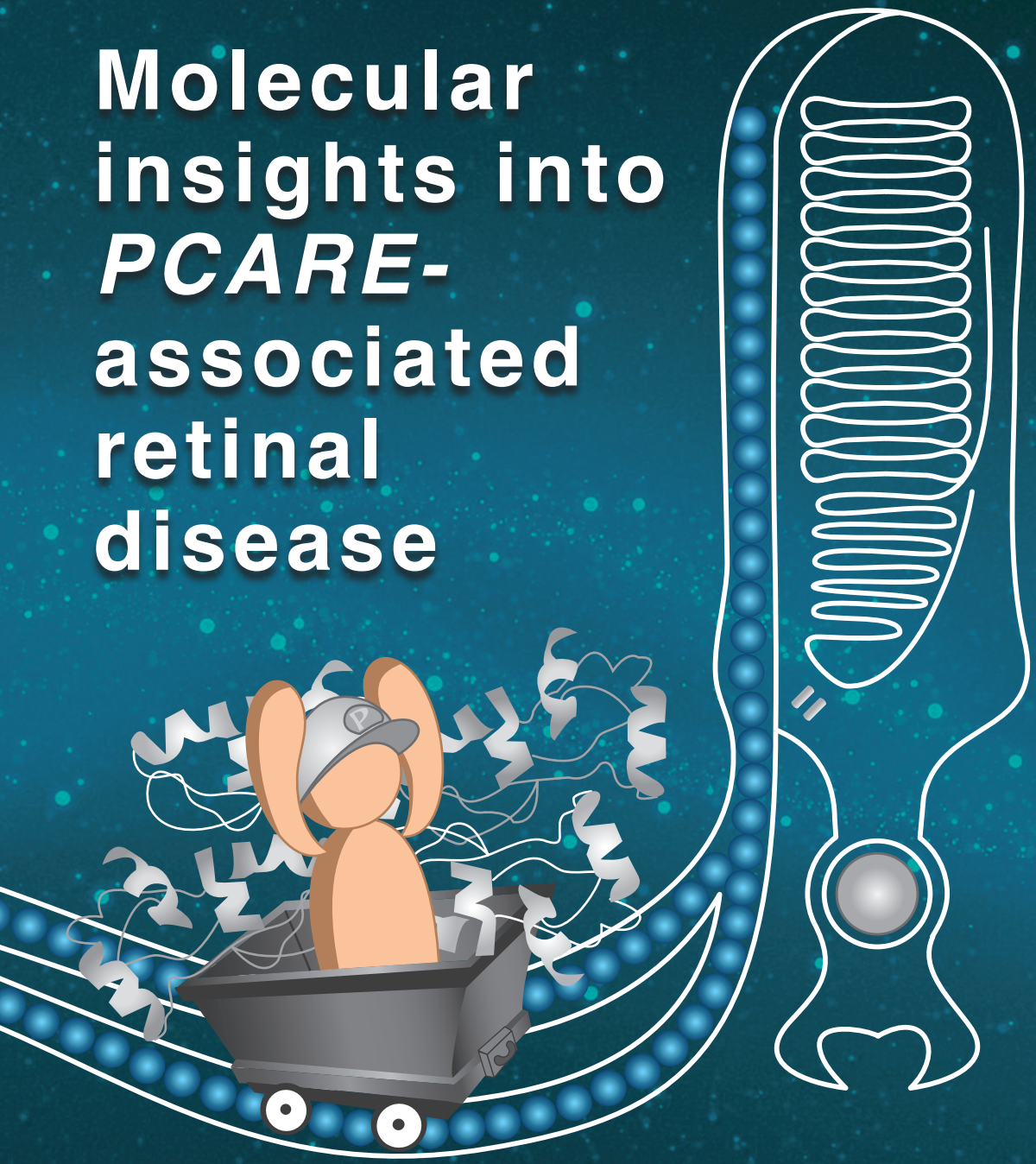

Julio César Corral Serrano

Molecular insights into *PCARE*-associated retinal disease

Julio César Corral Serrano

This project has received funding from the European Union's Seventh Framework Programme for research, technological development and demonstration under grant agreement no 317472 (EyeTN).

The work presented in this thesis was carried out within the Radboud Institute for Molecular Life Sciences (RIMLS).

The publication of this thesis was financially supported by the Radboud University Nijmegen, the Stichting Blindenhulp, the Landelijke Stichting voor Blinden en Slechtzienden, the Stichting Ooglijders and the Rotterdamse Stichting Blindenbelangen.

ISBN: 978-94-6380-031-0

Cover and chapter covers designed by M. Eugenia Castejón Lorite

Print and cover adaptation by Proefschrift Maken, proefschriftmaken.nl

Molecular insights into *PCARE*-associated retinal disease

Proefschrift

ter verkrijging van de graad van doctor
aan de Radboud Universiteit Nijmegen
op gezag van de rector magnificus prof. dr. J.H.J.M. van Krieken,
volgens besluit van het college van decanen
in het openbaar te verdedigen op

maandag 3 december 2018
om 12.30 uur precies

door

Julio César Corral Serrano
geboren op 17 oktober 1989
te Madrid, Spanje

Promotoren

Dr. Rob W.J. Collin

Prof. dr. ir. Ronald Roepman

Copromotor

Dr. Alejandro Garanto

Manuscriptcommissie

Prof. dr. Anneke I. den Hollander

Prof. dr. Colin A. Johnson (University of Leeds, Verenigd Koninkrijk)

Prof. dr. Nine V.A.M. Knoers (Rijksuniversiteit Groningen)

Paranimfen

Daniel Lôpo Polla

Laura Lorés de Motta

Marc Pauper

Molecular insights into *PCARE*-associated retinal disease

Doctoral Thesis

to obtain the degree of doctor
from Radboud University Nijmegen
on the authority of the Rector Magnificus prof. dr. J.H.J.M. van Krieken,
according to the decision of the Council of Deans
to be defended in public on

Monday, December 3, 2018
at 12:30 hours

by

Julio César Corral Serrano
Born on October 17, 1989
in Madrid, Spain

Supervisors

Dr. Rob W.J. Collin

Prof. dr. ir. Ronald Roepman

Co-supervisor

Dr. Alejandro Garanto

Doctoral thesis committee

Prof. dr. Anneke I. den Hollander

Prof. dr. Colin A. Johnson (University of Leeds, UK)

Prof. dr. Nine V.A.M. Knoers (University of Groningen)

Paranymphs

Daniel Lôpo Polla

Laura Lorés de Motta

Marc Pauper

a Popó

Table of contents

List of abbreviations

*	Stop codon
3D	Three-dimensional
aa	Amino acid
AAV	Adeno-associated virus
ABCA4	ATP binding cassette subfamily A member 4
ACTN1	α-actinin
ad	Autosomal dominant
ar	Autosomal recessive
AON	Antisense oligonucleotide
Arp2/3	Actin-related protein 2/actin-related protein 3
Ax	Axoneme
BB	Basal body
BBS	Bardet-Biedl syndrome
bGHpA	Bovine growth hormone polyadenylation signal
BODIPY	Boron-dipyrromethene
C2ORF71	Chromosome 2 open reading frame 71
CaP	Calyceal processes
Cap	Capsid gene
CC	Connecting cilium
CCT	Chaperonin containing TCP-1
CD	Cone dystrophy
CEN3	Centrin-3
CEP250	Centrosomal protein 250 kDa
CEP290	Centrosomal protein 290 kDa
cDNA	Complementary deoxyribonucleic acid
cGMP	Cyclic guanosine monophosphate
CHM	Choroideremia
CJ	Connecting junctions
CR	Ciliary rootlet
CRD	Cone-rod dystrophy
CRISPR	Clustered regularly interspaced short palindromic repeat
CRX	Cone-rod homeobox
CP	Ciliary pocket

DA	Distal appendages
dC	Daughter centriole
DCTN2	Dynactin subunit 2
DNA	Deoxyribonucleic acid
dpf	Days post fertilization
dup	Duplication
ENA/VASP	Enabled/vasodilator-stimulated phosphoprotein
ER	Endoplasmic reticulum
ESC	Embryonic stem cell
FBS	Fetal bovine serum
FDA	US Food and drug administration
FL	Fiber links
Gli	Glioma-associated oncogene
GMP	Guanosine monophosphate
GT335	Polyglutamylated tubulin
HDR	Homology-directed repair
HEK293T	Human embryonic kidney 293T
hpf	Hours post fertilization
hTERT RPE-1	Human telomerase-immortalized retinal pigmented epithelial-1
IFT	Intraflagellar transport
IFT57	Intraflagellar transport 57 kDa
ins	Insertion
iPSC	Induced pluripotent stem cell
IRD	Inherited retinal disease
IS	Inner segment
ITR	Inverted terminal repeat
JBS	Joubert syndrome
kb	Kilobase
kDa	Kilodalton
KIF17	Kinesin family member 17
LCA	Leber congenital amaurosis
LCA5	Leber congenital amaurosis 5
LIMA1	LIM domain and actin binding 1
MI	Mitochondria

mIMCD-3	Mouse inner medullary collecting duct-3
MKS	Meckel-Gruber syndrome
mpf	Months post fertilization
mRNA	Messenger ribonucleic acid
MT	Microtubules
NHEJ	Non-homologous end joining
NR	Neural retina
OFD1	Oral-facial-digital syndrome 1
OS	Outer segment
PCARE	Photoreceptor cilium actin regulator
PCM1	Pericentriolar material 1
PDE	Phosphodiesterase
PolyA	Polyadenylation signal
PRA	Progressive retinal atrophy
PRPH2	Peripherin 2
rd	Retinal degeneration
Rep	Replication gene
RHO	Rhodopsin
RK	Rhodopsin kinase
RNA	Ribonucleic acid
RNA-Seq	RNA sequencing
ROM1	Retinal outer segment membrane protein 1
RP	Retinitis Pigmentosa
RP1	Retinitis Pigmentosa 1
RP1L1	Retinitis Pigmentosa 1-Like 1
RP2	Retinitis Pigmentosa 2
RP54	Retinitis pigmentosa type 54
RPE	Retinal pigment epithelium
RPGR	Retinitis Pigmentosa GTPase Regulator
RPGRIP1L	RPGR-interacting protein 1-like protein
SA	Sub-distal appendages
Shh	Sonic hedgehog
SPATA7	Spermatogenesis associated 7
ST	Synaptic terminal

SV40	Simian vacuolating virus 40 intron
TAP	Tandem affinity purification
TZ	Transition zone
USH2A	Usher syndrome type IIa
WASF3	Wiskott-Aldrich syndrome protein family member 3
WAVE	WASP-family verprolin-homologous protein family
WPRE	Woodchuck hepatitis virus (WHP) post-transcriptional regulatory element
WRC	WAVE regulatory complex
Y2H	Yeast two-hybrid
YL	Y-linkers

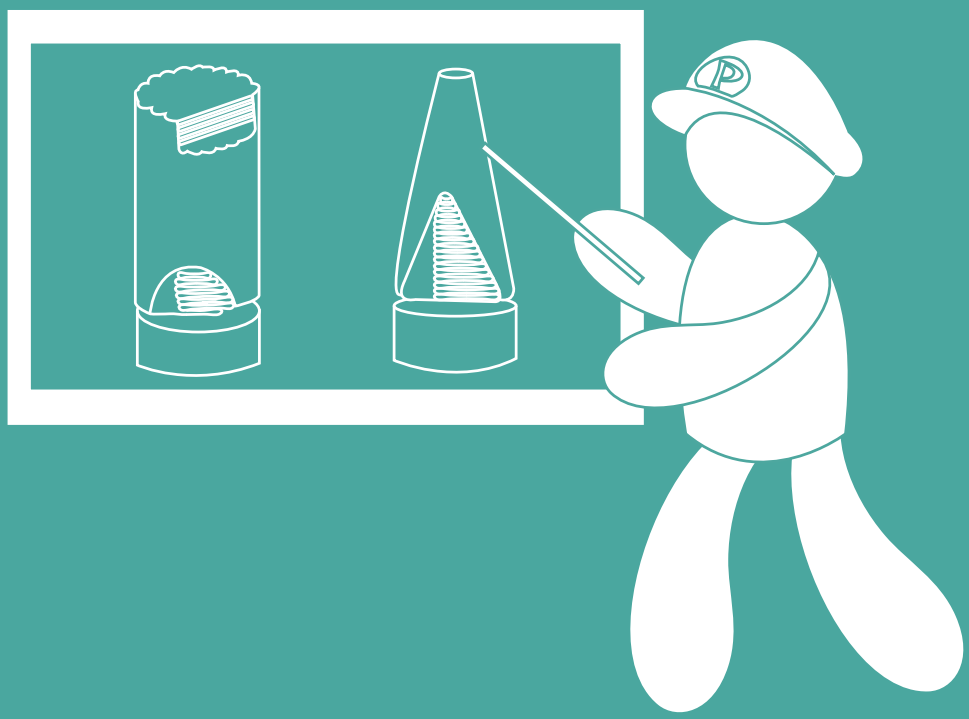

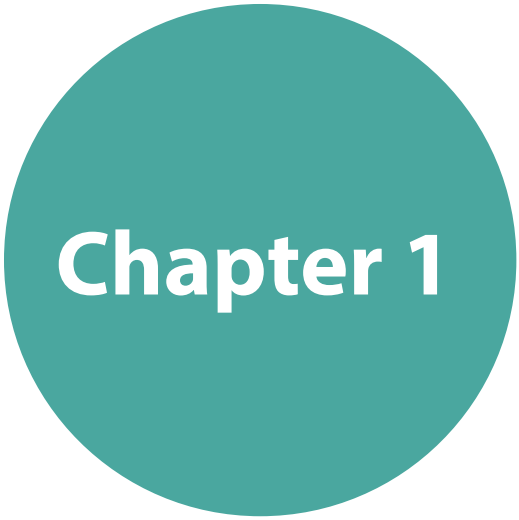

General introduction

"We were born into a mystery, one that has haunted us since at least as long as we've been human." (Quote from Cosmos: A Spacetime Odyssey, 2014, s01e03).

Our world is filled with an infinite amount of colors and shapes. Sight enables us to perceive actions, while vision allows us to make assessments about those actions. Animals have been sensing brightness for a very long time. ''The 'race' between predator and prey and the need 'to see' and 'to be seen' or 'not to be seen' were drivers for the origin and subsequent evolution of efficient visual systems'' (quote from Schoenemann et al., 2017).[1] The oldest eye recorded dates from the Cambrian period, about 530 million years ago, and belongs to a hard-shelled species, the trilobite.[1] The first light-sensing cell would have evolved much earlier, and since then, evolution of light-sensing organs has come a long way.

In this introductory chapter, we will give a general overview of the process of human vision and its main components: the eye and the retina. Because the content of this thesis will mainly cover molecular studies on the photoreceptor-specific ciliary gene *C2ORF71*/*PCARE*, we will particularly focus on the photoreceptor cell and its ciliary axoneme, discuss the current status of research of retinal ciliopathies, introduce different cellular and animal models that are used to model these diseases, and give an overview of potential therapies.

1.1 The eye

The eye is the sensory organ for vision. When light enters the eye, it travels through the cornea to the iris and pupil, which regulate the amount of light that passes, just like a shutter in a camera. The pupil constricts when light enters the eye, and it widens when it becomes dark. Light rays continue their path through the lens, which focuses the light, and cross the vitreous humor that fills the eyeball to maintain its intraocular pressure and thus spherical shape. Finally, the rays reach the retina, a layered tissue of neuroepithelial origin that is composed of different cell types. In the retina, photoreceptor cells receive the light and convert it into electrochemical impulses, that are transferred through the optic nerve to the visual centers in the brain (Figure 1).

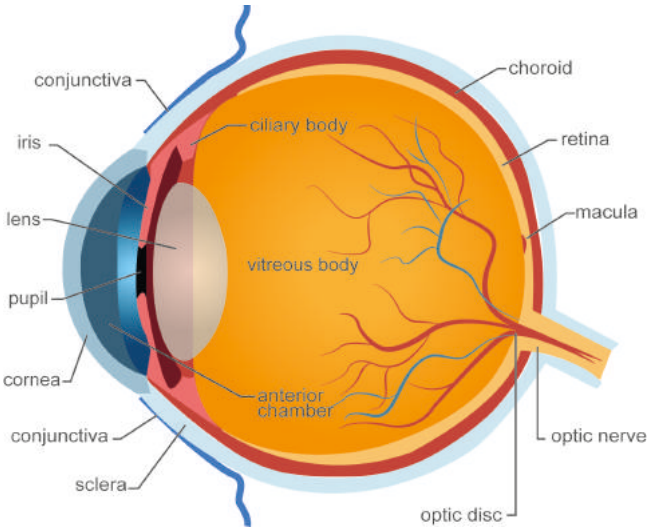

Figure 1. Anatomy of the eye. The eye is composed of a cornea, iris, pupil, lens, vitreous, retina, macula, choroid and optic nerve. Vision starts when light rays enter the eye through the cornea, and reach the retina at the back of the eye. Photoreceptor cells in the retina transform the light photons into electrical signals that are transferred through the optic nerve to the brain.

1.2 Anatomy of the retina

The father of neuroscience, Santiago Ramón y Cajal, was fascinated by the retina, and described it as "an advantageous structure for the neurobiologist because of its accessibility, its orderly organization in alternate layers of cell bodies and intercellular contacts, and the easy identification of the main direction of the nervous message flow".[2] His studies were fundamental to understand the retinal architecture as a neural tissue.

The **retina** is the light-receptive tissue at the back of the eye, located between the choroid and the vitreous. The retina arises from neural ectoderm and consists of a pigmented layer, derived from the outer layer of the optic cup, and the neural retina, derived from the inner layer of the optic cup.[3] The retina is composed of **ten representative layers** (Figure 2).

The layer closest to the vitreous body is the *inner limiting membrane*, composed of astrocytes and terminations of Müller cells. Astrocytes are special glial cells[4] which provide neurotrophic support, mechanical support for degenerating axons, and are important for the maintenance of the blood-retina barrier.[5] The Müller cells are the predominant glial cells in the retina, and they provide homeostatic and metabolic support to the retinal neurons.

The next layer, the *(optic) nerve fiber layer*, is formed by the axons of ganglion cells. Ganglion cells receive electrical signals from bipolar and amacrine cells that were generated by the photoreceptor cells, and transmit them through the continuation of their axons in the optic nerve to the brain. The *ganglion cell layer* consists of retinal ganglion cells and displaced amacrine cells.

The dendrites of the ganglion cells connect in the *inner plexiform layer* with the axons of the bipolar cells through the synapses. Amacrine cells in the inner plexiform layer receive information from bipolar neurons and transfer this information to ganglion cells.

The *inner nuclear layer* contains the nuclei of amacrine cells, bipolar cells, horizontal cells and Müller cells. Bipolar cells are neurons that receive signals from a set of photoreceptor cells and transmit it to ganglion cells. In the dark, photoreceptor cells are depolarized and release glutamate. This glutamate activates OFF-center bipolar cells, named so because they are active when the light is off, and inhibits ON-center bipolar cells. When exposed to light, photoreceptors release less glutamate, which activates the ON-center bipolar cells, which are active when the light is on.[6] Horizontal cells are horizontally oriented neurons with dendrites that connect with the synaptic terminations of the photoreceptor cells.

The *outer plexiform layer* is composed by the synapses between rod spherules or cone pedicles and dendrites of bipolar cells and processes of the horizontal cells. The *outer nuclear layer* contains the cell bodies of rod and cone photoreceptors. The *external* (or outer) *limiting membrane* is made of tight junction and adherent junction proteins that help to maintain the structure of the retina through mechanical strength.[7]

The outermost layer of the retina is the *photoreceptor cell layer*, composed by the inner and outer segments of rod and cone photoreceptor cells.

The retina is supported by the *retinal pigment epithelium (RPE)*, which sits between the photoreceptor cell layer and the choroid. The RPE is composed of pigmented cells important for many physiological functions. Some of these functions are the maintenance of adhesion of the neural retina,[8,9] phagocytosis of shed photoreceptor outer segments,[10] participation in the visual cycle,[11] and transport plus storage of metabolites and vitamins.[12]

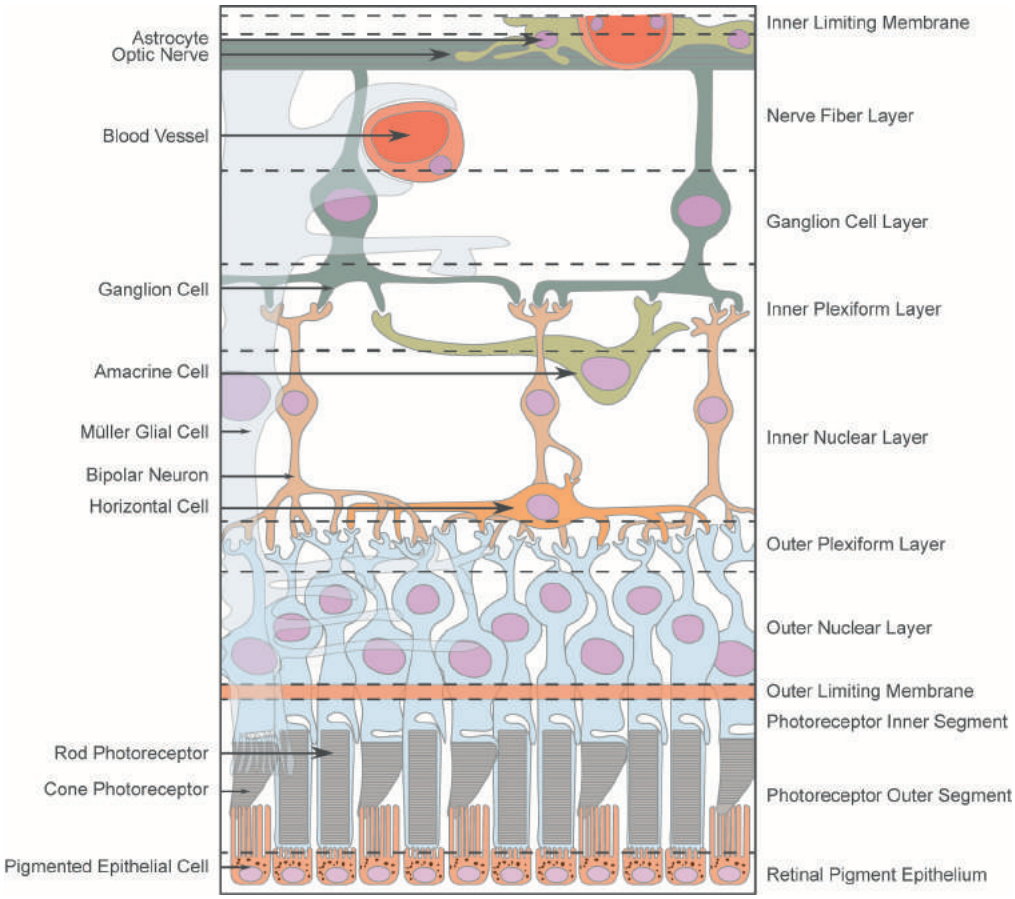

Figure 2. Anatomy of the retina. The retina is a multilayered tissue that consists of different cell types: the photoreceptor cells (rods and cones), the interneuronal cells (bipolar, amacrine and horizontal cells), the ganglion cells, the astrocytes and the Müller cells.

1.3 The photoreceptor cells

Photoreceptors are sensory neurons in the retina that are in charge of receiving the light and transforming it into electrical signals, a process named phototransduction. There are two main types of photoreceptor cells in the retina: the *rods* and the *cones*. The human retina is composed of ~120 million rod photoreceptor cells (~95% of the total number of photoreceptors) and 6 million cone photoreceptor cells (~5%).[13] The rods mediate highly sensitive vision in dim light, which is perceived as colorless "greyscale" since only one type of rod cells exist. The cones mediate color vision in bright light, and the human retina contains three types of cone cells. Cones sensitive to low-frequency photons (λmax~555–565 nm) are named L-cones, M-cones detect middle-frequency photons (λmax~530–537 nm), and supra-frequency photons (λmax~415–430 nm) are detected by S-cones.[14]

In humans, the center of the retina is constituted by a cone-enriched region, called the *fovea*, which is responsible for high visual acuity as its central positioning allows sharp focusing of the received light.[15] Each photoreceptor cell is organized in four distinct compartments: the outer segment (OS), the inner segment (IS), the nucleus and the synaptic terminal (Figure 3).

1.3.1 The phototransduction cascade

The phototransduction cascade takes place in the outer segments of photoreceptor cells.

In the dark, the cyclic guanosine monophosphate (cGMP) levels are high inside the outer segments, inducing the depolarization of the photoreceptor membrane. As a result, the Ca^{2+}-channels are open at the photoreceptor synapse, and the cell releases the neurotransmitter glutamate. Because of this, ON-center bipolar cells are hyperpolarized as they have inhibitory (metabotropic) glutamate receptors. When the ON-center bipolar cells are hyperpolarized, they do not release glutamate onto the ganglion cells, which therefore remain at rest and do not relay information to the brain. The other type of bipolar cells (the OFF-center bipolar cells) have excitatory glutamate receptors and are depolarized in absence of light, allowing for specific relay of information regarding fluctuating variation in light intensity to complex receptive fields in the retina.

The phototransduction cascade is activated when a photon reaches an opsin G-protein coupled receptor molecule (e.g. rhodopsin). The chromophore it contains, 11-*cis* retinal, then undergoes photoisomerization to all-trans retinal, becomes enzymatically activated, and catalyzes the activation of the G-protein transducin. Transducin, in turn, activates the effector phosphodiesterase (PDE). PDE hydrolyzes cyclic guanosine monophosphate (cGMP) into 5'-GMP. The decrease in cytoplasmic free cGMP concentration leads to the closure of the cGMP-gated cation channels on the plasma membrane. The closure of these channels leads to reduction of cation influx into the outer segment (while the efflux of cations continues undisturbed). This results in membrane hyperpolarization, meaning the intracellular voltage becomes more negative. Hyperpolarization of the photoreceptor cell membrane inhibits its glutamate release at the synapse.[16] This reduction of glutamate causes depolarization of the ON-center bipolar cells in absence of the inhibitory signal, which then release glutamate neurotransmitter to the ganglion cells. These are in turn activated to release action potentials that are transferred to the brain through the optic nerve. Hyperpolarization of OFF-center bipolar cells has the opposite effect, and stops release of glutamate onto the ganglion cells, increasing the ability to rapidly and accurately relay differences in lighting information.

Within the outer segment, the drop in intracellular Ca^{2+} triggers the recovery phase of phototransduction, which involves active turnoff and recycling of the transduction components. This

mediates light adaptation in the case of a sustained stimulus, which is important in order to maintain visual sensitivity under light conditions. It also rapidly restores the cell to its pre-activated state in the case of a transient stimulus, which is essential to maintain the ability to respond to a single light photon.

1.3.2 The outer segments

The **outer segments (OS)** of photoreceptor cells are highly modified and specialized sensory cilia.[17-19] Primary cilia are microtubule-based protrusions of the plasma membrane found in nearly all cell types. Cilia modulate different signaling pathways that regulate proliferation, differentiation, transcription, migration, polarity and tissue morphology.[20] The OS is composed by hundreds of stacked membrane discs essential for phototransduction. Outer segments connect to the biosynthetic compartment, the inner segment (IS), by a narrow microtubule-based connecting cilium (CC) that is homologous to the transition zone of a primary non-motile cilium.[21] Daily, approximately 10% of the rod photoreceptor opsin-loaded discs are shed and phagocytized by the adjacent RPE cells,[22] while the same amount of new membrane discs are generated and restacked at the OS base, ensuring photoreceptor homeostasis.

1.3.3 The photoreceptor ciliary axoneme

Back in the 17th century, Antony van Leeuwenhoek was first to identify cilia in protozoa.[23] He described them as “incredibly thin feet, or little legs, which were moved very nimbly”. The word ‘*cilium*’ (latin word for eyelash) was probably first formulated by Otto Muller in 1786.[24] This organelle was named *primary cilium* in 1968,[25] when the first cilia were observed to arise directly from the walls of pre-existing centrioles. The primary cilium is linked to other cellular organelles and regulates many important cellular processes such as the cell cycle, division and cytokinesis, and signaling pathways important for development: Hedgehog, Wnt and Notch.[26]

The *connecting cilium (CC)* of photoreceptors is homologous to the *transition zone (TZ)* of a primary cilium and is part of the **photoreceptor ciliary axoneme**. The connecting cilium was named by De Robertis in 1956, when he was studying some of the first electron micrographs of photoreceptor cells.[27] However, some authors refer to this region as the transition zone of photoreceptor cilia.[18] The photoreceptor ciliary axoneme is composed of nine microtubule doublets arranged in a circle (9 + 0), lacking the central pair of microtubules characteristic of motile cilia (9 + 2), and expands from the basal body until two-thirds into the outer segments.[27,28] The basal part of the photoreceptor axoneme connects with the basal body. The *basal body (BB)* is composed of nine sets of microtubule triplets and has a rootlet extending basally into the IS. The distal part of the photoreceptor ciliary

axoneme contains singlets of microtubules (Figure 3B).[29,30] As in primary cilia, the CC is distal of the mother centriole and forms a barrier to regulate protein entry into the cilium.[31] The CC measures ~0.3 mm in diameter and 1–1.5 mm in length, and it is composed of transition fibers, the ciliary necklace, and Y-fibers essential for membrane anchoring and formation of a selectively permeable pore that prevents random diffusion and ciliary entry of cytoplasmic components.[31,32] At the tip of the CC, newly outer segment discs are believed to form by an evagination mechanism of the ciliary plasma membrane.[33-36]

1.3.4 Ciliary transport to the outer segments

The daily renewal of photoreceptor outer segments requires a high level of protein synthesis. Because of this, proteins are constantly transported from the biosynthetic compartment in the inner segment through the connecting cilium to the outer segments. There are two known types of protein transport to the outer segments: protein transport by molecular motors and protein transport by diffusion.

1.3.4.1 Protein transport by molecular motors

The process of protein movement along the axoneme for ciliogenesis and cilia maintenance is called *intraflagellar transport (IFT)*. Ciliary axonemal microtubules serve as tracks for protein transport driven by two families of molecular motors, kinesins and dyneins. This transport occurs in two directions helped by the IFT trains, the primary cargo of the motor proteins: anterograde from the base to the tip of the cilium, and retrograde, from the tip to the ciliary base (Figure 3C).[37] The anterograde transport of cargoes along the axoneme is regulated by the IFT protein subcomplex B and powered by the motor protein kinesin-2. Retrograde transport from the OS to the IS is regulated by the IFT protein subcomplex A and driven by a dynein motor complex.[30] The major protein in the membrane of rod outer segments, rhodopsin,[38,39] is transported by actin filament-based and microtubule-associated transport mechanisms driven by the motor proteins myosin VIIa[40,41] and kinesin-2.[42] The BBSome, composed by eight Bardet-Biedl syndrome (BBS) proteins, moves associated to IFT trains, and regulates IFT assembly and turnaround in cilia.[43-45] The importance of correct IFT transport has been frequently reported, and mutations in genes encoding for IFT proteins (e.g. *TTC21B*,[46,47] *IFT80,*[48] *IFT144,*[49] *IFT140*[50,51]) can lead to defects in the cilium that lead to diseases (ciliopathies) that may also display retinal degeneration (see **section 1.4** for retinal ciliopathies).

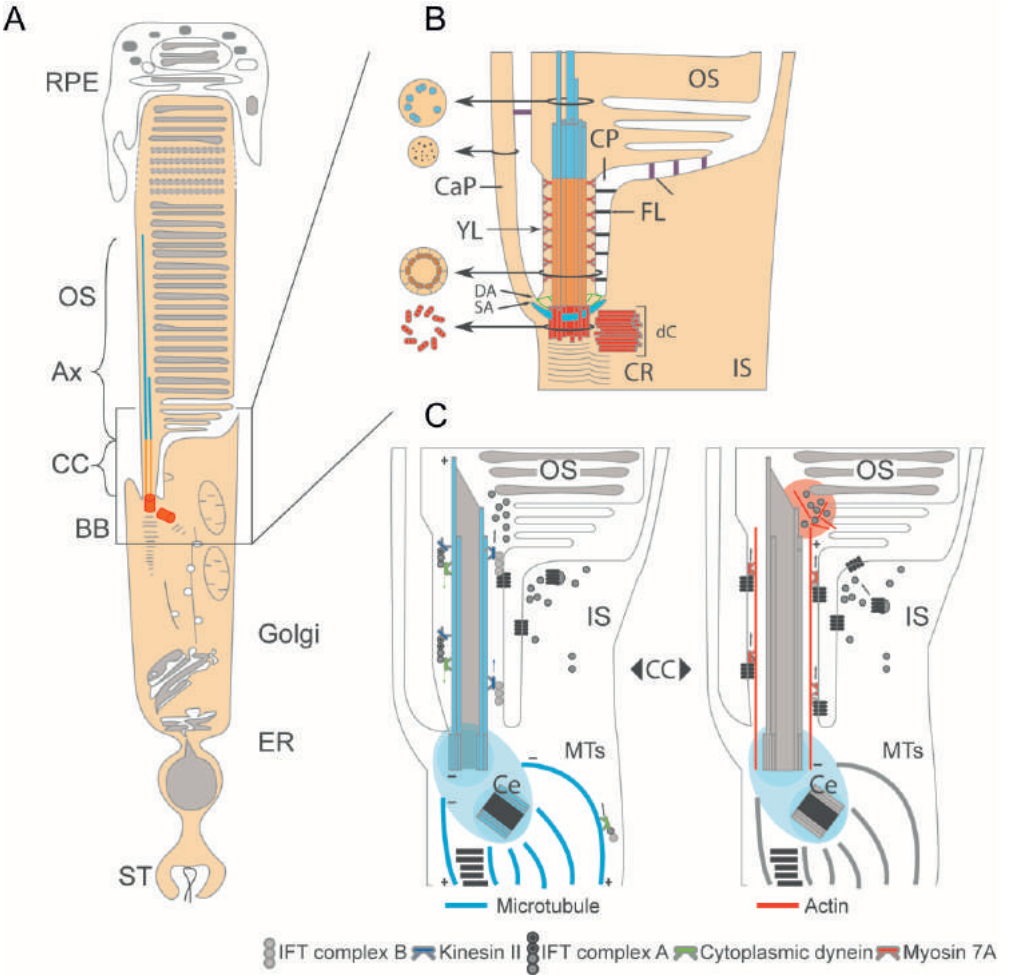

Figure 3. The photoreceptor cilium. A, Schematic representation of a rod photoreceptor. The outer segment (OS) is connected to the adjacent inner segment (IS) through the connecting cilium (CC). The photoreceptor ciliary axoneme (Ax) extends from the basal body (BB) up to two thirds into the outer segments. **B**, Magnification of the CC region. The basal body is localized basally from the CC, and is an anchor point of the ciliary rootlet (CR). Calyceal processes (CaP) extend from the inner segment. **C**, Transport of cargoes to the CC is mediated by cytoplasmic dynein 1 towards the minus-end along microtubules (MTs). Anterograde transport along the CC is mediated by the IFT protein subcomplex B and powered by the motor protein kinesin-2 towards the plus-end. The retrograde transport along the CC is regulated by the IFT protein subcomplex A and cytoplasmic dynein 2 towards the minus-end. Some proteins are transported to the OS by myosin 7a-driven transport along actin filaments. CR: ciliary rootlet, Ax: axoneme, CJ: Connecting junctions, CP: ciliary pocket, DA: Distal appendages, ER: endoplasmic reticulum, FL: fiber links, MI: mitochondria, RPE: Retinal pigment epithelium, SA: Sub-distal appendages, ST: Synaptic terminal. YL: Y-linkers. (Figure adapted from May-Simera et al., 2017[52] and Falk et al., 2015[53]).

1.3.4.2 Protein transport by diffusion

Protein diffusion has recently gained attention as an alternative or complementary mechanism to flagella and cilia protein transport.[54,55] Diffusion of soluble proteins in the CC was first reported by Calvert et al.[56] Although the microtubular arrangement impedes diffusion at the axoneme periphery, the core of the axoneme is permeable to diffusion. It is known that phototransduction proteins can translocate by simple diffusion.[57] This translocation depends on the size and shape of the molecules and the geometry of the compartment, limiting the entry of high molecular-weight molecules.[58] The work of Kuznetsov[59] describes a model to quantify transport of OS proteins through the CC. In this model, because protein concentration is higher in the OS than in the IS, the diffusion would occur from the OS to the IS if protein diffusivity in the CC is not zero. More recently, Luo et al.[60] have found a passive-diffusion route in the axonemal lumen in primary cilia. While IFT20, a component of the IFT subcomplex B,[61] is transported solely using the IFT train pathway, up to half of the kinesin-2 family motor protein KIF17 and one third of α-tubulin, a protein known as "cargo" of the IFT train,[62] diffuse through the axonemal lumen in addition to the directional movements with the IFT train.[60]

1.4 Retinal ciliopathies

Ciliopathies are a group of rare genetic disorders that occur as a consequence of cilia dysfunction. *Retinal ciliopathies* are *inherited retinal diseases (IRDs)* in which the function of the photoreceptor outer segments or the ciliary axoneme is disturbed. IRDs caused by mutations in genes expressed in the RPE or that encode proteins from a different compartment of the photoreceptor cell (e.g., splicing factor genes) are excluded from the "retinal ciliopathies" classification. Retinal ciliopathies can include *retinitis pigmentosa (RP)*, *cone-rod dystrophy (CRD) and Leber congenital amaurosis (LCA)*, although not all genes mutated in these subtypes of IRD code for ciliary proteins.

1.4.1 Prevalence and inheritance patterns

Retinitis pigmentosa (**RP**, OMIM #268000), caused by degeneration of rod photoreceptors, is the most common form of IRD, affecting around 1 in 4,000 individuals worldwide.[63,64] RP can be inherited in an autosomal dominant (adRP), autosomal recessive (arRP) or X-linked (XL-RP) manner. Mutations in the gene *RHO*, coding for the protein rhodopsin, account for 20-30% of adRP cases.[65,66] Over 40 genes and loci have been implicated in autosomal recessive RP (RetNet, https://sph.uth.edu/retnet/), and most of them are responsible for around 1% or fewer cases.[67] Around 10-15% of RP patients show X-linked inheritance.[68] Two genes, *RP2* and *RPGR*, account for 10-20% and 70-90% of cases, respectively.[69-72] Rare digenic forms have been reported in individuals who are heterozygous for both

a *ROM1* pathogenic variant and a *PRPH2* pathogenic variant,[73] and in one family with syndromic RP, heterozygous *RP1L1* and *C2ORF71/PCARE* null mutations have been described.[74]

Cone dystrophy (**CD**, OMIM #602093), which affects solely the cones, and **cone-rod dystrophy** (**CRD**, OMIM #120970), affecting first the cones and later the rods, have a prevalence of 1-30,000-40,000 individuals.[75,76] Mutations in more than 20 genes can cause autosomal recessive cone-rod dystrophy, most commonly in the *ABCA4* gene, which accounts for 30-60% of cases. At least 10 genes have been associated with cone-rod dystrophy that is inherited in an autosomal dominant pattern. Mutations in the *GUCY2D* and *CRX* genes account for about half of these cases.[77,78] *CRX*-associated autosomal dominant cone-rod dystrophy, however, would not be included in the spectrum of retinal ciliopathies, since it codes for a transcription factor.[79,80]

Leber congenital amaurosis (**LCA**; OMIM #204000) is a rare subtype of IRD that occurs in ~1:50,000 individuals, but it is the most common cause of blindness in children. LCA has an autosomal recessive pattern of inheritance in most cases. Mutations in 24 genes have been associated with LCA (RetNet, https://sph.uth.edu/retnet/). The most frequently mutated genes in LCA are *CEP290* (15%),[81] *GUCY2D* (12%)[82] and *CRB1* (10%).[83] A small number of dominant cases have been reported in patients with mutations in *CRX*[84] or *IMPDH1*.[85]

1.4.2 Symptoms

RP, LCA, and CD/CRD in general are considered progressive diseases, meaning that the visual impairment worsens with time. The most common symptom in RP is night blindness, caused by initial loss of rod photoreceptors, which develops into impairment of peripheral vision (tunnel vision) and eventually leads to complete blindness at the end-stage of the disease. In CD/CRD, the cones are primarily affected, leading to reduced visual acuity, light sensitivity (photophobia), involuntary movements of the eyes (nystagmus) and abnormal color vision. When the rods also become affected, patients with CRD can suffer from night vision loss. LCA is more severe than RP and CRD, since it affects both rods and cones at early stages. Patients diagnosed with LCA are usually infants,[86,87] and the most common symptoms include photophobia, nystagmus and extreme farsightedness.

1.4.3 Non-syndromic retinal ciliopathies

Non-syndromic retinal ciliopathies are ciliopathies of the retina that do not present systemic abnormalities. Nineteen genes that encode ciliary proteins have only been identified mutated in patients with non-syndromic retinal ciliopathies: *C2ORF71/PCARE,*[88,89] *C8ORF37,*[90] *CDHR1,*[91] *EYS,*[92,93] *FAM161A,*[94,95] *KIZ,*[96] *LCA5,*[97] *MAK,*[98,99] *NEK2,*[100] *PROM1,*[101] *PRPH2,*[102] *RAB28,*[103] *ROM1,*[73] *RPGRIP1,*[104] *RP1,*[105,106] *RP2,*[71,72] *SPATA7,*[107] *TOPORS,*[108] *TULP1.*[109,110] Diseases caused by mutations in genes

encoding phototransduction cascade and visual cycle proteins are also considered retinal ciliopathies by some authors, since they reside in the sensory cilium.[18] Non-syndromic forms have been described for the genes *ABCA4*,[111] *CNGA1*,[112] *CNGA3*,[113] *CNGB1*,[114] *CNGB3*,[115] *GNAT1*,[116] *GNAT2*,[117,118] *GRK*,[119] *GUCA1A*,[120,121] *GUCA1B*,[122] *GUCY2D*,[77] *LRAT*,[123] *OPN1LW*,[124-126] *OPN1MW*,[124,126] *OPN1SW*,[127,128] *PDE6A*,[129] *PDE6B*,[130] *PDE6C*,[131] *PDE6G*,[132] *RDH5*,[133,134] *RDH12*,[135,136] *RGS9*,[137] *RGS9BP*,[137] *RHO*,[138] *RPE65*,[139] and *SAG*.[140] The exclusive retinal expression of some of these genes explains the retina-specific phenotype.[141] However, the specificity of the phenotype is unknown for those genes who are expressed in other tissues, and genetic modifiers of the disease may explain some of the cases.[18]

1.4.4 Syndromic retinal ciliopathies

Mutations in the same gene can also lead to different phenotypes.[142-144] For example, specific mutations in the gene *IFT140* can cause short rib thoracic dysplasia 9 with or without polydactyly,[51,145] while other *IFT140* mutations can cause non-syndromic retinal degeneration.[50] Because of this, the spectrum of ciliopathies is broad, and accurate diagnosis is needed. Below, we review the most common forms of syndromic retinal ciliopathies: Usher syndrome, Joubert syndrome, Meckel-Gruber syndrome and Bardet-Biedl syndrome.

Usher syndrome (OMIM #276900-902) is the most frequent syndromic form of retinitis pigmentosa with a prevalence of ~1:25,000 individuals.[146] Usher syndrome is characterized by hearing impairment combined with vision loss. Mutations in at least eleven genes can cause Usher syndrome type I, II or III. The most frequent type is Usher syndrome type IIa, caused by mutations in the *USH2A* gene.[147,148] *USH2A* is required for the long-term maintenance of retinal photoreceptors and for the development of cochlear hair cells.[149] Mutations in *GPR98*[150,151] and *DFNB31*[152] are causative of the remaining Usher syndrome type II cases. Usher syndrome type III is caused by mutations in *CLRN1* or *HARS*. CLRN1 locates to the base of photoreceptor cilia and to synaptic ribbons.[153] HARS codes for a histidyl-tRNA synthetase and its relation to cilia is still unknown.[154]

Usher syndrome type I is not strictly a ciliopathy because the function of the protein encoded by these genes (*MYO7A*, *USH1C*, *CDH23*, *PCDH15*, *USH1G* and *CIB2*) is related to actin-based structures in the periciliary region, the calyceal processes, and not directly to cilia.[155] However, since the protein encoded by *MYO7A* has a role in transport of rhodopsin and the visual retinoid cycle enzyme RPE65 to the outer segments,[41,156] Usher syndrome type I caused by mutations in *MYO7A* could be included in the retinal ciliopathies as well.

Rare forms of Usher syndrome have been reported in which the phenotype is explained by mutations in two different genes simultaneously: *USH2A* with *PDZD7*,[157] and *CEP250* with *C2ORF71/PCARE*.[158]

Additionally, mutations in *CEP78* can cause cone-rod dystrophy and hearing loss associated with primary-cilia defects.[159]

Joubert syndrome (**JBTS**, OMIM #213300) and **Meckel-Gruber syndrome** (**MKS**, OMIM #249000) are recessive neurodevelopmental conditions that overlap genetically, in the sense that both JBTS and MKS are caused by mutations in genes encoding proteins that are structural or functional components of the primary cilium.[160] JBTS is characterized by a distinctive cerebellar and brain stem malformation called the molar tooth sign. Patients may also present with hypotonia (low muscle tone), developmental delay, ataxia, retinal degeneration, renal or hepatic defects, polydactyly, and orofacial dysmorphism.[161,162] The most common genetic causes of JBTS involve mutations in the genes *AHI1*,[163,164] *C5orf42*,[165] *CC2D2A*,[166,167] *CEP290*,[168] *CSPP1*,[169,170] *INPP5E*,[171,172] *KIAA0586*,[173,174] *MKS1*,[175] *NPHP1*,[176] *RPGRIP1L*,[177] *TCTN2*,[178] *TEMEM67*,[179] *TMEM216*.[180]

Clinical features of Meckel-Gruber syndrome include central nervous system malformation, cystic kidneys, and fibrotic changes to the liver. Other frequent features are optic disc coloboma, postaxial polydactyly, heart defects, skeletal dysplasia, microphthalmia, genital anomalies and cleft lip.[181] Mutations in twelve genes have been reported to cause MKS (*B9D1*,[182,183] *B9D2*,[182] *CC2D2A*,[184] *CEP290*,[185,186] *KIF14*,[187] *MKS1*,[188] *NPHP3*,[189] *RPGRIP1L*,[177] *TCTN2*,[190] *TMEM67*,[191] *TMEM216*,[192] *TMEM231*[193]).[18] Garcia-Gonzalo et al., 2011, identified a transition zone complex of Meckel and Joubert syndrome proteins that regulates ciliary assembly and trafficking, and are important for modulation of Sonic Hedgehog (Shh) signaling transduction, suggesting that transition zone dysfunction is the cause of these ciliopathies.[178]

Bardet-Biedl syndrome (**BBS**) is an autosomal recessive disorder caused by mutations in genes important for proper cilia function. Some of these genes code for the BBSome proteins, a complex of proteins that localize to the ciliary basal body and associate to and regulate the IFT trains, travelling together with it along the axoneme.[194] The clinical features of BBS include kidney dysfunction, photoreceptor degeneration, obesity, polydactyly, behavioral dysfunction and hypogonadism.[195,196] The majority of BBS mutations are present in the gene *BBS1*.[197,198] Nineteen other genes have been associated with BBS (*ARL6*,[199] *BBIP1*,[200] *BBS2*,[201] *BBS4*,[202] *BBS5*,[203] *BBS7*,[204] *BBS9*,[205] *BBS10*,[206] *BBS12*,[207] *CEP290*,[208] *IFT27*,[209] *IFT172*,[210] *LZTFL1*,[211] *MKKS*,[212,213] *MKS1*,[208] *SDCCAG8*,[214] *TRIM32*,[215] *TTC8*,[216] *WDPCP*[217]).[18] Two diseases have a similar phenotype to BBS: Alström syndrome, for which only one gene, *ALMS1*,[218] has been identified to date, and MORM (mental retardation, truncal obesity, retinal disease and micropenis) syndrome, for which only one family with a homozygous mutation in *INPP5E* has been described.[219,220]

1.5 From gene to protein function

For many of the newly discovered genes associated to retinal diseases, the function remains a mystery. Nowadays, the molecular characterization of proteins is coming to light thanks to the systematic study of protein-protein interactions. Proteins and other biological molecules never work alone, and they tend to either interact stably with other proteins in multi-subunit protein complexes that act as molecular machines or interact transiently with other proteins as part of a biochemical reaction or pathway. Inherited defects in the components of such complexes or pathways can affect human health. The first high-quality maps of the human interactome have recently been published.[221-224] There are several high-throughput complementary methods to study protein-protein interactions, two of which are most commonly used: protein-protein interaction trap screens in yeast (yeast two-hybrid system) and protein complex affinity purification followed by mass spectrometry. Yeast two-hybrid systems are identifying direct, binary interactions between two proteins that are ectopically expressed in a yeast cell, while mass-spectrometry-based approaches are able to map entire interacting protein complexes without obtaining detailed knowledge about direct interactions.

1.5.1 Interaction trap screening in yeast

The *GAL4-based yeast two-hybrid system (Y2H)* was generated by Fields and Song,[225,226] taking advantage of the GAL4 protein of the yeast *Saccharomyces cerevisiae*. GAL4 is a transcriptional activator required for the expression of genes encoding enzymes required for galactose utilization. In this Y2H, the cDNA encoding the DNA binding domain of the GAL4 protein is N-terminally fused to a bait protein 'X', and subsequently subcloned in a yeast expression plasmid vector. The cDNA encoding the GAL4 activating region is C-terminally fused to a prey protein 'Y' and subcloned in a different plasmid. When these two plasmids are co-transformed in yeast, only if proteins X and Y interact, they will reconstitute a functional GAL4 transcription factor by recruiting all required components of the RNA polymerase complex such that the transcription of several reporter genes that are under GAL4 control is activated. The yeast cells are then grown in selective media, and only the yeast cells expressing two interacting proteins that activate the auxotrophic markers will grow (Figure 4A). Additional reporter genes such as colorimetric markers are evaluated simultaneously to improve the specificity of the system. Genes expressing the prey proteins can subsequently be identified by Sanger sequencing. This system can be applied to study the direct binding of a specific bait-prey combination, or to screen prey protein-expressing cDNA libraries of a specific tissue with a bait protein of interest.

1.5.2 Tandem affinity purification (TAP)

The *tandem affinity purification (TAP)* method was described in 2001 by Puig et al.[227] The TAP method is based on the strongly enhanced specificity of a sequential double affinity purification of the protein complex associated with a protein of interest in a cell, compared to a single purification step. The original TAP tag consists of two IgG binding domains of *Staphylococcus aureus* protein A and a calmodulin binding peptide separated by a TEV protease cleavage site. An advanced purification approach combines a Strep-tag II and a FLAG-tag with the TAP tag (SF-TAP).[228] Because this is a very small tag that displays a very limited nonspecific binding capacity, the inefficient protease cleavage step can be omitted. Once the TAP-tagged bait protein is ectopically expressed, proteins are extracted from the cell, and the SF-TAP fusion protein and its associated complex are recovered by two rounds of affinity purification/elution. The first round of purification uses the tandem Strep-tag II moiety, and the second round uses the FLAG-tag moiety. After purification, the complexes are eluted and subjected to mass spectrometry in order to identify the affinity purified members of the protein complex associating with the protein of interest (Figure 4B).

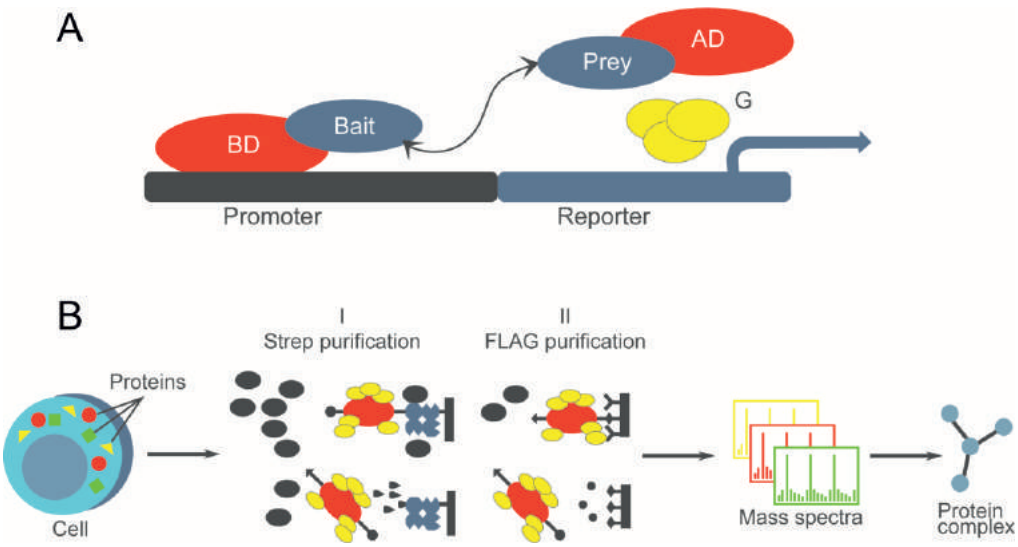

Figure 4. Schematic overview of **A**, yeast two-hybrid system (adapted from Giorgini and Muchowski, 2005[229]) and **B**, tandem affinity purification. (B is partially adapted from Marissa Fessenden, 2017[230] and https://www.helmholtz-muenchen.de/proteinscience/research/proteomics-technology-development/interaction-proteomics/overview/index.html). BD= Binding Domain, AD= Activation Domain, G= General transcription machinery.

1.6 Animal models of retinal disease

The importance of animal models for studying retinal dystrophies rests not only in understanding the pathogenesis of the disease, but also in assessing the efficacy of new means of treatment. Mendelian inheritance was first observed in retinal degeneration animal models of **mice** and **rats** back in the early 20th century by Keeler[231] and Bourne et al.[232] Some decades later, retinal degeneration (*rd*) mice,[233] harboring a mutation in *Pde6b*[234] and retinal degeneration slow (*rds*) mice,[235] with a defect in *Prph2*[236] were described. The generation of mutant animal models and the discovery of human mutations came hand in hand. For instance, mutations in the gene *CHM*, associated to choroideraemia[237] and in *RHO*, associated to adRP[138] were discovered in 1990, while their respective mouse models appeared just few years after.[238,239] To date, over 100 different genes that underlie human retinal diseases have been modeled in mice.[240]

An advantage of using mice for retinal degeneration research is their genetic similarity with humans, with 75% of mouse genes being in 1:1 orthologous relationship with human genes.[241] Importantly, mice and humans share 79% of amino acid sequence identity of proteins encoded by IRD genes.[240] The mice genome is well covered,[242] and the techniques available for targeted manipulation of their genome are well developed (Knockout Mouse Project (KOMP), http://www.knockoutmouse.org/).[243] However, the use of mice to study retinal degeneration also has certain drawbacks. Contrary to humans, mice are nocturnal animals, they lack the cone cell-enriched area of the retina, the fovea, and instead, their cones are spread throughout the retina.[244] The photoreceptor anatomy of the mice is different from the humans, since mice lack photoreceptor calyceal processes,[155] although this has been debated.[245] Moreover, some retinal genes are not present in the mice (i.e. *EYS*), whereas others are duplicated (i.e. *TIMM8A*).

The **zebrafish**, *Danio rerio*, is a tropical freshwater fish frequently used as a vertebrate model in research given the number of offspring, its amenability to genetic manipulation, and the transparent nature of the embryo, which allows to readily study developmental processes. Lately, the zebrafish has gained attention as an excellent animal model to study retinal degeneration. Like humans, zebrafish are diurnal animals, although they have a higher proportion of cone photoreceptors *versus* rods. Besides short (S), medium (M) and long (L) wavelength cone photoreceptors, zebrafish contain an additional cone photoreceptor sensitive to UV light, which is also the first to mature. Importantly, between 72 to 96 hours post fertilization (hpf), most major classes of cells can be identified in the central retina.[246] Research using zebrafish has generated different mutant models of retinal degeneration to date (*cacna1fa*,[247] *ush1c*,[248] *gnat2*,[249] *gc3*,[250] *gucy2f*,[251] *myo7a*,[252,253] *crb2a*,[254,255] *pde6c*,[256] *eys*,[257,258] *ift57*,[259,260] *ift88*,[260] *ift172*[260]).

Unlike mammals, however, zebrafish are able to regenerate the retina once damaged.[261] Factors secreted by dying cells are received by Müller glia cells, which stimulate their proliferation.[262] This regeneration process may be an impediment to study retinal degeneration. Moreover, a whole-genome duplication event that occurred during the divergence of the teleost fish[263,264] made the present-day zebrafish genome to contain many duplicated genes, of which more than 67 correspond to genes mutated in IRDs. These, together with the evolutionary distance of zebrafish to humans,[240] are the major drawbacks of using zebrafish for retinal research.

Pigs are diurnal animals with a cone-enriched retina,[155] which make them a good choice for the study of cone-associated disorders. Models for the genes *rho*,[265-267] *elovl4*,[268] and *Gucy2d*,[269] have been generated in pigs. However, the large space needed for housing pigs and the elevated maintenance costs, make this model less attractive for research.

Not only research models but also naturally occurring animal models of IRD have been identified. The most commonly reported one is the **dog**, a domestic animal that is often inbred, expressing many recessively inherited disorders. Retinal degeneration in dogs is named progressive retinal atrophy (PRA), and has been described for more than 100 breeds, while more than twenty causative mutant genes have been identified. Importantly, gene therapy successfully restored vision in *RPE65* mutant dogs,[270-272] and built a path for its translation to humans.

1.7 Cellular models of retinal disease

Many of the genes associated with retinal ciliopathies still have an unknown function. Given the difficulty to access the retina, study of the disease has been limited to animal models, which do not always portrait the same human traits. In recent years, **induced pluripotent stem cell (iPSC)** technology[273,274] has opened the possibility to study retinal degeneration *in vitro*. To generate a proper disease cellular model, there are three important factors to consider in advance: a selection of somatic patient cells, a reprogramming strategy, and a differentiation protocol that allows researchers to mimic the physiological conditions of the tissue of interest.

The somatic cell type of choice is important due to epigenetic memory, which may influence the differentiation capacity of iPSCs towards a different lineage than the original one.[275] Most studies use fibroblasts, while there are studies that generated RPE and photoreceptor cells using lymphocytes[276] or keratinocytes.[277] iPSCs can be easily obtained from patient's blood cells with minimal risk to the donor.[278-280] Peripheral blood-derived human iPS lines are similar to human embryonic stem cells in

relation to morphology, expression of surface antigens, activation of endogenous pluripotency genes, DNA methylation and differentiation potential.

An even less invasive source of somatic cells is urine. Exfoliated cells present in the urine are an excellent source for noninvasive reprogramming. The advantage of using urine is that it can be obtained at any age, gender and ethnic origin, and allows sample collection under any circumstance except for renal failure.[281] Other somatic cell sources to generate iPSCs are adipose stem cells,[282,283] periosteum membrane,[282] periodontal ligament,[284] neural stem cells, hepatocytes, or amniocytes.

Modeling of retinitis pigmentosa has been performed in two-dimensional cultures using specific medium supplemented with developmental signaling molecules. The first differentiation was done by the group of Takahashi.[285,286] Their studies consisted in the differentiation of iPSCs derived from patients with mutations in the genes *RP1*, *RP9*, *PRPH2* or *RHO*. Because the proteins encoded by these genes have roles in the phototransduction cascade and OS morphogenesis of rod photoreceptors, the iPSCs were induced to differentiate towards a photoreceptor cell fate. Scientists observed expression of photoreceptor-specific markers, like rhodopsin and recoverin. Additionally, there was decreased rod cell survival and increased endoplasmic reticulum stress, indicating that the *in vitro* model of rod degeneration was successful.

Yoshida et al. generated induced pluripotent stem cells (iPSCs) from an RP patient carrying a mutation in *RHO* (p.E181K).[287] They went one step further and re-inserted the correct copy of the gene using a helper-dependent adenoviral vector gene transfer. In a different study, Tucker and colleagues performed exome sequencing of iPSCs from a patient with RP to identify a homozygous insertion in a retina-specific isoform of male germ cell-associated kinase (MAK) as a cause of RP.[99] The same group used next-generation and Sanger sequencing on iPSC-derived retinal cells to identify disease-causing *USH2A* mutations in a patient with autosomal recessive RP.[277]

Obtaining RPE cells from iPSCs *in vitro* is less challenging than obtaining photoreceptors. To generate RPE *in vitro*, scientists take advantage of the tendency of pluripotent cells to differentiate towards ectoderm upon fibroblast growth factor withdrawal. A number of studies have investigated the disease mechanisms of RP when the primary defect resides in the RPE cells. Examples of this include mutations in *MERTK*,[288] *MFRP*,[289] *HADHA*,[290] or *BEST1*.[291] Schwarz et al. generated iPSC-derived RPE from a patient carrying the mutation p.R120* in the gene *RP2* [PMID: 25292197], encoding a GTPase-activating protein for Arf-like 3.[292]

Several protocols for retinal differentiation of non-disease cell types have been successfully published, which recapitulate *in vitro* key structural and functional features of the native retina, in

particular the presence of photoreceptors with outer segment discs and light sensitivity.[293-295] These protocols share the formation of optic cups in a three-dimensional (3D) culture. After differentiation, the optic cups develop into retinal organoids that contain the cells and organization of the neural retina: horizontal, amacrine, bipolar, ganglion cells, Müller cells and photoreceptors.

Phillips et al. modeled microphthalmia associated to mutations in the transcription factor visual system homeobox 2 (*VSX2*).[276] The differentiated cultures failed to produce bipolar cells, a distinctive feature previously observed in *Vsx2* mutant mice. *VSX2*-deficient iPSCs also demonstrated delayed photoreceptor maturation, which was overcome via exogenous expression of wild-type VSX2 at early stages of retinal differentiation.

Parfitt et al. modeled LCA associated with mutations in the gene encoding the ciliary protein CEP290.[296] Treating optic cups with an antisense morpholino effectively blocked aberrant splicing and restored expression of full-length CEP290, restoring normal cilia-based protein trafficking. Modulation of X-linked RP caused by mutations in the retinitis pigmentosa GTPase regulator (*RPGR*) gene by iPSCs showed a clinically-significant role for RPGR in the activation of the actin-severing protein gelsolin linked to photoreceptor actin dynamics.[297] Human 3D optic cups were also used to investigate REEP6 expression levels and confirmed the expression of a retina-specific isoform REEP6.1, and that disruption of this isoform alone within rod photoreceptors can lead to retinal disease.[298]

1.8 Therapies for inherited retinal diseases

The retina is a highly suitable tissue for gene therapy, due to its accessibility, immune privilege, and compartmentalization. Given the high heterogeneity of retinal ciliopathies, development of generally applicable therapies is still a challenge. Therefore, different therapeutic strategies are being developed that depend on the causative gene, the mutation, and the inheritance pattern (Figure 5).

1.8.1 Viral vectors

Recessive mutations are a good target for gene augmentation therapy because they generally cause absence of protein, and consequently, the expression of wild-type protein is likely to ameliorate the disease phenotype. **Adeno-associated virus (AAV)**, **lentivirus** and **adenovirus** are the preferred viral vectors for this type of therapy. Adenovirus and lentivirus, while having a relatively larger packaging capacity (>5 kb), do not target photoreceptor cells very efficiently.[299] AAVs have been the preferentially used vectors due to their safety and ease of manipulation.[300] Among the different

serotypes, AAV2/5, 2/7, 2/8 and 2/9 have demonstrated more efficient transduction of photoreceptor cells and RPE.[301-304] The drawback of using AAVs is its small packaging capacity of ~4,8 kb, which is not suitable for large transgenes. Different clinical trials for mutations in *RPE65* have been completed to date, with a very variable outcome (ClinicalTrials.gov, identifiers NCT00749957, NCT01496040, NCT00643747). Some patients show improved retinal activity but some of them also showed deterioration after some time. In 2017, a phase III clinical trial using AAV2-hRPE65v2 for patients with mutations in *RPE65* showed effectiveness in improvement of visual function in the intervention group versus the control group,[305] and by the end of 2017, this study lead to the commercialization approval of this vector by the FDA under the name Luxturna™.

1.8.2 Non-viral vectors

Gene therapy using non-viral vectors is also a promising therapy for the treatment of retinal degeneration. **Liposomes**, **polymers**, **polypeptides** and **nanoparticles** are non-viral vectors, which have the advantage of having low immunogenicity, high capacity and the possibility of large-scale production. CK30PEG10K nanoparticles containing the wild-type *Rds* gene under the control of the MOP promoter provided a therapeutically effective gene delivery system for rescuing the disease phenotype in a mouse model for RP (*rds*$^{+/-}$).[306] The lack of long-term gene expression however is a major drawback for these types of vectors.[300,307] One study, nonetheless, showed long-term expression of the *Rpe65* gene in mice lacking *Rpe65* using a nanoparticle, liposome-protamine-DNA complex (LPD).[308]

1.8.3 Stem cell therapy

Transplantation of healthy cells able to generate retinal cells is a treatment alternative for patients with severe retinal degeneration. The advantage of stem cell therapy lies in that it may be applied independently of the gene and mutation. To date, there are a few clinical trials that have tested the efficacy of cell transplantation for patients with retinal dystrophies. A phase III clinical trial using bone marrow-derived mononuclear cells showed no adverse effects and visual improvement in patients with RP and CRD.[309] A different trial in twenty RP patients showed an improvement in the quality of life after three months of treatment, however, the improvement stopped after one year.[310]

Retinal stem cells may be obtained *in vitro* using two different sources: induced pluripotent stem cells (iPSCs) or embryonic stem cells (ESCs). As mentioned in **section 1.7**, different groups have been able to generate functional photoreceptor cells from human iPSCs. Transplantion of iPSCs-derived retinal cells, however, has been only studied in animal models so far. MacLaren et al. showed that only stage-specific photoreceptor precursors, corresponding to postmitotic committed

photoreceptors, are able to efficiently integrate into the degenerating retina, differentiate into mature photoreceptors, form synaptic connections, and possibly lead to recovery of visual function.[311] Transplantation of differentiated photoreceptor cells derived from human ESCs into a mouse model was able to restore vision in *Crx*-deficient mice.[312] Transplantation of ESCs- and iPSCs-derived 3D retinal sheets showed to be efficacious in the advanced retinal degeneration mouse model *rd1*,[313] and in two primate models of retinal degeneration.[314]

The use of iPSCs overcomes the risks of rejection associated to use of ESCs from an allogenic donor. However, iPSCs may be associated to malignant characteristics due to the use of transcription factors for its production, impurities in the culture, unwanted differentiation, and the presence of the patient's mutation.[315] Transplantation of photoreceptor cells derived from iPSCs or ESCs in humans have not yet been reported, but clinical trials for retinitis pigmentosa patients are underway (ClinicalTrials.gov, identifiers NCT02320812, NCT03073733, NCT02464436).

1.8.4 Genome-targeted retinal therapy

Clustered Regularly Interspaced Short Palindromic Repeat (CRISPR)/Cas9 is a DNA cleavage system that originates from the immune defense system of bacteria and archaea, first identified by Mojica et al. in the 1990s.[316,317] The Cas9 nuclease cleaves double-stranded DNA at a target genomic locus. After that, the targeted locus is repaired by either the non-homologous end joining (NHEJ) pathway, which results in insertions and/or deletions in the targeted locus, or by the homology-directed repair (HDR) pathway, which allows precise gene editing in the presence of an exogenously introduced repair template. This genome editing technique represents nowadays a powerful tool for the treatment of genetic diseases. Use of CRISPR/Cas9 technology to disrupt the dominant Rho p.S334* mutation in adRP rat models has recently been reported.[318] Interestingly, AAV-mediated CRISPR/Cas9 delivery to post-mitotic photoreceptors to disrupt *Nrl*, helps rod survival and preserves cone function in three different mouse models of retinal degeneration.[319] Although promising, translation of CRISPR/Cas9 genome editing of retinal diseases into the clinic may be delayed by several factors.[320] One factor is the few studies that report off-target effects of CRISPR/Cas9. Reports have shown off-target mutations at sites that differ by five nucleotides.[321] Additionally, replacement of a mutation by HDR is not only challenging, but unlike NHEJ, HDR occurs only substantially in dividing cells and hardly in post-mitotic photoreceptor or RPE cells. Therefore, CRISPR/Cas9-based systems are better suited for degrading mutant alleles.

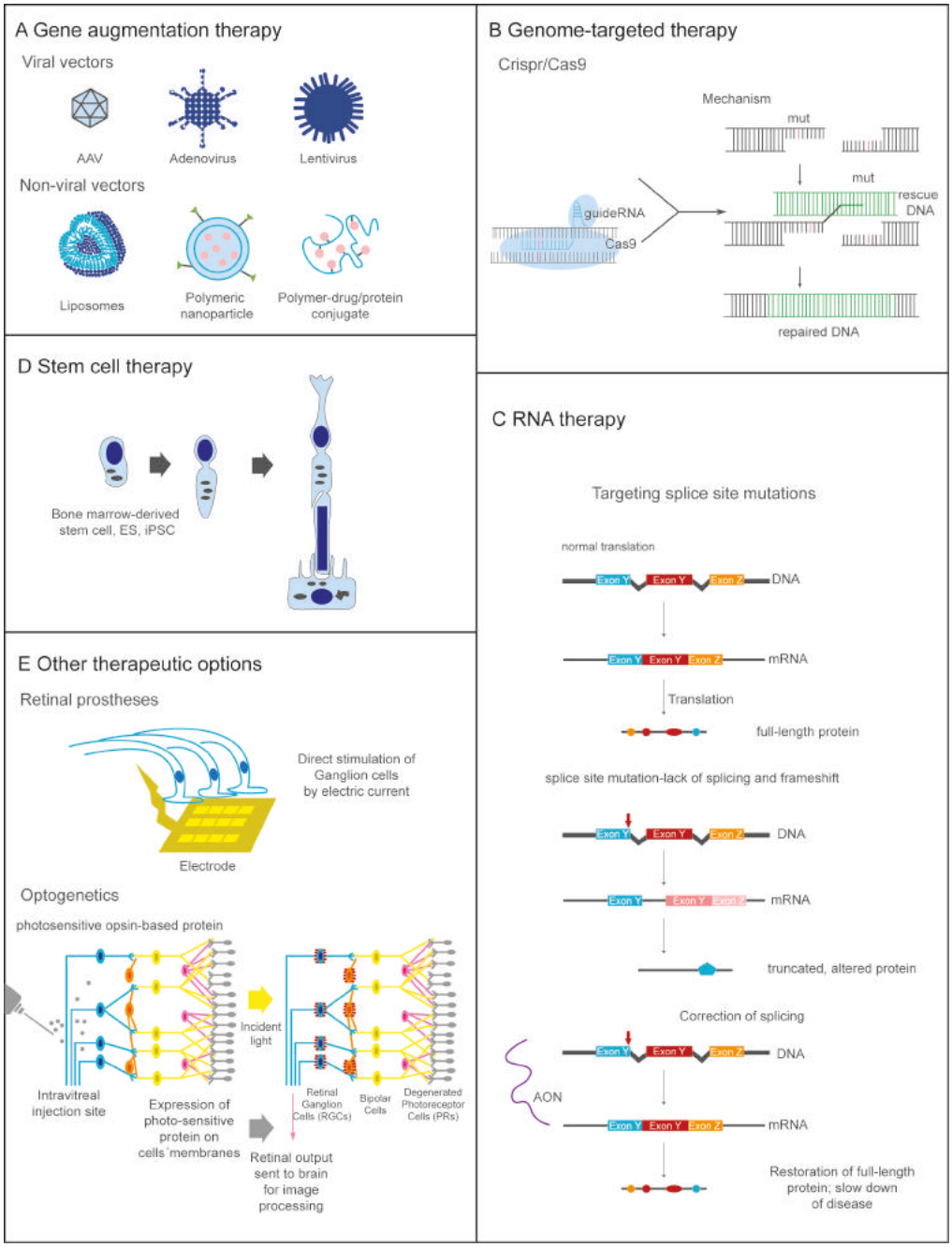

Figure 5. Current therapeutic strategies to treat inherited retinal diseases. A, Gene augmentation therapy using adeno-associated virus (AAV), adenovirus, lentivirus, liposomes, nanoparticles or polymers. These vectors carry wild-type cDNA of the mutated gene, and restore the wild-type protein exogenously. **B,** Genome-targeted therapy using CRISPR/Cas9 to correct DNA defects, or **C,** RNA therapy to correct mRNA defects. **D,** Stem cell transplantation of healthy retinal cells. **E,** Retinal prostheses and optogenetics are options for advanced stages of the disease. (Partially adapted from May-Simera et al., 2017[52]; França Dias et al., 2017[322] and GenSight, https://labiotech.eu/company/gensightbiologics/?nabe=6526793858416640:1)

RNA therapy is a mutation-specific treatment option for retinal disease patients.[323] Antisense oligonucleotides (AONs) are small DNA or RNA molecules that can complementary bind to target pre-mRNA sequences to control the splicing or the degradation of transcripts. Garanto et al. showed that delivery of AONs targeting a deep-intronic *CEP290* mutation in fibroblasts restored normal *CEP290* pre-mRNA splicing.[324] In a recent study by the group of Michael Cheetham, AON delivery to differentiated iPSCs-derived photoreceptor cells was able to restore *CEP290* splice defects and photoreceptor ciliary structures.[296] Although yet in its early stages, RNA therapy is thus a promising treatment for retinal disease when the mutations occur outside the coding sequence.

1.8.5 Other therapeutic options

When the disease is diagnosed in an advanced stage, the few remaining photoreceptor cells might not be sufficient for patients to benefit from gene therapy, or even cell transplantation. **Retinal prostheses** are a therapeutic option in these cases. The concept of retinal prostheses consists on the stimulation of the retinal cells by application of an electrical charge by an electrode activated by light.[325] Another emerging technique to treat patients with advanced retinal degeneration is **optogenetics**. Optogenetics is a type of gene therapy that aims at photosensitizing remnant bipolar or ganglion cells by genetically introducing photosensitive opsin-based proteins into the cell membrane. Ectopic expression of human rhodopsin has been shown effective in restoring some visual responses and behavior in mutant rd1 mice.[326] A phase I/II clinical trial using optogenetic therapies for a patient with advanced RP is ongoing (ClinicalTrials.gov, identifier: NCT02556736). Vision through light-sensitive ganglion cells is different than vision through photoreceptor cells, therefore the aim of this type of therapy is not to fully restore vision, but to provide the eye with some vision, thus improving the life quality of the patients.

1.9 Aim of this thesis

The main purpose of this thesis is to unravel the molecular mechanisms behind *PCARE*-associated retinal disease, and to build a path towards a therapy for this disease.

In **chapter 2**, we show that PCARE directly interacts with several proteins involved in the dynamic actin filament biogenesis. PCARE is able to recruit this actin module to the primary cilium to evaginate the ciliary plasma membrane. We propose that a similar actin dynamics-driven membrane evagination process is operational at the base of the photoreceptor outer segments where the PCARE module and actin co-localize, thereby shedding light on the mechanistic context of outer segment disc biogenesis.

In **chapter 3**, we offer an overview of all the reported mutations in *PCARE* and analyze any potential correlation between the genotype and the severity of *PCARE*-associated retinal disease.

In **chapter 4**, we report the duplication of the *pcare* gene in zebrafish. Generation of a *pcare1* mutant zebrafish using CRISPR/Cas9 technology shows that this gene is essential for proper outer segment morphogenesis and visual function in zebrafish.

In **chapter 5**, we study the potential of an iPS cell line derived from a patient with a homozygous mutation in *PCARE* to differentiate into a retinal fate. Transcriptome analysis reveals differences between wild-type and patient-derived cell lines, such as the downregulation of the expression of genes encoding cytoskeleton-associated proteins in *PCARE*-deficient iPSCs compared to controls. Moreover, wild-type cells are able to differentiate into a neuronal fate, contrary to patient-derived iPSCs.

Chapter 6 describes the generation and characterization of an adeno-associated virus (AAV) vector containing full-length *PCARE* cDNA for future therapeutic purposes.

In **chapter 7** the main topics of this thesis are discussed, focusing on the molecular mechanisms behind actin-driven outer segment disc morphogenesis. We also analyze *PCARE*-associated retinal disease, different models currently available to further study the disease features, and potential therapeutic strategies.

1.10 References

1. Schoenemann, B., Parnaste, H., and Clarkson, E.N.K. (2017). Structure and function of a compound eye, more than half a billion years old. Proc Natl Acad Sci U S A 114, 13489-13494.
2. Ramón y Cajal, S. (1893) La Cellule 9, 119-257 [English translation (1972) by S. A. Thorpe and M. Glickstein in The Structure of the Retina C. Thomas].
3. Arey, L.B. (1942). Visual mechanisms. Edited by Heinrich Klüver. The Jacques Cattell Press, Lancaster, Pa. 8vo. 8 + 322 pp. 1942. The Anatomical Record 84, 423-424.
4. Bussow, H. (1980). The astrocytes in the retina and optic nerve head of mammals: a special glia for the ganglion cell axons. Cell Tissue Res 206, 367-378.
5. Vecino, E., Rodriguez, F.D., Ruzafa, N., Pereiro, X., and Sharma, S.C. (2016). Glia-neuron interactions in the mammalian retina. Prog Retin Eye Res 51, 1-40.
6. Feher, J.J. (2017). Quantitative human physiology : an introduction.(Amsterdam ; Boston: Elsevier/AP, Academic Press is an imprint of Elsevier). Pages 456-470.
7. Omri, S., Omri, B., Savoldelli, M., Jonet, L., Thillaye-Goldenberg, B., Thuret, G., Gain, P., Jeanny, J.C., Crisanti, P., and Behar-Cohen, F. (2010). The outer limiting membrane (OLM) revisited: clinical implications. Clin Ophthalmol 4, 183-195.
8. Opas, M. (1985). The focal adhesions of chick retinal pigmented epithelial cells. Can J Biochem Cell Biol 63, 553-563.
9. Opas, M., Turksen, K., and Kalnins, V.I. (1985). Adhesiveness and distribution of vinculin and spectrin in retinal pigmented epithelial cells during growth and differentiation in vitro. Dev Biol 107, 269-280.
10. Kevany, B.M., and Palczewski, K. (2010). Phagocytosis of retinal rod and cone photoreceptors. Physiology (Bethesda) 25, 8-15.
11. Strauss, O. (2005). The retinal pigment epithelium in visual function. Physiol Rev 85, 845-881.
12. Bok, D. (1993). The retinal pigment epithelium: a versatile partner in vision. J Cell Sci Suppl 17, 189-195.
13. Sung, C.H., and Chuang, J.Z. (2010). The cell biology of vision. J Cell Biol 190, 953-963.
14. Mustafi, D., Engel, A.H., and Palczewski, K. (2009). Structure of cone photoreceptors. Prog Retin Eye Res 28, 289-302.
15. Curcio, C.A., Sloan, K.R., Kalina, R.E., and Hendrickson, A.E. (1990). Human photoreceptor topography. J Comp Neurol 292, 497-523.
16. Fu, Y. (1995). Phototransduction in Rods and Cones. In Webvision: The Organization of the Retina and Visual System, H. Kolb, E. Fernandez, andR. Nelson, eds. (Salt Lake City (UT).
17. Khanna, H. (2015). Photoreceptor Sensory Cilium: Traversing the Ciliary Gate. Cells 4, 674-686.
18. Bujakowska, K.M., Liu, Q., and Pierce, E.A. (2017). Photoreceptor Cilia and Retinal Ciliopathies. Cold Spring Harb Perspect Biol 9.
19. Liu, Q., Tan, G., Levenkova, N., Li, T., Pugh, E.N., Jr., Rux, J.J., Speicher, D.W., and Pierce, E.A. (2007). The proteome of the mouse photoreceptor sensory cilium complex. Mol Cell Proteomics 6, 1299-1317.
20. Oh, E.C., and Katsanis, N. (2012). Cilia in vertebrate development and disease. Development 139, 443-448.
21. Roepman, R., and Wolfrum, U. (2007). Protein networks and complexes in photoreceptor cilia. Subcell Biochem 43, 209-235.
22. Young, R.W. (1967). The renewal of photoreceptor cell outer segments. J Cell Biol 33, 61-72.
23. Dobell, C., and Leeuwenhoek, A.v. (1932). Antony van Leeuwenhoek and his "Little animals"; being some account of the father of protozoology and bacteriology and his multifarious discoveries in these disciplines.(New York,: Harcourt, Brace and company).
24. Müller, O.F., and Fabricius, O. (1786). Animalcula infusoria fluvia tilia et marina.(Hauniae :: Typis N. Mölleri).
25. Sorokin, S.P. (1968). Reconstructions of centriole formation and ciliogenesis in mammalian lungs. J Cell Sci 3, 207-230.
26. Beales, P., and Jackson, P.K. (2012). Cilia - the prodigal organelle. Cilia 1, 1.
27. De Robertis, E. (1956). Morphogenesis of the retinal rods; an electron microscope study. J Biophys Biochem Cytol 2, 209-218.
28. Kaplan, M.W., Iwata, R.T., and Sears, R.C. (1987). Lengths of immunolabeled ciliary microtubules in frog photoreceptor outer segments. Exp Eye Res 44, 623-632.
29. Pearring, J.N., Salinas, R.Y., Baker, S.A., and Arshavsky, V.Y. (2013). Protein sorting, targeting and trafficking in photoreceptor cells. Prog Retin Eye Res 36, 24-51.
30. Rosenbaum, J.L., and Witman, G.B. (2002). Intraflagellar transport. Nat Rev Mol Cell Biol 3, 813-825.
31. Garcia-Gonzalo, F.R., and Reiter, J.F. (2012). Scoring a backstage pass: mechanisms of ciliogenesis and ciliary access. J Cell Biol 197, 697-709.

32. Besharse, J.C., Forestner, D.M., and Defoe, D.M. (1985). Membrane assembly in retinal photoreceptors. III. Distinct membrane domains of the connecting cilium of developing rods. J Neurosci 5, 1035-1048.
33. Steinberg, R.H., Fisher, S.K., and Anderson, D.H. (1980). Disc morphogenesis in vertebrate photoreceptors. J Comp Neurol 190, 501-508.
34. Ding, J.D., Salinas, R.Y., and Arshavsky, V.Y. (2015). Discs of mammalian rod photoreceptors form through the membrane evagination mechanism. J Cell Biol 211, 495-502.
35. Pugh, E.N., Jr. (2015). Photoreceptor disc morphogenesis: The classical evagination model prevails. J Cell Biol 211, 491-493.
36. Burgoyne, T., Meschede, I.P., Burden, J.J., Bailly, M., Seabra, M.C., and Futter, C.E. (2015). Rod disc renewal occurs by evagination of the ciliary plasma membrane that makes cadherin-based contacts with the inner segment. Proc Natl Acad Sci U S A 112, 15922-15927.
37. Kozminski, K.G., Johnson, K.A., Forscher, P., and Rosenbaum, J.L. (1993). A motility in the eukaryotic flagellum unrelated to flagellar beating. Proc Natl Acad Sci U S A 90, 5519-5523.
38. Nickell, S., Park, P.S., Baumeister, W., and Palczewski, K. (2007). Three-dimensional architecture of murine rod outer segments determined by cryoelectron tomography. J Cell Biol 177, 917-925.
39. Hofmann, L., and Palczewski, K. (2015). The G protein-coupled receptor rhodopsin: a historical perspective. Methods Mol Biol 1271, 3-18.
40. Wolfrum, U., and Schmitt, A. (2000). Rhodopsin transport in the membrane of the connecting cilium of mammalian photoreceptor cells. Cell Motil Cytoskeleton 46, 95-107.
41. Liu, X., Udovichenko, I.P., Brown, S.D., Steel, K.P., and Williams, D.S. (1999). Myosin VIIa participates in opsin transport through the photoreceptor cilium. J Neurosci 19, 6267-6274.
42. Williams, D.S. (2002). Transport to the photoreceptor outer segment by myosin VIIa and kinesin II. Vision Res 42, 455-462.
43. Taschner, M., Bhogaraju, S., and Lorentzen, E. (2012). Architecture and function of IFT complex proteins in ciliogenesis. Differentiation 83, S12-22.
44. Williams, C.L., McIntyre, J.C., Norris, S.R., Jenkins, P.M., Zhang, L., Pei, Q., Verhey, K., and Martens, J.R. (2014). Direct evidence for BBSome-associated intraflagellar transport reveals distinct properties of native mammalian cilia. Nat Commun 5, 5813.
45. Wei, Q., Zhang, Y., Li, Y., Zhang, Q., Ling, K., and Hu, J. (2012). The BBSome controls IFT assembly and turnaround in cilia. Nat Cell Biol 14, 950-957.
46. Davis, E.E., Zhang, Q., Liu, Q., Diplas, B.H., Davey, L.M., Hartley, J., Stoetzel, C., Szymanska, K., Ramaswami, G., Logan, C.V., et al. (2011). TTC21B contributes both causal and modifying alleles across the ciliopathy spectrum. Nat Genet 43, 189-196.
47. Huynh Cong, E., Bizet, A.A., Boyer, O., Woerner, S., Gribouval, O., Filhol, E., Arrondel, C., Thomas, S., Silbermann, F., Canaud, G., et al. (2014). A homozygous missense mutation in the ciliary gene TTC21B causes familial FSGS. J Am Soc Nephrol 25, 2435-2443.
48. Beales, P.L., Bland, E., Tobin, J.L., Bacchelli, C., Tuysuz, B., Hill, J., Rix, S., Pearson, C.G., Kai, M., Hartley, J., et al. (2007). IFT80, which encodes a conserved intraflagellar transport protein, is mutated in Jeune asphyxiating thoracic dystrophy. Nat Genet 39, 727-729.
49. Fehrenbach, H., Decker, C., Eisenberger, T., Frank, V., Hampel, T., Walden, U., Amann, K.U., Kruger-Stollfuss, I., Bolz, H.J., Haffner, K., et al. (2014). Mutations in WDR19 encoding the intraflagellar transport component IFT144 cause a broad spectrum of ciliopathies. Pediatr Nephrol 29, 1451-1456.
50. Xu, M., Yang, L., Wang, F., Li, H., Wang, X., Wang, W., Ge, Z., Wang, K., Zhao, L., Li, H., et al. (2015). Mutations in human IFT140 cause non-syndromic retinal degeneration. Hum Genet 134, 1069-1078.
51. Perrault, I., Saunier, S., Hanein, S., Filhol, E., Bizet, A.A., Collins, F., Salih, M.A., Gerber, S., Delphin, N., Bigot, K., et al. (2012). Mainzer-Saldino syndrome is a ciliopathy caused by IFT140 mutations. Am J Hum Genet 90, 864-870.
52. May-Simera, H., Nagel-Wolfrum, K., and Wolfrum, U. (2017). Cilia - The sensory antennae in the eye. Prog Retin Eye Res 60, 144-180.
53. Falk, N., Losl, M., Schroder, N., and Giessl, A. (2015). Specialized Cilia in Mammalian Sensory Systems. Cells 4, 500-519.
54. Ye, F., Breslow, D.K., Koslover, E.F., Spakowitz, A.J., Nelson, W.J., and Nachury, M.V. (2013). Single molecule imaging reveals a major role for diffusion in the exploration of ciliary space by signaling receptors. Elife 2, e00654.
55. Harris, J.A., Liu, Y., Yang, P., Kner, P., and Lechtreck, K.F. (2016). Single-particle imaging reveals intraflagellar transport-independent transport and accumulation of EB1 in Chlamydomonas flagella. Mol Biol Cell 27, 295-307.

56. Calvert, P.D., Schiesser, W.E., and Pugh, E.N., Jr. (2010). Diffusion of a soluble protein, photoactivatable GFP, through a sensory cilium. J Gen Physiol 135, 173-196.
57. Nair, K.S., Hanson, S.M., Mendez, A., Gurevich, E.V., Kennedy, M.J., Shestopalov, V.I., Vishnivetskiy, S.A., Chen, J., Hurley, J.B., Gurevich, V.V., et al. (2005). Light-dependent redistribution of arrestin in vertebrate rods is an energy-independent process governed by protein-protein interactions. Neuron 46, 555-567.
58. Najafi, M., Maza, N.A., and Calvert, P.D. (2012). Steric volume exclusion sets soluble protein concentrations in photoreceptor sensory cilia. Proc Natl Acad Sci U S A 109, 203-208.
59. Kuznetsov, A.V. (2013). Protein transport in the connecting cilium of a photoreceptor cell: modeling the effects of bidirectional protein transitions between the diffusion-driven and motor-driven kinetic states. Comput Biol Med 43, 758-764.
60. Luo, W., Ruba, A., Takao, D., Zweifel, L.P., Lim, R.Y.H., Verhey, K.J., and Yang, W. (2017). Axonemal Lumen Dominates Cytosolic Protein Diffusion inside the Primary Cilium. Sci Rep 7, 15793.
61. Follit, J.A., Tuft, R.A., Fogarty, K.E., and Pazour, G.J. (2006). The intraflagellar transport protein IFT20 is associated with the Golgi complex and is required for cilia assembly. Mol Biol Cell 17, 3781-3792.
62. Craft, J.M., Harris, J.A., Hyman, S., Kner, P., and Lechtreck, K.F. (2015). Tubulin transport by IFT is upregulated during ciliary growth by a cilium-autonomous mechanism. J Cell Biol 208, 223-237.
63. Hartong, D.T., Berson, E.L., and Dryja, T.P. (2006). Retinitis pigmentosa. Lancet 368, 1795-1809.
64. Haim, M. (2002). Epidemiology of retinitis pigmentosa in Denmark. Acta Ophthalmol Scand Suppl, 1-34.
65. Audo, I., Manes, G., Mohand-Said, S., Friedrich, A., Lancelot, M.E., Antonio, A., Moskova-Doumanova, V., Poch, O., Zanlonghi, X., Hamel, C.P., et al. (2010). Spectrum of rhodopsin mutations in French autosomal dominant rod-cone dystrophy patients. Invest Ophthalmol Vis Sci 51, 3687-3700.
66. Sohocki, M.M., Daiger, S.P., Bowne, S.J., Rodriquez, J.A., Northrup, H., Heckenlively, J.R., Birch, D.G., Mintz-Hittner, H., Ruiz, R.S., Lewis, R.A., et al. (2001). Prevalence of mutations causing retinitis pigmentosa and other inherited retinopathies. Hum Mutat 17, 42-51.
67. Ferrari, S., Di Iorio, E., Barbaro, V., Ponzin, D., Sorrentino, F.S., and Parmeggiani, F. (2011). Retinitis pigmentosa: genes and disease mechanisms. Curr Genomics 12, 238-249.
68. Daiger, S.P., Sullivan, L.S., and Bowne, S.J. (2013). Genes and mutations causing retinitis pigmentosa. Clin Genet 84, 132-141.
69. Vervoort, R., Lennon, A., Bird, A.C., Tulloch, B., Axton, R., Miano, M.G., Meindl, A., Meitinger, T., Ciccodicola, A., and Wright, A.F. (2000). Mutational hot spot within a new RPGR exon in X-linked retinitis pigmentosa. Nat Genet 25, 462-466.
70. Fahim, A.T., Bowne, S.J., Sullivan, L.S., Webb, K.D., Williams, J.T., Wheaton, D.K., Birch, D.G., and Daiger, S.P. (2011). Allelic heterogeneity and genetic modifier loci contribute to clinical variation in males with X-linked retinitis pigmentosa due to RPGR mutations. PLoS One 6, e23021.
71. Hardcastle, A.J., Thiselton, D.L., Van Maldergem, L., Saha, B.K., Jay, M., Plant, C., Taylor, R., Bird, A.C., and Bhattacharya, S. (1999). Mutations in the RP2 gene cause disease in 10% of families with familial X-linked retinitis pigmentosa assessed in this study. Am J Hum Genet 64, 1210-1215.
72. Mears, A.J., Gieser, L., Yan, D., Chen, C., Fahrner, S., Hiriyanna, S., Fujita, R., Jacobson, S.G., Sieving, P.A., and Swaroop, A. (1999). Protein-truncation mutations in the RP2 gene in a North American cohort of families with X-linked retinitis pigmentosa. Am J Hum Genet 64, 897-900.
73. Kajiwara, K., Berson, E.L., and Dryja, T.P. (1994). Digenic retinitis pigmentosa due to mutations at the unlinked peripherin/RDS and ROM1 loci. Science 264, 1604-1608.
74. Liu, Y.P., Bosch, D.G., Siemiatkowska, A.M., Rendtorff, N.D., Boonstra, F.N., Moller, C., Tranebjaerg, L., Katsanis, N., and Cremers, F.P. (2017). Putative digenic inheritance of heterozygous RP1L1 and C2orf71 null mutations in syndromic retinal dystrophy. Ophthalmic Genet 38, 127-132.
75. Hamel, C.P. (2007). Cone rod dystrophies. Orphanet J Rare Dis 2, 7.
76. Michaelides, M., Hunt, D.M., and Moore, A.T. (2004). The cone dysfunction syndromes. Br J Ophthalmol 88, 291-297.
77. Perrault, I., Rozet, J.M., Calvas, P., Gerber, S., Camuzat, A., Dollfus, H., Chatelin, S., Souied, E., Ghazi, I., Leowski, C., et al. (1996). Retinal-specific guanylate cyclase gene mutations in Leber's congenital amaurosis. Nat Genet 14, 461-464.
78. Freund, C.L., Gregory-Evans, C.Y., Furukawa, T., Papaioannou, M., Looser, J., Ploder, L., Bellingham, J., Ng, D., Herbrick, J.A., Duncan, A., et al. (1997). Cone-rod dystrophy due to mutations in a novel photoreceptor-specific homeobox gene (CRX) essential for maintenance of the photoreceptor. Cell 91, 543-553.

79. Chen, S., Wang, Q.L., Nie, Z., Sun, H., Lennon, G., Copeland, N.G., Gilbert, D.J., Jenkins, N.A., and Zack, D.J. (1997). Crx, a novel Otx-like paired-homeodomain protein, binds to and transactivates photoreceptor cell-specific genes. Neuron 19, 1017-1030.
80. Furukawa, T., Morrow, E.M., and Cepko, C.L. (1997). Crx, a novel otx-like homeobox gene, shows photoreceptor-specific expression and regulates photoreceptor differentiation. Cell 91, 531-541.
81. den Hollander, A.I., Koenekoop, R.K., Yzer, S., Lopez, I., Arends, M.L., Voesenek, K.E., Zonneveld, M.N., Strom, T.M., Meitinger, T., Brunner, H.G., et al. (2006). Mutations in the CEP290 (NPHP6) gene are a frequent cause of Leber congenital amaurosis. Am J Hum Genet 79, 556-561.
82. Koenekoop, R.K., Fishman, G.A., Iannaccone, A., Ezzeldin, H., Ciccarelli, M.L., Baldi, A., Sunness, J.S., Lotery, A.J., Jablonski, M.M., Pittler, S.J., et al. (2002). Electroretinographic abnormalities in parents of patients with Leber congenital amaurosis who have heterozygous GUCY2D mutations. Arch Ophthalmol 120, 1325-1330.
83. Lotery, A.J., Jacobson, S.G., Fishman, G.A., Weleber, R.G., Fulton, A.B., Namperumalsamy, P., Heon, E., Levin, A.V., Grover, S., Rosenow, J.R., et al. (2001). Mutations in the CRB1 gene cause Leber congenital amaurosis. Arch Ophthalmol 119, 415-420.
84. Sohocki, M.M., Sullivan, L.S., Mintz-Hittner, H.A., Birch, D., Heckenlively, J.R., Freund, C.L., McInnes, R.R., and Daiger, S.P. (1998). A range of clinical phenotypes associated with mutations in CRX, a photoreceptor transcription-factor gene. Am J Hum Genet 63, 1307-1315.
85. Bowne, S.J., Sullivan, L.S., Mortimer, S.E., Hedstrom, L., Zhu, J., Spellicy, C.J., Gire, A.I., Hughbanks-Wheaton, D., Birch, D.G., Lewis, R.A., et al. (2006). Spectrum and frequency of mutations in IMPDH1 associated with autosomal dominant retinitis pigmentosa and leber congenital amaurosis. Invest Ophthalmol Vis Sci 47, 34-42.
86. den Hollander, A.I., Roepman, R., Koenekoop, R.K., and Cremers, F.P.M. (2008). Leber congenital amaurosis: genes, proteins and disease mechanisms. Prog Retin Eye Res 27, 391-419.
87. Weleber, R.G. (2002). Infantile and childhood retinal blindness: a molecular perspective (The Franceschetti Lecture). Ophthalmic Genet 23, 71-97.
88. Collin, R.W.J., Safieh, C., Littink, K.W., Shalev, S.A., Garzozi, H.J., Rizel, L., Abbasi, A.H., Cremers, F.P.M., den Hollander, A.I., Klevering, B.J., et al. (2010). Mutations in C2ORF71 cause autosomal-recessive retinitis pigmentosa. Am J Hum Genet 86, 783-788.
89. Nishimura, D.Y., Baye, L.M., Perveen, R., Searby, C.C., Avila-Fernandez, A., Pereiro, I., Ayuso, C., Valverde, D., Bishop, P.N., Manson, F.D., et al. (2010). Discovery and functional analysis of a retinitis pigmentosa gene, C2ORF71. Am J Hum Genet 86, 686-695.
90. Ravesh, Z., El Asrag, M.E., Weisschuh, N., McKibbin, M., Reuter, P., Watson, C.M., Baumann, B., Poulter, J.A., Sajid, S., Panagiotou, E.S., et al. (2015). Novel C8orf37 mutations cause retinitis pigmentosa in consanguineous families of Pakistani origin. Mol Vis 21, 236-243.
91. Duncan, J.L., Roorda, A., Navani, M., Vishweswaraiah, S., Syed, R., Soudry, S., Ratnam, K., Gudiseva, H.V., Lee, P., Gaasterland, T., et al. (2012). Identification of a novel mutation in the CDHR1 gene in a family with recessive retinal degeneration. Arch Ophthalmol 130, 1301-1308.
92. Abd El-Aziz, M.M., Barragan, I., O'Driscoll, C.A., Goodstadt, L., Prigmore, E., Borrego, S., Mena, M., Pieras, J.I., El-Ashry, M.F., Safieh, L.A., et al. (2008). EYS, encoding an ortholog of Drosophila spacemaker, is mutated in autosomal recessive retinitis pigmentosa. Nat Genet 40, 1285-1287.
93. Collin, R.W.J., Littink, K.W., Klevering, B.J., van den Born, L.I., Koenekoop, R.K., Zonneveld, M.N., Blokland, E.A., Strom, T.M., Hoyng, C.B., den Hollander, A.I., et al. (2008). Identification of a 2 Mb human ortholog of Drosophila eyes shut/spacemaker that is mutated in patients with retinitis pigmentosa. Am J Hum Genet 83, 594-603.
94. Langmann, T., Di Gioia, S.A., Rau, I., Stohr, H., Maksimovic, N.S., Corbo, J.C., Renner, A.B., Zrenner, E., Kumaramanickavel, G., Karlstetter, M., et al. (2010). Nonsense mutations in FAM161A cause RP28-associated recessive retinitis pigmentosa. Am J Hum Genet 87, 376-381.
95. Bandah-Rozenfeld, D., Mizrahi-Meissonnier, L., Farhy, C., Obolensky, A., Chowers, I., Pe'er, J., Merin, S., Ben-Yosef, T., Ashery-Padan, R., Banin, E., et al. (2010). Homozygosity mapping reveals null mutations in FAM161A as a cause of autosomal-recessive retinitis pigmentosa. Am J Hum Genet 87, 382-391.
96. El Shamieh, S., Neuille, M., Terray, A., Orhan, E., Condroyer, C., Demontant, V., Michiels, C., Antonio, A., Boyard, F., Lancelot, M.E., et al. (2014). Whole-exome sequencing identifies KIZ as a ciliary gene associated with autosomal-recessive rod-cone dystrophy. Am J Hum Genet 94, 625-633.
97. den Hollander, A.I., Koenekoop, R.K., Mohamed, M.D., Arts, H.H., Boldt, K., Towns, K.V., Sedmak, T., Beer, M., Nagel-Wolfrum, K., McKibbin, M., et al. (2007). Mutations in LCA5, encoding the ciliary protein lebercilin, cause Leber congenital amaurosis. Nat Genet 39, 889-895.

98. Ozgul, R.K., Siemiatkowska, A.M., Yucel, D., Myers, C.A., Collin, R.W.J., Zonneveld, M.N., Beryozkin, A., Banin, E., Hoyng, C.B., van den Born, L.I., et al. (2011). Exome sequencing and cis-regulatory mapping identify mutations in MAK, a gene encoding a regulator of ciliary length, as a cause of retinitis pigmentosa. Am J Hum Genet 89, 253-264.
99. Tucker, B.A., Scheetz, T.E., Mullins, R.F., DeLuca, A.P., Hoffmann, J.M., Johnston, R.M., Jacobson, S.G., Sheffield, V.C., and Stone, E.M. (2011). Exome sequencing and analysis of induced pluripotent stem cells identify the cilia-related gene male germ cell-associated kinase (MAK) as a cause of retinitis pigmentosa. Proc Natl Acad Sci U S A 108, E569-576.
100. Nishiguchi, K.M., Tearle, R.G., Liu, Y.P., Oh, E.C., Miyake, N., Benaglio, P., Harper, S., Koskiniemi-Kuendig, H., Venturini, G., Sharon, D., et al. (2013). Whole genome sequencing in patients with retinitis pigmentosa reveals pathogenic DNA structural changes and NEK2 as a new disease gene. Proc Natl Acad Sci U S A 110, 16139-16144.
101. Maw, M.A., Kennedy, B., Knight, A., Bridges, R., Roth, K.E., Mani, E.J., Mukkadan, J.K., Nancarrow, D., Crabb, J.W., and Denton, M.J. (1997). Mutation of the gene encoding cellular retinaldehyde-binding protein in autosomal recessive retinitis pigmentosa. Nat Genet 17, 198-200.
102. Kajiwara, K., Hahn, L.B., Mukai, S., Travis, G.H., Berson, E.L., and Dryja, T.P. (1991). Mutations in the human retinal degeneration slow gene in autosomal dominant retinitis pigmentosa. Nature 354, 480-483.
103. Roosing, S., Rohrschneider, K., Beryozkin, A., Sharon, D., Weisschuh, N., Staller, J., Kohl, S., Zelinger, L., Peters, T.A., Neveling, K., et al. (2013). Mutations in RAB28, encoding a farnesylated small GTPase, are associated with autosomal-recessive cone-rod dystrophy. Am J Hum Genet 93, 110-117.
104. Dryja, T.P., Adams, S.M., Grimsby, J.L., McGee, T.L., Hong, D.H., Li, T., Andreasson, S., and Berson, E.L. (2001). Null RPGRIP1 alleles in patients with Leber congenital amaurosis. Am J Hum Genet 68, 1295-1298.
105. Guillonneau, X., Piriev, N.I., Danciger, M., Kozak, C.A., Cideciyan, A.V., Jacobson, S.G., and Farber, D.B. (1999). A nonsense mutation in a novel gene is associated with retinitis pigmentosa in a family linked to the RP1 locus. Hum Mol Genet 8, 1541-1546.
106. Pierce, E.A., Quinn, T., Meehan, T., McGee, T.L., Berson, E.L., and Dryja, T.P. (1999). Mutations in a gene encoding a new oxygen-regulated photoreceptor protein cause dominant retinitis pigmentosa. Nat Genet 22, 248-254.
107. Wang, H., den Hollander, A.I., Moayedi, Y., Abulimiti, A., Li, Y., Collin, R.W., Hoyng, C.B., Lopez, I., Abboud, E.B., Al-Rajhi, A.A., et al. (2009). Mutations in SPATA7 cause Leber congenital amaurosis and juvenile retinitis pigmentosa. Am J Hum Genet 84, 380-387.
108. Bowne, S.J., Sullivan, L.S., Gire, A.I., Birch, D.G., Hughbanks-Wheaton, D., Heckenlively, J.R., and Daiger, S.P. (2008). Mutations in the TOPORS gene cause 1% of autosomal dominant retinitis pigmentosa. Mol Vis 14, 922-927.
109. Hagstrom, S.A., Duyao, M., North, M.A., and Li, T. (1999). Retinal degeneration in tulp1-/- mice: vesicular accumulation in the interphotoreceptor matrix. Invest Ophthalmol Vis Sci 40, 2795-2802.
110. Banerjee, P., Kleyn, P.W., Knowles, J.A., Lewis, C.A., Ross, B.M., Parano, E., Kovats, S.G., Lee, J.J., Penchaszadeh, G.K., Ott, J., et al. (1998). TULP1 mutation in two extended Dominican kindreds with autosomal recessive retinitis pigmentosa. Nat Genet 18, 177-179.
111. Allikmets, R., Singh, N., Sun, H., Shroyer, N.F., Hutchinson, A., Chidambaram, A., Gerrard, B., Baird, L., Stauffer, D., Peiffer, A., et al. (1997). A photoreceptor cell-specific ATP-binding transporter gene (ABCR) is mutated in recessive Stargardt macular dystrophy. Nat Genet 15, 236-246.
112. Dryja, T.P., Finn, J.T., Peng, Y.W., McGee, T.L., Berson, E.L., and Yau, K.W. (1995). Mutations in the gene encoding the alpha subunit of the rod cGMP-gated channel in autosomal recessive retinitis pigmentosa. Proc Natl Acad Sci U S A 92, 10177-10181.
113. Kohl, S., Marx, T., Giddings, I., Jagle, H., Jacobson, S.G., Apfelstedt-Sylla, E., Zrenner, E., Sharpe, L.T., and Wissinger, B. (1998). Total colourblindness is caused by mutations in the gene encoding the alpha-subunit of the cone photoreceptor cGMP-gated cation channel. Nat Genet 19, 257-259.
114. Bareil, C., Hamel, C.P., Delague, V., Arnaud, B., Demaille, J., and Claustres, M. (2001). Segregation of a mutation in CNGB1 encoding the beta-subunit of the rod cGMP-gated channel in a family with autosomal recessive retinitis pigmentosa. Hum Genet 108, 328-334.
115. Kohl, S., Baumann, B., Broghammer, M., Jagle, H., Sieving, P., Kellner, U., Spegal, R., Anastasi, M., Zrenner, E., Sharpe, L.T., et al. (2000). Mutations in the CNGB3 gene encoding the beta-subunit of the cone photoreceptor cGMP-gated channel are responsible for achromatopsia (ACHM3) linked to chromosome 8q21. Hum Mol Genet 9, 2107-2116.

116. Dryja, T.P., Hahn, L.B., Reboul, T., and Arnaud, B. (1996). Missense mutation in the gene encoding the alpha subunit of rod transducin in the Nougaret form of congenital stationary night blindness. Nat Genet 13, 358-360.
117. Aligianis, I.A., Forshew, T., Johnson, S., Michaelides, M., Johnson, C.A., Trembath, R.C., Hunt, D.M., Moore, A.T., and Maher, E.R. (2002). Mapping of a novel locus for achromatopsia (ACHM4) to 1p and identification of a germline mutation in the alpha subunit of cone transducin (GNAT2). J Med Genet 39, 656-660.
118. Kohl, S., Baumann, B., Rosenberg, T., Kellner, U., Lorenz, B., Vadala, M., Jacobson, S.G., and Wissinger, B. (2002). Mutations in the cone photoreceptor G-protein alpha-subunit gene GNAT2 in patients with achromatopsia. Am J Hum Genet 71, 422-425.
119. Yamamoto, S., Sippel, K.C., Berson, E.L., and Dryja, T.P. (1997). Defects in the rhodopsin kinase gene in the Oguchi form of stationary night blindness. Nat Genet 15, 175-178.
120. Payne, A.M., Downes, S.M., Bessant, D.A., Taylor, R., Holder, G.E., Warren, M.J., Bird, A.C., and Bhattacharya, S.S. (1998). A mutation in guanylate cyclase activator 1A (GUCA1A) in an autosomal dominant cone dystrophy pedigree mapping to a new locus on chromosome 6p21.1. Hum Mol Genet 7, 273-277.
121. Sokal, I., Li, N., Surgucheva, I., Warren, M.J., Payne, A.M., Bhattacharya, S.S., Baehr, W., and Palczewski, K. (1998). GCAP1 (Y99C) mutant is constitutively active in autosomal dominant cone dystrophy. Mol Cell 2, 129-133.
122. Sato, M., Nakazawa, M., Usui, T., Tanimoto, N., Abe, H., and Ohguro, H. (2005). Mutations in the gene coding for guanylate cyclase-activating protein 2 (GUCA1B gene) in patients with autosomal dominant retinal dystrophies. Graefes Arch Clin Exp Ophthalmol 243, 235-242.
123. Thompson, D.A., Li, Y., McHenry, C.L., Carlson, T.J., Ding, X., Sieving, P.A., Apfelstedt-Sylla, E., and Gal, A. (2001). Mutations in the gene encoding lecithin retinol acyltransferase are associated with early-onset severe retinal dystrophy. Nat Genet 28, 123-124.
124. Nathans, J., Thomas, D., and Hogness, D.S. (1986). Molecular genetics of human color vision: the genes encoding blue, green, and red pigments. Science 232, 193-202.
125. Winderickx, J., Sanocki, E., Lindsey, D.T., Teller, D.Y., Motulsky, A.G., and Deeb, S.S. (1992). Defective colour vision associated with a missense mutation in the human green visual pigment gene. Nat Genet 1, 251-256.
126. Ayyagari, R., Kakuk, L.E., Coats, C.L., Bingham, E.L., Toda, Y., Felius, J., and Sieving, P.A. (1999). Bilateral macular atrophy in blue cone monochromacy (BCM) with loss of the locus control region (LCR) and part of the red pigment gene. Mol Vis 5, 13.
127. Weitz, C.J., Miyake, Y., Shinzato, K., Montag, E., Zrenner, E., Went, L.N., and Nathans, J. (1992). Human tritanopia associated with two amino acid substitutions in the blue-sensitive opsin. Am J Hum Genet 50, 498-507.
128. Weitz, C.J., Went, L.N., and Nathans, J. (1992). Human tritanopia associated with a third amino acid substitution in the blue-sensitive visual pigment. Am J Hum Genet 51, 444-446.
129. Huang, S.H., Pittler, S.J., Huang, X., Oliveira, L., Berson, E.L., and Dryja, T.P. (1995). Autosomal recessive retinitis pigmentosa caused by mutations in the alpha subunit of rod cGMP phosphodiesterase. Nat Genet 11, 468-471.
130. McLaughlin, M.E., Sandberg, M.A., Berson, E.L., and Dryja, T.P. (1993). Recessive mutations in the gene encoding the beta-subunit of rod phosphodiesterase in patients with retinitis pigmentosa. Nat Genet 4, 130-134.
131. Thiadens, A.A., den Hollander, A.I., Roosing, S., Nabuurs, S.B., Zekveld-Vroon, R.C., Collin, R.W., De, B.E., Koenekoop, R.K., van Schooneveld, M.J., Strom, T.M., et al. (2009). Homozygosity mapping reveals PDE6C mutations in patients with early-onset cone photoreceptor disorders. Am J Hum Genet 85, 240-247.
132. Dvir, L., Srour, G., Abu-Ras, R., Miller, B., Shalev, S.A., and Ben-Yosef, T. (2010). Autosomal-recessive early-onset retinitis pigmentosa caused by a mutation in PDE6G, the gene encoding the gamma subunit of rod cGMP phosphodiesterase. Am J Hum Genet 87, 258-264.
133. Yamamoto, H., Simon, A., Eriksson, U., Harris, E., Berson, E.L., and Dryja, T.P. (1999). Mutations in the gene encoding 11-cis retinol dehydrogenase cause delayed dark adaptation and fundus albipunctatus. Nat Genet 22, 188-191.
134. Gonzalez-Fernandez, F., Kurz, D., Bao, Y., Newman, S., Conway, B.P., Young, J.E., Han, D.P., and Khani, S.C. (1999). 11-cis retinol dehydrogenase mutations as a major cause of the congenital night-blindness disorder known as fundus albipunctatus. Mol Vis 5, 41.

135. Perrault, I., Hanein, S., Gerber, S., Barbet, F., Ducroq, D., Dollfus, H., Hamel, C., Dufier, J.L., Munnich, A., Kaplan, J., et al. (2004). Retinal dehydrogenase 12 (RDH12) mutations in leber congenital amaurosis. Am J Hum Genet 75, 639-646.
136. Janecke, A.R., Thompson, D.A., Utermann, G., Becker, C., Hubner, C.A., Schmid, E., McHenry, C.L., Nair, A.R., Ruschendorf, F., Heckenlively, J., et al. (2004). Mutations in RDH12 encoding a photoreceptor cell retinol dehydrogenase cause childhood-onset severe retinal dystrophy. Nat Genet 36, 850-854.
137. Nishiguchi, K.M., Sandberg, M.A., Kooijman, A.C., Martemyanov, K.A., Pott, J.W., Hagstrom, S.A., Arshavsky, V.Y., Berson, E.L., and Dryja, T.P. (2004). Defects in RGS9 or its anchor protein R9AP in patients with slow photoreceptor deactivation. Nature 427, 75-78.
138. Dryja, T.P., McGee, T.L., Hahn, L.B., Cowley, G.S., Olsson, J.E., Reichel, E., Sandberg, M.A., and Berson, E.L. (1990). Mutations within the rhodopsin gene in patients with autosomal dominant retinitis pigmentosa. N Engl J Med 323, 1302-1307.
139. Gu, S.M., Thompson, D.A., Srikumari, C.R., Lorenz, B., Finckh, U., Nicoletti, A., Murthy, K.R., Rathmann, M., Kumaramanickavel, G., Denton, M.J., et al. (1997). Mutations in RPE65 cause autosomal recessive childhood-onset severe retinal dystrophy. Nat Genet 17, 194-197.
140. Fuchs, S., Nakazawa, M., Maw, M., Tamai, M., Oguchi, Y., and Gal, A. (1995). A homozygous 1-base pair deletion in the arrestin gene is a frequent cause of Oguchi disease in Japanese. Nat Genet 10, 360-362.
141. Kim, M.S., Pinto, S.M., Getnet, D., Nirujogi, R.S., Manda, S.S., Chaerkady, R., Madugundu, A.K., Kelkar, D.S., Isserlin, R., Jain, S., et al. (2014). A draft map of the human proteome. Nature 509, 575-581.
142. Perrault, I., Delphin, N., Hanein, S., Gerber, S., Dufier, J.L., Roche, O., Defoort-Dhellemmes, S., Dollfus, H., Fazzi, E., Munnich, A., et al. (2007). Spectrum of NPHP6/CEP290 mutations in Leber congenital amaurosis and delineation of the associated phenotype. Hum Mutat 28, 416.
143. Ferrante, M.I., Giorgio, G., Feather, S.A., Bulfone, A., Wright, V., Ghiani, M., Selicorni, A., Gammaro, L., Scolari, F., Woolf, A.S., et al. (2001). Identification of the gene for oral-facial-digital type I syndrome. Am J Hum Genet 68, 569-576.
144. Estrada-Cuzcano, A., Koenekoop, R.K., Coppieters, F., Kohl, S., Lopez, I., Collin, R.W.J., De Baere, E.B., Roeleveld, D., Marek, J., Bernd, A., et al. (2011). IQCB1 mutations in patients with leber congenital amaurosis. Invest Ophthalmol Vis Sci 52, 834-839.
145. Schmidts, M., Frank, V., Eisenberger, T., Al Turki, S., Bizet, A.A., Antony, D., Rix, S., Decker, C., Bachmann, N., Bald, M., et al. (2013). Combined NGS approaches identify mutations in the intraflagellar transport gene IFT140 in skeletal ciliopathies with early progressive kidney Disease. Hum Mutat 34, 714-724.
146. Kremer, H., van Wijk, E., Marker, T., Wolfrum, U., and Roepman, R. (2006). Usher syndrome: molecular links of pathogenesis, proteins and pathways. Hum Mol Genet 15 Spec No 2, R262-270.
147. Eudy, J.D., Weston, M.D., Yao, S., Hoover, D.M., Rehm, H.L., Ma-Edmonds, M., Yan, D., Ahmad, I., Cheng, J.J., Ayuso, C., et al. (1998). Mutation of a gene encoding a protein with extracellular matrix motifs in Usher syndrome type IIa. Science 280, 1753-1757.
148. Millan, J.M., Aller, E., Jaijo, T., Blanco-Kelly, F., Gimenez-Pardo, A., and Ayuso, C. (2011). An update on the genetics of usher syndrome. J Ophthalmol 2011, 417217.
149. Liu, X., Bulgakov, O.V., Darrow, K.N., Pawlyk, B., Adamian, M., Liberman, M.C., and Li, T. (2007). Usherin is required for maintenance of retinal photoreceptors and normal development of cochlear hair cells. Proc Natl Acad Sci U S A 104, 4413-4418.
150. Jacobson, S.G., Cideciyan, A.V., Aleman, T.S., Sumaroka, A., Roman, A.J., Gardner, L.M., Prosser, H.M., Mishra, M., Bech-Hansen, N.T., Herrera, W., et al. (2008). Usher syndromes due to MYO7A, PCDH15, USH2A or GPR98 mutations share retinal disease mechanism. Hum Mol Genet 17, 2405-2415.
151. Ebermann, I., Wiesen, M.H., Zrenner, E., Lopez, I., Pigeon, R., Kohl, S., Lowenheim, H., Koenekoop, R.K., and Bolz, H.J. (2009). GPR98 mutations cause Usher syndrome type 2 in males. J Med Genet 46, 277-280.
152. Mustapha, M., Chouery, E., Chardenoux, S., Naboulsi, M., Paronnaud, J., Lemainque, A., Megarbane, A., Loiselet, J., Weil, D., Lathrop, M., et al. (2002). DFNB31, a recessive form of sensorineural hearing loss, maps to chromosome 9q32-34. Eur J Hum Genet 10, 210-212.
153. Zallocchi, M., Meehan, D.T., Delimont, D., Askew, C., Garige, S., Gratton, M.A., Rothermund-Franklin, C.A., and Cosgrove, D. (2009). Localization and expression of clarin-1, the Clrn1 gene product, in auditory hair cells and photoreceptors. Hear Res 255, 109-120.
154. Puffenberger, E.G., Jinks, R.N., Sougnez, C., Cibulskis, K., Willert, R.A., Achilly, N.P., Cassidy, R.P., Fiorentini, C.J., Heiken, K.F., Lawrence, J.J., et al. (2012). Genetic mapping and exome sequencing identify variants associated with five novel diseases. PLoS One 7, e28936.

155. Sahly, I., Dufour, E., Schietroma, C., Michel, V., Bahloul, A., Perfettini, I., Pepermans, E., Estivalet, A., Carette, D., Aghaie, A., et al. (2012). Localization of Usher 1 proteins to the photoreceptor calyceal processes, which are absent from mice. J Cell Biol 199, 381-399.
156. Lopes, V.S., Gibbs, D., Libby, R.T., Aleman, T.S., Welch, D.L., Lillo, C., Jacobson, S.G., Radu, R.A., Steel, K.P., and Williams, D.S. (2011). The Usher 1B protein, MYO7A, is required for normal localization and function of the visual retinoid cycle enzyme, RPE65. Hum Mol Genet 20, 2560-2570.
157. Ebermann, I., Phillips, J.B., Liebau, M.C., Koenekoop, R.K., Schermer, B., Lopez, I., Schafer, E., Roux, A.F., Dafinger, C., Bernd, A., et al. (2010). PDZD7 is a modifier of retinal disease and a contributor to digenic Usher syndrome. J Clin Invest 120, 1812-1823.
158. Khateb, S., Zelinger, L., Mizrahi-Meissonnier, L., Ayuso, C., Koenekoop, R.K., Laxer, U., Gross, M., Banin, E., and Sharon, D. (2014). A homozygous nonsense CEP250 mutation combined with a heterozygous nonsense C2orf71 mutation is associated with atypical Usher syndrome. J Med Genet 51, 460-469.
159. Nikopoulos, K., Farinelli, P., Giangreco, B., Tsika, C., Royer-Bertrand, B., Mbefo, M.K., Bedoni, N., Kjellstrom, U., El Zaoui, I., Di Gioia, S.A., et al. (2016). Mutations in CEP78 Cause Cone-Rod Dystrophy and Hearing Loss Associated with Primary-Cilia Defects. Am J Hum Genet 99, 770-776.
160. Szymanska, K., Hartill, V.L., and Johnson, C.A. (2014). Unraveling the genetics of Joubert and Meckel-Gruber syndromes. J Pediatr Genet 3, 65-78.
161. Valente, E.M., Dallapiccola, B., and Bertini, E. (2013). Joubert syndrome and related disorders. Handb Clin Neurol 113, 1879-1888.
162. Parisi, M., and Glass, I. (1993). Joubert Syndrome. In GeneReviews((R)), M.P. Adam, H.H. Ardinger, R.A. Pagon, S.E. Wallace, L.J.H. Bean, K. Stephens, andA. Amemiya, eds. (Seattle (WA).
163. Dixon-Salazar, T., Silhavy, J.L., Marsh, S.E., Louie, C.M., Scott, L.C., Gururaj, A., Al-Gazali, L., Al-Tawari, A.A., Kayserili, H., Sztriha, L., et al. (2004). Mutations in the AHI1 gene, encoding jouberin, cause Joubert syndrome with cortical polymicrogyria. Am J Hum Genet 75, 979-987.
164. Ferland, R.J., Eyaid, W., Collura, R.V., Tully, L.D., Hill, R.S., Al-Nouri, D., Al-Rumayyan, A., Topcu, M., Gascon, G., Bodell, A., et al. (2004). Abnormal cerebellar development and axonal decussation due to mutations in AHI1 in Joubert syndrome. Nat Genet 36, 1008-1013.
165. Srour, M., Schwartzentruber, J., Hamdan, F.F., Ospina, L.H., Patry, L., Labuda, D., Massicotte, C., Dobrzeniecka, S., Capo-Chichi, J.M., Papillon-Cavanagh, S., et al. (2012). Mutations in C5ORF42 cause Joubert syndrome in the French Canadian population. Am J Hum Genet 90, 693-700.
166. Gorden, N.T., Arts, H.H., Parisi, M.A., Coene, K.L., Letteboer, S.J., van Beersum, S.E., Mans, D.A., Hikida, A., Eckert, M., Knutzen, D., et al. (2008). CC2D2A is mutated in Joubert syndrome and interacts with the ciliopathy-associated basal body protein CEP290. Am J Hum Genet 83, 559-571.
167. Noor, A., Windpassinger, C., Patel, M., Stachowiak, B., Mikhailov, A., Azam, M., Irfan, M., Siddiqui, Z.K., Naeem, F., Paterson, A.D., et al. (2008). CC2D2A, encoding a coiled-coil and C2 domain protein, causes autosomal-recessive mental retardation with retinitis pigmentosa. Am J Hum Genet 82, 1011-1018.
168. Sayer, J.A., Otto, E.A., O'Toole, J.F., Nurnberg, G., Kennedy, M.A., Becker, C., Hennies, H.C., Helou, J., Attanasio, M., Fausett, B.V., et al. (2006). The centrosomal protein nephrocystin-6 is mutated in Joubert syndrome and activates transcription factor ATF4. Nat Genet 38, 674-681.
169. Shaheen, R., Shamseldin, H.E., Loucks, C.M., Seidahmed, M.Z., Ansari, S., Ibrahim Khalil, M., Al-Yacoub, N., Davis, E.E., Mola, N.A., Szymanska, K., et al. (2014). Mutations in CSPP1, encoding a core centrosomal protein, cause a range of ciliopathy phenotypes in humans. Am J Hum Genet 94, 73-79.
170. Tuz, K., Bachmann-Gagescu, R., O'Day, D.R., Hua, K., Isabella, C.R., Phelps, I.G., Stolarski, A.E., O'Roak, B.J., Dempsey, J.C., Lourenco, C., et al. (2014). Mutations in CSPP1 cause primary cilia abnormalities and Joubert syndrome with or without Jeune asphyxiating thoracic dystrophy. Am J Hum Genet 94, 62-72.
171. Bielas, S.L., Silhavy, J.L., Brancati, F., Kisseleva, M.V., Al-Gazali, L., Sztriha, L., Bayoumi, R.A., Zaki, M.S., Abdel-Aleem, A., Rosti, R.O., et al. (2009). Mutations in INPP5E, encoding inositol polyphosphate-5-phosphatase E, link phosphatidyl inositol signaling to the ciliopathies. Nat Genet 41, 1032-1036.
172. Thomas, S., Wright, K.J., Le Corre, S., Micalizzi, A., Romani, M., Abhyankar, A., Saada, J., Perrault, I., Amiel, J., Litzler, J., et al. (2014). A homozygous PDE6D mutation in Joubert syndrome impairs targeting of farnesylated INPP5E protein to the primary cilium. Hum Mutat 35, 137-146.
173. Bachmann-Gagescu, R., Phelps, I.G., Dempsey, J.C., Sharma, V.A., Ishak, G.E., Boyle, E.A., Wilson, M., Marques Lourenco, C., Arslan, M., University of Washington Center for Mendelian, G., et al. (2015). KIAA0586 is Mutated in Joubert Syndrome. Hum Mutat 36, 831-835.
174. Yin, Y., Bangs, F., Paton, I.R., Prescott, A., James, J., Davey, M.G., Whitley, P., Genikhovich, G., Technau, U., Burt, D.W., et al. (2009). The Talpid3 gene (KIAA0586) encodes a centrosomal protein that is essential for primary cilia formation. Development 136, 655-664.

175. Romani, M., Micalizzi, A., Kraoua, I., Dotti, M.T., Cavallin, M., Sztriha, L., Ruta, R., Mancini, F., Mazza, T., Castellana, S., et al. (2014). Mutations in B9D1 and MKS1 cause mild Joubert syndrome: expanding the genetic overlap with the lethal ciliopathy Meckel syndrome. Orphanet J Rare Dis 9, 72.
176. Parisi, M.A., Bennett, C.L., Eckert, M.L., Dobyns, W.B., Gleeson, J.G., Shaw, D.W., McDonald, R., Eddy, A., Chance, P.F., and Glass, I.A. (2004). The NPHP1 gene deletion associated with juvenile nephronophthisis is present in a subset of individuals with Joubert syndrome. Am J Hum Genet 75, 82-91.
177. Delous, M., Baala, L., Salomon, R., Laclef, C., Vierkotten, J., Tory, K., Golzio, C., Lacoste, T., Besse, L., Ozilou, C., et al. (2007). The ciliary gene RPGRIP1L is mutated in cerebello-oculo-renal syndrome (Joubert syndrome type B) and Meckel syndrome. Nat Genet 39, 875-881.
178. Garcia-Gonzalo, F.R., Corbit, K.C., Sirerol-Piquer, M.S., Ramaswami, G., Otto, E.A., Noriega, T.R., Seol, A.D., Robinson, J.F., Bennett, C.L., Josifova, D.J., et al. (2011). A transition zone complex regulates mammalian ciliogenesis and ciliary membrane composition. Nat Genet 43, 776-784.
179. Baala, L., Romano, S., Khaddour, R., Saunier, S., Smith, U.M., Audollent, S., Ozilou, C., Faivre, L., Laurent, N., Foliguet, B., et al. (2007). The Meckel-Gruber syndrome gene, MKS3, is mutated in Joubert syndrome. Am J Hum Genet 80, 186-194.
180. Edvardson, S., Shaag, A., Zenvirt, S., Erlich, Y., Hannon, G.J., Shanske, A.L., Gomori, J.M., Ekstein, J., and Elpeleg, O. (2010). Joubert syndrome 2 (JBTS2) in Ashkenazi Jews is associated with a TMEM216 mutation. Am J Hum Genet 86, 93-97.
181. Logan, C.V., Abdel-Hamed, Z., and Johnson, C.A. (2011). Molecular Genetics and Pathogenic Mechanisms for the Severe Ciliopathies: Insights into Neurodevelopment and Pathogenesis of Neural Tube Defects. Molecular Neurobiology 43, 12-26.
182. Dowdle, W.E., Robinson, J.F., Kneist, A., Sirerol-Piquer, M.S., Frints, S.G., Corbit, K.C., Zaghloul, N.A., van Lijnschoten, G., Mulders, L., Verver, D.E., et al. (2011). Disruption of a ciliary B9 protein complex causes Meckel syndrome. Am J Hum Genet 89, 94-110.
183. Hopp, K., Heyer, C.M., Hommerding, C.J., Henke, S.A., Sundsbak, J.L., Patel, S., Patel, P., Consugar, M.B., Czarnecki, P.G., Gliem, T.J., et al. (2011). B9D1 is revealed as a novel Meckel syndrome (MKS) gene by targeted exon-enriched next-generation sequencing and deletion analysis. Hum Mol Genet 20, 2524-2534.
184. Tallila, J., Jakkula, E., Peltonen, L., Salonen, R., and Kestila, M. (2008). Identification of CC2D2A as a Meckel syndrome gene adds an important piece to the ciliopathy puzzle. Am J Hum Genet 82, 1361-1367.
185. Baala, L., Audollent, S., Martinovic, J., Ozilou, C., Babron, M.C., Sivanandamoorthy, S., Saunier, S., Salomon, R., Gonzales, M., Rattenberry, E., et al. (2007). Pleiotropic effects of CEP290 (NPHP6) mutations extend to Meckel syndrome. Am J Hum Genet 81, 170-179.
186. Frank, V., den Hollander, A.I., Bruchle, N.O., Zonneveld, M.N., Nurnberg, G., Becker, C., Du, B.G., Kendziorra, H., Roosing, S., Senderek, J., et al. (2008). Mutations of the CEP290 gene encoding a centrosomal protein cause Meckel-Gruber syndrome. Hum Mutat 29, 45-52.
187. Filges, I., Nosova, E., Bruder, E., Tercanli, S., Townsend, K., Gibson, W.T., Rothlisberger, B., Heinimann, K., Hall, J.G., Gregory-Evans, C.Y., et al. (2014). Exome sequencing identifies mutations in KIF14 as a novel cause of an autosomal recessive lethal fetal ciliopathy phenotype. Clin Genet 86, 220-228.
188. Kyttala, M., Tallila, J., Salonen, R., Kopra, O., Kohlschmidt, N., Paavola-Sakki, P., Peltonen, L., and Kestila, M. (2006). MKS1, encoding a component of the flagellar apparatus basal body proteome, is mutated in Meckel syndrome. Nat Genet 38, 155-157.
189. Bergmann, C., Fliegauf, M., Bruchle, N.O., Frank, V., Olbrich, H., Kirschner, J., Schermer, B., Schmedding, I., Kispert, A., Kranzlin, B., et al. (2008). Loss of nephrocystin-3 function can cause embryonic lethality, Meckel-Gruber-like syndrome, situs inversus, and renal-hepatic-pancreatic dysplasia. Am J Hum Genet 82, 959-970.
190. Shaheen, R., Faqeih, E., Seidahmed, M.Z., Sunker, A., Alali, F.E., AlQahtani, K., and Alkuraya, F.S. (2011). A TCTN2 mutation defines a novel Meckel Gruber syndrome locus. Hum Mutat 32, 573-578.
191. Smith, U.M., Consugar, M., Tee, L.J., McKee, B.M., Maina, E.N., Whelan, S., Morgan, N.V., Goranson, E., Gissen, P., Lilliquist, S., et al. (2006). The transmembrane protein meckelin (MKS3) is mutated in Meckel-Gruber syndrome and the wpk rat. Nat Genet 38, 191-196.
192. Valente, E.M., Logan, C.V., Mougou-Zerelli, S., Lee, J.H., Silhavy, J.L., Brancati, F., Iannicelli, M., Travaglini, L., Romani, S., Illi, B., et al. (2010). Mutations in TMEM216 perturb ciliogenesis and cause Joubert, Meckel and related syndromes. Nat Genet 42, 619-625.
193. Shaheen, R., Ansari, S., Mardawi, E.A., Alshammari, M.J., and Alkuraya, F.S. (2013). Mutations in TMEM231 cause Meckel-Gruber syndrome. J Med Genet 50, 160-162.

194. Klink, B.U., Zent, E., Juneja, P., Kuhlee, A., Raunser, S., and Wittinghofer, A. (2017). A recombinant BBSome core complex and how it interacts with ciliary cargo. Elife 6.
195. Beales, P.L., Elcioglu, N., Woolf, A.S., Parker, D., and Flinter, F.A. (1999). New criteria for improved diagnosis of Bardet-Biedl syndrome: results of a population survey. J Med Genet 36, 437-446.
196. Mockel, A., Perdomo, Y., Stutzmann, F., Letsch, J., Marion, V., and Dollfus, H. (2011). Retinal dystrophy in Bardet-Biedl syndrome and related syndromic ciliopathies. Prog Retin Eye Res 30, 258-274.
197. Koenekoop, R. (2003). The major gene for Bardet-Biedl syndrome is BBS1. Ophthalmic Genet 24, 127.
198. Mykytyn, K., Nishimura, D.Y., Searby, C.C., Shastri, M., Yen, H.J., Beck, J.S., Braun, T., Streb, L.M., Cornier, A.S., Cox, G.F., et al. (2002). Identification of the gene (BBS1) most commonly involved in Bardet-Biedl syndrome, a complex human obesity syndrome. Nat Genet 31, 435-438.
199. Fan, Y., Esmail, M.A., Ansley, S.J., Blacque, O.E., Boroevich, K., Ross, A.J., Moore, S.J., Badano, J.L., May-Simera, H., Compton, D.S., et al. (2004). Mutations in a member of the Ras superfamily of small GTP-binding proteins causes Bardet-Biedl syndrome. Nat Genet 36, 989-993.
200. Scheidecker, S., Etard, C., Pierce, N.W., Geoffroy, V., Schaefer, E., Muller, J., Chennen, K., Flori, E., Pelletier, V., Poch, O., et al. (2014). Exome sequencing of Bardet-Biedl syndrome patient identifies a null mutation in the BBSome subunit BBIP1 (BBS18). J Med Genet 51, 132-136.
201. Nishimura, D.Y., Searby, C.C., Carmi, R., Elbedour, K., Van Maldergem, L., Fulton, A.B., Lam, B.L., Powell, B.R., Swiderski, R.E., Bugge, K.E., et al. (2001). Positional cloning of a novel gene on chromosome 16q causing Bardet-Biedl syndrome (BBS2). Hum Mol Genet 10, 865-874.
202. Mykytyn, K., Braun, T., Carmi, R., Haider, N.B., Searby, C.C., Shastri, M., Beck, G., Wright, A.F., Iannaccone, A., Elbedour, K., et al. (2001). Identification of the gene that, when mutated, causes the human obesity syndrome BBS4. Nat Genet 28, 188-191.
203. Li, J.B., Gerdes, J.M., Haycraft, C.J., Fan, Y., Teslovich, T.M., May-Simera, H., Li, H., Blacque, O.E., Li, L., Leitch, C.C., et al. (2004). Comparative genomics identifies a flagellar and basal body proteome that includes the BBS5 human disease gene. Cell 117, 541-552.
204. Badano, J.L., Ansley, S.J., Leitch, C.C., Lewis, R.A., Lupski, J.R., and Katsanis, N. (2003). Identification of a novel Bardet-Biedl syndrome protein, BBS7, that shares structural features with BBS1 and BBS2. Am J Hum Genet 72, 650-658.
205. Nishimura, D.Y., Swiderski, R.E., Searby, C.C., Berg, E.M., Ferguson, A.L., Hennekam, R., Merin, S., Weleber, R.G., Biesecker, L.G., Stone, E.M., et al. (2005). Comparative genomics and gene expression analysis identifies BBS9, a new Bardet-Biedl syndrome gene. Am J Hum Genet 77, 1021-1033.
206. Stoetzel, C., Laurier, V., Davis, E.E., Muller, J., Rix, S., Badano, J.L., Leitch, C.C., Salem, N., Chouery, E., Corbani, S., et al. (2006). BBS10 encodes a vertebrate-specific chaperonin-like protein and is a major BBS locus. Nat Genet 38, 521-524.
207. Stoetzel, C., Muller, J., Laurier, V., Davis, E.E., Zaghloul, N.A., Vicaire, S., Jacquelin, C., Plewniak, F., Leitch, C.C., Sarda, P., et al. (2007). Identification of a novel BBS gene (BBS12) highlights the major role of a vertebrate-specific branch of chaperonin-related proteins in Bardet-Biedl syndrome. Am J Hum Genet 80, 1-11.
208. Leitch, C.C., Zaghloul, N.A., Davis, E.E., Stoetzel, C., Diaz-Font, A., Rix, S., Alfadhel, M., Lewis, R.A., Eyaid, W., Banin, E., et al. (2008). Hypomorphic mutations in syndromic encephalocele genes are associated with Bardet-Biedl syndrome. Nat Genet 40, 443-448.
209. Aldahmesh, M.A., Li, Y., Alhashem, A., Anazi, S., Alkuraya, H., Hashem, M., Awaji, A.A., Sogaty, S., Alkharashi, A., Alzahrani, S., et al. (2014). IFT27, encoding a small GTPase component of IFT particles, is mutated in a consanguineous family with Bardet-Biedl syndrome. Hum Mol Genet 23, 3307-3315.
210. Bujakowska, K.M., Zhang, Q., Siemiatkowska, A.M., Liu, Q., Place, E., Falk, M.J., Consugar, M., Lancelot, M.E., Antonio, A., Lonjou, C., et al. (2015). Mutations in IFT172 cause isolated retinal degeneration and Bardet-Biedl syndrome. Hum Mol Genet 24, 230-242.
211. Marion, V., Stutzmann, F., Gerard, M., De Melo, C., Schaefer, E., Claussmann, A., Helle, S., Delague, V., Souied, E., Barrey, C., et al. (2012). Exome sequencing identifies mutations in LZTFL1, a BBSome and smoothened trafficking regulator, in a family with Bardet--Biedl syndrome with situs inversus and insertional polydactyly. J Med Genet 49, 317-321.
212. Katsanis, N., Beales, P.L., Woods, M.O., Lewis, R.A., Green, J.S., Parfrey, P.S., Ansley, S.J., Davidson, W.S., and Lupski, J.R. (2000). Mutations in MKKS cause obesity, retinal dystrophy and renal malformations associated with Bardet-Biedl syndrome. Nat Genet 26, 67-70.
213. Slavotinek, A.M., Stone, E.M., Mykytyn, K., Heckenlively, J.R., Green, J.S., Heon, E., Musarella, M.A., Parfrey, P.S., Sheffield, V.C., and Biesecker, L.G. (2000). Mutations in MKKS cause Bardet-Biedl syndrome. Nat Genet 26, 15-16.

214. Otto, E.A., Hurd, T.W., Airik, R., Chaki, M., Zhou, W., Stoetzel, C., Patil, S.B., Levy, S., Ghosh, A.K., Murga-Zamalloa, C.A., et al. (2010). Candidate exome capture identifies mutation of SDCCAG8 as the cause of a retinal-renal ciliopathy. Nat Genet 42, 840-850.
215. Chiang, A.P., Beck, J.S., Yen, H.J., Tayeh, M.K., Scheetz, T.E., Swiderski, R.E., Nishimura, D.Y., Braun, T.A., Kim, K.Y., Huang, J., et al. (2006). Homozygosity mapping with SNP arrays identifies TRIM32, an E3 ubiquitin ligase, as a Bardet-Biedl syndrome gene (BBS11). Proc Natl Acad Sci U S A 103, 6287-6292.
216. Ansley, S.J., Badano, J.L., Blacque, O.E., Hill, J., Hoskins, B.E., Leitch, C.C., Kim, J.C., Ross, A.J., Eichers, E.R., Teslovich, T.M., et al. (2003). Basal body dysfunction is a likely cause of pleiotropic Bardet-Biedl syndrome. Nature 425, 628-633.
217. Kim, S.K., Shindo, A., Park, T.J., Oh, E.C., Ghosh, S., Gray, R.S., Lewis, R.A., Johnson, C.A., Attie-Bittach, T., Katsanis, N., et al. (2010). Planar cell polarity acts through septins to control collective cell movement and ciliogenesis. Science 329, 1337-1340.
218. Collin, G.B., Marshall, J.D., Ikeda, A., So, W.V., Russell-Eggitt, I., Maffei, P., Beck, S., Boerkoel, C.F., Sicolo, N., Martin, M., et al. (2002). Mutations in ALMS1 cause obesity, type 2 diabetes and neurosensory degeneration in Alstrom syndrome. Nat Genet 31, 74-78.
219. Hampshire, D.J., Ayub, M., Springell, K., Roberts, E., Jafri, H., Rashid, Y., Bond, J., Riley, J.H., and Woods, C.G. (2006). MORM syndrome (mental retardation, truncal obesity, retinal dystrophy and micropenis), a new autosomal recessive disorder, links to 9q34. Eur J Hum Genet 14, 543-548.
220. Jacoby, M., Cox, J.J., Gayral, S., Hampshire, D.J., Ayub, M., Blockmans, M., Pernot, E., Kisseleva, M.V., Compere, P., Schiffmann, S.N., et al. (2009). INPP5E mutations cause primary cilium signaling defects, ciliary instability and ciliopathies in human and mouse. Nat Genet 41, 1027-1031.
221. Rolland, T., Tasan, M., Charloteaux, B., Pevzner, S.J., Zhong, Q., Sahni, N., Yi, S., Lemmens, I., Fontanillo, C., Mosca, R., et al. (2014). A proteome-scale map of the human interactome network. Cell 159, 1212-1226.
222. Huttlin, E.L., Ting, L., Bruckner, R.J., Gebreab, F., Gygi, M.P., Szpyt, J., Tam, S., Zarraga, G., Colby, G., Baltier, K., et al. (2015). The BioPlex Network: A Systematic Exploration of the Human Interactome. Cell 162, 425-440.
223. Wan, C., Borgeson, B., Phanse, S., Tu, F., Drew, K., Clark, G., Xiong, X., Kagan, O., Kwan, J., Bezginov, A., et al. (2015). Panorama of ancient metazoan macromolecular complexes. Nature 525, 339-344.
224. Hein, M.Y., Hubner, N.C., Poser, I., Cox, J., Nagaraj, N., Toyoda, Y., Gak, I.A., Weisswange, I., Mansfeld, J., Buchholz, F., et al. (2015). A human interactome in three quantitative dimensions organized by stoichiometries and abundances. Cell 163, 712-723.
225. Fields, S., and Song, O. (1989). A novel genetic system to detect protein-protein interactions. Nature 340, 245-246.
226. Chien, C.T., Bartel, P.L., Sternglanz, R., and Fields, S. (1991). The two-hybrid system: a method to identify and clone genes for proteins that interact with a protein of interest. Proc Natl Acad Sci U S A 88, 9578-9582.
227. Puig, O., Caspary, F., Rigaut, G., Rutz, B., Bouveret, E., Bragado-Nilsson, E., Wilm, M., and Seraphin, B. (2001). The tandem affinity purification (TAP) method: a general procedure of protein complex purification. Methods 24, 218-229.
228. Gloeckner, C.J., Boldt, K., Schumacher, A., Roepman, R., and Ueffing, M. (2007). A novel tandem affinity purification strategy for the efficient isolation and characterisation of native protein complexes. Proteomics 7, 4228-4234.
229. Giorgini, F., and Muchowski, P.J. (2005). Connecting the dots in Huntington's disease with protein interaction networks. Genome Biol 6, 210.
230. Fessenden, M. (2017). Protein maps chart the causes of disease. Nature 549, 293-295.
231. Keeler, C.E. (1924). The Inheritance of a Retinal Abnormality in White Mice. Proc Natl Acad Sci U S A 10, 329-333.
232. Bourne, M.C., Campbell, D.A., and Tansley, K. (1938). Hereditary Degeneration of the Rat Retina. Br J Ophthalmol 22, 613-623.
233. Sidman, R.L., and Green, M.C. (1965). Retinal Degeneration in the Mouse: Location of the Rd Locus in Linkage Group Xvii. J Hered 56, 23-29.
234. Bowes, C., Li, T., Danciger, M., Baxter, L.C., Applebury, M.L., and Farber, D.B. (1990). Retinal degeneration in the rd mouse is caused by a defect in the beta subunit of rod cGMP-phosphodiesterase. Nature 347, 677-680.
235. Sanyal, S., De Ruiter, A., and Hawkins, R.K. (1980). Development and degeneration of retina in rds mutant mice: light microscopy. J Comp Neurol 194, 193-207.

236. Travis, G.H., Brennan, M.B., Danielson, P.E., Kozak, C.A., and Sutcliffe, J.G. (1989). Identification of a photoreceptor-specific mRNA encoded by the gene responsible for retinal degeneration slow (rds). Nature 338, 70-73.
237. Cremers, F.P., van de Pol, D.J., van Kerkhoff, L.P., Wieringa, B., and Ropers, H.H. (1990). Cloning of a gene that is rearranged in patients with choroideraemia. Nature 347, 674-677.
238. van den Hurk, J.A., Hendriks, W., van de Pol, D.J., Oerlemans, F., Jaissle, G., Ruther, K., Kohler, K., Hartmann, J., Zrenner, E., van Bokhoven, H., et al. (1997). Mouse choroideremia gene mutation causes photoreceptor cell degeneration and is not transmitted through the female germline. Hum Mol Genet 6, 851-858.
239. Olsson, J.E., Gordon, J.W., Pawlyk, B.S., Roof, D., Hayes, A., Molday, R.S., Mukai, S., Cowley, G.S., Berson, E.L., and Dryja, T.P. (1992). Transgenic mice with a rhodopsin mutation (Pro23His): a mouse model of autosomal dominant retinitis pigmentosa. Neuron 9, 815-830.
240. Slijkerman, R.W., Song, F., Astuti, G.D., Huynen, M.A., van Wijk, E., Stieger, K., and Collin, R.W. (2015). The pros and cons of vertebrate animal models for functional and therapeutic research on inherited retinal dystrophies. Prog Retin Eye Res 48, 137-159.
241. Church, D.M., Goodstadt, L., Hillier, L.W., Zody, M.C., Goldstein, S., She, X., Bult, C.J., Agarwala, R., Cherry, J.L., DiCuccio, M., et al. (2009). Lineage-specific biology revealed by a finished genome assembly of the mouse. PLoS Biol 7, e1000112.
242. Smith, C.L., Blake, J.A., Kadin, J.A., Richardson, J.E., Bult, C.J., and Mouse Genome Database, G. (2018). Mouse Genome Database (MGD)-2018: knowledgebase for the laboratory mouse. Nucleic Acids Res 46, D836-D842.
243. Gurumurthy, C., M. Quadros, R., Sato, M., Mashimo, T., C. Kent Lloyd, K., and Ohtsuka, M. (2016). CRISPR/Cas9 and the Paradigm Shift in Mouse Genome Manipulation Technologies.
244. Volland, S., Esteve-Rudd, J., Hoo, J., Yee, C., and Williams, D.S. (2015). A comparison of some organizational characteristics of the mouse central retina and the human macula. PLoS One 10, e0125631.
245. Volland, S., Hughes, L.C., Kong, C., Burgess, B.L., Linberg, K.A., Luna, G., Zhou, Z.H., Fisher, S.K., and Williams, D.S. (2015). Three-dimensional organization of nascent rod outer segment disk membranes. Proc Natl Acad Sci U S A 112, 14870-14875.
246. Fadool, J.M., and Dowling, J.E. (2008). Zebrafish: a model system for the study of eye genetics. Prog Retin Eye Res 27, 89-110.
247. Jia, S., Muto, A., Orisme, W., Henson, H.E., Parupalli, C., Ju, B., Baier, H., and Taylor, M.R. (2014). Zebrafish Cacna1fa is required for cone photoreceptor function and synaptic ribbon formation. Hum Mol Genet 23, 2981-2994.
248. Phillips, J.B., Blanco-Sanchez, B., Lentz, J.J., Tallafuss, A., Khanobdee, K., Sampath, S., Jacobs, Z.G., Han, P.F., Mishra, M., Titus, T.A., et al. (2011). Harmonin (Ush1c) is required in zebrafish Muller glial cells for photoreceptor synaptic development and function. Dis Model Mech 4, 786-800.
249. Brockerhoff, S.E., Rieke, F., Matthews, H.R., Taylor, M.R., Kennedy, B., Ankoudinova, I., Niemi, G.A., Tucker, C.L., Xiao, M., Cilluffo, M.C., et al. (2003). Light stimulates a transducin-independent increase of cytoplasmic Ca2+ and suppression of current in cones from the zebrafish mutant nof. J Neurosci 23, 470-480.
250. Muto, A., Orger, M.B., Wehman, A.M., Smear, M.C., Kay, J.N., Page-McCaw, P.S., Gahtan, E., Xiao, T., Nevin, L.M., Gosse, N.J., et al. (2005). Forward genetic analysis of visual behavior in zebrafish. PLoS Genet 1, e66.
251. Collery, R.F., Cederlund, M.L., and Kennedy, B.N. (2013). Transgenic zebrafish expressing mutant human RETGC-1 exhibit aberrant cone and rod morphology. Exp Eye Res 108, 120-128.
252. Ernest, S., Rauch, G.J., Haffter, P., Geisler, R., Petit, C., and Nicolson, T. (2000). Mariner is defective in myosin VIIA: a zebrafish model for human hereditary deafness. Hum Mol Genet 9, 2189-2196.
253. Wasfy, M.M., Matsui, J.I., Miller, J., Dowling, J.E., and Perkins, B.D. (2014). myosin 7aa(-/-) mutant zebrafish show mild photoreceptor degeneration and reduced electroretinographic responses. Exp Eye Res 122, 65-76.
254. Malicki, J., and Driever, W. (1999). oko meduzy mutations affect neuronal patterning in the zebrafish retina and reveal cell-cell interactions of the retinal neuroepithelial sheet. Development 126, 1235-1246.
255. Omori, Y., and Malicki, J. (2006). oko meduzy and related crumbs genes are determinants of apical cell features in the vertebrate embryo. Curr Biol 16, 945-957.

256. Stearns, G., Evangelista, M., Fadool, J.M., and Brockerhoff, S.E. (2007). A mutation in the cone-specific pde6 gene causes rapid cone photoreceptor degeneration in zebrafish. J Neurosci 27, 13866-13874.
257. Yu, M., Liu, Y., Li, J., Natale, B.N., Cao, S., Wang, D., Amack, J.D., and Hu, H. (2016). Eyes shut homolog is required for maintaining the ciliary pocket and survival of photoreceptors in zebrafish. Biol Open 5, 1662-1673.
258. Lu, Z., Hu, X., Liu, F., Soares, D.C., Liu, X., Yu, S., Gao, M., Han, S., Qin, Y., Li, C., et al. (2017). Ablation of EYS in zebrafish causes mislocalisation of outer segment proteins, F-actin disruption and cone-rod dystrophy. Sci Rep 7, 46098.
259. Krock, B.L., and Perkins, B.D. (2008). The intraflagellar transport protein IFT57 is required for cilia maintenance and regulates IFT-particle-kinesin-II dissociation in vertebrate photoreceptors. J Cell Sci 121, 1907-1915.
260. Sukumaran, S., and Perkins, B.D. (2009). Early defects in photoreceptor outer segment morphogenesis in zebrafish ift57, ift88 and ift172 Intraflagellar Transport mutants. Vision Res 49, 479-489.
261. Wan, J., and Goldman, D. (2016). Retina regeneration in zebrafish. Curr Opin Genet Dev 40, 41-47.
262. Nelson, C.M., Ackerman, K.M., O'Hayer, P., Bailey, T.J., Gorsuch, R.A., and Hyde, D.R. (2013). Tumor necrosis factor-alpha is produced by dying retinal neurons and is required for Muller glia proliferation during zebrafish retinal regeneration. J Neurosci 33, 6524-6539.
263. Meyer, A., and Schartl, M. (1999). Gene and genome duplications in vertebrates: the one-to-four (-to-eight in fish) rule and the evolution of novel gene functions. Curr Opin Cell Biol 11, 699-704.
264. Howe, K., Clark, M.D., Torroja, C.F., Torrance, J., Berthelot, C., Muffato, M., Collins, J.E., Humphray, S., McLaren, K., Matthews, L., et al. (2013). The zebrafish reference genome sequence and its relationship to the human genome. Nature 496, 498-503.
265. Ross, J.W., Fernandez de Castro, J.P., Zhao, J., Samuel, M., Walters, E., Rios, C., Bray-Ward, P., Jones, B.W., Marc, R.E., Wang, W., et al. (2012). Generation of an inbred miniature pig model of retinitis pigmentosa. Invest Ophthalmol Vis Sci 53, 501-507.
266. Petters, R.M., Alexander, C.A., Wells, K.D., Collins, E.B., Sommer, J.R., Blanton, M.R., Rojas, G., Hao, Y., Flowers, W.L., Banin, E., et al. (1997). Genetically engineered large animal model for studying cone photoreceptor survival and degeneration in retinitis pigmentosa. Nat Biotechnol 15, 965-970.
267. Li, Z.Y., Wong, F., Chang, J.H., Possin, D.E., Hao, Y., Petters, R.M., and Milam, A.H. (1998). Rhodopsin transgenic pigs as a model for human retinitis pigmentosa. Invest Ophthalmol Vis Sci 39, 808-819.
268. Sommer, J.R., Estrada, J.L., Collins, E.B., Bedell, M., Alexander, C.A., Yang, Z., Hughes, G., Mir, B., Gilger, B.C., Grob, S., et al. (2011). Production of ELOVL4 transgenic pigs: a large animal model for Stargardt-like macular degeneration. Br J Ophthalmol 95, 1749-1754.
269. Kostic, C., Lillico, S.G., Crippa, S.V., Grandchamp, N., Pilet, H., Philippe, S., Lu, Z., King, T.J., Mallet, J., Sarkis, C., et al. (2013). Rapid cohort generation and analysis of disease spectrum of large animal model of cone dystrophy. PLoS One 8, e71363.
270. Annear, M.J., Mowat, F.M., Bartoe, J.T., Querubin, J., Azam, S.A., Basche, M., Curran, P.G., Smith, A.J., Bainbridge, J.W., Ali, R.R., et al. (2013). Successful gene therapy in older Rpe65-deficient dogs following subretinal injection of an adeno-associated vector expressing RPE65. Hum Gene Ther 24, 883-893.
271. Mowat, F.M., Breuwer, A.R., Bartoe, J.T., Annear, M.J., Zhang, Z., Smith, A.J., Bainbridge, J.W., Petersen-Jones, S.M., and Ali, R.R. (2013). RPE65 gene therapy slows cone loss in Rpe65-deficient dogs. Gene Ther 20, 545-555.
272. Petersen-Jones, S.M., Annear, M.J., Bartoe, J.T., Mowat, F.M., Barker, S.E., Smith, A.J., Bainbridge, J.W., and Ali, R.R. (2012). Gene augmentation trials using the Rpe65-deficient dog: contributions towards development and refinement of human clinical trials. Adv Exp Med Biol 723, 177-182.
273. Takahashi, K., and Yamanaka, S. (2006). Induction of pluripotent stem cells from mouse embryonic and adult fibroblast cultures by defined factors. Cell 126, 663-676.
274. Yu, J., Vodyanik, M.A., Smuga-Otto, K., Antosiewicz-Bourget, J., Frane, J.L., Tian, S., Nie, J., Jonsdottir, G.A., Ruotti, V., Stewart, R., et al. (2007). Induced pluripotent stem cell lines derived from human somatic cells. Science 318, 1917-1920.
275. Hu, Q., Friedrich, A.M., Johnson, L.V., and Clegg, D.O. (2010). Memory in induced pluripotent stem cells: reprogrammed human retinal-pigmented epithelial cells show tendency for spontaneous redifferentiation. Stem Cells 28, 1981-1991.
276. Phillips, M.J., Perez, E.T., Martin, J.M., Reshel, S.T., Wallace, K.A., Capowski, E.E., Singh, R., Wright, L.S., Clark, E.M., Barney, P.M., et al. (2014). Modeling human retinal development with patient-specific

induced pluripotent stem cells reveals multiple roles for visual system homeobox 2. Stem Cells 32, 1480-1492.
277. Tucker, B.A., Mullins, R.F., Streb, L.M., Anfinson, K., Eyestone, M.E., Kaalberg, E., Riker, M.J., Drack, A.V., Braun, T.A., and Stone, E.M. (2013). Patient-specific iPSC-derived photoreceptor precursor cells as a means to investigate retinitis pigmentosa. Elife 2, e00824.
278. Loh, Y.H., Hartung, O., Li, H., Guo, C., Sahalie, J.M., Manos, P.D., Urbach, A., Heffner, G.C., Grskovic, M., Vigneault, F., et al. (2010). Reprogramming of T cells from human peripheral blood. Cell Stem Cell 7, 15-19.
279. Seki, T., Yuasa, S., Oda, M., Egashira, T., Yae, K., Kusumoto, D., Nakata, H., Tohyama, S., Hashimoto, H., Kodaira, M., et al. (2010). Generation of induced pluripotent stem cells from human terminally differentiated circulating T cells. Cell Stem Cell 7, 11-14.
280. Staerk, J., Dawlaty, M.M., Gao, Q., Maetzel, D., Hanna, J., Sommer, C.A., Mostoslavsky, G., and Jaenisch, R. (2010). Reprogramming of human peripheral blood cells to induced pluripotent stem cells. Cell Stem Cell 7, 20-24.
281. Zhou, T., Benda, C., Dunzinger, S., Huang, Y., Ho, J.C., Yang, J., Wang, Y., Zhang, Y., Zhuang, Q., Li, Y., et al. (2012). Generation of human induced pluripotent stem cells from urine samples. Nat Protoc 7, 2080-2089.
282. Esteban, M.A., Wang, T., Qin, B., Yang, J., Qin, D., Cai, J., Li, W., Weng, Z., Chen, J., Ni, S., et al. (2010). Vitamin C enhances the generation of mouse and human induced pluripotent stem cells. Cell Stem Cell 6, 71-79.
283. Sun, N., Panetta, N.J., Gupta, D.M., Wilson, K.D., Lee, A., Jia, F., Hu, S., Cherry, A.M., Robbins, R.C., Longaker, M.T., et al. (2009). Feeder-free derivation of induced pluripotent stem cells from adult human adipose stem cells. Proc Natl Acad Sci U S A 106, 15720-15725.
284. Wada, N., Wang, B., Lin, N.H., Laslett, A.L., Gronthos, S., and Bartold, P.M. (2011). Induced pluripotent stem cell lines derived from human gingival fibroblasts and periodontal ligament fibroblasts. J Periodontal Res 46, 438-447.
285. Jin, Z.B., Okamoto, S., Osakada, F., Homma, K., Assawachananont, J., Hirami, Y., Iwata, T., and Takahashi, M. (2011). Modeling retinal degeneration using patient-specific induced pluripotent stem cells. PLoS One 6, e17084.
286. Jin, Z.B., Okamoto, S., Xiang, P., and Takahashi, M. (2012). Integration-free induced pluripotent stem cells derived from retinitis pigmentosa patient for disease modeling. Stem Cells Transl Med 1, 503-509.
287. Yoshida, T., Ozawa, Y., Suzuki, K., Yuki, K., Ohyama, M., Akamatsu, W., Matsuzaki, Y., Shimmura, S., Mitani, K., Tsubota, K., et al. (2014). The use of induced pluripotent stem cells to reveal pathogenic gene mutations and explore treatments for retinitis pigmentosa. Mol Brain 7, 45.
288. Lukovic, D., Artero Castro, A., Delgado, A.B., Bernal Mde, L., Luna Pelaez, N., Diez Lloret, A., Perez Espejo, R., Kamenarova, K., Fernandez Sanchez, L., Cuenca, N., et al. (2015). Human iPSC derived disease model of MERTK-associated retinitis pigmentosa. Sci Rep 5, 12910.
289. Li, Y., Wu, W.H., Hsu, C.W., Nguyen, H.V., Tsai, Y.T., Chan, L., Nagasaki, T., Maumenee, I.H., Yannuzzi, L.A., Hoang, Q.V., et al. (2014). Gene therapy in patient-specific stem cell lines and a preclinical model of retinitis pigmentosa with membrane frizzled-related protein defects. Mol Ther 22, 1688-1697.
290. Polinati, P.P., Ilmarinen, T., Trokovic, R., Hyotylainen, T., Otonkoski, T., Suomalainen, A., Skottman, H., and Tyni, T. (2015). Patient-Specific Induced Pluripotent Stem Cell-Derived RPE Cells: Understanding the Pathogenesis of Retinopathy in Long-Chain 3-Hydroxyacyl-CoA Dehydrogenase Deficiency. Invest Ophthalmol Vis Sci 56, 3371-3382.
291. Singh, R., Shen, W., Kuai, D., Martin, J.M., Guo, X., Smith, M.A., Perez, E.T., Phillips, M.J., Simonett, J.M., Wallace, K.A., et al. (2013). iPS cell modeling of Best disease: insights into the pathophysiology of an inherited macular degeneration. Hum Mol Genet 22, 593-607.
292. Veltel, S., Gasper, R., Eisenacher, E., and Wittinghofer, A. (2008). The retinitis pigmentosa 2 gene product is a GTPase-activating protein for Arf-like 3. Nat Struct Mol Biol 15, 373-380.
293. Zhong, X., Gutierrez, C., Xue, T., Hampton, C., Vergara, M.N., Cao, L.H., Peters, A., Park, T.S., Zambidis, E.T., Meyer, J.S., et al. (2014). Generation of three-dimensional retinal tissue with functional photoreceptors from human iPSCs. Nat Commun 5, 4047.
294. Gonzalez-Cordero, A., Kruczek, K., Naeem, A., Fernando, M., Kloc, M., Ribeiro, J., Goh, D., Duran, Y., Blackford, S.J.I., Abelleira-Hervas, L., et al. (2017). Recapitulation of Human Retinal Development from Human Pluripotent Stem Cells Generates Transplantable Populations of Cone Photoreceptors. Stem Cell Reports 9, 820-837.

295. Nakano, T., Ando, S., Takata, N., Kawada, M., Muguruma, K., Sekiguchi, K., Saito, K., Yonemura, S., Eiraku, M., and Sasai, Y. (2012). Self-formation of optic cups and storable stratified neural retina from human ESCs. Cell Stem Cell 10, 771-785.
296. Parfitt, D.A., Lane, A., Ramsden, C.M., Carr, A.J., Munro, P.M., Jovanovic, K., Schwarz, N., Kanuga, N., Muthiah, M.N., Hull, S., et al. (2016). Identification and Correction of Mechanisms Underlying Inherited Blindness in Human iPSC-Derived Optic Cups. Cell Stem Cell 18, 769-781.
297. Megaw, R., Abu-Arafeh, H., Jungnickel, M., Mellough, C., Gurniak, C., Witke, W., Zhang, W., Khanna, H., Mill, P., Dhillon, B., et al. (2017). Gelsolin dysfunction causes photoreceptor loss in induced pluripotent cell and animal retinitis pigmentosa models. Nat Commun 8, 271.
298. Arno, G., Agrawal, S.A., Eblimit, A., Bellingham, J., Xu, M., Wang, F., Chakarova, C., Parfitt, D.A., Lane, A., Burgoyne, T., et al. (2016). Mutations in REEP6 Cause Autosomal-Recessive Retinitis Pigmentosa. Am J Hum Genet 99, 1305-1315.
299. Puppo, A., Cesi, G., Marrocco, E., Piccolo, P., Jacca, S., Shayakhmetov, D.M., Parks, R.J., Davidson, B.L., Colloca, S., Brunetti-Pierri, N., et al. (2014). Retinal transduction profiles by high-capacity viral vectors. Gene Ther 21, 855-865.
300. Dalkara, D., Goureau, O., Marazova, K., and Sahel, J.A. (2016). Let There Be Light: Gene and Cell Therapy for Blindness. Hum Gene Ther 27, 134-147.
301. Allocca, M., Mussolino, C., Garcia-Hoyos, M., Sanges, D., Iodice, C., Petrillo, M., Vandenberghe, L.H., Wilson, J.M., Marigo, V., Surace, E.M., et al. (2007). Novel adeno-associated virus serotypes efficiently transduce murine photoreceptors. J Virol 81, 11372-11380.
302. Auricchio, A., Kobinger, G., Anand, V., Hildinger, M., O'Connor, E., Maguire, A.M., Wilson, J.M., and Bennett, J. (2001). Exchange of surface proteins impacts on viral vector cellular specificity and transduction characteristics: the retina as a model. Human Molecular Genetics 10, 3075-3081.
303. Lebherz, C., Maguire, A., Tang, W., Bennett, J., and Wilson, J.M. (2008). Novel AAV serotypes for improved ocular gene transfer. J Gene Med 10, 375-382.
304. Lotery, A.J., Yang, G.S., Mullins, R.F., Russell, S.R., Schmidt, M., Stone, E.M., Lindbloom, J.D., Chiorini, J.A., Kotin, R.M., and Davidson, B.L. (2003). Adeno-associated virus type 5: transduction efficiency and cell-type specificity in the primate retina. Hum Gene Ther 14, 1663-1671.
305. Russell, S., Bennett, J., Wellman, J.A., Chung, D.C., Yu, Z.F., Tillman, A., Wittes, J., Pappas, J., Elci, O., McCague, S., et al. (2017). Efficacy and safety of voretigene neparvovec (AAV2-hRPE65v2) in patients with RPE65-mediated inherited retinal dystrophy: a randomised, controlled, open-label, phase 3 trial. Lancet 390, 849-860.
306. Cai, X., Conley, S.M., Nash, Z., Fliesler, S.J., Cooper, M.J., and Naash, M.I. (2010). Gene delivery to mitotic and postmitotic photoreceptors via compacted DNA nanoparticles results in improved phenotype in a mouse model of retinitis pigmentosa. FASEB J 24, 1178-1191.
307. Trapani, I., Puppo, A., and Auricchio, A. (2014). Vector platforms for gene therapy of inherited retinopathies. Prog Retin Eye Res 43, 108-128.
308. Rajala, A., Wang, Y., Zhu, Y., Ranjo-Bishop, M., Ma, J.X., Mao, C., and Rajala, R.V. (2014). Nanoparticle-assisted targeted delivery of eye-specific genes to eyes significantly improves the vision of blind mice in vivo. Nano Lett 14, 5257-5263.
309. Siqueira, A.P., Wallgren, M., Hossain, M.S., Johannisson, A., Sanz, L., Calvete, J.J., and Rodriguez-Martinez, H. (2011). Quality of boar spermatozoa from the sperm-peak portion of the ejaculate after simplified freezing in MiniFlatpacks compared to the remaining spermatozoa of the sperm-rich fraction. Theriogenology 75, 1175-1184.
310. Siqueira, R.C., Messias, A., Messias, K., Arcieri, R.S., Ruiz, M.A., Souza, N.F., Martins, L.C., and Jorge, R. (2015). Quality of life in patients with retinitis pigmentosa submitted to intravitreal use of bone marrow-derived stem cells (Reticell -clinical trial). Stem Cell Res Ther 6, 29.
311. MacLaren, R.E., Pearson, R.A., MacNeil, A., Douglas, R.H., Salt, T.E., Akimoto, M., Swaroop, A., Sowden, J.C., and Ali, R.R. (2006). Retinal repair by transplantation of photoreceptor precursors. Nature 444, 203-207.
312. Lamba, D.A., Gust, J., and Reh, T.A. (2009). Transplantation of human embryonic stem cell-derived photoreceptors restores some visual function in Crx-deficient mice. Cell Stem Cell 4, 73-79.
313. Assawachananont, J., Mandai, M., Okamoto, S., Yamada, C., Eiraku, M., Yonemura, S., Sasai, Y., and Takahashi, M. (2014). Transplantation of embryonic and induced pluripotent stem cell-derived 3D retinal sheets into retinal degenerative mice. Stem Cell Reports 2, 662-674.

314. Shirai, H., Mandai, M., Matsushita, K., Kuwahara, A., Yonemura, S., Nakano, T., Assawachananont, J., Kimura, T., Saito, K., Terasaki, H., et al. (2016). Transplantation of human embryonic stem cell-derived retinal tissue in two primate models of retinal degeneration. Proc Natl Acad Sci U S A 113, E81-90.
315. MacLaren, R.E., Bennett, J., and Schwartz, S.D. (2016). Gene Therapy and Stem Cell Transplantation in Retinal Disease: The New Frontier. Ophthalmology 123, S98-S106.
316. Mojica, F.J., Diez-Villasenor, C., Garcia-Martinez, J., and Soria, E. (2005). Intervening sequences of regularly spaced prokaryotic repeats derive from foreign genetic elements. J Mol Evol 60, 174-182.
317. Mojica, F.J., and Rodriguez-Valera, F. (2016). The discovery of CRISPR in archaea and bacteria. FEBS J 283, 3162-3169.
318. Bakondi, B. (2016). In vivo versus ex vivo CRISPR therapies for retinal dystrophy. Expert Rev Ophthalmol 11, 397-400.
319. Yu, W., Mookherjee, S., Chaitankar, V., Hiriyanna, S., Kim, J.W., Brooks, M., Ataeijannati, Y., Sun, X., Dong, L., Li, T., et al. (2017). Nrl knockdown by AAV-delivered CRISPR/Cas9 prevents retinal degeneration in mice. Nat Commun 8, 14716.
320. Yiu, G. Genome Editing in Retinal Diseases using CRISPR Technology. Ophthalmology Retina 2, 1-3.
321. Fu, Y., Foden, J.A., Khayter, C., Maeder, M.L., Reyon, D., Joung, J.K., and Sander, J.D. (2013). High-frequency off-target mutagenesis induced by CRISPR-Cas nucleases in human cells. Nat Biotechnol 31, 822-826.
322. Dias, M.F., Joo, K., Kemp, J.A., Fialho, S.L., da Silva Cunha, A., Jr., Woo, S.J., and Kwon, Y.J. (2018). Molecular genetics and emerging therapies for retinitis pigmentosa: Basic research and clinical perspectives. Prog Retin Eye Res 63, 107-131.
323. Collin, R.W., and Garanto, A. (2017). Applications of antisense oligonucleotides for the treatment of inherited retinal diseases. Curr Opin Ophthalmol 28, 260-266.
324. Garanto, A., Chung, D.C., Duijkers, L., Corral-Serrano, J.C., Messchaert, M., Xiao, R., Bennett, J., Vandenberghe, L.H., and Collin, R.W. (2016). In vitro and in vivo rescue of aberrant splicing in CEP290-associated LCA by antisense oligonucleotide delivery. Hum Mol Genet 25, 2552-2563.
325. Weiland, J.D., and Humayun, M.S. (2014). Retinal prosthesis. IEEE Trans Biomed Eng 61, 1412-1424.
326. Cehajic-Kapetanovic, J., Eleftheriou, C., Allen, A.E., Milosavljevic, N., Pienaar, A., Bedford, R., Davis, K.E., Bishop, P.N., and Lucas, R.J. (2015). Restoration of Vision with Ectopic Expression of Human Rod Opsin. Curr Biol 25, 2111-2122.

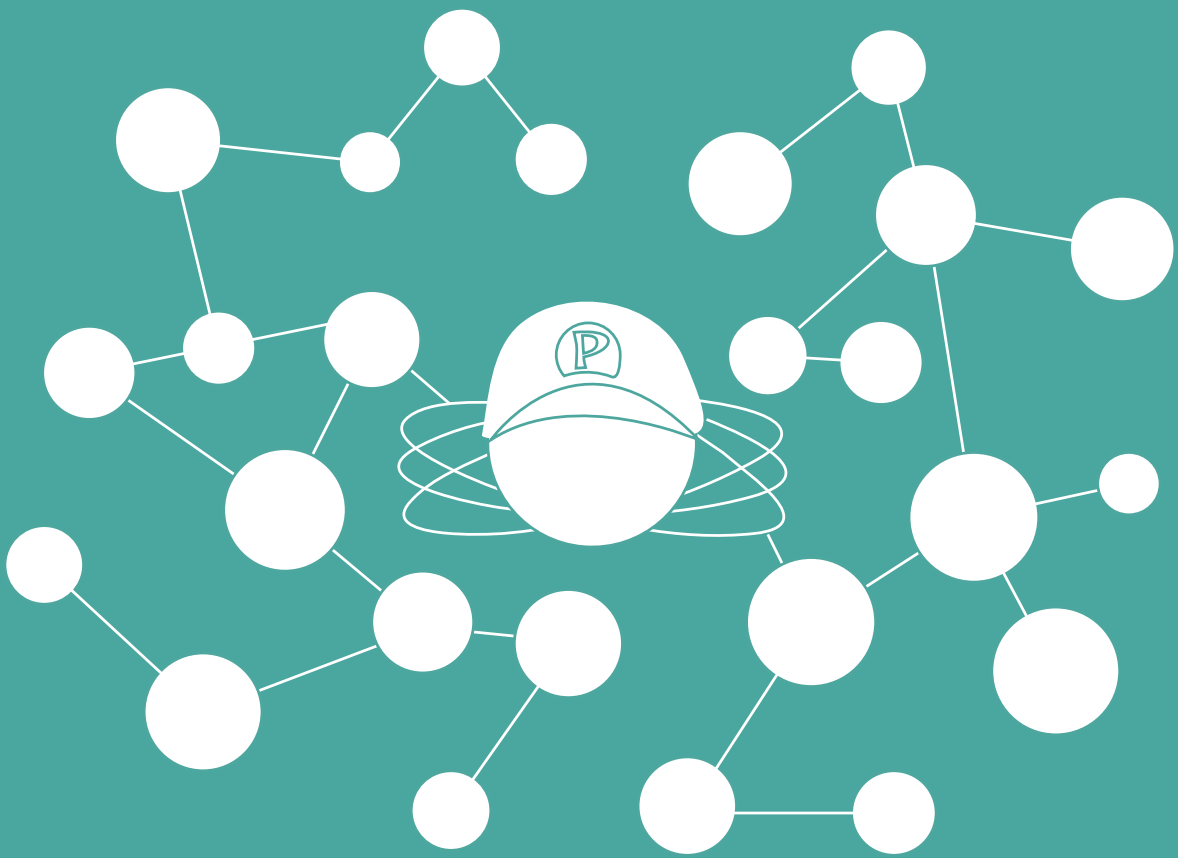

Chapter 2

The photoreceptor-specific protein PCARE interacts with WASF3 to deploy a ciliary actin dynamics module

The photoreceptor-specific protein PCARE interacts with WASF3 to deploy a ciliary actin dynamics module

Julio C. Corral-Serrano[1,2], Jeroen van Reeuwijk[1,2], Anita D.M. Hoogendoorn[1], Renate A.A. Ruigrok[1], Adem Yildirim[4], Lonneke Duijkers[1], Ideke J.C. Lamers[1], Stef J.F. Letteboer[1], Max D. van Essen[1], Sanae Sakami[5], Sylvia E.C. van Beersum[1], Krzysztof Palczewski[5], Karsten Boldt[6], Uwe Wolfrum[4], Marius Ueffing[6], Alejandro Garanto[1,3], Ronald Roepman[1,2,*,#], Rob W.J. Collin[1,3,#]

[1]Department of Human Genetics, Radboud University Medical Center, Nijmegen, The Netherlands; [2]Radboud Institute for Molecular Life Sciences, Radboud University Medical Center, Nijmegen, The Netherlands; [3]Donders Institute for Cognitive Neuroscience, Radboud University Medical Center, Nijmegen, The Netherlands; [4]Institute of Molecular Physiology, Johannes Gutenberg University of Mainz, Mainz, Germany; [5]Department of Pharmacology, School of Medicine, Case Western Reserve University, Cleveland, OH, USA; [6]Center of Ophthalmology, Institute for Ophthalmic Research, University of Tübingen, Tübingen, Germany.

#shared last authors

Revised version in preparation

2.1 Abstract

The outer segments (OS) of rod and cone photoreceptor cells are specialized sensory cilia that contain hundreds of opsin-loaded stacked membrane discs that enable phototransduction. The biogenesis of these discs is initiated at the OS base, but the driving force has been debated. Here, we show that the protein encoded by the photoreceptor-specific gene *C2ORF71*, which is mutated in inherited retinal dystrophy (RP54), localizes to the OS base. We demonstrate that C2ORF71/PCARE (photoreceptor cilium actin regulator) can interact directly with the Arp2/3 activator WASF3, and several other proteins involved in the dynamic actin filament biogenesis, which it efficiently recruits to the primary cilium. Ectopic co-expression of PCARE and WASF3 in ciliated cells results in the activation of an evagination process at the ciliary tip resembling that of lamellipodia, a process that was disrupted by a retinal dystrophy-associated missense mutation in PCARE. We propose that a similar actin dynamics-driven evagination process is operational at the base of the photoreceptor OS where the PCARE module and actin co-localize, but which is abrogated in *Pcare*$^{-/-}$ mice. The observation that several proteins involved in retinal ciliopathies are translocated to this evagination process renders it a potential common denominator in the pathomechanisms of these hereditary disorders. Together, our findings show that a tightly regulated deployment of actin dynamics is orchestrated by the photoreceptor-specific protein PCARE, thereby shedding more light on the mechanistic context of outer segment disc biogenesis.

2.2 Introduction

Photoreceptor cells in the neural retina of vertebrates are postmitotic, neuroepithelial cells that are highly polarized and compartmentalized.[1-3] The apical phototransductive outer segment is connected to the biosynthetic compartment, the inner segment (IS), by a narrow microtubule-based connecting cilium (CC) that is homologous to the transition zone of a primary non-motile cilium.[4] The replacement of damaged molecular OS components requires renewal by a specialized refurbishing mechanism. Daily, approximately 10% of the rod photoreceptor's opsin-loaded discs are shed at the apical OS tip,[5] and phagocytised by the adjacent RPE cells, while the same amount of new membrane discs are generated and restacked at the OS base, ensuring photoreceptor homeostasis. The canonical mechanism behind the onset of the formation of new discs was recently established to be evagination and subsequent expansion of the ciliary plasma membrane at the region where the CC enters the OS base.[6,7] Actin was proposed to be a critical factor in this, after a branched actin network was observed at the site of evagination initiation over three decades ago,[8,9] and inhibition of actin polymerization interfered with this process.[10] Despite these observations, detailed molecular insights into the dynamics or regulation of this actin-driven membrane evagination process have remained elusive.

We set out to identify the molecular disease mechanism of a progressive subtype of inherited retinal dystrophy, autosomal recessive retinitis pigmentosa type 54 (RP54) that is caused by mutations in *C2orf71*.[11,12] Using an affinity capture approach, we here show that the ciliary protein encoded by this gene interacts with basal body/centriole-associated proteins, microtubule-associated proteins and, intriguingly, also with several proteins involved in the assembly and activation of actin. Localization studies in human and mouse retinae, both of wild-type and *C2orf71* knockout mice, confirmed the C2orf71-dependent localization of these proteins to the base of the photoreceptor outer segments. Subsequent studies in ciliated cells demonstrated the capacity of this protein module to form structures resembling membrane evaginations. We have renamed *C2orf71* to *PCARE*, which stands for 'photoreceptor cilium actin regulator', as our study indicates that this protein plays an important role in delivering an actin module to the base of outer segment discs.

2.3 Results

2.3.1 PCARE is a ciliary and actin-associated protein

PCARE is predominantly expressed in the retina[11] and encodes a 140-kDa ciliary protein that is predicted to be myristoylated and palmitoylated at its N-terminus (Figure 1a).[12] These post-translational modifications promote stable attachment to membranes and are critically important in ciliary translocation.[13] PCARE does not contain any highly conserved functional domains, but several structural protein sequence motifs are predicted, including a tentative actin-binding motif (Figure 1a). Evaluation of the localization of full-length and three subfragments of PCARE in ciliated hTERT RPE-1 cells (Supplemental Figure 1a) showed that both full-length PCARE and the N-terminal fragment 1 (PCARE-F1; amino acids (aa) 2-449) localize to the basal body and axoneme of the primary cilium. The middle fragment 2 (PCARE-F2; aa450-900) localizes to the cytosol where it appears to induce and/or decorate cellular cytoskeletal filaments. Co-staining with phalloidin indicated that these filaments are actin-based (Supplemental Figure 1b). The C-terminal fragment 3 (PCARE-F3; aa901-1289) that contains a predicted nuclear localization signal, mainly localizes to the nucleus, although some axonemal staining was also observed (Supplemental Figure 1a).

2.3.2 PCARE interacts with microtubule-, centrosome-, and actin-associated proteins

We used PCARE as a bait in protein-protein interaction screens to identify potential physical links to known biochemical pathways. Screens for binary retinal interactors of PCARE and its three subfragments were carried out using the yeast two-hybrid system (Supplemental Table 1). Assessment of the resulting 41 candidate interactors, after confirmation by co-transformation in yeast, revealed six proteins that are known to be associated with the centriole(s) of the centrosome and/or the ciliary basal body, of which three are known to be involved in retinal ciliopathies, i.e. OFD1, CEP290, and CEP250 (Figure 1b).[14] Other interacting proteins are also microtubule-associated, like the dynactin subunits DCTN1/p150-glued and DCTN2/p50 dynamitin, PCM1, NINL, and KNSTRN. In addition, three components of microtubule-based kinesin motors (KIF20A, KLC2 and KLC4) were found to interact with PCARE. Importantly, a direct association with one of the key proteins involved in activating actin dynamics was identified, the WAVE regulatory complex (WRC) member WAVE3/WASF3 (Wiskott-Aldrich syndrome protein family member 3). This protein is required for the nucleation of a dynamic branched F-actin network by activating the Arp2/3 complex.[15]

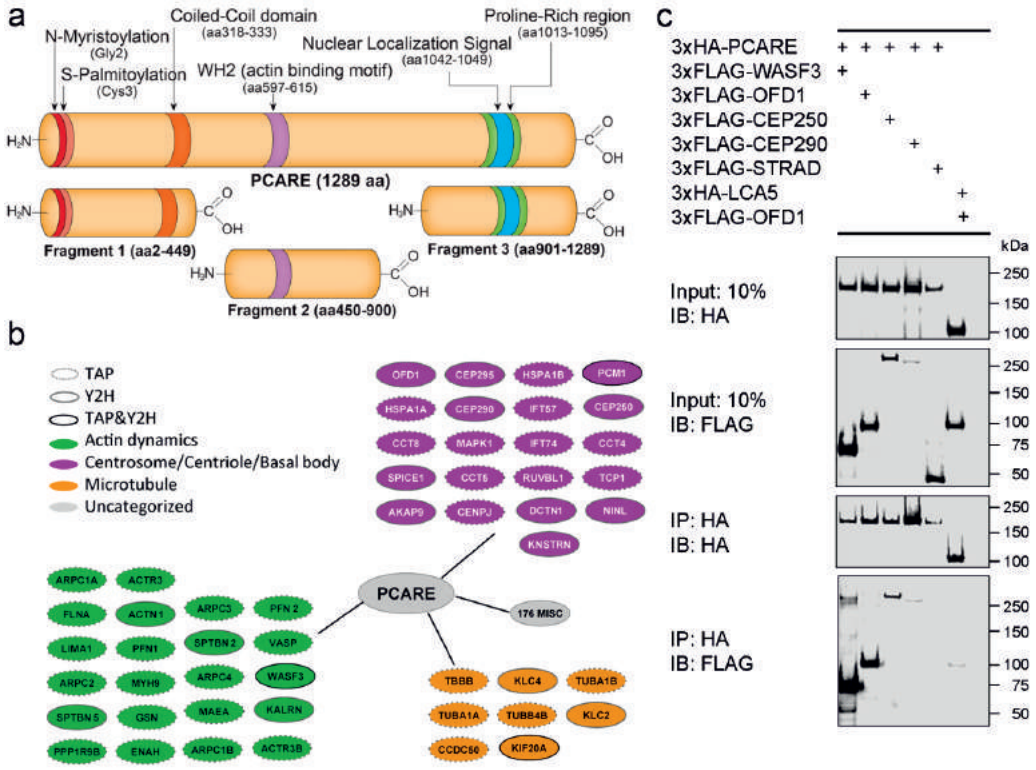

Figure 1. PCARE interacts with microtubule-, centrosome-, and actin-associated proteins. a, Schematic representation of the PCARE protein structure and subdivision into three fragments. Indicated are the N-myristoylation and S-palmitoylation residues, a predicted coiled coil domain (by COILS Server, http://embnet.vital-it.ch/software/COILS_form.html), a WH2 actin binding motif (by ELM, http://elm.eu.org/), a nuclear localization signal (by ELM) and a proline-rich region (by HHpred, https://toolkit.tuebingen.mpg.de/hhpred). **b**, Overview of the main protein modules associated to PCARE, as found in the Y2H and TAP studies. Three prominent modules can be distinguished: a module composed by proteins linked to actin dynamics (in green), a module of centrosomal/centriolar/basal body proteins (in purple), and a module of microtubule-associated proteins (in orange). **c**, Validation of the binary interactions by co-immunoprecipitation. HEK293T cells were co-transfected with cDNA constructs encoding 3xHA-PCARE and 3xFLAG-WASF3, 3xFLAG-OFD1, 3xFLAG-CEP250 or 3xFLAG-CEP290. The unrelated protein 3xFLAG-STRAD was used as negative control of PCARE interaction. As positive control, the interaction between 3xHA-LCA5 and 3xFLAG-OFD1 was used. Protein complexes were immunoprecipitated with anti-HA antibodies, while input or immunoprecipitated fractions were immunoblotted with anti-HA or anti-FLAG antibodies.

Next to WASF3, four other proteins with different roles in actin dynamics were identified as putative PCARE interactors (Figure 1b, Supplemental Table 1). To validate the specificity of the direct binding of PCARE to a representative subset of potential binary interacting partners identified in the Y2H screens,

we performed co-immunoprecipitations using HEK293T cells ectopically expressing 3xHA-PCARE and 3xFLAG-tagged WASF3, OFD1, CEP250 or CEP290 (Figure 1c). All four putative PCARE-interacting proteins were indeed found to specifically co-immunoprecipitate with PCARE, albeit somewhat less strong for CEP290. For WASF3, the main interacting region was delineated to the N-terminal PCARE Fragment 1, while PCARE Fragment 2 also had some affinity for this protein (Supplemental Figure 1c).

To further explore the PCARE interactome, we performed tandem affinity purification (TAP) of Strep-II/FLAG-tagged full-length PCARE expressed in HEK293T cells. Interacting proteins were subsequently identified by mass spectrometry (Figure 1b, Supplemental Table 2). Although limited overlap is generally observed in Y2H and TAP-MS data,[16] five proteins, DCTN2, KIF20A, IFFO1, PCM1 and WASF3, were found to interact with PCARE in both the Y2H and the TAP assay, again demonstrating the importance of these interactions. Moreover, the three functional protein modules we identified by the Y2H assays could also be distinguished in this experiment: a microtubule-associated module (6 proteins), a centrosome/basal body module (12 proteins), and 18 proteins that are known to play diverse roles in *de novo* actin network assembly, including most members of the ARP2/3 complex that regulates actin polymerization. These proteins include the actin assembly regulator ENAH, the actin capping/severing protein gelsolin, the actin cytoskeleton restructuring factors profilin 1 and 2, myosin regulatory subunits 12A and 12B, the actin bundling protein LIMA1, the actin bundling and membrane-associating protein filamin A, and several chaperonins (Figure 1b, Supplemental Table 2).

2.3.3 PCARE co-localizes with an actin dynamics module at the OS base

We next evaluated the localization of representative components of these three modules in the retina. Immunofluorescence staining of PCARE and its direct interactors WASF3 and α-actinin (ACTN1) in human retina showed staining in the area of the connecting cilium (Figure 2a). Co-staining with centrin-3 (CEN3) that marks the axoneme of the connecting cilium (CC) and the daughter centriole (dC) showed that all three proteins localized at the site of initiation of OS disc morphogenesis in the apical CC region of photoreceptors, where F-actin co-localized with WASF3. The three proteins also localized to the base of the connecting cilium and the daughter centriole (Figure 2a). Immunofluorescence co-staining of WASF3 and F-actin at the apical and basal CC regions was also confirmed (Figure 2b). Although suitable for western-blot, PCARE antibody did not yield a specific staining in immunohistochemical analyses on mouse retinae (Supplemental Figure 5).

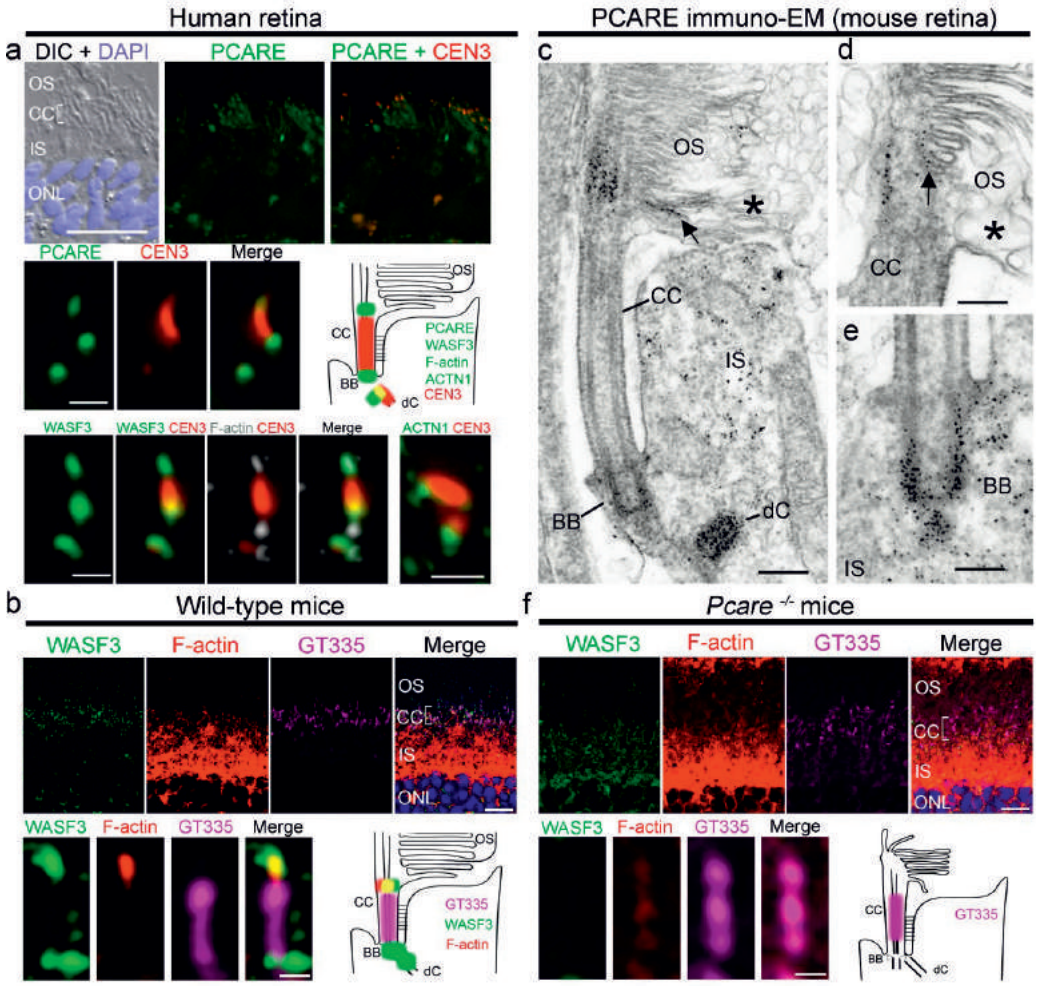

Figure 2. PCARE co-localizes with actin-associated proteins at the OS base in the retina. a-b, Localization of PCARE, WASF3, ACTN1 and F-actin in a human donor retina (66 years old) and in wild-type mouse retinas (1 month old). PCARE co-localizes with WASF3, ACTN1 and F-actin at the tip of the connecting cilium (CC, counterstained with anti-centrin (CEN3) or GT335) and at the basal body (BB) and the adjacent daughter centriole (dC). **c-e**, Immuno-EM localization of PCARE in mouse photoreceptors (3 months old) affirm localization in the outer segment (OS) at the tip of the CC (asterisks) associated with nascent discs (arrows) and the centrioles of photoreceptors. **f**, In age-matched *Pcare*$^{-/-}$ mouse retinas, WASF3 and F-actin mislocalize from the apical part of the CC. Outer nuclear layer, ONL; IS, inner segment; BB, basal body; dC, daughter centriole. Scale bars: a: upper panel: 25 µm, middle and lower panels: 1 µm; b,f: upper panels 10 µm, lower panels: 0.5 µm; c: 300 nm; d: 150 nm; e: 175 nm.

High-resolution localization analysis of PCARE in mouse photoreceptors by immuno-electron microscopy (EM) further validated and specified these findings (Figure 2c-e), demonstrating that PCARE decorates the microtubules of the apical region of the connecting cilium, and extends to the first nascent discs of the OS base (Figure 2c,d). Furthermore, it decorates the microtubules of the ciliary basal body (Figure 2e) and daughter centriole (Figure 2c), while some more dispersed signal around the basal body and in the inner segment/calyceal process could also be observed (Figure 2c,e). Evaluation of the actin dynamics module in retinae of one-month old *Pcare*$^{-/-}$ mice that develop early-onset retinal degeneration[17] showed that WASF3 and F-actin were absent from the CC region, while the CC itself remained present, as indicated by the staining of the axonemal marker polyglutamylated tubulin (GT335) (Figure 2f).

2.3.4 PCARE recruits WASF3 to the ciliary tip and induces membrane evaginations

To further study the importance of the interactions of PCARE and its binding partners, we first evaluated the localization of ectopically expressed PCARE and the Arp2/3 complex activating factor WASF3 in ciliated hTERT RPE-1 cells (Figure 3a,b), and compared this with their localization upon co-expression (Figure 3c,d). In the absence of PCARE, which is not endogenously expressed in these cells, WASF3 associates to F-actin in the vicinity of the nucleus (Figure 3b). When PCARE was co-expressed, it efficiently recruited WASF3 and translocated it into the cilium (Figure 3c), where actin filaments could be identified (Figure 3d). Intriguingly, this induced the formation of a membrane evagination, appearing as a bulge with some variety in shape and size (Figure 3c,d). This process was not cell-type specific, as it could also be observed in murine ciliated mIMCD-3 cells (Supplemental Figure 2). Several intermediate stages of this process could be observed, suggesting a progressively extensive evagination in time at the ciliary tip (Figure 3c-e). A more detailed evaluation of several confocal planes of a cell ectopically co-expressing PCARE, WASF3 and the centrosomal/basal body protein DCTN2, one of the binary PCARE interactors, further demonstrated that docking of the module at the ciliary tip initiates ciliary membrane evagination (Figure 3f). To validate that actin dynamics is involved in the formation of these evaginations, we treated the cells with actin polymerization inhibitors. Cytochalasin D administration, which prevents polymerization of the barbed ends of F-actin filaments,[18] did not affect the formation of these structures. In contrast, treatment with latrunculin B, which sequesters G-actin monomers and thereby prevents its polymerization,[19] completely blocked the formation of the evaginations (Figure 3g). Other compounds such as CK-660 and nocodazole did not affect this process (Figure 3g).

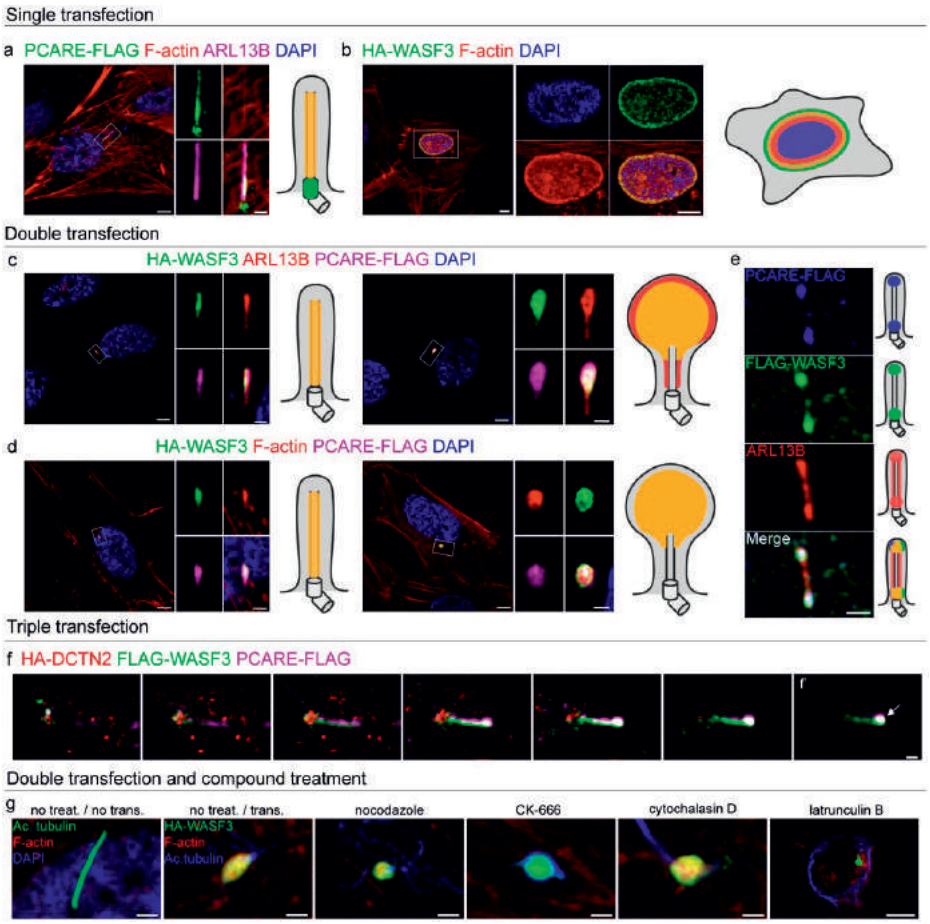

Figure 3. Formation of ciliary evaginations upon ectopic co-expression of PCARE and WASF3. **a,** Ectopic expression of PCARE in hTERT RPE-1 cells shows localization of PCARE (green) at both the ciliary base and axoneme, and presence of F-actin (red) inside the primary cilium, stained with ARL13B (purple). **b,** Overexpression of WASF3 (green) recruits F-actin (red) to the nucleus. **c**, Co-expression of PCARE and WASF3 translocates the latter from the nucleus into the cilium (left panel). An evagination of the ciliary membrane forms at the ciliary tip (right panel). **d,** This evagination is filled with polymerized actin. **e,** Cells were transfected with plasmids expressing FLAG-WASF3 and PCARE-FLAG and stained 4 hours after transfection with antibodies directed against ARL13B (red), WASF3 (green) and PCARE (blue). At this point we can already observe accumulation of the proteins at the ciliary base and tip. **f,** hTERT RPE-1 cells were transfected with plasmids expressing HA-DCTN2, FLAG-WASF3 and PCARE-FLAG and stained with antibodies directed against HA (red), WASF3 (green) and PCARE (purple). Recombinant WASF3 (green) and PCARE (purple) proteins accumulate at the tip of the primary cilium (**f'**, arrows). DCTN2 (red) marks the base of the cilium. Imaging was performed using focal plane merging in a Zeiss LSM 800 microscope with Airyscan. **g**, PCARE/WASF3 co-transfected cells were treated for 18 h with 1 µM of cytochalasin D, the ARP2/3 complex inhibitor CK-666, nocodazole or latrunculin B, and stained with WASF3 (green), F-actin (red) and acetylated tubulin (blue). Nocodazole, cytochalasin D or CK-666 treatment did not disrupt the formation of the ciliary evaginations, while latrunculin B caused complete disruption of these. Scale bars: a-b: left panels: 20 µm, middle panels: 5 µm, insets: 1 µm; c-d: left panels: 5 µm, insets: 1 µm; e,f: 1 µm; g: all 1 µm, except latrunculin B-treated cells: 5 µm.

2.3.5 Actin- and tubulin-associated proteins localize to the ciliary tip evaginations

Evaluation of the constitution of these evaginations by immunofluorescence showed that they contain all tested core components of the PCARE-associated actin dynamics module we identified in our affinity screens: ENA/VASP (Figure 4a) and the RhoGEF kinase kalirin (Figure 4b), that is known to affect the actin cytoskeleton and is a RAC1 activator.[20] Its substrate RAC1, which was not identified in our affinity screen but is known to activate the Wave regulatory complex,[21] indeed was also present at the evaginations (Figure 4c). Co-expression of PCARE, WASF3, and the ARP3 protein, a member of the Arp2/3 complex and involved in activation of the branched actin network,[22] did confirm co-localization of these proteins and F-actin throughout the evagination structure (Figure 4d). Evaluation of the localization of markers of the ciliary microtubule axoneme, acetylated tubulin (Supplemental Figure 3a) and polyglutamylated tubulin (Supplemental Figure 3b) upon ectopic co-expression of PCARE and WASF3 showed a partial colocalization, which was also the case for the intraflagellar transport protein IFT88 (Supplemental Figure 3c).

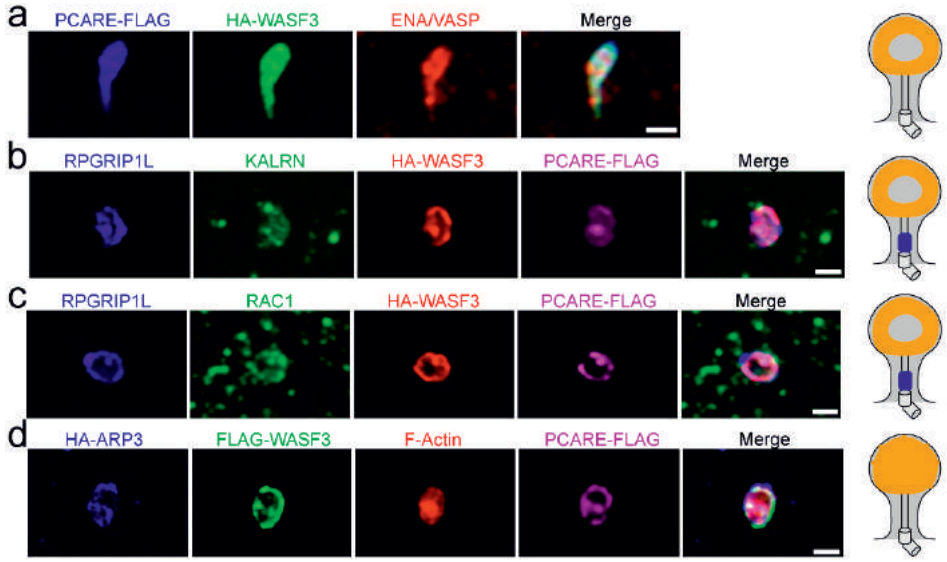

Figure 4. Actin-associated proteins localize to the ciliary evagination. Ciliated hTERT RPE-1 cells were transfected with plasmids expressing PCARE-FLAG and HA-WASF3 (**a-c**) or FLAG-WASF3 (**d**), and stained with antibodies directed against: **a,** PCARE (blue), WASF3 (green, ENA/VASP (red); **b**, RPGRIP1L (blue), KALRN (green), WASF3 (red), PCARE (purple); **c**, RPGRIP1L (blue), RAC1 (green), WASF3 (red), PCARE (purple); **d,** HA to detect HA-ARP3 (blue), WASF3 (green), F-actin (red), PCARE (purple). Scale bars are 1 µm.

2.3.6 Mutant p.(I201F) PCARE alters the formation of evaginations

To investigate the pathophysiology underlying *PCARE*-associated RP54, the p.(I201F) missense mutation [12] was introduced into PCARE. Although p.(I201F) mutant PCARE still translocated to the ciliary axoneme, there were observable differences between the evaginations formed by wild-type and mutant PCARE (Figure 5). To analyse these differences in more detail, we classified the different cilia phenotypes of co-transfected cells in three types: type I (large, extended evagination), type II (small bulge), type III (no bulge) (Figure 5a,b). Three independent evaluations of these cilia were performed in a total of 40 cilia for the wild-type condition and 41 cilia for the mutant condition (Figure 5c). The majority of the cilia (~79% of the total for the WT and ~65% for the mutant) presented some degree of bulging. Importantly, cells transfected with wild-type PCARE contained predominantly cilia with the large, extended evaginations (type I, 56% on average) compared to the PCARE p.(I201F) mutant (16% on average). Moreover, the area of the bulges was significantly increased in the wild-type condition compared to the mutant (Figure 5d).

2.3.7 Distinct retinal ciliopathy proteins modify the structure of the ciliary evaginations

Interestingly, we observed that the ciliary marker ARL13B (Fig. 3c,e) and the ciliary transition zone marker RPGRIP1L (Figure 4b,c) also localized to the evaginations. As mutations in these two proteins cause the retinal ciliopathy Joubert syndrome, and genes encoding several of the identified PCARE interactors have also been found to be mutated in ciliopathies, we evaluated the relevance of the encoded proteins to the evagination process. Upon ectopic co-expression of PCARE and WASF3, several of these proteins are co-translocated into the ciliary tip evaginations, similar to RPGRIP1L and ARL13B. These include the basal body protein OFD1 (Figure 6a) and the ciliary axonemal proteins spermatogenesis-associated protein 7 (SPATA7, Figure 6b) and lebercilin/LCA5 (Figure 6c). Two PCARE interactors of the centrosomal/basal body module that we tested, DCTN2 (Figure 3f) and CEP250 (Figure 6d) however were not translocated to the ciliary evaginations and remained at the ciliary basal body. Although OFD1, SPATA7 and lebercilin were all efficiently translocated to the evagination structures, different expression patterns and effects were observed. Lebercilin was predominantly found at the base of the structures (Figure 6c), in contrast to OFD1 and SPATA7 (Figure 6a,b). Intriguingly, the latter two were found to expand the size of the evagination structures by, on average, 40% (Figure 6e).

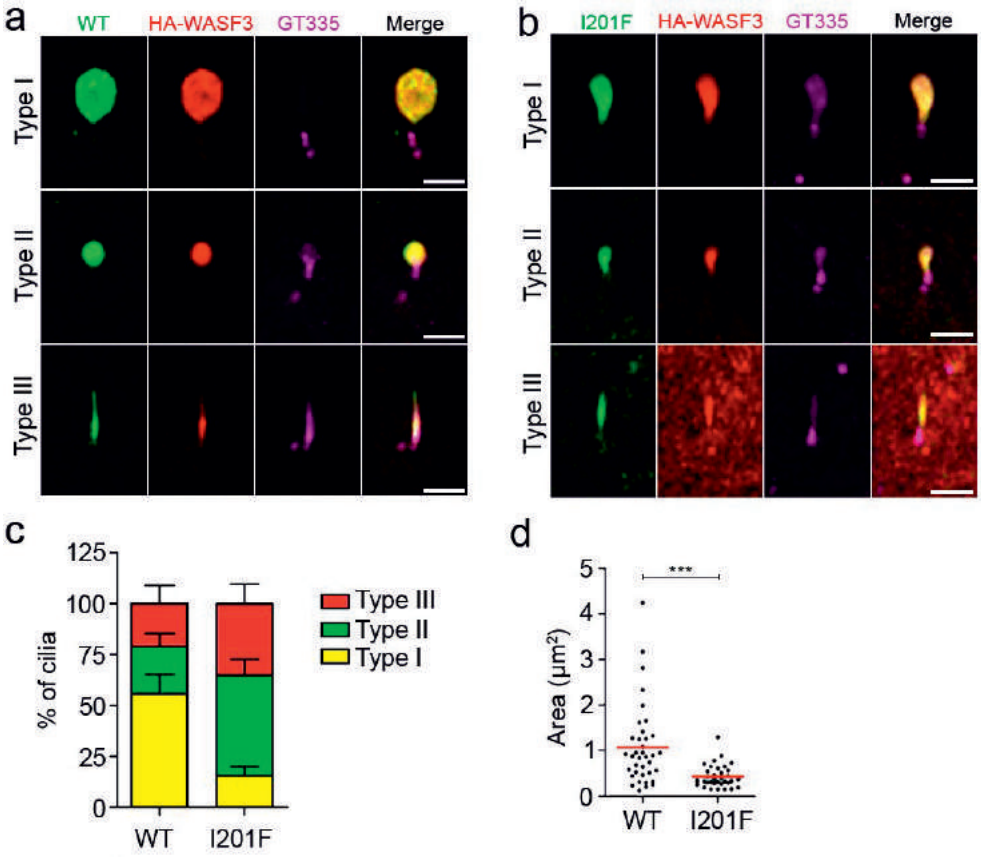

Figure 5. RP-associated mutant p.(I201F) PCARE generates distinct ciliary evaginations. hTERT RPE-1 cells were co-transfected with plasmids expressing FLAG-tagged WASF3, and either wild-type PCARE or mutant PCARE p.(I201F) fused to HA (**a, b**). Cells were stained with antibodies recognizing PCARE (green), WASF3 (red) and polyglutamylated tubulin (GT335, purple). Scale bars are 2 µm. To compare the cilia transfected with wild-type PCARE (WT) to mutant PCARE (I201F), we categorized the different phenotypes in type I (expanded evagination / ring structure), II (small bulged cilium) or III (regular cilium) structures. Cells transfected with wild-type PCARE contain more type I cilia than mutant transfected cells (**c**). **d**) Quantifications of the area of the evaginations is represented for each measured cilia, and shows that cilia transfected with the I201F mutant present smaller evaginated areas than the wild type; n=37 (WT), I201F (n=34), p-value = 0.0001.

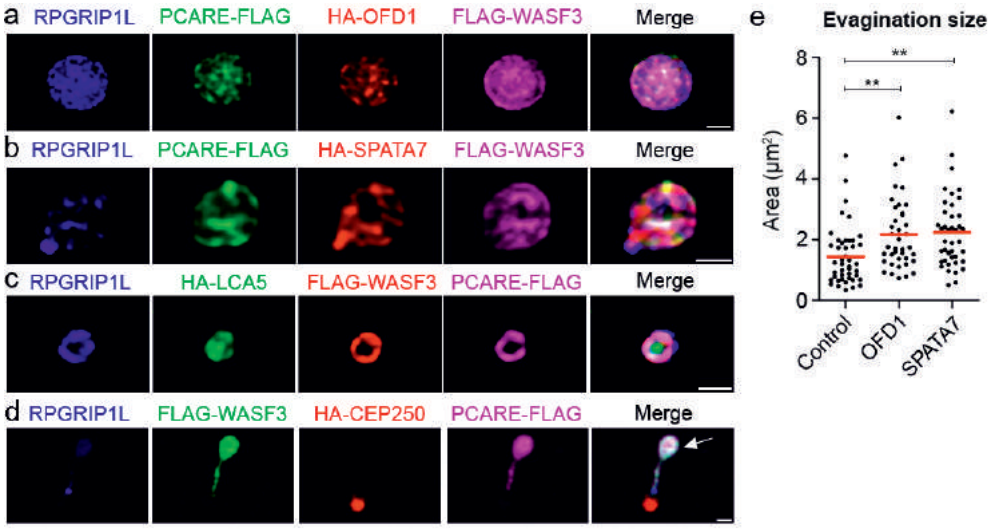

Figure 6. Retinal ciliopathy proteins modify the structure of the ciliary evaginations. Triple co-expression of PCARE (**a**, **b**, green; **c**, **d**, purple), WASF3 (**a**, **b**, purple; **c**, red; **d**, green) and OFD1 (**a**, red) or SPATA7 (**b**, red) increases the size of the ciliary evaginations in hTERT RPE-1 cells, but it does not increase for LCA5 (**c,** green) and CEP250 (**d,** red). In these evaginations, the transition zone marker RPGRIP1L (blue) shows different localization patterns. **e,** Quantifications of the area of the evaginations is represented for each cilia, and revealed a statistically significant increase in size for the OFD1 and SPATA7 transfected cilia. The mean for each condition is indicated in red. *OFD1 (p-value = 0.0027), *SPATA7 (p-value = 0.0011); n=44 (Control), n=39 (OFD1); n=41 (SPATA7). Scale bars are 1 µm.

2.4 Discussion

The neogenesis of photopigment-loaded membrane discs of a vertebrate photoreceptor cell is a tightly regulated, multistep process that takes place at the base of the sensory primary cilium of this cell.[23] This results in the assembly of hundreds of new discs each day at the OS base where it connects to the ciliary stalk. The shedding and subsequent phagocytosis by the RPE at the tip of the OS tip balances this process that allows, at least in humans, a complete renewal cycle every 10 days. This elegant evolution towards high resolution colour vision requires over a thousand proteins for its function, but comes with a prize: critical defects in these processes due to genetic mutations that disrupt ciliary proteins are a major cause for non-syndromic and syndromic hereditary blindness, collectively known as the retinal ciliopathies.[4,24,25] The combination of high-resolution imaging studies with protein-protein interaction analyses has shown to be an effective way to expand our knowledge of cilium function in health and disease in an iterative way.[4,26] In this study, we took this approach to investigate the role of PCARE in the photoreceptor cilium to understand the disease pathogenesis of RP54.

Although PCARE is expressed specifically in the retina,[11,17] the full-length protein efficiently localizes to the cilium upon ectopic expression in cultured ciliated cells (i.e. hTERT RPE-1 and mIMCD-3 cells). The subdivision of PCARE into three fragments was done to avoid potential size restraints and increase the sensitivity of our Y2H screening.[27] This also allowed the evaluation of the contribution of the predicted domains residing in these fragments to the PCARE localization. Only N-terminal fragment 1 (aa2-449) efficiently localized to the entire cilium including the basal body, similar to the full-length protein, which is likely to be induced by the predicted N-Myristoylation (Gly2) and S-Palmitoylation (Cys3) signals present in this fragment. The C-terminal fragment 3 (aa901-1289) seems to use its predicted nuclear localization signal to translocate to the nucleus, although the relevance of this signal in full-length PCARE is unclear. The central fragment 2 (aa450-900) contains a predicted actin-binding motif, and is indeed capable of decorating actin filaments. The relevance of this latter finding became clear when we evaluated the protein-protein interaction data. Besides the identification of several centrosomal/basal body-, and microtubule-associated interacting proteins that matched the ciliary localization of PCARE, our yeast two-hybrid screen for binary PCARE interactors yielded several proteins that have been shown to be involved in the regulation of actin. This process concerns the dynamic cycling between polymerization and disassembly of the 42 kDa monomeric, globular actin (G-actin) protein into filamentous actin (F-actin), and the subsequent formation of higher order, branched F-actin networks. This allows cells to efficiently and rapidly remodel their cytoskeleton, and has been adopted as their main and most versatile force-generating system, as it facilitates most cellular processes that require cell membrane protrusion, contraction, and remodelling.[28,29] Most interestingly, we identified WASF3/WAVE3 as a direct PCARE interactor. This protein is incorporated into a conserved, heteropentameric WAVE regulatory complex (WRC) that activates the Arp2/3 complex for actin filament nucleation and assembly of a branched F-actin network.[15] Specific subtypes of the wide variety of actin dynamics-regulated processes can be distinguished by their protein constitution. The WRC is known to activate the Arp2/3 complex specifically in lamellipodia, ribbon-like flat cell membrane protrusions driven by actin dynamics that provide cellular motility across a surface.[30] In turn, the Arp2/3 complex activation occurs downstream of the Rho GTPase family member RAC1. Interestingly, RAC1 can be activated by the Rho GEF kalirin. Both kalirin and alpha-actinin, direct interactors of PCARE, are proteins with spectrin-like repeats that allow the interaction with a variety of substrates.[31] The association of PCARE with an extensive actin dynamics module was further solidified and extended by our tandem affinity purification experiments, identifying a further 18 proteins associated with actin dynamics. These included most members of the Arp2/3 complex (that can be activated by WASF3), the actin assembly regulator ENAH, the actin capping/severing protein gelsolin, the

actin cytoskeleton restructuring factors profilin 1 and 2, myosin regulatory subunits 12A and 12B, the actin bundling protein LIMA1, the actin bundling and membrane-associating protein filamin A, and several chaperonins of the CCT family, all known to be important for correct actin filament folding.

As several differentially localized actin-based processes have been suggested to regulate photoreceptor outer segment neogenesis and homeostasis,[23] it was important to accurately determine the location of PCARE in the retina. As its capacity to localize to the primary cilium of cultured cells already suggested, PCARE was indeed found at the photoreceptor connecting cilium. More precise localization by immunofluorescence and immuno-EM determined that PCARE localizes to three prominent sites: the ciliary basal body, the accompanying daughter centriole, and a narrow region at the tip of the connecting cilium stalk, directly adjacent to the site of the neogenesis of the first outer segment membrane discs. WASF3 also localized to these three sites, while F-actin localized with WASF3 at the tip of the connecting cilium. This latter finding was particularly exciting, as it directly links to one of the axioms in photoreceptor cell biology: the observation of a branched F-actin network at this exact location over thirty years ago, when the involvement of F-actin in the neogenesis of OS discs was first suggested.[8] This hypothesis was later strengthened by results of treatment with the actin poison cytochalasin D that prohibited the generation of new discs, but not the (over)growth of existing ones.[10] Further support was obtained from immuno-EM observations that demonstrated the presence of alpha-actinin at this site.[9] This hypothesis of actin dynamics-driven membrane evagination has been challenged several times since then, as different fixation and imaging techniques showed different results.[23] We here demonstrate that ectopic co-expression of PCARE and WASF3 in cultured ciliated cells, in which PCARE is not endogenously expressed, recruits all WASF3 from the cytoplasm to the cilium, and induces membrane evagination at the ciliary tip. The fact that the formation of these evaginations can be prohibited by the F-actin poison latrunculin-B, suggests the involvement of actin in this process. Evaluation of the components present in these ciliary evaginations, either by co-localization or co-expression, confirmed that they contained all tested proteins of the actin dynamics module that were identified in our protein-protein interaction studies (Figure 7).

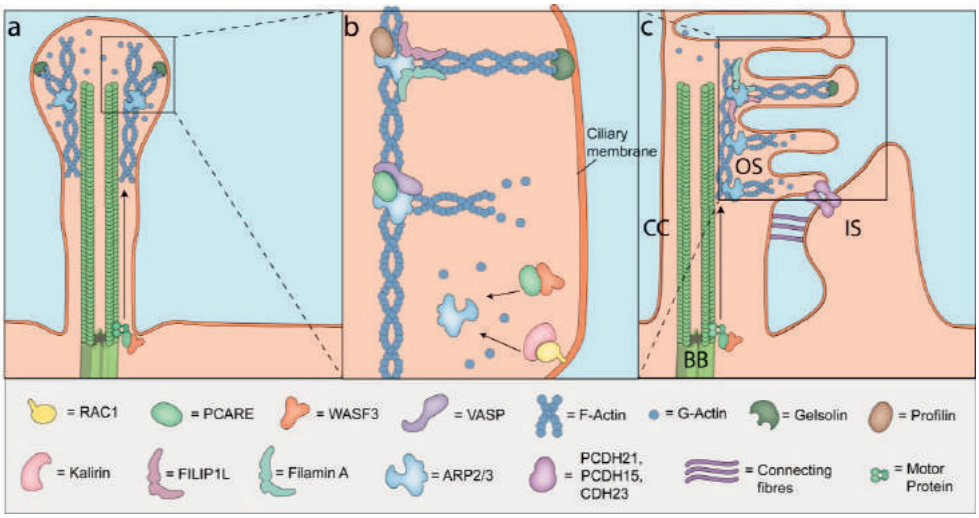

Figure 7. Proposed model of actin network formation at the photoreceptor ciliary membrane. Accurate delivery of a multimeric actin assembly module by PCARE, paired with the WAVE regulatory complex member WASF3 and several other modifiers of a dynamic F-actin network assembly at the primary cilium (**a**) and at the photoreceptor connecting cilium (**c**). Most of these actin modifiers are found in the process of lamellipodia formation. **b**, Zoom-in of the marked region. In this hypothetical scheme, the Arp2/3 complex acts as main nucleator of actin polymerization at the edge of the membrane.[32]PCARE recruits WASF3 to the ciliary tip, where they may act as nucleator promoting factors, probably by use of their WH2 domain and proline-rich region, contributing to the extension of the evagination.[33] The PCARE interactor kalirin (Supplemental Table 1), a Rho-GEF, activates the Rho GTPase RAC1.[34] RAC1, a WAVE complex activator,[21] would be responsible for WASF3 activation. ENAH/VASP (VASP) and profilin would act as elongation factors, tethering actin filaments to the membrane.[35] Potent actin cross-linkers in this network like filamin A and FILIP1L (filamin A-interacting protein 1-like, Supplemental Table 1) would help to stabilize the network. Capping proteins like gelsolin act to prevent the loss of actin subunits at the barbed end and increase the rate of nucleation.

Several aspects of our study provide important new insights into the molecular disease mechanisms underlying the disturbed photoreceptor function observed in not only *PCARE*-associated RP but also in several other retinal ciliopathies. First, as we identified that a missense mutation (p.I201F) in PCARE alters the ciliary tip evaginations, we propose that the disturbance of actin dynamics-driven OS disc neogenesis is the underlying mechanism in *PCARE*-associated retinal dystrophy. Both the phenotype of the photoreceptors of *Pcare*$^{-/-}$ mice,[17] and the absence of Wasf3, and F-actin that we observed at the tip of the connecting cilium stalk of the photoreceptors in these mice, validate this hypothesis. Second, in a recent whole genome sequencing effort, *WASF3* variants were found in a patient with cone-rod dystrophy.[36] As WASF3 is a direct interactor of PCARE, our data suggest *WASF3* could be a *bona fide* gene in which mutations could underlie retinal dystrophy. Third, we identified and validated three retinal ciliopathy proteins as binary interactors of PCARE: CEP250, CEP290, and OFD1. Disruption of their

function, or their interaction with PCARE, may therefore be associated to the retinal disease pathogenesis. Intriguingly, homozygosity mapping combined with whole exome sequencing in an Iranian cohort revealed nonsense mutations in both *CEP250* and *PCARE* to be responsible for atypical Usher syndrome with early-onset hearing loss and mild retinal degeneration,[37] suggesting that the proteins encoded by these genes could be involved in the same molecular processes. Here, we show that CEP250 strictly localizes to base of the cilium and it is not recruited into the ciliary lumen by PCARE, in contrast to most other interacting and ciliary proteins that we tested. This may indicate that CEP250 forms a docking base for PCARE at the ciliary base prior to its ciliary entry, allowing assembly of its actin dynamics module. Fourth, several other retinal ciliary proteins that we tested are also translocated to the ciliary tip evaginations upon ectopic co-expression of PCARE and WASF3. These proteins include RPGRIP1L, ARL13B, SPATA7, and Lebercilin/LCA5. Interestingly, the co-expression of OFD1 and SPATA7 significantly expanded the size of the structures, suggesting a dynamic participation of these proteins in the evagination process. RPGRIP1L was the only protein that clearly translocated to the ciliary lumen and tip only by PCARE without expression of WASF3 (Supplemental Figure 4). Fifth, the previous detection of both Rpgrip1l and Lebercilin at the apical CC region of mouse photoreceptors by immuno-EM,[38,39] and the recent discovery of the interaction of the X-linked RP-associated protein RPGR with gelsolin[40] (which was also present in our TAP dataset), strengthens the hypothesis that several retinal ciliopathy proteins play a role in the actin-driven membrane evagination process, either as their primary function or as an alternative one.

To conclude, we here demonstrate that the protein PCARE, encoded by the former *C2orf71* gene that is mutated in inherited retinal dystrophy, interacts with several ciliary proteins as well as those that are involved in the regulation of actin. The membrane evaginations that were observed in our cellular transfection studies, as well as the localization of the endogenous proteins within the photoreceptor cell suggests that PCARE could be involved in the first steps of outer segment disc neogenesis by the recruitment of an actin dynamics module to the ciliary base and the subsequent transfer of this module to the apical connecting cilium region. We do not yet have sufficient information about the precise mode of subsequent steps involved in this process that even may still involve membrane blebbing and/or ectocytosis. Also, we obtained the identity of likely only a subset of the components that are part of this machinery. Further analysis of the developing *Pcare*$^{-/-}$ mouse retina by EM, would be needed to address the exact defect in OS formation. We did however show that we can model the process of ciliary tip evagination in cultured mammalian cells by ectopic expression of PCARE and WASF3, which allows the future evaluation and elucidation of many components that may participate in this critical step in outer

segment development and homeostasis. Finally, our study provides unique insights into the accurate delivery and activation of a multimeric module of actin dynamics regulating proteins, at a tightly restricted sub-organellar site of action by a single trafficking molecule, PCARE. This expands the already broad repertoire of the cell to dynamically activate and modulate filamentous actin networks to drive membrane morphogenesis.

2.5 Methods

2.5.1 DNA constructs

Human *C2orf71/PCARE* [NCBI GeneID:388939] full length cDNA was obtained by PCR using Human Retina Marathon®-Ready cDNA (Clontech). Upon Sanger sequencing, two deviations from the reference sequence were identified, both of which are known as common polymorphisms (rs10166913:p.(Thr580Met); rs139768554:p.(Ser1225dup)). PCARE fragments F1 (aa2-449), F2 (aa450-900) and F3 (901-1,289) were generated using pENTR-PCARE as template. The PCARE p.(I201F) mutant (c.601A>T) was generated via site-directed mutagenesis using primers 5'-TCCAAATATGAAGCATTTCTGTGCATCATCC-3' and 5'-GGATGATGCACAGAAATGCTTCATATTTGGA-3' (mutated nucleotide underlined). The eGFP-CEP250 plasmid was kindly donated by Dr. Erich Nigg (Biozentrum, University of Basel, Basel, Switzerland) and used as template to obtain CEP250 full length cDNA by PCR. pENTR-WASF3 [NP_001278894.1] and pENTR-SPATA7 [NP_001035518.1] were a generous gift from Prof. N. Katsanis (Duke University School of Medicine, Durham, US). pENTR-CEP290 was produced using human testis cDNA (Clontech) as starting material. pENTR-ARP3 [NCBI GeneID: 10096] was generated using brain cDNA as input. pENTR-LCA5, pENTR-OFD1 and pENTR-DCTN2 were previously generated in-house.[41] The sequence of all entry clones was verified by Sanger sequencing. Expression constructs for yeast-two-hybrid assay, tandem affinity purification, co-immunoprecipitation or immunolocalization experiments were created by transferring the entry clones into the appropriate destination clones using Gateway Technology (Life Technologies).

2.5.2 Yeast-two-hybrid assay

For the yeast-two-hybrid assays, full length PCARE (aa2-1,289) and the three PCARE fragments (F1-F3, see above) were cloned into a plasmid containing the binding domain of the GAL4 transcription factor (pBD vector, Gateway cloning, Life Technologies). These pBD vectors were used as bait to screen both human (oligo-dT primed) and bovine (random primed) retinal cDNA libraries, as described previously [27].

Interactions were analyzed by assessment of reporter gene (HIS3 and ADE2) activation via growth on selective media and β-galactosidase colorimetric filter lift assays (LacZ reporter gene). cDNA inserts of clones containing putative interaction partners were confirmed by Sanger sequencing.

2.5.3 Cell culture

For co-immunoprecipitation and tandem affinity purification experiments, HEK293T (ATCC® CRL-3216™) cells were grown in DMEM medium (Sigma-Aldrich, D0819) supplemented with 10% FCS (Sigma-Aldrich, F0392), 1% sodium pyruvate (Sigma-Aldrich, S8636) and 1% penicillin/streptavidin (Sigma-Aldrich, P4333). For immunolocalization studies, hTERT RPE-1 (ATCC® CRL-4000™) and mIMCD-3 (ATCC® CRL-2123™) cells were grown in DMEM/F12, supplemented with 10% FCS (Sigma-Aldrich, F0392), 1% sodium pyruvate (Sigma-Aldrich, S8636) and 1% penicillin/streptavidin (Sigma-Aldrich, P4333).

2.5.4 Tandem Affinity Purification

N-terminal and C-terminal Strep-FLAG-PCARE constructs were transfected into HEK293T cells using Effectene Transfection Reagent (QIAGEN). Forty-eight hours post-transfection, cleared cell lysates were obtained by lysing cells in a buffer containing 0.5% Nonidet-P40 (NP-40), protease inhibitor cocktail (Roche), and phosphatase inhibitor cocktails II (Sigma-Aldrich) and III (GBiosciences) in TBS (50 mM Tris-HCl, pH 7.4 and 150 mM NaCl) for 20 min at 4 °C. Cell debris and nuclei were removed by centrifugation at 10,000 *g* for 10 min. The Streptavidin- and FLAG-based tandem affinity purification steps were performed as described previously.[42,43] Five percent of the final eluate was evaluated by SDS-PAGE followed by silver staining, according to standard protocols, while the remaining 95% was subjected to protein precipitation with chloroform and methanol. Protein precipitates were subsequently subjected to mass spectrometry analysis and peptide identification as described before.[44,45]

2.5.5 Antibodies

Rabbit anti-PCARE polyclonal antibody was generated in our lab. A human PCARE C-terminal peptide corresponding to amino acids 1192 to 1286 was selected based on antigenicity, hydrophilicity, surface accessibility and linearity. This peptide was cloned into pGEX-6P vector (Gateway technologies) and expression of the GST-fusion protein was induced in BL21-DE3 cells. The GST-fused antigen was then cleaved by Prescission protease (Sigma-Aldrich), after which the purified antigen was used to immunize rabbits (Eurogentec). Affinity purification of the antibody was achieved by running 6xHis-MBP tagged

PCARE C-terminal peptide on nitrocellulose blots, subsequent binding of serum antibody, and final elutions using an acidic glycine buffer (glycine/HCl 100 mM, pH 2.5). Specificity of the antibody was confirmed by immunocytochemistry and western blot analysis to detect the recombinant PCARE protein (Supplemental Figure 5). All other primary and secondary antibodies used in this study are listed in Supplemental Table 3, including their origin and the antibody dilutions used for each experiment type.

2.5.6 Co-immunoprecipitation

A plasmid expressing 3xHA-PCARE was co-transfected with plasmids expressing 3xFLAG-WASF3, 3xFLAG-OFD1, 3xFLAG-CEP250 and 3xFLAG-CEP290 into HEK293T cells using FuGENE HD Transfection Reagent (Promega) following manufacturer's instructions. As a negative control, 3xHA-PCARE was co-transfected with 3xFLAG-STRAD. The interaction between 3xHA-LCA5 and 3xFLAG-OFD1 was used as positive control[41]. Forty-eight hours post-transfection, cells were washed and lysed on ice using lysis buffer (50 mM Tris-HCl pH 7.5, 150 mM NaCl, 1% NP-40, 10% glycerol) supplemented with cOmplete™ Protease Inhibitor Cocktail (Roche Diagnostics). Lysates were incubated with anti-HA Affinity Matrix beads (SigmaAldrich) and processed as described previously.[41] Beads were precipitated by centrifugation and supernatant was run on NuPAGE Novex 3-8% Tris-Acetate gels. The interactions were assessed by immunoblotting, followed by staining with monoclonal mouse α-FLAG or monoclonal mouse α-HA as primary antibody and goat-anti mouse RDye800 or RDye680 as secondary antibody (Supplemental Table 3).

2.5.7 Western blot analysis

HEK293T cell pellets were resuspended in 150 µl RIPA buffer (50 mM Tris pH 7.5, 1 mM EDTA, 150 mM NaCl, 0.5% Na-Deoxycholate, 1% NP-40 plus protease inhibitors) rotating for 30 min at 4 °C. Cells were sonicated for 15 seconds and centrifuged for 5 min at 12,000 *g*, 4 °C. The supernatant was mixed with loading buffer supplemented with 0.1 M DTT and proteins were separated on a 3-8% NuPAGE Tris-Acetate Gel. Proteins were transferred onto a nitrocellulose membrane (Amersham Protran 0.45 NC, GE Healthcare Life Sciences) overnight at 4 °C. After transfer, membrane was briefly washed in PBS and blocked for 1 h at RT in 5% Blotting-Grade Blocker (Bio-Rad) in PBS. Primary antibodies were incubated overnight in 2.5% blocker (Blotting Grade Blocker Non-Fat Dry Milk, Bio-Rad) in PBS. Subsequently, the membrane was washed three times in PBS-Tween 0.2% at RT and incubated with secondary antibodies in 2.5% blocking milk for 45 min. After secondary antibody incubation, the membrane was washed three

times for 10 min in PBS-Tween 0.2% followed by a finally wash in 1xPBS. Fluorescence was analyzed on a Li-Cor Odyssey 2.1 infrared scanner using Image Studio 4.0 software.

2.5.8 Immunocytochemistry

hTERT RPE-1 or mIMCD-3 cells were grown on 12-well plates until reaching 90% confluency. To induce cilia growth, cells were fed with serum starvation medium (DMEM/F12, 0.2% FCS + 1% Pen/Strep + 1% NaPy). Twenty-four hours post-starvation, cells were transfected with DNA plasmids using lipofectamine 2000 in a 1:2.5 ratio following manufacturer's instructions. Twenty hours post-transfection, cultured cells were fixed in PFA 2% for 20 min at RT, followed by 1% Triton-X-100 treatment for 3 min and blocking in 2% BSA for 20 min. Subsequently, cells were incubated with primary antibodies diluted in blocking solution for 1 h. After incubation, cells were washed three times in PBS and incubated with the corresponding Alexa Fluor conjugated secondary antibody (Supplemental Table 3). Finally, slides were washed three times in PBS for 5 min and mounted in ProLong(R) Gold antifade reagent (P36930, Life Technologies).

2.5.9 Compound treatments

Prior to treatment, hTERT RPE-1 cells were seeded, serum starved and transfected as described above. Cells were treated with cytochalasin D 1.0 µM and 5.0 µM, and CK-666 1 µM, nocodazole 1 µM or Latrunculin B 1 µM for 18 hours before fixation. Cells were fixed and stained as described in the immunocytochemistry section above.

2.5.10 Animals

C57BL/6J JAX™ wild-type mice were purchased from Charles River. *Pcare*$^{-/-}$ mice were previously described.[17] Animal experiments were approved by the national authorities (Centrale Commissie Dierproeven, project number AVD103002016758) and the local animal welfare committee, and conducted according to the regulations of the Association for Research in Vision and Ophthalmology.

2.5.11 Immunohistochemistry

The retina from a 66 year-old female human donor with no history of retinal disease was obtained from the Department of Ophthalmology, University Medical Center Mainz, Germany, adhering to the guidelines of the Declaration of Helsinki (http://www.wma.net/en/30publications/10policies/b3/), and were processed for indirect immunofluorescence staining as described previously.[46] For the mouse sections,

eyes of sacrificed animals were enucleated, embedded in OCT and slowly frozen in liquid nitrogen. Seven-micron cryosections of one-month old wild-type or *Pcare*$^{-/-}$ mouse retinas were used for immunohistochemistry purposes as described before.[47] Primary antibodies were incubated overnight at 4 °C in blocking solution in a humid and dark atmosphere. Subsequently, sections were washed three times in PBS and secondary antibody, including DAPI, was incubated. Finally, sections were washed three times in PBS, mounted in ProLong® Gold Antifade Mountant (ThermoFisher Scientific) and sealed with nail polish. Slides were imaged using a Z1 Axio Imager (Zeiss) microscope.

2.5.12 Electron microscopy (pre-embedding labelling)

Immunoelectron microscopy on mouse retinae (3 months old) was performed as described previously.[48,49] Ultrathin sections were analyzed in a transmission electron microscope (Tecnai 12 BioTwin) and processed as previously described.

2.5.13 Statistical Analysis

To study the size changes in the cilium, the area of bulged cilia (in μm^2) was measured using ImageJ.
In Figure 5, the area was measured in 37 cells for the wild-type (double transfection of hTERT RPE-1 cells with constructs expressing HA-PCARE-WT and HA-WASF3) and 34 cells for the PCARE p.I201F mutant (double transfection of hTERT RPE-1 cells with constructs expressing PCARE-I201F-FLAG and HA-WASF3). For the comparison in figure 5, the p-value = 0,0001; t=4,207; df=42.
In Figure 6, the area of the bulged cilia was measured using ImageJ in 44 cells for the control (double transfection of hTERT RPE-1 cells with constructs expressing PCARE-FLAG and HA-WASF3), 39 cells for OFD1 (triple transfection of hTERT RPE-1 cells with constructs expressing PCARE-FLAG, HA-WASF3 and HA-OFD1) and 41 cells for SPATA7 (triple transfection of hTERT RPE-1 cells with constructs expressing PCARE-FLAG, HA-WASF3 and HA-SPATA7). For control *vs*. OFD1, p-value = 0,0032; t=3,054; df=72. For control *vs*. SPATA7, p-value = 0,0013; t=3,351; df=76.
Statistical analysis was performed using a two-tailed Student t-test with Welch's correction.

2.6 References

1. Anderson, D.H., Fisher, S.K., and Steinberg, R.H. (1978). Mammalian cones: disc shedding, phagocytosis, and renewal. Invest Ophthalmol Vis Sci 17, 117-133.
2. Nilsson, S.E. (1964). Receptor Cell Outer Segment Development and Ultrastructure of the Disk Membranes in the Retina of the Tadpole (Rana Pipiens). J Ultrastruct Res 11, 581-602.
3. Goldberg, A.F., and Molday, R.S. (1996). Defective subunit assembly underlies a digenic form of retinitis pigmentosa linked to mutations in peripherin/rds and rom-1. Proc Natl Acad Sci U S A 93, 13726-13730.
4. Roepman, R., and Wolfrum, U. (2007). Protein networks and complexes in photoreceptor cilia. Subcell Biochem 43, 209-235.
5. Young, R.W. (1967). The renewal of photoreceptor cell outer segments. J Cell Biol 33, 61-72.
6. Burgoyne, T., Meschede, I.P., Burden, J.J., Bailly, M., Seabra, M.C., and Futter, C.E. (2015). Rod disc renewal occurs by evagination of the ciliary plasma membrane that makes cadherin-based contacts with the inner segment. Proc Natl Acad Sci U S A 112, 15922-15927.
7. Steinberg, R.H., Fisher, S.K., and Anderson, D.H. (1980). Disc morphogenesis in vertebrate photoreceptors. J Comp Neurol 190, 501-508.
8. Chaitin, M.H., Schneider, B.G., Hall, M.O., and Papermaster, D.S. (1984). Actin in the photoreceptor connecting cilium: immunocytochemical localization to the site of outer segment disk formation. J Cell Biol 99, 239-247.
9. Arikawa, K., and Williams, D.S. (1989). Organization of actin filaments and immunocolocalization of alpha-actinin in the connecting cilium of rat photoreceptors. J Comp Neurol 288, 640-646.
10. Williams, D.S., Linberg, K.A., Vaughan, D.K., Fariss, R.N., and Fisher, S.K. (1988). Disruption of microfilament organization and deregulation of disk membrane morphogenesis by cytochalasin D in rod and cone photoreceptors. J Comp Neurol 272, 161-176.
11. Collin, R.W.J., Safieh, C., Littink, K.W., Shalev, S.A., Garzozi, H.J., Rizel, L., Abbasi, A.H., Cremers, F.P.M., den Hollander, A.I., Klevering, B.J., et al. (2010). Mutations in C2ORF71 cause autosomal-recessive retinitis pigmentosa. Am J Hum Genet 86, 783-788.
12. Nishimura, D.Y., Baye, L.M., Perveen, R., Searby, C.C., Avila-Fernandez, A., Pereiro, I., Ayuso, C., Valverde, D., Bishop, P.N., Manson, F.D., et al. (2010). Discovery and functional analysis of a retinitis pigmentosa gene, C2ORF71. Am J Hum Genet 86, 686-695.
13. Godsel, L.M., and Engman, D.M. (1999). Flagellar protein localization mediated by a calcium-myristoyl/palmitoyl switch mechanism. EMBO J 18, 2057-2065.
14. Reiter, J.F., and Leroux, M.R. (2017). Genes and molecular pathways underpinning ciliopathies. Nat Rev Mol Cell Biol.
15. Suetsugu, S., Miki, H., and Takenawa, T. (1999). Identification of two human WAVE/SCAR homologues as general actin regulatory molecules which associate with the Arp2/3 complex. Biochem Biophys Res Commun 260, 296-302.
16. Jensen, L.J., and Bork, P. (2008). Biochemistry. Not comparable, but complementary. Science 322, 56-57.
17. Kevany, B.M., Zhang, N., Jastrzebska, B., and Palczewski, K. (2015). Animals deficient in C2Orf71, an autosomal recessive retinitis pigmentosa-associated locus, develop severe early-onset retinal degeneration. Hum Mol Genet 24, 2627-2640.
18. MacLean-Fletcher, S., and Pollard, T.D. (1980). Mechanism of action of cytochalasin B on actin. Cell 20, 329-341.
19. Spector, I., Shochet, N.R., Blasberger, D., and Kashman, Y. (1989). Latrunculins--novel marine macrolides that disrupt microfilament organization and affect cell growth: I. Comparison with cytochalasin D. Cell Motil Cytoskeleton 13, 127-144.
20. Penzes, P., Johnson, R.C., Alam, M.R., Kambampati, V., Mains, R.E., and Eipper, B.A. (2000). An isoform of kalirin, a brain-specific GDP/GTP exchange factor, is enriched in the postsynaptic density fraction. J Biol Chem 275, 6395-6403.
21. Chen, B., Chou, H.T., Brautigam, C.A., Xing, W., Yang, S., Henry, L., Doolittle, L.K., Walz, T., and Rosen, M.K. (2017). Rac1 GTPase activates the WAVE regulatory complex through two distinct binding sites. Elife 6.
22. Bisi, S., Disanza, A., Malinverno, C., Frittoli, E., Palamidessi, A., and Scita, G. (2013). Membrane and actin dynamics interplay at lamellipodia leading edge. Curr Opin Cell Biol 25, 565-573.
23. Goldberg, A.F., Moritz, O.L., and Williams, D.S. (2016). Molecular basis for photoreceptor outer segment architecture. Prog Retin Eye Res 55, 52-81.

24. Estrada-Cuzcano, A., Roepman, R., Cremers, F.P., den Hollander, A.I., and Mans, D.A. (2012). Non-syndromic retinal ciliopathies: translating gene discovery into therapy. Hum Mol Genet 21, R111-124.
25. Bujakowska, K.M., Liu, Q., and Pierce, E.A. (2017). Photoreceptor Cilia and Retinal Ciliopathies. Cold Spring Harb Perspect Biol 9.
26. Nachury, M.V., Loktev, A.V., Zhang, Q., Westlake, C.J., Peranen, J., Merdes, A., Slusarski, D.C., Scheller, R.H., Bazan, J.F., Sheffield, V.C., et al. (2007). A core complex of BBS proteins cooperates with the GTPase Rab8 to promote ciliary membrane biogenesis. Cell 129, 1201-1213.
27. Letteboer, S.J., and Roepman, R. (2008). Versatile screening for binary protein-protein interactions by yeast two-hybrid mating. Methods Mol Biol 484, 145-159.
28. Michelot, A., and Drubin, D.G. (2011). Building distinct actin filament networks in a common cytoplasm. Curr Biol 21, R560-569.
29. Rottner, K., Faix, J., Bogdan, S., Linder, S., and Kerkhoff, E. (2017). Actin assembly mechanisms at a glance. J Cell Sci 130, 3427-3435.
30. Chen, Z., Borek, D., Padrick, S.B., Gomez, T.S., Metlagel, Z., Ismail, A.M., Umetani, J., Billadeau, D.D., Otwinowski, Z., and Rosen, M.K. (2010). Structure and control of the actin regulatory WAVE complex. Nature 468, 533-538.
31. Djinovic-Carugo, K., Gautel, M., Ylanne, J., and Young, P. (2002). The spectrin repeat: a structural platform for cytoskeletal protein assemblies. FEBS Lett 513, 119-123.
32. Mullins, R.D., Heuser, J.A., and Pollard, T.D. (1998). The interaction of Arp2/3 complex with actin: nucleation, high affinity pointed end capping, and formation of branching networks of filaments. Proc Natl Acad Sci U S A 95, 6181-6186.
33. Dominguez, R. (2016). The WH2 Domain and Actin Nucleation: Necessary but Insufficient. Trends Biochem Sci 41, 478-490.
34. Wu, J.H., Fanaroff, A.C., Sharma, K.C., Smith, L.S., Brian, L., Eipper, B.A., Mains, R.E., Freedman, N.J., and Zhang, L. (2013). Kalirin promotes neointimal hyperplasia by activating Rac in smooth muscle cells. Arterioscler Thromb Vasc Biol 33, 702-708.
35. Breitsprecher, D., Kiesewetter, A.K., Linkner, J., Urbanke, C., Resch, G.P., Small, J.V., and Faix, J. (2008). Clustering of VASP actively drives processive, WH2 domain-mediated actin filament elongation. EMBO J 27, 2943-2954.
36. Carss, K.J., Arno, G., Erwood, M., Stephens, J., Sanchis-Juan, A., Hull, S., Megy, K., Grozeva, D., Dewhurst, E., Malka, S., et al. (2017). Comprehensive Rare Variant Analysis via Whole-Genome Sequencing to Determine the Molecular Pathology of Inherited Retinal Disease. Am J Hum Genet 100, 75-90.
37. Khateb, S., Zelinger, L., Mizrahi-Meissonnier, L., Ayuso, C., Koenekoop, R.K., Laxer, U., Gross, M., Banin, E., and Sharon, D. (2014). A homozygous nonsense CEP250 mutation combined with a heterozygous nonsense C2orf71 mutation is associated with atypical Usher syndrome. J Med Genet 51, 460-469.
38. Arts, H.H., Doherty, D., van Beersum, S.E., Parisi, M.A., Letteboer, S.J., Gorden, N.T., Peters, T.A., Marker, T., Voesenek, K., Kartono, A., et al. (2007). Mutations in the gene encoding the basal body protein RPGRIP1L, a nephrocystin-4 interactor, cause Joubert syndrome. Nat Genet 39, 882-888.
39. den Hollander, A.I., Koenekoop, R.K., Mohamed, M.D., Arts, H.H., Boldt, K., Towns, K.V., Sedmak, T., Beer, M., Nagel-Wolfrum, K., McKibbin, M., et al. (2007). Mutations in LCA5, encoding the ciliary protein lebercilin, cause Leber congenital amaurosis. Nat Genet 39, 889-895.
40. Megaw, R., Abu-Arafeh, H., Jungnickel, M., Mellough, C., Gurniak, C., Witke, W., Zhang, W., Khanna, H., Mill, P., Dhillon, B., et al. (2017). Gelsolin dysfunction causes photoreceptor loss in induced pluripotent cell and animal retinitis pigmentosa models. Nat Commun 8, 271.
41. Coene, K.L., Roepman, R., Doherty, D., Afroze, B., Kroes, H.Y., Letteboer, S.J., Ngu, L.H., Budny, B., van Wijk, E., Gorden, N.T., et al. (2009). OFD1 is mutated in X-linked Joubert syndrome and interacts with LCA5-encoded lebercilin. Am J Hum Genet 85, 465-481.
42. Boldt, K., van Reeuwijk, J., Gloeckner, C.J., Ueffing, M., and Roepman, R. (2009). Tandem affinity purification of ciliopathy-associated protein complexes. Methods in cell biology 91, 143-160.
43. Gloeckner, C.J., Boldt, K., Schumacher, A., Roepman, R., and Ueffing, M. (2007). A novel tandem affinity purification strategy for the efficient isolation and characterisation of native protein complexes. Proteomics 7, 4228-4234.

44. Texier, Y., Toedt, G., Gorza, M., Mans, D.A., van Reeuwijk, J., Horn, N., Willer, J., Katsanis, N., Roepman, R., Gibson, T.J., et al. (2014). Elution profile analysis of SDS-induced subcomplexes by quantitative mass spectrometry. Molecular & cellular proteomics : MCP 13, 1382-1391.
45. Boldt, K., van Reeuwijk, J., Lu, Q., Koutroumpas, K., Nguyen, T.M., Texier, Y., van Beersum, S.E., Horn, N., Willer, J.R., Mans, D.A., et al. (2016). An organelle-specific protein landscape identifies novel diseases and molecular mechanisms. Nat Commun 7, 11491.
46. Overlack, N., Kilic, D., Bauss, K., Marker, T., Kremer, H., van Wijk, E., and Wolfrum, U. (2011). Direct interaction of the Usher syndrome 1G protein SANS and myomegalin in the retina. Biochim Biophys Acta 1813, 1883-1892.
47. Garanto, A., Chung, D.C., Duijkers, L., Corral-Serrano, J.C., Messchaert, M., Xiao, R., Bennett, J., Vandenberghe, L.H., and Collin, R.W. (2016). In vitro and in vivo rescue of aberrant splicing in CEP290-associated LCA by antisense oligonucleotide delivery. Hum Mol Genet 25, 2552-2563.
48. Sedmak, T., Sehn, E., and Wolfrum, U. (2009). Immunoelectron microscopy of vesicle transport to the primary cilium of photoreceptor cells. Methods Cell Biol 94, 259-272.
49. Sedmak, T., and Wolfrum, U. (2010). Intraflagellar transport molecules in ciliary and nonciliary cells of the retina. J Cell Biol 189, 171-186.

2.7 Acknowledgements

We thank Lisette Hetterschijt, Elisabeth Sehn and Gabriele B. Stern-Schneider for technical assistance, Drs. Erich Nigg and Nicholas Katsanis for providing expression constructs, Dr. Carsten Janke for providing antibodies, and Dr. Zhiqian Dong (CWRU), Dr. Wendy Sun (CWRU) and David Peck (CWRU) for technical help on *Pcare*$^{-/-}$ mouse experiments. This work was funded by the FP7-PEOPLE-2012-ITN programme EyeTN, Brussels, Belgium (grant agreement no.: 317472) to RWJC, the Tistou & Charlotte Kerstan Stiftung to MU, the European Community's Seventh Framework FP7/2009 programme SYSCILIA (grant agreement no: 241955) to UW, MU, and RR, by the Netherlands Organization for Scientific Research (NWO Vici-865.12.005) to RR, and by The Netherlands Organisation for Health Research and Development (ZonMW-91216051) to RR and RWJC.

2.8 Supplemental Data

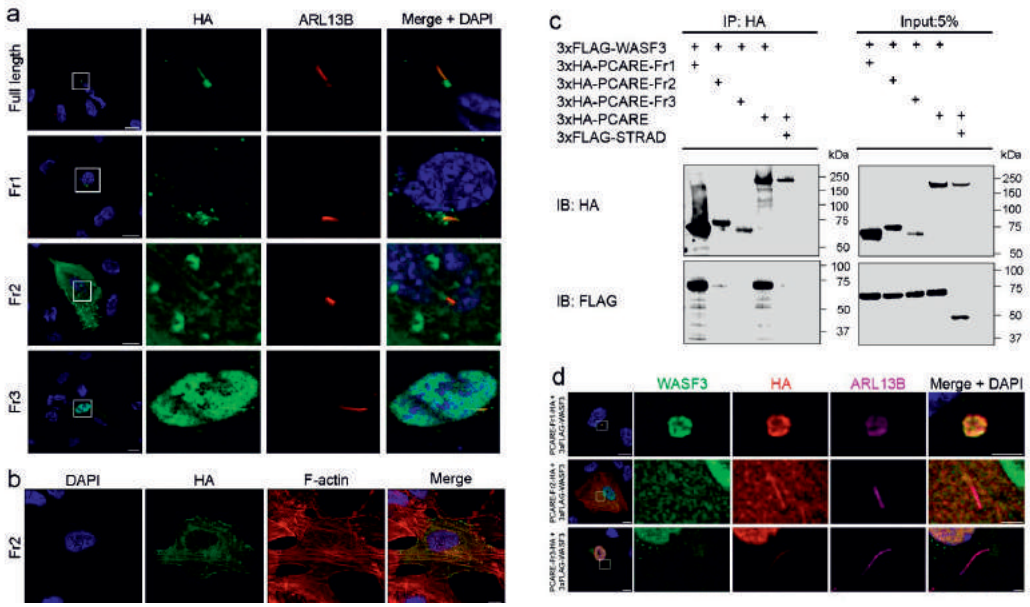

Supplemental Figure 1. Intracellular localization of PCARE fragments and validation of their interaction with WASF3. a, Subcellular localization of PCARE full length and three fragments. hTERT RPE-1 cells were transfected with constructs encoding C-terminally HA-tagged full length PCARE or fragments 1, 2 or 3 (Fr1, Fr2, Fr3). PCARE was detected using anti-HA antibody (green). ARL13B (red) was used as a marker of the axonemal cilium. Nuclei were stained with DAPI (blue). **b,** Localization of C-terminally HA-tagged PCARE-Fr2 (anti-HA staining, green) to filamentous structures, co-localizing with F-actin (phalloidin staining, red) . Scale bars are 20 µm (b), and 10 µm (c). **c.** PCARE fragments Fr1, Fr2 and Fr3 fused to HA were co-transfected with 3xFLAG-WASF3 in HEK293T cells. The interaction between full length PCARE and WASF3 was used as a positive control, while the protein 3xFLAG-STRAD was used as a negative control. In addition, a non-transfected control was taken along. Notice that WASF3 is present in the immunoprecipitated fraction when co-transfected with PCARE-Fr1-HA, and only at low levels when co-expressed with PCARE-Fr2. **d**, Subcellular localization of PCARE fragments when co-transfected with WASF3 in hTERT RPE-1 cells. PCARE fragments were detected using anti-HA antibodies (red) and WASF3 using anti-WASF3 (green). ARL13B (purple) was used as axonemal marker. While all PCARE fragments are able to locate to the cilium, only PCARE-Fr1 is able to transport WASF3 into the cilium and generate ciliary evaginations. Scale bar: 10 µm, for insets: 2.0 µm.

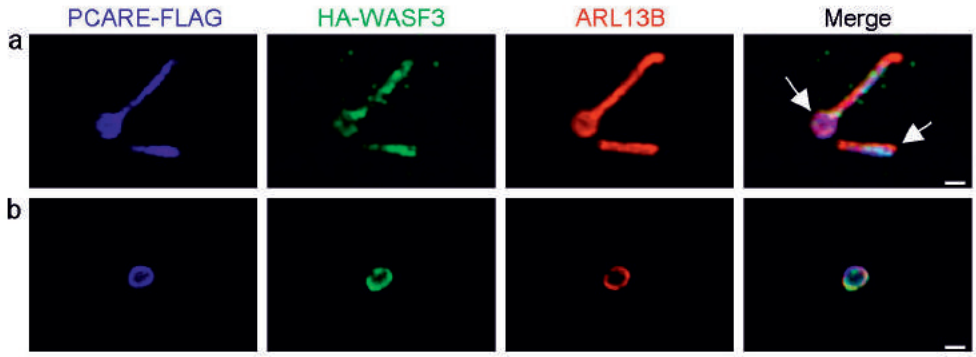

Supplemental Figure 2. Ciliary membrane evaginations in murine inner medullary collecting duct (mIMCD-3) cells. mIMCD-3 cells were co-transfected with constructs expressing HA-WASF3 and PCARE-FLAG cells and stained with antibodies recognizing PCARE (blue), WASF3 (green) and the ciliary membrane marker ARL13B (red). In **a,** the ciliary evagination is visible at one end of the primary cilium (arrows). In **b,** a completely modified cilium with disc-like appearance of the ciliary membrane evagination is shown, with all three detected proteins colocalizing at the periphery of the structure, indicating close proximity to the ciliary membrane. Scale bars are 1 µm.

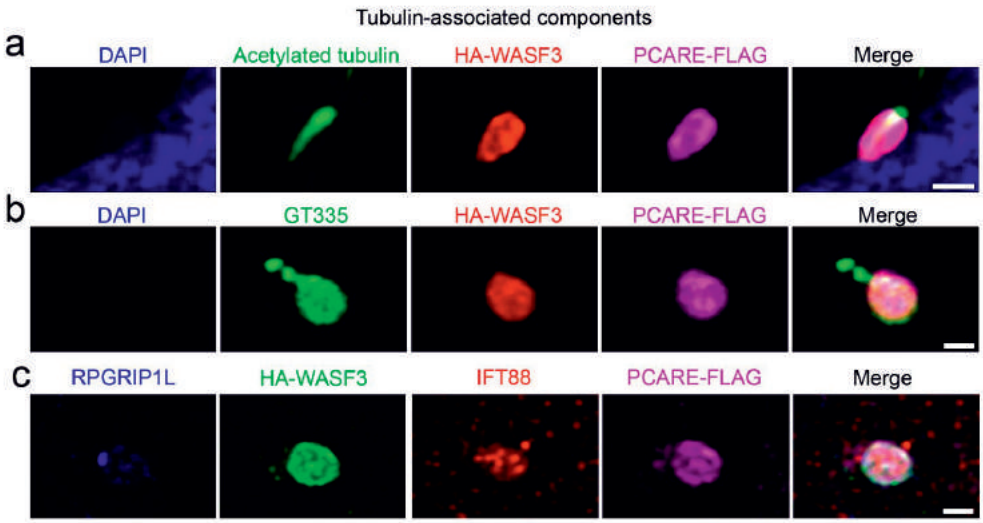

Supplemental Figure 3. Localization of tubulin-associated components in the ciliary membrane evaginations. Ciliated hTERT RPE-1 cells were transfected with plasmids expressing PCARE-FLAG and HA-WASF3 (**a-c**) and stained with antibodies directed against: **a**, acetylated tubulin (green), WASF3 (red), PCARE (purple); **b**, polyglutamylated tubulin GT335 (green), WASF3 (red), PCARE (purple); **c**, RPGRIP1L (blue), WASF3 (green), IFT88 (red), PCARE (purple). Scale bars are 1 µm.

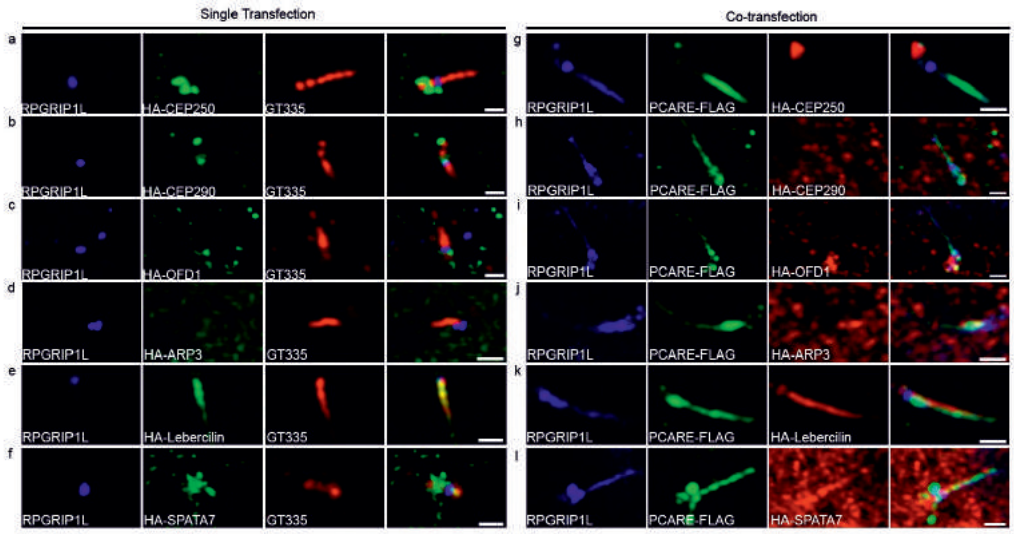

Supplemental Figure 4. Localization of PCARE interacting proteins in hTERT RPE-1 cells. Ciliated hTERT RPE-1 cells were either transfected with plasmids expressing PCARE interacting proteins (**a-f**) or co-transfected with these plasmids and plasmids expressing PCARE-FLAG (**g-l**) to study the ciliary localization of PCARE in presence of the following proteins: **a**, **g**, CEP250, **b**, **h**, CEP290, **c**, **i**, OFD1, **d**, **j**, ARP3, **e**, **k**, Lebercilin and **f**, **l**, SPATA7. In single transfected cells, GT335 (red) marks the ciliary axoneme (**a-f**). In co-transfected cells, PCARE-FLAG (green) decorates the entire cilium (**g-l**). RPGRIP1L (blue) was used as transition zone marker (**a-l**). Interestingly, PCARE is able to transport RPGRIP1L, ARP3 and SPATA7 into the axoneme of the cilium, but not CEP250, CEP290 or OFD1. Scale bars are 1 µm.

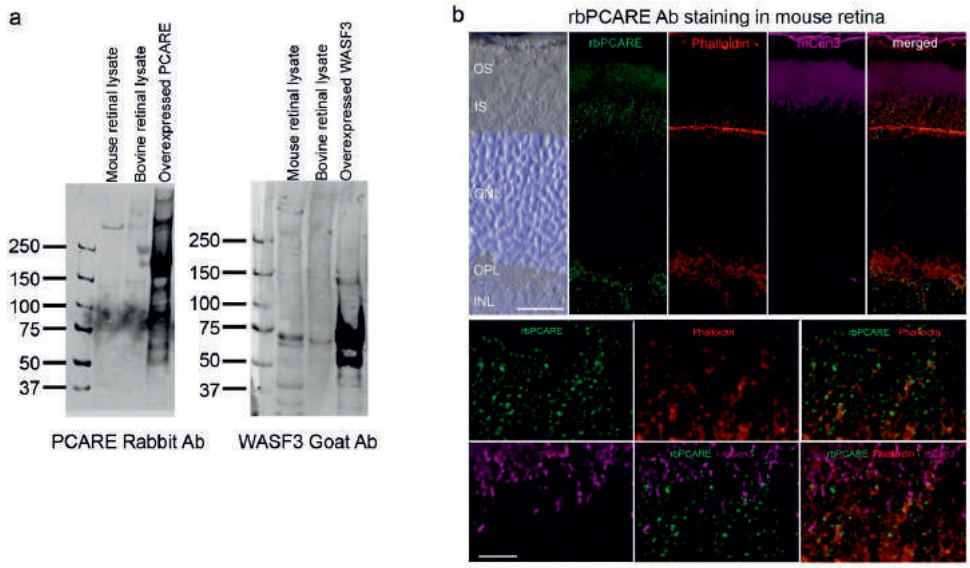

Supplemental Figure 5. Antibody characterization. a, PCARE and WASF3 antibody test in mouse and bovine retina lysates. Blot was incubated with PCARE and WASF3 antibodies, respectively. The first line corresponds to mouse retinal lysate, the second line to bovine retinal lysate, and the third line to a lysate of HEK293T cells transfected with either PCARE or WASF3 construct. A band at the expected size of ~140kDa can be observed when incubating the blot with PCARE antibody. A second, stronger band can be also observed at ~280 kDa. A band for WASF3 can be observed at ~55 kDa in all three lysates. **b**, Immunohistochemistry in mouse retina using PCARE antibody. While there is observable staining at the inner segment (IS) and connecting cilium (CC) region, it does not seem to be specific. Scale bars = 25 µm (upper panel), 10 µm (lower panel). OS: Outer Segments; IS: Inner Segments; ONL: Outer Nuclear Layer; OPL: Outer Plexiform Layer; INL: Inner Nuclear Layer.

Supplemental Table 1. PCARE interactors found in the yeast-2-hybrid experiments. **A**, results of the yeast-2-hybrid screen on human retinal cDNA library and **B**, results of the yeast-2-hybrid screen on bovine retinal cDNA library. Number of clones = number of colonies growing after library mating, sequence verified. All clones were confirmed by co-transformation with the correspondent PCARE fragment. Number of unique clones = number of single clones based on sequence. PCARE fragment used in the screen; F1: amino acid 2 to 459, F2: amino acid 450-900, F3: amino acid 901-1289, FL: amino acid 2-1289.

A	Yeast-2-Hybrid screen on human retinal cDNA library					
	Gene ID	**Gene Full Name**	**EntrezGeneID**	**N° of clones**	**N° of unique clones**	**PCARE Fragment**
	CDR2	Cerebellar Degeneration-Related Protein 2	1039	70	9	F1, F2, FL
	PCM1	Pericentriolar Material 1	5108	9	1	F1
	NINL	Ninein-like	22981	2	2	F2
	ACTN1	Actinin, Alpha 1	87	2	1	F2
	DCTN2	Dynactin 2 (P50)	10540	2	1	F1
	KIF20A	Kinesin Family Member 20A	8481	2	1	F1
	CCDC148	Coiled-Coil Domain Containing 148	10112	1	1	F1
	HSBP1	Heat Shock Factor Binding Protein 1	130940	1	1	F1
	KNSTRN	Kinetochore-Localized Astrin/SPAG5 Binding Protein	3281	1	1	F1
	OFD1	Oral-Facial-Digital Syndrome 1	90417	1	1	F1

B	Yeast-2-Hybrid screen on bovine retinal cDNA library					
	Gene ID	**Gene Full Name**	**EntrezGeneID**	**N° of clones**	**N° of unique clones**	**PCARE Fragment**
	CDR2	Cerebellar Degeneration-Related Protein 2	1039	14	2	F1, FL
	FILIP1L	Filamin A Interacting Protein 1-Like	11259	11	1	F1
	AKAP9	A Kinase (PRKA) Anchor Protein 9	10142	10	2	F1
	WASF3	WAS Protein Family, Member 3	10810	8	1	F1
	ANKHD1	Ankyrin Repeat And KH Domain Containing 1	54882	7	1	F1
	DCTN1	Dynactin 1	1639	3	2	F1
	GOLGA3	Golgin A3	2802	2	2	F1
	CCDC150	Coiled-Coil Domain Containing 150	284992	2	1	F1
	EMILIN3	Elastin Microfibril Interfacer 3	90187	2	1	F1
	IFFO1	Intermediate Filament Family Orphan 1	25900	2	1	F1
	IL4I1	Interleukin 4 Induced 1	259307	2	1	F1
	KANSL1	KAT8 Regulatory NSL Complex Subunit 1	284058	2	1	F1

CEP295	Centrosomal Protein 295kDa	85459	2	1	F1
SPTBN2	Spectrin, Beta, Non-Erythrocytic 2	6712	2	1	F1
SPTBN5	Spectrin, Beta, Non-Erythrocytic 5	51332	2	1	F1
TAX1BP1	Tax1 (Human T-Cell Leukemia Virus Type I) Binding Protein 1	8887	2	1	F1
ANGPTL2	Angiopoietin-Like Protein 2 3	23452	1	1	F1
CEP250	Centrosomal Protein 250kDa	11190	1	1	F1
CEP290	Centrosomal Protein 290kDa	80184	1	1	F2
KALRN	Kalirin, RhoGEF Kinase	8997	1	1	F2
KLC4	Kinesin Light Chain 4	89953	1	1	F1
BORCS5	BLOC-1-related complex subunit 5	118426	1	1	F1
LRRC70	Leucine Rich Repeat Containing 70	100130733	1	1	F1
NBPF12	Neuroblastoma Breakpoint Family, Member 12	149013	1	1	F1
NEFH	Neurofilament, Heavy Polypeptide	4744	1	1	F2
RABEP1	Rabaptin, RAB GTPase Binding Effector Protein 1	9135	1	1	F1
RNF40	Ring Finger Protein 40, E3 Ubiquitin Protein Ligase	9810	1	1	F1
SPICE1	Spindle and centriole associated protein 1	152185	1	1	F1
SYBU	Syntabulin (Syntaxin-Interacting)	55638	1	1	F1
TPR	Translocated Promoter Region, Nuclear Basket Protein	7175	1	1	F1
KLC2	Kinesin Light Chain 2	64837	1	1	F1
TEF	Thyrotrophic Embryonic Factor	7008	1	1	FL

FL: full-length PCARE
F1: PCARE fragment 1
F2: PCARE fragment 2
F3: PCARE fragment 3

Actin dynamics*
Centrosome/centriole*
Microtubule*

*Color coding also valid for supplemental table 2

Supplemental Table 2. TAP-MS protein identifications from HEK293T cells for PCARE N- or C-terminally SF-tagged proteins. The last column (PMID_27173435_TAPbaitCount) provides the number of different bait proteins that identified this protein in similar TAP-MS experiments as a reference for specificity of identification in this study.

Symbol	Entrez GeneID	unique peptides 1	sequence coverage 1	unique peptides 2	sequence coverage 2	unique peptides 3	sequence coverage 3	unique peptides 4	sequence coverage 4	unique peptides 5	sequence coverage 5	unique peptides 6	sequence coverage 6	PMID_27173435_TAPbaitCount
		NTAP_PCARE_exp1	NTAP_PCARE_exp1	NTAP_PCARE_exp2	NTAP_PCARE_exp2	NTAP_PCARE_exp3	NTAP_PCARE_exp3	NTAP_PCARE_exp4	NTAP_PCARE_exp4	CTAP_PCARE_exp5	CTAP_PCARE_exp5	CTAP_PCARE_exp6	CTAP_PCARE_exp6	Out of 217
ABCB1	5243							6	0.048					2
ABCB10	23456			10	0.141	7	0.102	7	0.091					1
ABHD12	26090					2	0.050	3	0.070					5
ACACA	31			2	0.008	9	0.047	21	0.112					176
ACTB	60	16	0.611	14	0.485	14	0.395	14	0.405					179
ACTR3	10096	6	0.206	7	0.213	8	0.230	6	0.132					4
ACTR3B	57180					2	0.091	2	0.112					0
AHCY	191					2	0.053	5	0.127					25
AIFM1	9131					2	0.056	2	0.039					149
ALB	213			3	0.051	3	0.049	2	0.036					154
ANXA1	301									2	0.072			22
ANXA2	302											4	0.109	89
ARG1	383											2	0.062	77
ARPC1A	10552					3	0.092	3	0.097					0
ARPC1B	10095					2	0.075	2	0.075					1
ARPC2	10109					3	0.097	2	0.077					0
ARPC3	10094	2	0.135	3	0.174	5	0.253	4	0.242					1
ARPC4	10093					2	0.119	2	0.119					2
ATP1A1	476					2	0.024	6	0.078					120
ATP5A1	498					8	0.165	9	0.161					135
ATP5B	506					3	0.085	3	0.085					102
ATP5C1	509							2	0.074					100
ATP5D	513							2	0.137					10
ATP5O	539					2	0.108							15
BAG2	9532					5	0.213	5	0.218					94

BAG3	9531					8	0.202	4	0.085					3
BAG4	9530					4	0.118	5	0.164					2
BAG5	9529					5	0.157	6	0.166					33
BCAP31	10134					2	0.102	2	0.069					8
BSG	682					2	0.073	2	0.073					69
C2orf71 (PCARE)	388939	87	0.733	83	0.719	129	0.791	116	0.800	58	0.487	48	0.418	1
CAD	790					11	0.068	8	0.039					138
CANX	821					9	0.157	11	0.182					99
CASP14	23581											2	0.095	113
CCDC138	165055							3	0.054					1
CCDC50	152137							2	0.065					0
CCDC87	55231							3	0.029					0
CCT2	10576					2	0.049	2	0.067					122
CCT4	10575					2	0.048	3	0.056					139
CCT5	22948					6	0.115	6	0.135					136
CCT6A	908					5	0.102	7	0.136					129
CCT7	10574					2	0.026							120
CCT8	10694					4	0.088	2	0.044					139
CDK13	8621					2	0.013							1
CDSN	1041											2	0.051	51
CENPJ	55835					3	0.019							0
CISD3	284106					2	0.087							5
CKAP4	10970			2	0.041	8	0.173	10	0.211					25
CPVL	54504			2	0.038			2	0.038					32
CS	1431					2	0.054	2	0.054					2
CSTA	1475											2	0.194	104
CTU1	90353							2	0.069					1
DCAF7	10238	5	0.178	7	0.260	8	0.284	5	0.208					12
DCAF8	50717					3	0.067	5	0.097					19
DCD	117159							3	0.327	2	0.200	2	0.200	160
DCTN2	10540					7	0.227	3	0.080					24

DDB1	1642	2	0.018	5	0.039	17	0.179	16	0.136				130
DNAJC10	54431							2	0.023				6
DNAJC7	7266							2	0.051				41
DSC1	1823							2	0.032	3	0.041		124
DSG1	1828									7	0.079		138
DSP	1832							3	0.011	22	0.075		136
EEF1A1	1915	2	0.074			4	0.097	2	0.048	2	0.050		195
ELL	8178					3	0.056	6	0.077				1
ENAH	55740	32	0.504	28	0.418	37	0.503	33	0.494	2	0.054		4
ERCC3	2071					3	0.072						0
ESYT2	57488					2	0.024	4	0.058				36
EXOG	9941							2	0.076				2
FABP5	2171									2	0.133		91
FBXO17	115290					4	0.162	2	0.086				0
FBXW11	23291					7	0.157	3	0.048				2
FKBP10	60681					2	0.052						0
FLG	2312							4	0.010	5	0.008		123
FLG2	388698									6	0.031		165
FLNA	2316					2	0.013						17
GALNT2	2590					2	0.063	2	0.049				1
GAPDH	2597					3	0.087	3	0.116	3	0.125		147
GGCT	79017									3	0.170		48
GID8	54994					4	0.246						12
GRPEL1	80273							2	0.129				1
GSN	2934					5	0.084						2
HACD3	51495							2	0.088				91
HRNR	388697							7	0.052	7	0.047		156
HSD17B10	3028					4	0.291	2	0.077				5
HSD17B4	3295							3	0.073				3
HSP90AA1	3320					4	0.057	3	0.044				169
HSP90AB1	3326					4	0.087	4	0.066				180

HSPA1A	3303	94	0.743	88	0.761	120	0.871	120	0.841	64	0.588	54	0.538	214
HSPA1B	3304	94	0.743	88	0.761	120	0.871	120	0.841	64	0.588	54	0.538	214
HSPA1L	3305	2	0.321			3	0.374	3	0.401					64
HSPA2	3306					2	0.254							43
HSPA4	3308	43	0.665	36	0.515	50	0.670	52	0.679	22	0.343	8	0.123	156
HSPA4L	22824	27	0.470	20	0.358	26	0.414	34	0.490	4	0.097	5	0.092	105
HSPA5	3309	26	0.526	27	0.531	38	0.606	35	0.564	10	0.265	3	0.096	208
HSPA8	3312	38	0.675	32	0.656	38	0.686	42	0.698	29	0.554	22	0.437	214
HSPA9	3313	28	0.498	29	0.533	41	0.594	41	0.504	10	0.222	5	0.091	203
HSPD1	3329					2	0.044							133
HSPH1	10808	28	0.443	25	0.355	28	0.435	23	0.350	10	0.141	5	0.070	152
HYOU1	10525					2	0.019							1
IFFO1	25900							2	0.079					1
IFFO2	126917							4	0.099					0
IFT57	55081					2	0.058							9
IFT74	80173							2	0.040					21
IMPDH2	3615							2	0.056					57
IRS4	8471					6	0.056	3	0.045					129
JUP	3728											8	0.103	122
TMEM131L	23240							3	0.017					0
KIF20A	10112					2	0.024							0
KPRP	448834											4	0.071	149
KRT1	3848	18	0.332	21	0.337	19	0.307	33	0.506	28	0.498	40	0.543	192
KRT10	3858	14	0.298	23	0.509	17	0.289	35	0.604	21	0.409	38	0.608	191
KRT13	3860									7	0.236			77
KRT14	3861					2	0.112	13	0.345	7	0.225	21	0.549	187
KRT16	3868							4	0.243			6	0.349	159
KRT17	3872											3	0.225	143
KRT2	3849	14	0.261	19	0.385	20	0.401	36	0.723	24	0.510	36	0.648	192
KRT4	3851									11	0.275			63
KRT5	3852			2	0.085	3	0.120	7	0.200	9	0.227	19	0.412	186

KRT6A	3853							5	0.239			9	0.387	171
KRT6B	3854											2	0.371	101
KRT6C	286887									7	0.301	2	0.387	76
KRT78	196374											3	0.092	104
KRT80	144501											2	0.082	52
KRT9	3857	8	0.185	12	0.230	22	0.612	21	0.470	21	0.414	31	0.650	192
LANCL1	10314							2	0.050					1
LCLAT1	253558					3	0.070	2	0.056					0
LIMA1	51474							2	0.032					1
LRP1	4035							2	0.006					3
LRRC59	55379	2	0.098	5	0.218	3	0.088	4	0.140					11
LYZ	4069											2	0.101	64
MAD2L1	4085					3	0.122	2	0.117					86
MAEA	10296							2	0.071					12
MAPK1	5594							2	0.083					10
MOGS	7841							2	0.037					21
MYH9	4627					5	0.027	4	0.025					28
MYL12A	10627			2		0.180								4
MYL12B	103910			2		0.180								3
NCL	4691					2	0.025	2	0.025					60
NIPSNAP1	8508					2	0.067							5
NIPSNAP3A	25934					3	0.126	3	0.126					0
OGFOD3	79701	2	0.053	2	0.053	4	0.135	2	0.053					2
PCCA	5095					2	0.026	4	0.069					62
PCCB	5096					3	0.063	4	0.089					69
PCM1	5108							2	0.009					5
PFN1	5216					4	0.350	2	0.179					22
PFN2	5217					2	0.186	4	0.343					2
PGAM5	192111					2	0.066	8	0.343					75
PGRMC1	10857					2	0.113							67
PHGDH	26227					2	0.038							118

PIP4K2C	79837					2	0.074	2	0.038					5
PITRM1	10531	11	0.140	23	0.289	25	0.321	26	0.343					1
POLDIP2	26073					2	0.065							3
PPIA	5478			3	0.152	2	0.127	2	0.127					51
PPM1B	5495					3	0.063	5	0.125					40
PPP1R9B	84687					4	0.074	6	0.087					2
PPP2CB	5516						5	0.204						18
PPP2R1A	5518					7	0.156	7	0.115					63
PPP2R2A	5520					5	0.114	5	0.107					31
PRDX1	5052					5	0.427	7	0.412			2	0.151	131
PRDX3	10935					3	0.145	4	0.195					19
PRDX4	10549	3	0.125	2	0.055	9	0.432	8	0.347			2	0.066	68
PRMT5	10419	2	0.047			10	0.171	19	0.338	5	0.088	4	0.056	162
PSMD2	5708							2	0.025					53
PSMD3	5709							2	0.045					70
PTPRF	5792					3	0.029	2	0.019					6
PTPRU	10076					3	0.026							2
RPN1	6184							4	0.074					77
RUVBL1	8607	6	0.154	6	0.180	12	0.366	12	0.355					140
RUVBL2	10856	3	0.097	4	0.106	12	0.371	15	0.406					139
S100A9	6280							3	0.333					84
SERPINB12	89777											3	0.067	94
SFPQ	6421					3	0.061	2	0.032					19
SHMT2	6472							3	0.083					5
SKP1	6500	2	0.153			2	0.153							19
SLC25A3	5250			2	0.052									154
SLC25A5	292	2	0.080	4	0.141	2	0.067	2	0.057					197
SRPRA	6734					4	0.061	2	0.045					3
SRPRB	58477					3	0.148	2	0.074					17
STUB1	10273					7	0.244	10	0.307					58
STX4	6810					2	0.074							0

SUGP1	57794					2	0.026							0
TARS2	80222					2	0.036							30
ELOB	6923					3	0.263							21
TCP1	6950					4	0.086	4	0.072					143
TGM3	7053											3	0.039	107
THOP1	7064							2	0.022					0
TMED10	10972					4	0.233	3	0.137					27
TMED2	10959					2	0.124							6
TMEM199	147007					2	0.106							0
TMEM33	55161							2	0.097					41
TMPO	7112					2	0.049	2	0.064					20
TUBA1A	7846			10	0.337									67
TUBA1B	10376	12	0.366			12	0.353	9	0.268					196
TUBB	203068	10	0.315	11	0.340			2	0.288					205
TUBB4B	10383					9	0.308	6	0.193					163
TYK2	7297							3	0.033					1
UBB	7314	2	0.079	3	0.148	3	0.148	3	0.166			2	0.109	104
UFM1	51569	3	0.600	4	0.682	4	0.506	3	0.682					1
USMG5	84833							2	0.431					62
USP7	7874					5	0.067	4	0.063					32
USP9X	8239					2	0.007	4	0.014					56
VASP	7408	13	0.439	11	0.379	15	0.461	12	0.416					2
WASF3	10810			2	0.062	7	0.191	8	0.301					1
WDR26	80232							4	0.076					20
WDR77	79084					3	0.155	5	0.211	2	0.105	4	0.170	160
WDTC1	23038					4	0.064	6	0.094					8
XRCC5	7520					2	0.022	2	0.022					24
XRCC6	2547					6	0.149	3	0.054					32
YPEL5	51646							2	0.182					9
YWHAB	7529	3	0.313	3	0.272	3	0.415	2	0.305	2	0.301			55
YWHAE	7531	13	0.537	14	0.624	23	0.675	17	0.596	15	0.616	11	0.510	168

YWHAG	7532	5	0.356	5	0.352	7	0.413	6	0.381	3	0.267	3	0.182	63
YWHAH	7533	8	0.459	5	0.350	7	0.337	11	0.382	5	0.333	3	0.232	40
YWHAZ	7534	5	0.380	4	0.359	8	0.412	8	0.465	5	0.367			92

Supplemental Table 3. Overview of all the primary and secondary antibodies used in this study, including the dilutions used for each of the different experiments. IP: Immuno-precipitation; WB: Western blot; ICC: immunocytochemistry; IHC: immunohistochemistry.

Primary Antibody Target	Host species	Supplier	Catalog N°	WB	ICC	IHC	immuno-EM
Acetylated tubulin	Mouse	Sigma-Aldrich	T6793	-	1:500	-	
ACTN1	Rabbit	Sigma-Aldrich	HPA006035	-	1:500	1:250	_
ARL13B	Rabbit	Proteintech	17711-1-AP	-	1:500	-	_
ARL13B	Mouse	NeuroMab	75-287	-	1:500	-	_
Centrin-3	Mouse	*Custom made*	-	-	-	1:100	_
CEP290	Rabbit	Novus Biological	NB100-86991	-	-	1:300	_
FILIP1L	Rabbit	Sigma-Aldrich	HPA043133	-	1:500	-	_
FLAG-tag	Mouse	Sigma-Aldrich	F3165	1:1,000	1:500	_	_
FLAG-tag	Rabbit	Sigma-Aldrich	F7425	-	1:500	_	_
HA-tag	Mouse	Sigma-Aldrich	H3663	1:1,000	1:500	-	_
HA-tag	Rabbit	Sigma-Aldrich	H6908	-	1:500	-	_
HA-tag Affinity Matrix clone 3F10	Rat	Sigma-Aldrich	11815016001	-	-	-	_
KALRN	Goat	Novus Biological	NB100-41371	-	1:500	-	_
PCARE	Rabbit	*Custom made*	-	1:500	1:250	1:100/1:500	1:100
Polyglutamylated tubulin (GT335)	Mouse	*Dr. Carsten Janke*	-	-	1:500	1:500	_
RAC1 clone 23A8	Mouse	Sigma-Aldrich	05-389	-	1:500	-	_
RPGRIP1L	Guinea Pig	*Custom made*	-	-	1:250	-	_
WASF3	Goat	R&D Systems	AF5515	1:1,000	1:250	1:250/1:500	_
Secondary Antibody Target							
Goat IgG, Alexa Fluor 488	Donkey	Molecular Probes	A 11055	-	1:500	-	_
Goat IgG, Alexa Fluor 568	Donkey	Molecular Probes	A11057	_	1:500	-	_
Guinea Pig IgG (H+L), highly cross-adsorbed, CF™405S	Donkey	Sigma-Aldrich	SAB4600230	-	1:100	-	_

Mouse IgG (H+L), RDye680	Goat	Thermo Fisher Scientific	A21057	1:10,000	-	-	-
Mouse IgG (H+L), RDye800	Goat	Li-cor	926-32210	1:10,000	-	-	-
Mouse IgG H&L, Alexa Fluor 405	Donkey	Abcam	ab175658	-	1:500	-	-
Mouse IgG, Alexa Fluor 488	Donkey	Life Technologies	A21202	-	1:500	-	-
Mouse IgG, Alexa Fluor 568	Donkey	Molecular Probes	A10037	-	1:500	-	-
Mouse IgG, Alexa Fluor 647	Chicken	Molecular Probes	A21463	-	1:500	-	-
Rabbit IgG H&L, Alexa Fluor 405	Donkey	Abcam	ab175651	-	1:500	-	-
Rabbit IgG, Alexa Fluor 647	Chicken	Molecular Probes	A21443	-	1:250	-	-
Others							
Alexa Fluor 568® phalloidin	-	Molecular Probes	A-12380	-	1:100	1:100	-

Chapter 3

Clinical and genetic overview of *PCARE*-associated retinal disease

Clinical and genetic overview of *PCARE*-associated retinal disease

Julio C. Corral-Serrano[1,2,*], Dyon Valkenburg[3,4,*], Ideke J.C. Lamers[1,2,*], Takeshi Iwata[5], Graeme C.M. Black[6], Tamar Ben-Yosef[7], Carel B. Hoyng[1,3], Alejandro Garanto[1,4], Ronald Roepman[1,2], Rob W.J. Collin[1,4]

[1]Department of Human Genetics, Radboud University Medical Center, Nijmegen, The Netherlands; [2]Radboud Institute for Molecular Life Sciences, Radboud University Medical Center, Nijmegen, The Netherlands; [3]Department of Ophthalmology, Radboud University Medical Center, Nijmegen, The Netherlands; [4]Donders Institute for Cognitive Neuroscience, Radboud University Medical Center, Nijmegen, The Netherlands; [5]Division of Molecular and Cellular Biology, National Institute of Sensory Organs, National Hospital Organization Tokyo Medical Center, Tokyo, Japan; [6]Centre for Genomic Medicine, St. Mary's Hospital, Manchester Academic Health Science Centre, University of Manchester, United Kingdom; [7]Rappaport Faculty of Medicine, Technion-Israel Institute of Technology, Haifa, Israel.

* shared first authors

Manuscript in preparation

3.1 Abstract

Mutations in the gene *PCARE* can cause non-syndromic autosomal recessive retinitis pigmentosa and occasionally cone-rod dystrophy. The aim of this study is to offer an overview of all the reported mutations in *PCARE* and analyze any potential correlation between the genotype and the severity of the disease. A literature search was conducted using PubMed and the Cochrane library. Clinical data of patients with disease-causing mutations in *PCARE* were extracted. A genotype-phenotype correlation analysis was performed based on mutation position and patient's age of onset. Clinical and genetic information was collected for 41 patients. The median age at first visit was 31.5 years, and the median best-corrected visual acuity was 0.30 for both eyes. Myopia was present in 12 (66.67%) patients, and night blindness in 16 (72.73%) patients. A total of 26 different mutations were identified. Homozygous *PCARE* mutations are mostly predicted to result in premature termination of protein synthesis, with only two homozygous missense mutations reported. The majority of patients (58.53%) present truncating or missense mutations at the N-terminus of PCARE, between amino acids 135 and 425. Finally, analysis of the position of the mutation in the PCARE protein and the age of onset revealed no clear correlation between these two variables. Our data suggest no clear correlation between the age of disease onset and the position of the *PCARE* mutation in patients with *PCARE*-associated retinal disease.

3.2 Introduction

Retinitis Pigmentosa (RP; MIM #268000) is an inherited retinal disease characterized by progressive vision loss, with a prevalence of around 1 in 4,000 individuals.[1-3] RP is clinically and genetically very heterogeneous and shows different patterns of inheritance: autosomal dominant (ad), autosomal recessive (ar) or X-linked (XL). The disease is characterized by progressive visual impairment, usually starting in childhood or adolescence, which may lead to blindness. Initially, the rod photoreceptor cells which regulate vision under low light conditions, degenerate. Subsequently, the cone cells, necessary for color vision and high visual acuity, also become affected. To date, more than 50 genes and loci have been implicated in arRP (RetNet; https://sph.uth.edu/retnet/), and most of them are responsible for around 1% or fewer cases.[4]

One of the genes found to be mutated in patients with arRP (OMIM #613428) is *C2orf71*/*PCARE* (photoreceptor cilium actin regulator, OMIM #613425).[5-11] In addition, one study reported cone-rod dystrophy in a patient with the nonsense mutation c.1837C>T;p.R613* in *PCARE*.[12] Of interest, *PCARE* mutations are a frequent cause of arRP in the Swiss population.[8] *PCARE* contains only two exons, and codes for a photoreceptor-specific ciliary protein of 1288 amino acids (aa). *Pcare*$^{-/-}$ mice present highly disorganized photoreceptor outer segments and severe retinal degeneration, strengthening the cilium photoreceptor-specific role of *PCARE*.[13] In **chapter 2**, we have shown that PCARE is an actin-associated protein important for the recruitment of the Arp2/3 complex activator WASF3 to the primary cilium and, subsequently, for the actin-driven evagination of the ciliary plasma membrane. Exogenous expression of mutant p.Ile201Phe PCARE together with WASF3 produces smaller and less evaginations than wild-type PCARE, suggesting this as one of the pathogenic mechanisms underlying *PCARE*-associated retinal disease.

In this study, we have collected all reported *PCARE* variants associated to retinal dystrophy up to April 2018. Given the presence of three predicted functional modules in the PCARE protein, we have assessed a potential correlation of the position of *PCARE* mutations with age of onset.

3.3 Results

3.3.1 Clinical phenotype of *PCARE*-associated retinal disease

Information of a total of 41 patients was collected (Table 1). The median age at first visit was 31.5 years (mean 33.46±16.20 years; range 12 – 75 years), and the median best-corrected visual acuity was 0.30 LogMAR (mean 0.47±0.52; range 0.10 – 2.50) for the right eye, and 0.30 LogMAR (mean 0.48±0.58; range -0.10 – 2.60) for the left eye at first visit. Refractive error was recorded for 18 patients, and myopia was present in 12 (66.67%). The presence or absence of night blindness was recorded for 22 patients, and night blindness was present in 16 (72.73%) patients. The general fundus image consisted of (mid-) peripheral retinal atrophy, with peripheral pigment changes and bone spicules, and vessel attenuation (Figure 1). Macular atrophy is often seen in later stages of the disease. Fundus autofluorescence revealed patches of hypofluorescence in 9 patients (out of 22 recorded, or 40.91%), and a speckled or atrophic macular area in 14 (out of 22 recorded, or 63.64%) patients. Optical coherence tomography data were available for 20 patients and revealed retinal thinning and loss of retinal lamination structure in all patients. Full-field electroretinography was performed in 25 patients and was severely reduced or non-recordable in 21 (84%) patients.

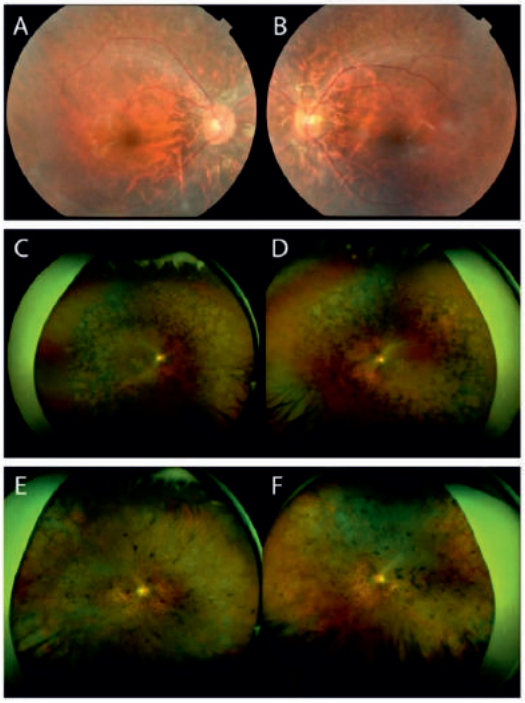

Figure 1. Fundus photographs of patients with *PCARE*-associated retinal disease. Paired fundus- (A, B) and ultra-widefield photographs (C-F) of the right (A, C, E) and left (B, D, F) eyes of three patients with two confirmed mutations in the PCARE gene. The phenotype *in fundo* resembles a classic retinitis pigmentosa, with optic disc pallor, vessel attenuation, bone-spicules in the (mid-) periphery and (mid-) peripheral RPE atrophy.

Table 1. Clinical characteristics of *PCARE*-associated retinal disease patients.

			Visual Acuity*		Refraction						
Pat. ID	**Fam. ID**	**Sex**	**OD**	**OS**	**OD**	**OS**	**Night blindness**	**ffERG**	**FAF**	**OCT**	**References**
1	17	F	20/60	20/50	-9.00	-7.00	Y	P very low	Small atrophic spots grouped in foveal area		[11]
2	11	F	20/32	20/32	-4.00	-2.90	Y	S severely reduced, P normal	Peripherally speckled	Retinal thinning, puckering	[8]
3	25	M	FC	FC				NR / NR			[14]
4	25	M	20/200	20/400				NR / NR			[14]
5	25	M	20/80	20/40	-8.50	-6.00		NR / NR			[14]
6	25	F									[14]
7	12	M	HM	HM			Y				[15]
8	22	F					Y		Perifoveal ring, central mottling atrophy ODS	photoreceptor loss, loss of retinal layer structure	[6]
9	22	F	20/125	20/32				Severely reduced ODS	Perifoveal ring, central mottling atrophy ODS	Vitelliform lesion subfoveal, photoreceptor layer loss	[6]
10	22	M	20/32	20/40				Flat ODS	Foveal sparing, hyper ring macula, hypo background and many nummular atrophic areas ODS	PR-loss with abnormal retina lamination	[6]
11	22	M	20/200	20/63	-0.75	-0.75	Y		Extensive widespread hypo, few small hyper areas throughout ODS		[6]
12	22	M			0.75	0.75	Y		Extensive widespread hypo, few small hyper areas throughout ODS	PR-loss with chaotic retinal structure	[6]
13	5	F	20/80	20/50	N/A	N/A	Y	NR	Macular and midperipheral speckled	Retinal thinning, puckering	[8]
14	24	M	20/60	20/30				Severely abnormal / Severely abnormal			[14]
15	24	F	20/60	20/60				NR / NR			[14]
16	24	M	20/25	20/16				Severely abnormal / NR			[14]
17	24	F	20/50	20/40				NR / NR			[14]
18	8	F	20/30	20/40	0	0	N	SP severely reduced	Perifoveal speckled	Retinal thinning, puckering	[8]
19	2	M	20/25	20/25	myopia	myopia	Y	S NR, P severely reduced	Macular large hypo area, speckled to midperipheral	Retinal thinning	[8]
20	2	F	LP	LP	myopia	myopia	N	NR		Retinal thinning, ORT	[8]
21	16	F									[9]
22	20	F									[7]
23	27	F	N/A	N/A			Y				[12]

24	4	F	20/25	20/30	-7.00	-6.50	N	NR		Retinal thinning	[8]
25	26	M	N/A	N/A				NR / NR			[14]
26	26	M	N/A	N/A				NR / NR			[14]
27	26	F	20/32	20/32			Y	NR			novel
28	3	M	20/200	20/400	-2.50	-1.30	Y	S NR, P severely reduced	Macular and midperipheral speckled	Retinal thinning, forming ORT	[8]
29	14	M	20/50	20/200			Y	Abolished	Peripheral bone spicules, circular patches of RPE, RPE pigmentation, vessel atenuation ODS		[16]
30	12	F					Y		Peripheral bone spicules, attenuated vessels, optic disc pallor		[17]
31	6	F	20/70	20/80	N/A	N/A		N/A	Large patches of hypo	Retinal thinning	[8]
32	9	M	20/30	20/30	0.40	0.80	N	S<P severely reduced	Perifoveal speckled	Retinal thinning	[8]
33	18	M	20/40	20/50	0	0	Y	NR			[7]
34	7	M	20/25	20/30	0.50	0.50	Y	N/A	Macular and nasal patchy hypo	Retinal thinning, puckering	[8]
35	21	M	20/40	20/40	1.50	1.50	Y	S barely detectable, P present although attenuated	Moderately heterogeneous macula, periphery normal	Retinal thinning, loss of IS/OS	[18]
36	21	M	20/30	20/30	-6.75	-5.75	Y	SP barely detectable	Heterogeneous macula, periphery normal	Retinal thinning, loss of IS/OS	[18]
37	1	M	20/30	20/30	-7.60	-3.00	N	SP severely reduced	Macular speckled	Retinal thinning	[8]
38	1	M	20/25	20/25	-4.40	-5.50	N	SP severely reduced	Perifoveal and midperipheral speckled	Retinal thinning	[8]
39	10	F	20/40	20/40	-3.00	-5.00	Y	S NR, P severely reduced	Foveal sparing hypo, speckled periphery, spared midperiphery	Retinal thinning, ORT	[8]
40	19	M	LP	LP	-3.50	-3.25	Y	NR			[7]
41	15	M	20/20	20/20	-3.50	-3.50	Y	NR	Ring-shaped macular hyperfluorescence	EZ present in the fovea	[19]

Clinical characteristics of the study cohort. All data reflect first available measurements. Refraction data reflect spherical errors.

FAF = fundus autofluorescence; OCT = optical coherence tomography; ffERG = full-field; LP = light perception; CF = counting fingers; HM = hand movements; N/A = not available; RPE = retinal pigment epithelium; NR = non-recordable; S = scotopic; P = photopic; ORT = outer retinal tabulation; IS/OS = inner segment / outer segment; Hypo = hypofluorescence; Hyper = hyperfluorescence.

*Visual acuity measures represent first available measurements.

3.3.2 Correlation analysis of *PCARE* mutation position with age of onset

Table 2 shows the summary of all reported patients and the corresponding *PCARE* mutations. Within the PCARE protein three defined regions can be observed: A conserved N-terminal region, which includes N-myristoylation and S-palmytoylation residues on aa 2 and 3 respectively, important for membrane attachment,[6,20] and a predicted globular domain (by ELM prediction tool; http://elm.eu.org/); a middle region with a predicted actin-binding motif (by ELM prediction tool; http://elm.eu.org/), and a C-terminal region rich in proline residues, which are known to be important for protein-protein interactions (Figure 2).[21,22] The different mutations identified in the patients are highlighted within the protein structure. Most of the patients (28 patients, 68.29%) present homozygous truncating mutations, whereas ten patients present heterozygous truncating mutations. Only two patients carry homozygous missense mutations, namely p.(Ile201Phe) or p.(Cys599Arg). In addition, one patient was reported with compound heterozygous missense mutations, p.(Arg29Trp) and p.(Arg1250Cys). The allele frequency of the p.Arg29Trp variant is 0.003 (gnomAD; gnomad.broadinstitute.org), whereas the p.Arg1250Cys variant has only been described in this patient. Whole-exome sequencing revealed heterozygous carriership of truncating mutations in recessive genes associated with retinal disease in this specific patient,[19] rendering the pathogenicity of the two *PCARE* missense mutations uncertain. To further examine the potential pathogenicity of these variants, we collected Grantham, PhyloP, SIFT and PolyPhen-2 pathogenicity prediction data, and the variants were classified based on the ACMG guidelines (Table 3).

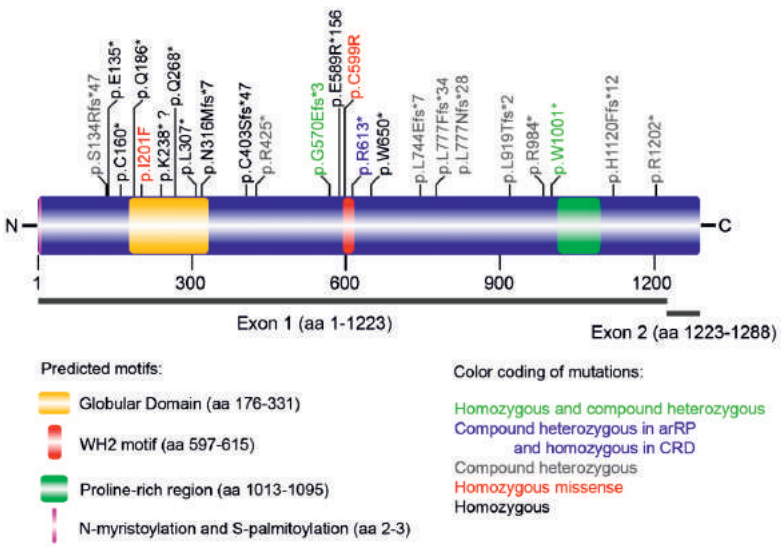

Figure 2. PCARE protein and mutation overview. At the N-terminus, PCARE protein contains N-myristoylation and S-palmytoylation residues and a predicted globular structure. An actin-binding WH2 motif is predicted between amino acids 597 and 615. At the C-terminus, PCARE contains a proline-rich region. Indicated are the aminoacidic positions of all reported disease-causing *PCARE* variants. To improve visibility, one instead of three-letter codes are used.

Table 2. Genetic characteristics of *PCARE*-associated retinal disease patients.

ID	Family ID	Sex	Age Onset (years)	Allele 1	Protein	Allele 2	Protein
1	17	F	14	c.403G>T	p.Glu135*	c.403G>T	p.Glu135*
2	11	F	20#	c.478_479insA	p.Cys160*	c.478_479insA	p.Cys160*
3	25	M	39	c.556C>T	p.Gln186*	c.556C>T	p.Gln186*
4	25	M	37	c.556C>T	p.Gln186*	c.556C>T	p.Gln186*
5	25	M	25	c.556C>T	p.Gln186*	c.556C>T	p.Gln186*
6	25	F	n.a.	c.556C>T	p.Gln186*	c.556C>T	p.Gln186*
7	12	M	23-24	c.712A>T	p.Lys238*	c.712A>T	p.Lys238*
8	22	F	26	c.758G>A	p.Trp253*	c.758G>A	p.Trp253*
9	22	F	17	c.758G>A	p.Trp253*	c.758G>A	p.Trp253*
10	22	M	26	c.758G>A	p.Trp253*	c.758G>A	p.Trp253*
11	22	M	41	c.758G>A	p.Trp253*	c.758G>A	p.Trp253*
12	22	M	20	c.758G>A	p.Trp253*	c.758G>A	p.Trp253*
13	5	F	42	c.920T>A	p.Leu307*	c.920T>A	p.Leu307*
14	24	M	37	c.946del	p.Asn316Metfs*7	c.946del	p.Asn316Metfs*7
15	24	F	32	c.946del	p.Asn316Metfs*7	c.946del	p.Asn316Metfs*7
16	24	M	30	c.946del	p.Asn316Metfs*7	c.946del	p.Asn316Metfs*7
17	24	F	31	c.946del	p.Asn316Metfs*7	c.946del	p.Asn316Metfs*7
18	8	F	22#	c.1206_1207dup	p.Cys403Serfs*47	c.1206_1207dup	p.Cys403Serfs*47
19	2	M	25#	c.1709_1728del	p.Gly570Glufs*3	c.1709_1728del	p.Gly570Glufs*3
20	2	F	50#	c.1709_1728del	p.Gly570Glufs*3	c.1709_1728del	p.Gly570lGufs*3
21	16	F	n.a.	c.1764del	p.Glu589Argfs*156	c.1764del	p.Glu589Argfs*156
22	20	F	n.a.	c.1764del	p.Glu589Argfs*156	c.1764del	p.Glu589Argfs*156
23	27	F	24	c.1837C>T	p.Arg613*	c.1837C>T	p.Arg613*
24	4	F	7.5#	c.1949G>A	p.Trp650*	c.1949G>A	p.Trp650*
25	26	M	47	c.2756_2768del	p.Lys919Thrfs*2	c.2756_2768del	p.Lys919Thrfs*2
26	26	M	59	c.2756_2768del	p.Lys919Thrfs*2	c.2756_2768del	p.Lys919Thrfs*2

27	26	F	6	c.2756_2768del	p.Lys919Thrfs*2	c.2756_2768del	p.Lys919Thrfs*2
28	3	M	32#	c.3002G>A	p.Trp1001*	c.3002G>A	p.Trp1001*
29	14	M	18	c.601A>T	p.Ile201Phe	c.601A>T	p.IleI201Phe
30	13	F	12	c.1795T>C	p.Cys599Arg	c.1795T>C	p.Cys599Arg
31	6	F	63#	c.402_405del	p.Ser134Argfs*47	c.3604C>T	p.Arg1202*
32	9	M	15#	c.802C>T	p.Gln268*	c.2756_2768del	p.Lys919Thrfs*2
33	18	M	18	c.946del	p.Asn316Metfs*7	c.3002G>A	p.Trp1001*
34	7	M	47#	c.1273C>T	p.Arg425*	c.3002G>A	p.Trp1001*
35	1	M	13#	c.1709_1728del	p.Gly570Glufs*3	c.2227_2228del	p.Leu744Glufs*7
36	1	M	22#	c.1709_1728del	p.Gly570Glufs*3	c.2227_2228del	p.Leu744Glufs*7
37	10	F	34#	c.1837C>T	p.Arg613*	c.3358_3359del	p.His1120Phefs*12
38	21	M	20	c.2327dup	p.Leu777Phefs*34	c.2328_2344del	p.Leu777Asnfs*28
39	21	M	14	c.2327dup	p.Leu777Phefs*34	c.2328_2344del	p.Leu777Asnfs*28
40	19	M	Early Childhood	c.2327dup	p.Leu777Phefs*34	c.2950C>T	p.Arg984*
41*	15	M	10	c.85C>T	p.Arg29Trp	c. 3748C>T	p.Arg1250Cys

= age at first visit. *patient with unknown pathogenicity. Patient genetic characteristics ordered by genetic composition: homozygous truncating mutations, followed by homozygous missense mutations, and compound heterozygous mutations.

Table 3. *In silico* analysis of *PCARE* missense variants.

Exon	cDNA change	Protein change	PhyloP	Grantham	PolyPhen-2 score	PolyPhen-2 Prediction	SIFT Score	SIFT Prediction	AC (gnomAD)	AF (gnomAD)	Classification
1	c.85C>T	p.Arg29Trp	-0.75	101	0.980	Probably damaging	0.02	Deleterious	64	0.0002334	Uncertain significance
1	c.601A>T	p.Ile201Phe	0.32	21	0.996	Probably damaging	0.02	Deleterious	1	0.000004061	Pathogenic
1	c.1795T>C	p.Cys599Arg	3.27	180	0.016	Benign	0.03	Deleterious	2	0.000008129	Pathogenic
2	c. 3748C>T	p.Arg1250Cys	-0.16	180	0.980	Probably damaging	0.13	Tolerated	1	0.00003230	Likely benign

AC: Allele count; AF: Allele frequency. Classification was assessed according to the ACMG guidelines.

Although PCARE lacks a structurally highly conserved domain, it does contain three predicted main functional domains. We therefore hypothesized that *PCARE* stop mutations affecting the N-terminal region of the protein could be more severe than those affecting the C-terminal part of the PCARE protein, and we tried to correlate the position of homozygous truncating mutations with the age of onset of disease (Figure 3). Three clusters can be distinguished, corresponding to the three defined protein regions. Two patients with the earliest onset, early childhood, carry mutations in the cluster of the middle (aa 570 to 650) and C-terminal regions (aa 744 to 1250). However, in these regions the disparity in age of onset is high, ranging from early childhood to an advanced age. For example, family 26 has two members with age at first visit of 47 and 59 years old, while one member visited the clinic at 6 years old. In contrast, the N-terminal region clusters all patients with an age at onset ranging from 17 to 42 years. Despite these observations, the limited total number of patients does not allow to establish a clear correlation between the age of disease onset and the position of the *PCARE* mutation.

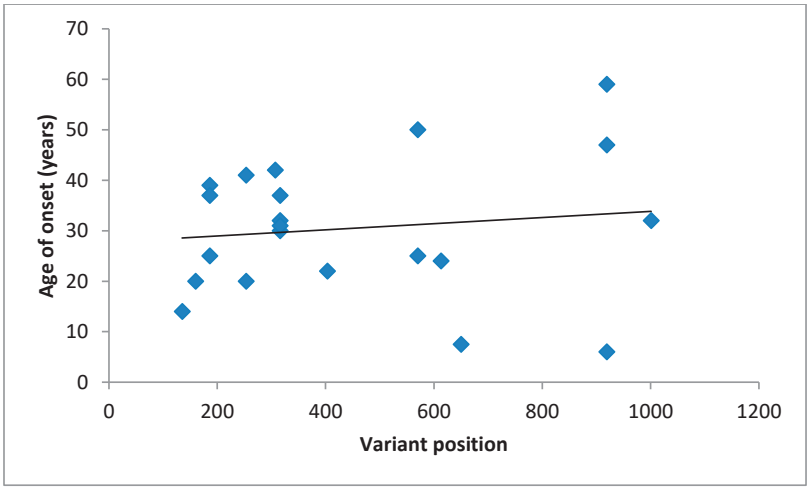

Figure 3. Correlation between the position of *PCARE* mutations and the age of onset in *PCARE*-associated retinal disease. Age of onset corresponds to the age of first visit to the clinic.

3.4 Discussion

Retinitis pigmentosa is the most common form of inherited retinal disease (IRD), a major cause of blindness. The full genetic spectrum of IRDs is not yet defined, and the information on genotype-phenotype correlations is limited, since mutations in different genes may result in a similar phenotype. Alternatively, many different clinical phenotypes may be caused by mutations in the same gene. The purpose of this study was to present an overview of all reported cases of *PCARE*-associated retinal disease and to determine any potential genotype-phenotype correlation for this specific subtype.

A total of 41 patients have been reported harboring mutations in *PCARE* associated with retinal disease. Interestingly, the median age at first visit was 31.5 years, an advanced age compared to other retinal disease genes.[23] As described in **chapter 2**, prediction programs show that PCARE contains three potential functional regions, and hypothesized that patients lacking two of the regions would have a more severe effect, *ergo* earlier age of onset, than those lacking only one of the regions. This is not the case, since some of the patients with mutations in the actin-binding motif seem to have an earlier onset than those where this motif remains intact. Several scenarios could underlie this result: first, *PCARE* mRNA can be degraded by non-sense mediated decay, preventing translation of any faulty truncated protein; second, mutated PCARE could be marked for degradation by the proteasome, with the same result; third, if the mutated protein is translated and stable, it may exhibit a negative effect on photoreceptor homeostasis. To further study the effect of missense and truncating mutations in the PCARE protein, we are currently performing localization studies in ciliated cells to analyze any potential effect in their localization and protein-protein interaction profiles.

The first limitation of studying *PCARE*-associated retinal disease is the small number of patients reported. This limitation is common for other IRDs, as the total number of genes associated to retinal diseases amounts to 261 (RetNet: https://sph.uth.edu/retnet/), and the majority of genes represent ~1% or less of all cases.[4] Even the most commonly mutated gene in arRP, *USH2A*, only accounts for about ~13% of cases.[23] Another constraint is a poor record of clinical data for some of the patients, that sometimes even lack any records of tests for visual acuity or electroretinograms. This calls for a better and more standardized protocol of clinical assessment of IRD patients. As a mutation in *PCARE* may be a modifier of Usher syndrome caused by mutations in *CEP250*,[24] it would also be important to include assessment of potential hearing loss in *PCARE* patients.

One patient harbored compound heterozygous missense mutations of unknown pathogenicity (p.Arg29Trp / p.Arg1250Cys). While clinical examinations revealed a classic retinitis pigmentosa

phenotype consisting of night blindness, concentrally constricted visual fields, non-recordable electroretinograms and typical fundus abnormalities, there is still some uncertainty that the encountered *PCARE* mutations are responsible for retinal disease in this patient. Based on current prediction programs and availability of population data, it may well be that (one of) these variants are benign, and thus mutations in *PCARE* are not the underlying cause of IRD in this patient. Segregation analysis, combined with functional studies on the missense mutant protein products, should be performed to determine whether these *PCARE* missense variants are truly disease-causing.

Because the age of onset is defined as the age of diagnosis, there may be a lot of divergence between the real age of onset of the disease and the first visit to the clinic. Interestingly, some families sharing the same causal mutation in *PCARE* have members with very early onset and others with late onset. This also obstructs the interpretation of the severity of the mutation. The presence of only one intron in the *PCARE* gene makes it less likely to encounter splice-site mutations, although it still should be investigated, as intronic mutations have been described for other retinal genes like *ABCA4*,[25,26] *CEP290*,[27] or *USH2A*.[28] Digenic forms of RP are known, therefore polygenic inheritance of retinal diseases cannot be ruled out.[29,30] Additionally, miRNAs may induce transcript degradation or translational inhibition of their target mRNAs,[31] and may also explain the differences in phenotypic severity when the causal mutation is the same.

In summary, we have presented an overview of the clinical and genetic characteristics of *PCARE*-associated retinal disease. The small number of patients reported and the limited clinical data collected from these patients makes it difficult to assess any potential genotype-phenotype correlation. Functional studies in different cellular and animal models are needed to shed more light into the function of *PCARE* and help to understand the disease better. A more detailed clinical examination of patients, together with a larger cohort of patients of *PCARE*-associated retinal disease, may help to obtain more accurate genotype-phenotype correlations and aid clinical diagnosis and personalized treatment for these patients.

3.5 Methods

3.5.1 Clinical data gathering

A literature search was conducted between October 1st 2017 and April 4th 2018. We searched PubMed and the Cochrane Library for "*C2orf71*" (as *PCARE* was previously known), which resulted in 21 results, and one more paper was found through references. All papers that included clinical data were selected, leading to the inclusion of a total of 11 papers with human clinical data on a total of

41 patients.[6-9,11,12,14-18] Clinical data were extracted, and authors were contacted to provide more information in case the published data were too limited.

3.5.2 Statistical analyses

Statistical analyses were performed using IBM SPSS version 22. Best-corrected visual acuity (BCVA) was transformed to the logarithm of the minimal angle of resolution (LogMAR) for statistical analysis. Counting fingers (CF) and light perception (LP) were assigned arbitrary BCVA values in order to perform Spearman ranked correlation analysis to assess inter-eye symmetry at baseline. Age of onset was defined as the age at which the patient first reported visual complaints. In case the age of onset was not reported or unknown, the age at first visit was considered the age of onset.

We investigated a genotype-phenotype correlation based on mutation position and the age of onset. Only patients that harbored homozygous mutations were included in this analysis, as the residual protein activity, and the contribution of individual mutations to this residual activity, is hard to predict for patients with compound heterozygous mutations.

3.6 References

1. Daiger, S.P., Sullivan, L.S., and Bowne, S.J. (2013). Genes and mutations causing retinitis pigmentosa. Clinical genetics 84, 132-141.
2. Parmeggiani, F. (2011). Clinics, epidemiology and genetics of retinitis pigmentosa. Current genomics 12, 236-237.
3. Haim, M. (2002). Epidemiology of retinitis pigmentosa in Denmark. Acta Ophthalmol Scand Suppl, 1-34.
4. Ferrari, S., Di Iorio, E., Barbaro, V., Ponzin, D., Sorrentino, F.S., and Parmeggiani, F. (2011). Retinitis pigmentosa: genes and disease mechanisms. Curr Genomics 12, 238-249.
5. Collin, R.W.J., Safieh, C., Littink, K.W., Shalev, S.A., Garzozi, H.J., Rizel, L., Abbasi, A.H., Cremers, F.P.M., den Hollander, A.I., Klevering, B.J., et al. (2010). Mutations in C2ORF71 cause autosomal-recessive retinitis pigmentosa. Am J Hum Genet 86, 783-788.
6. Nishimura, D.Y., Baye, L.M., Perveen, R., Searby, C.C., Avila-Fernandez, A., Pereiro, I., Ayuso, C., Valverde, D., Bishop, P.N., Manson, F.D., et al. (2010). Discovery and functional analysis of a retinitis pigmentosa gene, C2ORF71. Am J Hum Genet 86, 686-695.
7. Audo, I., Lancelot, M.E., Mohand-Said, S., Antonio, A., Germain, A., Sahel, J.A., Bhattacharya, S.S., and Zeitz, C. (2011). Novel C2orf71 mutations account for approximately 1% of cases in a large French arRP cohort. Hum Mutat 32, E2091-2103.
8. Gerth-Kahlert, C., Tiwari, A., Hanson, J.V.M., Batmanabane, V., Traboulsi, E., Pennesi, M.E., Al-Qahtani, A.A., Lam, B.L., Heckenlively, J., Zweifel, S.A., et al. (2017). C2orf71 Mutations as a Frequent Cause of Autosomal-Recessive Retinitis Pigmentosa: Clinical Analysis and Presentation of 8 Novel Mutations. Invest Ophthalmol Vis Sci 58, 3840-3850.
9. Coppieters, F., Van Schil, K., Bauwens, M., Verdin, H., De Jaegher, A., Syx, D., Sante, T., Lefever, S., Abdelmoula, N.B., Depasse, F., et al. (2014). Identity-by-descent-guided mutation analysis and exome sequencing in consanguineous families reveals unusual clinical and molecular findings in retinal dystrophy. Genet Med 16, 671-680.
10. Xu, Y., Guan, L., Shen, T., Zhang, J., Xiao, X., Jiang, H., Li, S., Yang, J., Jia, X., Yin, Y., et al. (2014). Mutations of 60 known causative genes in 157 families with retinitis pigmentosa based on exome sequencing. Hum Genet 133, 1255-1271.
11. Bocquet, B., Marzouka, N.A., Hebrard, M., Manes, G., Senechal, A., Meunier, I., and Hamel, C.P. (2013). Homozygosity mapping in autosomal recessive retinitis pigmentosa families detects novel mutations. Mol Vis 19, 2487-2500.

12. Mendonca, L.S.M., Avila, M.P., Silva, I.M.B.M., Lavigne, L.C., Oliveira, T., Chiang, J., Jordão, A., Rassi, A.T., Chaves, L.F.O.B., and Gabriel, L.A.R. (2014). Novel nonsense mutation in C2orf71 gene in a brazilian patient with autosomal recessive cone-rod dystrophy. Investigative Ophthalmology & Visual Science 55, 3275-3275.
13. Kevany, B.M., Zhang, N., Jastrzebska, B., and Palczewski, K. (2015). Animals deficient in C2Orf71, an autosomal recessive retinitis pigmentosa-associated locus, develop severe early-onset retinal degeneration. Hum Mol Genet 24, 2627-2640.
14. Collin, R.W., Safieh, C., Littink, K.W., Shalev, S.A., Garzozi, H.J., Rizel, L., Abbasi, A.H., Cremers, F.P., den Hollander, A.I., Klevering, B.J., et al. (2010). Mutations in C2ORF71 cause autosomal-recessive retinitis pigmentosa. Am J Hum Genet 86, 783-788.
15. Beheshtian, M., Saee Rad, S., Babanejad, M., Mohseni, M., Hashemi, H., Eshghabadi, A., Hajizadeh, F., Akbari, M.R., Kahrizi, K., Riazi Esfahani, M., et al. (2015). Impact of whole exome sequencing among Iranian patients with autosomal recessive retinitis pigmentosa. Arch Iran Med 18, 776-785.
16. Sanchez-Alcudia, R., Corton, M., Avila-Fernandez, A., Zurita, O., Tatu, S.D., Perez-Carro, R., Fernandez-San Jose, P., Lopez-Martinez, M.A., del Castillo, F.J., Millan, J.M., et al. (2014). Contribution of mutation load to the intrafamilial genetic heterogeneity in a large cohort of Spanish retinal dystrophies families. Invest Ophthalmol Vis Sci 55, 7562-7571.
17. Gonzalez-del Pozo, M., Mendez-Vidal, C., Bravo-Gil, N., Vela-Boza, A., Dopazo, J., Borrego, S., and Antinolo, G. (2014). Exome sequencing reveals novel and recurrent mutations with clinical significance in inherited retinal dystrophies. PLoS One 9, e116176.
18. Hebrard, M., Manes, G., Bocquet, B., Meunier, I., Coustes-Chazalette, D., Herald, E., Senechal, A., Bolland-Auge, A., Zelenika, D., and Hamel, C.P. (2011). Combining gene mapping and phenotype assessment for fast mutation finding in non-consanguineous autosomal recessive retinitis pigmentosa families. Eur J Hum Genet 19, 1256-1263.
19. Katagiri, S., Akahori, M., Sergeev, Y., Yoshitake, K., Ikeo, K., Furuno, M., Hayashi, T., Kondo, M., Ueno, S., Tsunoda, K., et al. (2014). Whole exome analysis identifies frequent CNGA1 mutations in Japanese population with autosomal recessive retinitis pigmentosa. PLoS One 9, e108721.
20. Godsel, L.M., and Engman, D.M. (1999). Flagellar protein localization mediated by a calcium-myristoyl/palmitoyl switch mechanism. EMBO J 18, 2057-2065.
21. Williamson, M.P. (1994). The structure and function of proline-rich regions in proteins. Biochem J 297 (Pt 2), 249-260.
22. Morgan, A.A., and Rubenstein, E. (2013). Proline: the distribution, frequency, positioning, and common functional roles of proline and polyproline sequences in the human proteome. PLoS One 8, e53785.
23. Bravo-Gil, N., Gonzalez-Del Pozo, M., Martin-Sanchez, M., Mendez-Vidal, C., Rodriguez-de la Rua, E., Borrego, S., and Antinolo, G. (2017). Unravelling the genetic basis of simplex Retinitis Pigmentosa cases. Sci Rep 7, 41937.
24. Khateb, S., Zelinger, L., Mizrahi-Meissonnier, L., Ayuso, C., Koenekoop, R.K., Laxer, U., Gross, M., Banin, E., and Sharon, D. (2014). A homozygous nonsense CEP250 mutation combined with a heterozygous nonsense C2orf71 mutation is associated with atypical Usher syndrome. J Med Genet 51, 460-469.
25. Sangermano, R., Bax, N.M., Bauwens, M., van den Born, L.I., De Baere, E., Garanto, A., Collin, R.W., Goercharn-Ramlal, A.S., den Engelsman-van Dijk, A.H., Rohrschneider, K., et al. (2016). Photoreceptor Progenitor mRNA Analysis Reveals Exon Skipping Resulting from the ABCA4 c.5461-10T-->C Mutation in Stargardt Disease. Ophthalmology 123, 1375-1385.
26. Bax, N.M., Sangermano, R., Roosing, S., Thiadens, A.A., Hoefsloot, L.H., van den Born, L.I., Phan, M., Klevering, B.J., Westeneng-van Haaften, C., Braun, T.A., et al. (2015). Heterozygous deep-intronic variants and deletions in ABCA4 in persons with retinal dystrophies and one exonic ABCA4 variant. Hum Mutat 36, 43-47.
27. den Hollander, A.I., Koenekoop, R.K., Yzer, S., Lopez, I., Arends, M.L., Voesenek, K.E., Zonneveld, M.N., Strom, T.M., Meitinger, T., Brunner, H.G., et al. (2006). Mutations in the CEP290 (NPHP6) gene are a frequent cause of Leber congenital amaurosis. Am J Hum Genet 79, 556-561.
28. Liquori, A., Vache, C., Baux, D., Blanchet, C., Hamel, C., Malcolm, S., Koenig, M., Claustres, M., and Roux, A.F. (2016). Whole USH2A Gene Sequencing Identifies Several New Deep Intronic Mutations. Hum Mutat 37, 184-193.
29. Kajiwara, K., Berson, E.L., and Dryja, T.P. (1994). Digenic retinitis pigmentosa due to mutations at the unlinked peripherin/RDS and ROM1 loci. Science 264, 1604-1608.
30. Gao, F.J., Zhang, S.H., Chen, J.Y., Xu, G.Z., and Wu, J.H. (2017). Digenic heterozygous mutations in EYS/LRP5 in a Chinese family with retinitis pigmentosa. Int J Ophthalmol 10, 325-328.

31. Karali, M., Persico, M., Mutarelli, M., Carissimo, A., Pizzo, M., Singh Marwah, V., Ambrosio, C., Pinelli, M., Carrella, D., Ferrari, S., et al. (2016). High-resolution analysis of the human retina miRNome reveals isomiR variations and novel microRNAs. Nucleic Acids Res 44, 1525-1540.

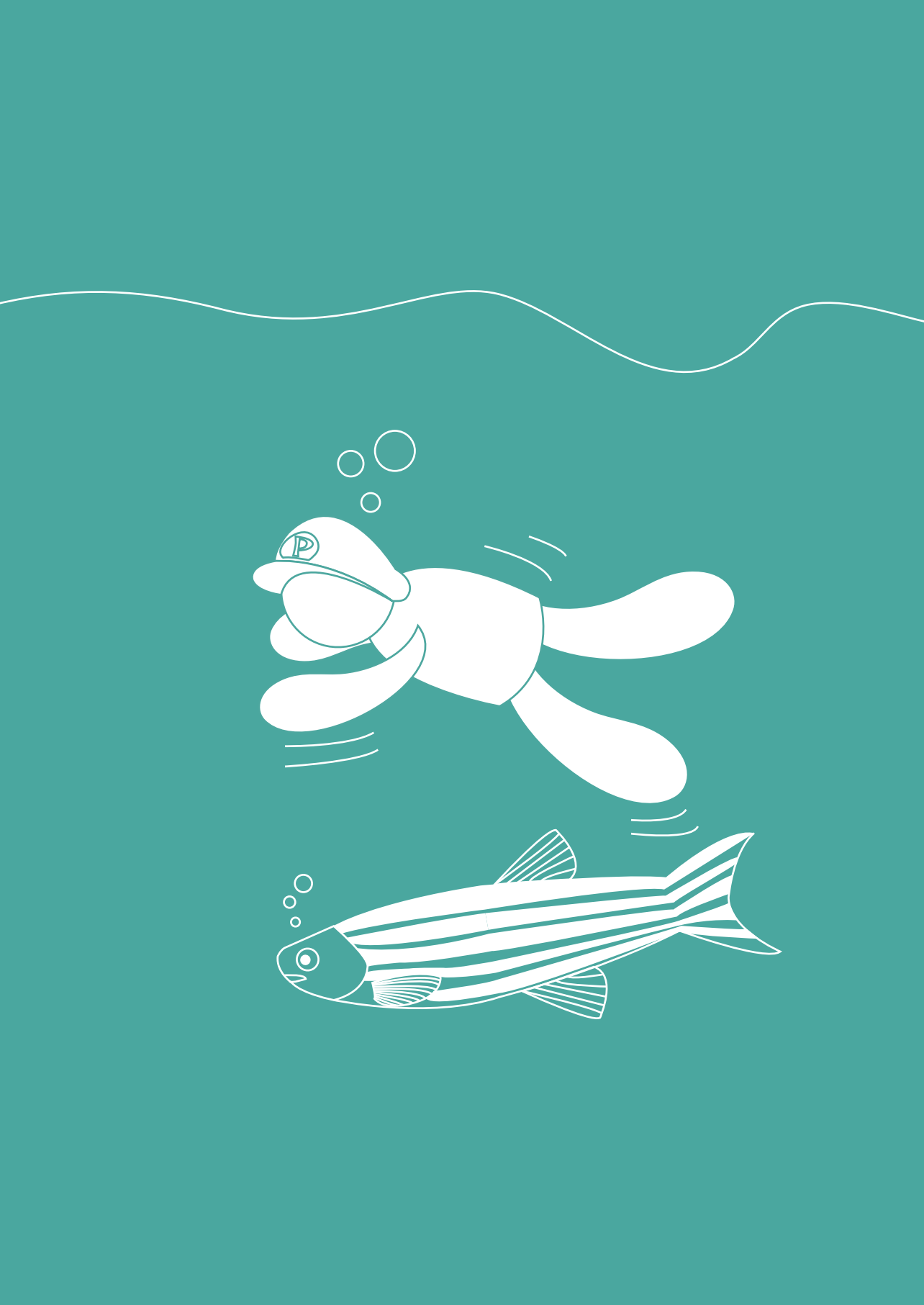

Chapter 4

C2orf71a/pcare1 is important for photoreceptor outer segment morphogenesis and visual function in zebrafish

C2orf71a/pcare1 is important for photoreceptor outer segment morphogenesis and visual function in zebrafish

Julio C. Corral-Serrano[1,2], Muriël Messchaert[1,3], Margo Dona[3,4], Theo A. Peters[3,4], Leonie M. Kamminga[2,5], Erwin van Wijk[3,4], Rob W.J. Collin[1,3]

[1]Department of Human Genetics, [2]Radboud Institute for Molecular Life Sciences, Radboud University Medical Center, Nijmegen, The Netherlands, [3]Donders Institute for Brain, Cognition and Behaviour, Radboud University, Nijmegen, The Netherlands, [4]Department of Otorhinolaryngology, Radboud University Medical Center, Nijmegen, The Netherlands, [5]Department of Molecular Biology, Radboud University, Nijmegen, The Netherlands.

Scientific Reports, ***8**: 9675*

4.1 Abstract

Mutations in *C2orf71* are causative for autosomal recessive retinitis pigmentosa and occasionally cone-rod dystrophy. We have recently discovered that the protein encoded by this gene is important for modulation of the ciliary membrane through the recruitment of an actin assembly module, and have therefore renamed the gene to *PCARE* (photoreceptor cilium actin regulator). Here, we report on the identification of two copies of the *c2orf71/pcare* gene in zebrafish, *pcare1* and *pcare2*. To study the role of the gene most similar to human *PCARE*, *pcare1*, we have generated a stable *pcare1* mutant zebrafish model (designated *pcare1*$^{rmc100/rmc100}$) in which the coding sequence was disrupted using CRISPR/Cas9 technology. Retinas of both embryonic (5 dpf) and adult (6 mpf) *pcare1*$^{rmc100/rmc100}$ zebrafish display a clear disorganization of photoreceptor outer segments, resembling the phenotype observed in *Pcare*$^{-/-}$ mice. Optokinetic response and visual motor response measurements indicated visual impairment in *pcare1*$^{rmc100/rmc100}$ zebrafish larvae at 5 dpf. In addition, electroretinogram measurements showed decreased b-wave amplitudes in *pcare1*$^{rmc100/rmc100}$ zebrafish as compared to age- and strain-matched wild-type larvae, indicating a defect in the transretinal current. Altogether, our data show that lack of pcare1 causes a retinal phenotype in zebrafish and indicate that the function of the *PCARE* gene is conserved across species.

4.2 Introduction

Retinitis pigmentosa (RP, MIM 268000) is an inherited retinal dystrophies (IRD) characterized by progressive visual impairment due to the loss of rod photoreceptors. The prevalence of RP in the population ranges between 1:3,000 and 1:5,000, making it the most common form of IRD. In 2010, we and others reported that mutations in *C2orf71* underlie non-syndromic autosomal recessive RP (arRP).[1,2] Consecutive studies detected additional *C2orf71* disease-causing missense and nonsense mutations along its entire coding sequence in cases with RP or cone-rod dystrophy (CRD).[3-8] Of interest, *C2orf71* mutations represent a frequent cause of arRP in the Swiss population.[9]

C2orf71 is almost exclusively expressed in the retina[1] and encodes a ciliary protein, C2orf71, that consists of 1,288 amino acids and localizes to the base of the outer segments (OS) in the retina, where OS disk neogenesis is initiated.[10] In *C2orf71*$^{-/-}$ mice, the OS are shortened and disorganized, and are marked by a mislocalization of proteins such as rhodopsin and cone opsins.[11] Recently, we have discovered that C2orf71 recruits a ciliary actin dynamics module that modifies the ciliary membrane, and hypothesize that this principle may be the driver of photoreceptor OS disks morphogenesis (as reported in **chapter 2**). Hence, we have renamed the *C2orf71* gene to *PCARE* which stands for photoreceptor cilium actin regulator. If *PCARE* indeed plays a conserved, actin-related role in vision, we would expect a similar function for this gene across vertebrates.

The zebrafish, *Danio rerio*, is a tropical freshwater fish that is commonly used in IRD research.[12-14] Advantages of using zebrafish for such studies are mainly their short life cycle and the large numbers of offspring. In addition, their *ex utero* development allows for easy tracking of eye development.[15] Despite being genetically distant to humans, zebrafish eyes share some similarities in morphology and physiology to human eyes. Like humans, zebrafish are also diurnal animals, and their retinas present a similar layered structure.[16] A whole-genome duplication event that occurred during the divergence of the teleost fish[17,18] made the present day zebrafish genome to contain many duplicated genes, of which over 64 correspond to genes mutated in IRD,[15] including *pcare*.

Transient morpholino-based knockdown of one of the two copies of *pcare* in zebrafish, *pcare1*, results in shortening of photoreceptor outer segments and visual dysfunction.[2] However, over the recent years, the specificity of morpholino-based knockdown studies have been debated, mostly due to non-specific binding that may occur.[19,20] In addition, the transient nature of the knock-down does not allow to study long-term effects.

Here, we have generated a stable *pcare1* zebrafish mutant using CRISPR/Cas9 technology to investigate the effect of the absence of pcare1 in a non-mammalian model, and demonstrate that, like in humans, the *pcare1* gene is essential for retinal function.

4.3 Results

4.3.1 *PCARE* is duplicated in the zebrafish genome

The zebrafish *pcare* paralogues, *pcare1* and *pcare2*, were identified by bioinformatic analysis using the software programs BLAST (https://blast.ncbi.nlm.nih.gov/Blast.cgi) and Ensembl (https://www.ensembl.org/index.html). Reciprocal BLAST searches revealed that both genes are true orthologues of the human *PCARE* gene. Bioinformatic analysis revealed that *pcare1* is located on chromosome 17 and codes for a protein of 1122 amino acids, while *pcare2* is locates to chromosome 20 and encodes a protein of 859 amino acids (Fig. 1). A synteny between part of the zebrafish chromosome 17 and the human chromosome 2 on which *PCARE* is located, suggests that *pcare1* is the true orthologue of the human counterpart. To study the expression of these genes, we performed RT-PCR on wild-type zebrafish eye cDNA at 5 days post fertilization (dpf). We observed that both genes are expressed in the zebrafish eye (Fig. 1B). Because of the higher similarity of pcare1 with the human PCARE protein sequence (32.1% of pcare1 vs 25.6% of pcare2, see Supplemental Figure S1) we decided to target the *pcare1* gene for disruption.

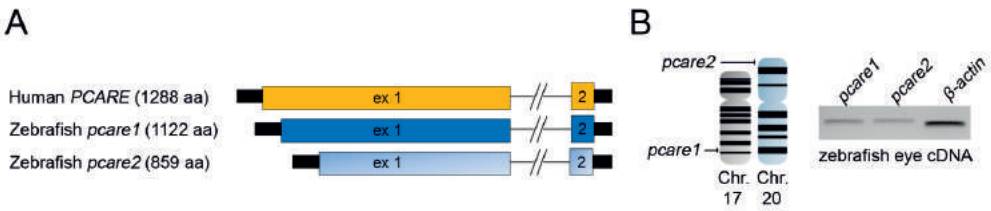

Figure 1. *PCARE* is duplicated in the zebrafish genome. A, Graphic representation of the human *PCARE* gene and the two *PCARE* orthologous zebrafish genes, *pcare1* and *pcare2.* **B**, Genomic location of the duplicated *pcare* genes in zebrafish. *Pcare1* is located in chromosome 17 and *pcare2* is located in chromosome 20 (left). Expression analysis using zebrafish eyes cDNA of *pcare1* and *pcare2* (right).

4.3.2 Generation of a *pcare1* mutant zebrafish line

For the generation of *pcare1* mutant zebrafish, a *pcare1* sequence-specific guide RNA was designed, and co-injected with *Cas9* mRNA into single cell zebrafish embryos. Mosaic fish containing indels around the target region were then outcrossed with wild-type fish to determine germline transmission and the exact genomic lesion that was introduced. We identified four adult F1 fish containing a heterozygous 29-basepair deletion in exon 1 of *pcare1* (c. 21_49del) (Fig. 2A-C). Subsequently, heterozygous *pcare1* carriers were mated to generate homozygous mutant fish, named *pcare1*$^{rmc100/rmc100}$, and subsequently crossed for a number of generations. Homozygous mutant fish did not show any signs of gross morphological abnormalities. The 29-basepair deletion is

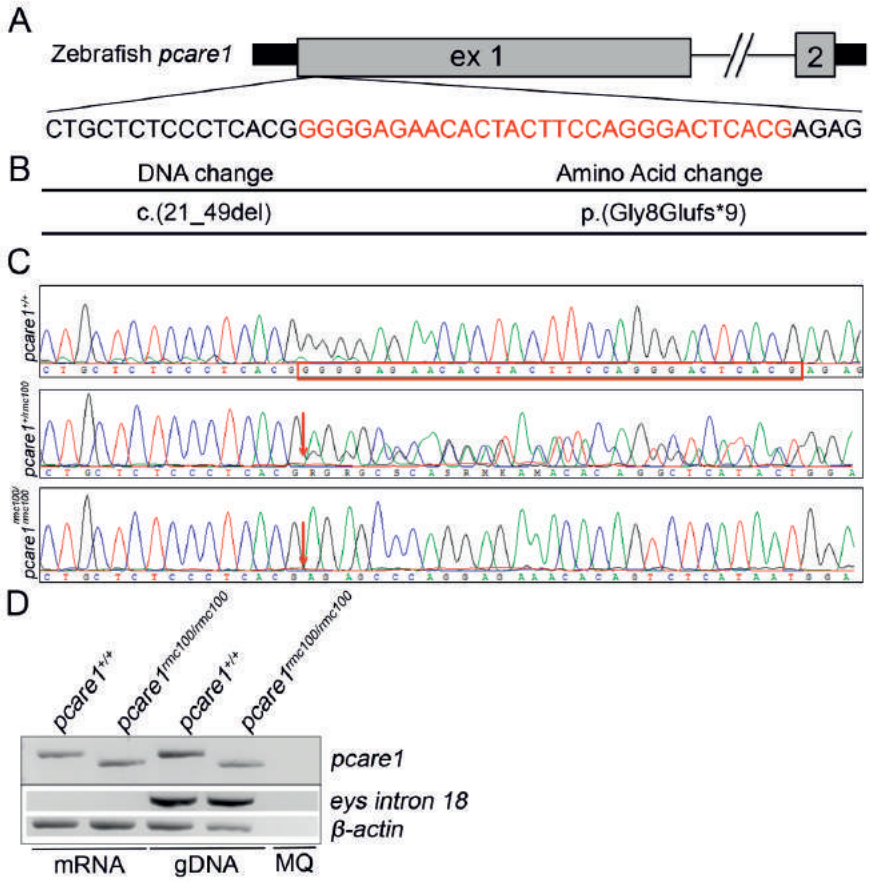

Figure 2. Generation of *pcare1*$^{rmc100/rmc100}$ zebrafish. A, The 2 exons of zebrafish *pcare1* gene are shown. In red, the sequence targeted by the *pcare1* guide RNA is indicated. **B**, The detected DNA change (c.21_49del) leads to a 29bp deletion causing a frame shift after aminoacid 8 of *pcare1*, predicted to result in a truncated protein (p.Gly8Glufs*9). **C**, Sequence validation of the targeted region in *pcare1*$^{+/+}$, *pcare1*$^{+/rmc100}$ and *pcare1*$^{rmc100/rmc100}$ zebrafish. The deleted 29bp are marked in red in the *pcare1*$^{+/+}$ sequence and absent from the heterozygous and homozygous sequences (red arrows).

predicted to result in the premature termination of translation after amino acid 16 of pcare1 (p.Gly8Glufs*9), most likely resulting in a functional null allele. RT-PCR analysis showed that mutant mRNA is expressed in the *pcare1* mutants, indicating that it does not, or at least not completely, undergo nonsense-mediated decay (Fig. 2D). Staining with different commercial and custom-made antibodies targeting the pcare protein in zebrafish did not yield any specific signals, nor any differences between wild-type and *pcare1*$^{rmc100/rmc100}$ mutant fish (data not shown). These results suggest that the antibodies targeting human PCARE do not recognize the zebrafish protein, most likely due to the low conservation between the human and zebrafish PCARE sequences (Supplemental Figure S1).

4.3.3 *Pcare1*$^{rmc100/rmc100}$ zebrafish show aberrant photoreceptor morphology

To analyze the morphology of the photoreceptor OS, *pcare1*$^{rmc100/rmc100}$ and wild-type strain-matched embryos of 5 dpf were sectioned and stained with boron-dipyrromethene (BODIPY). We observed a pronounced dysmorphology of the outer segments in the *pcare1*$^{rmc100/rmc100}$ zebrafish as compared to wild-type embryos (Fig. 3A). Since we recently discovered that the human PCARE protein is associated to actin, we also stained retinas, from embryonic (5 dpf) as well as adult (6 months post fertilization, mpf) fish, with an antibody against F-actin. The localization of actin further supported the disorganization of the OS (Fig. 3B,C) in the *pcare1*$^{rmc100/rmc100}$ retinas. In addition, both the rod-specific protein rhodopsin and the cone-specific protein Gnat2 exhibited a different pattern in *pcare1*$^{rmc100/rmc100}$ fish compared to wild-type fish, presumably affected by the change of morphology of the outer segments (Fig. 3B,C). Additionally, a reduction in the thickness of both outer and inner nuclear layers was observed in *pcare1*$^{rmc100/rmc100}$ fish of 6 months of age (Supplemental Figure S2).

4.3.4 *Pcare1*$^{rmc100/rmc100}$ larvae are visually impaired

To study the response of the zebrafish to visual stimuli, we performed optokinetic response (OKR) and visual motor response (VMR) measurements in wild-type and *pcare1*$^{rmc100/rmc100}$ larvae at 5 dpf. OKR analysis, that measures eye movements in a rotating drum, showed a significant decrease in the number of movements in *pcare1*$^{rmc100/rmc100}$ larvae compared to wild types (Fig. 4A). Twenty-one percent of the mutant larvae responded with less than 5 eye movements, which can be considered as spontaneous movements, while 5% of the mutant larvae showed no response at all (Fig. 4A). For VMR measurements, we employed the DanioVision system that enables automatic measurement of the activity of animals following a series of dark-to-light transitions. Our analysis showed a major decrease of the distance moved after the dark-to-light transitions between *pcare1*$^{rmc100/rmc100}$ and

wild-type larvae (Fig. 4B,C). The velocity of the movements was also higher in the wild-type larvae (Fig. 4D,E), though it was not statistically significant. To determine the response of the outer retina to a light stimulus, we performed ERG measurements in dark-adapted zebrafish larvae at 5 dpf. The b-wave response, which measures the action potentials of ON bipolar cells,[21] was drastically reduced in *pcare1*$^{rmc100/rmc100}$ compared to age-matched control larvae (Fig. 5).

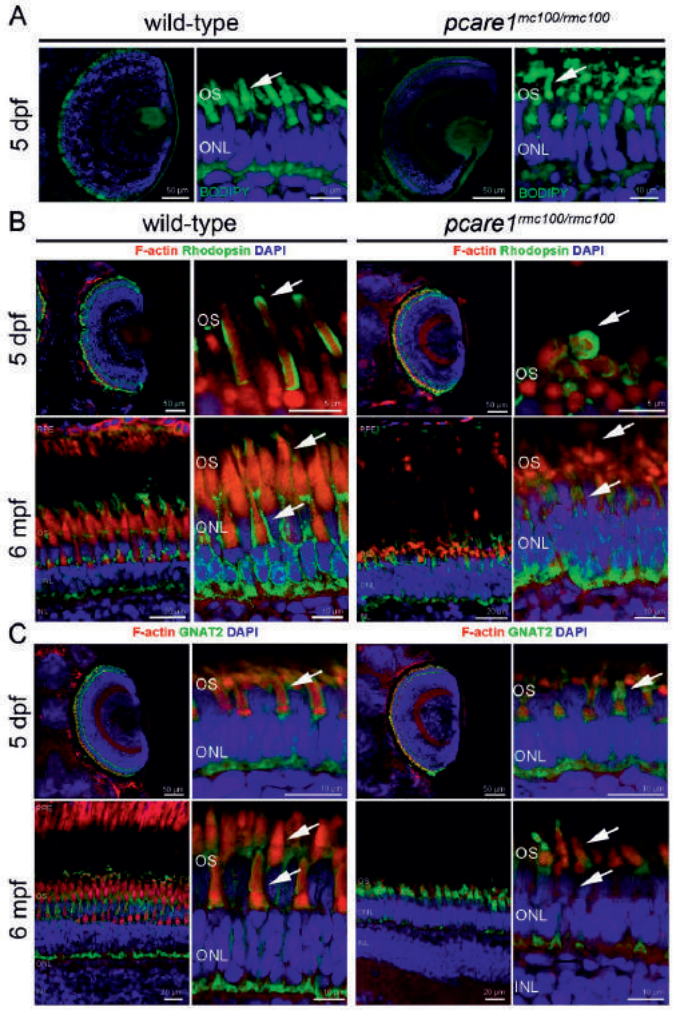

Figure 3. ***Pcare1***$^{rmc100/rmc100}$ **zebrafish show aberrant photoreceptor morphology. A**, Analysis of the morphology of the *pcare1*$^{rmc100/rmc100}$ zebrafish larval retina (5 dpf) using boron-dipyrromethene (BODIPY) revealed disorganization of photoreceptor outer segments as compared to those of strain- and age-matched wild-type larvae (arrows). **B**, Siblings of adult zebrafish without (wild-type) or containing (*pcare1*$^{rmc100/rmc100}$) the 29bp deletion in *pcare1* were sectioned and stained with antibodies against F-actin (red), Rhodopsin (green) or, in **C**, GNAT2 (green). Arrows indicate normal outer segments in control fish and dysmorphic outer segments in mutant fish. Nuclei were stained with DAPI.

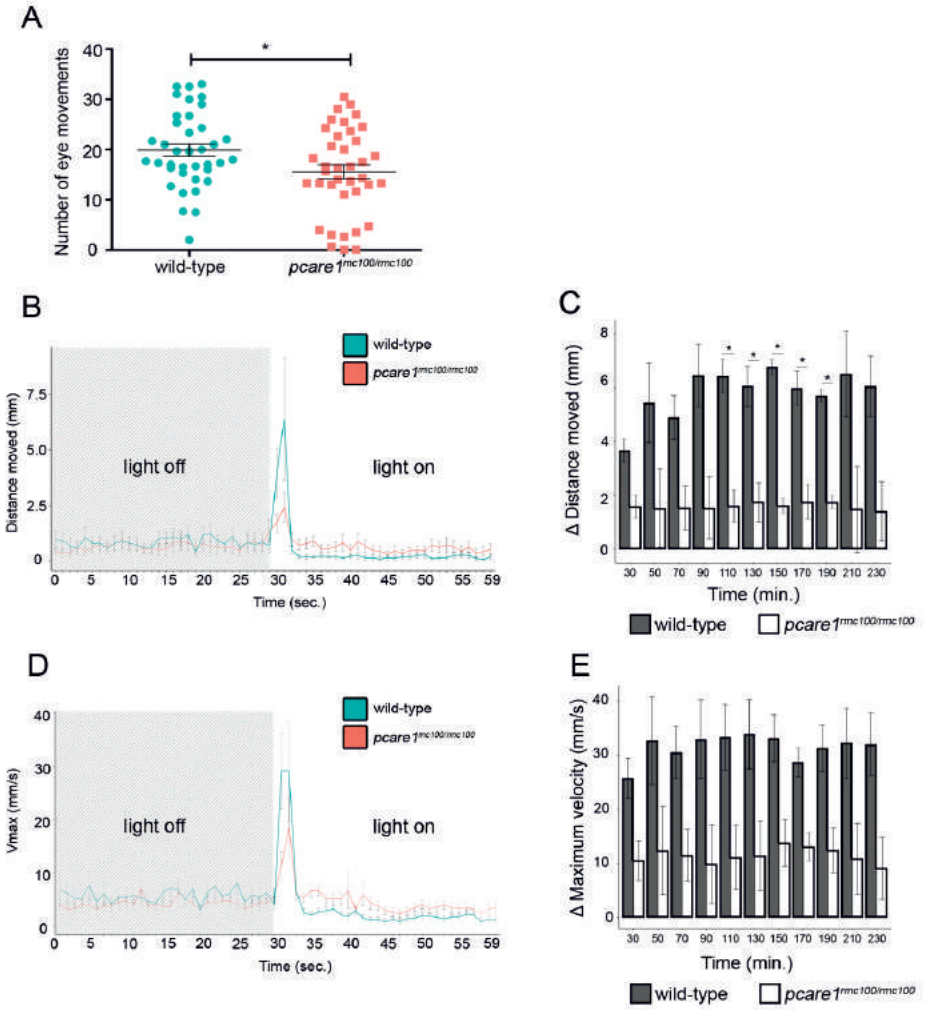

Figure 4. *Pcare1*$^{rmc100/rmc100}$ zebrafish are visually impaired. A, Optokinetic response (OKR) measurements revealed a decrease in the number of eye movements of *pcare1*$^{rmc100/rmc100}$ larvae (n=38) compared to control larvae (n=38). **B,** Representative graph showing the distance moved (maximum velocity in **D**) of the larvae between light-off to light-on change in a one-minute interval. **C**, Graphs showing the differences in the distance moved (maximum velocity in **E**) between wild-type and *pcare1*$^{rmc100/rmc100}$ larvae in different time points and combining three independent experiments. Bars indicate the standard error of the mean. P-values are corrected for multiple testing using Benjamini-Hochberg method; the comparisons marked with an asterisk showed statistical significance (*) = p-value < 0.05.

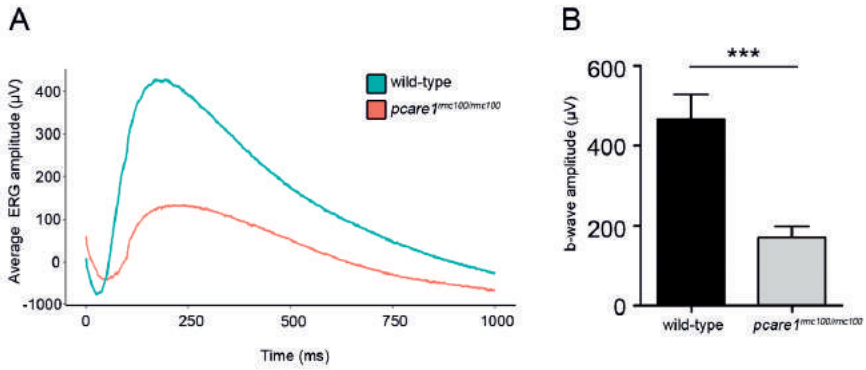

Figure 5. *Pcare1*$^{rmc100/rmc100}$ mutant zebrafish show reduced ERG responses. A, The average ERG amplitude to light stimuli of wild-type larvae (n=15) and *pcare1* mutant larvae (n=17) was measured. **B,** Comparison of maximal b-wave amplitudes between wild-type and *pcare1*$^{rmc100/rmc100}$ zebrafish larvae. The b-wave amplitude is significantly reduced in *pcare1*$^{rmc100/rmc100}$ mutants compared to wild-type larvae; p-value = 0.0004. Bars indicate the standard error of the mean.

4.4 Discussion

In humans, mutations in the gene *PCARE* lead to phenotypes where either the rod photoreceptors, in case of arRP, or the cone photoreceptors, in arCRD, are primarily affected. The outer segments of photoreceptor cells are specialized sensory cilia composed of stacked membrane discs that contain all the necessary elements for phototransduction.[22] Very recently, we have found evidence that PCARE could be an important ciliary actin modulator postulated to drive outer segment disk morphogenesis (**chapter 2**). This study was done using a *Pcare*$^{-/-}$ mouse model and human hTERT RPE-1 cells. Here, we have generated a zebrafish *pcare1* mutant (named *pcare1*$^{rmc100/rmc100}$) in order to obtain a better understanding of the function of pcare in a non-mammalian vertebrate. Based on the data presented here, it seems that the function of *PCARE* is conserved, as the photoreceptor outer segments are disorganized in *pcare1*$^{rmc100/rmc100}$ zebrafish.

The age of disease onset in patients with *PCARE* mutations ranges from the first to the sixth decade.[9] We observed that *pcare1*$^{rmc100/rmc100}$ zebrafish show a worse response than wild-type zebrafish, both in a behavioral assay and after electrophysiological recordings; however, *pcare1*$^{rmc100/rmc100}$ zebrafish are not completely blind. These observations correlate with the human phenotype, since patients do not become fully blind until a more advanced age. In mice, disruption of *Pcare* causes severe retinal dystrophy with an early onset, with flat ERG responses already at 8 weeks of age.[11] Behavioral assays using DanioVision did not show statistically significant differences for velocity and some points of distance moved; however, we can observe a clear different trend between wild-type and *pcare1*$^{rmc100/rmc100}$ larvae. This correlates with the high variability in results using visual motor assays

that other authors have reported.[23] Additionally, photoreceptive molecules in the zebrafish brain may mediate some of the behavioral responses to light.[24,25]

In our study, *pcare1*$^{rmc100/rmc100}$ zebrafish ERG responses show a reduction in the b-wave amplitude as early as 5 dpf, similar to the phenotype observed in mice. Since rod photoreceptors are still not functional in zebrafish at 5 dpf,[26,27] this indicates that cone photoreceptor cells and/or bipolar cells could be affected by depletion of *pcare1*, although we only measured b-wave responses that are derived from the bipolar cells. In addition, light detection through non-retinal tissues could be accounting for some of the responses.

Because the outer segments are not completely disrupted in *pcare1*$^{rmc100/rmc100}$ zebrafish, we hypothesize that other proteins involved in outer segment disc formation may still be functional at their action site. Unlike for other vertebrates, the common ancestor from the teleost lineage underwent a whole-genome duplication event.[18] A consequence of this is the presence of 26,206 protein-coding genes, more than any other sequenced vertebrate species.[28] For some of the duplicated genes, their function has diverged since then,[29,30] while for others it has remained unchanged.[31] Interestingly, parts of zebrafish chromosome 17 and 20 where *pcare1* and *pcare2* are located, descend from the same pre-duplication in the ancestral chromosome. Although disruption of the *pcare1* copy is sufficient to generate a strong retinal phenotype, there is still a possibility that *pcare2* may be involved in a similar process within the photoreceptor cells. Thus, a more severe retinal defect could be expected if both gene copies are disrupted, and future studies will be needed to address the function of pcare2.

Alternatively, other proteins involved in photoreceptor outer segment formation or maintenance could be responsible for our observations. Examples of such proteins are the subunits of the intraflagellar transport (IFT) particle, and the motor protein kinesin-2,[32] which are needed for axonemal protein traffic along the connecting cilium. Knockdown of IFT proteins in zebrafish causes severe retinal degeneration.[33] *Ift57*-deficient zebrafish mutants however are able to form a primitive photoreceptor connecting cilium, rod sacs and flattened outer segment discs, but the discs fail to acquire a proper length and subsequently the photoreceptors die.[33,34] Because of the similarities between the phenotypes of *Ift57* mutants and *pcare1*$^{rmc100/rmc100}$ zebrafish mutants, we hypothesize that a similar degenerative process of *pcare1*$^{rmc100/rmc100}$ zebrafish outer segments might take place.

Contrary to mammals, where Müller glia cells rarely divide followed by retinal injury, retinal regeneration does occur in zebrafish.[35,36] Upon injury, Müller glia are able to reprogram into retinal stem cells.[37] We however observed a disorganization of the photoreceptor outer segments and

degeneration of the outer nuclear layer at *pcare1*$^{rmc100/rmc100}$ zebrafish, both at 5 dpf and at 6 mpf. Therefore, the regeneration occurring in zebrafish is apparently not sufficient to halt the photoreceptor degeneration caused by absence of pcare1.

In summary, we have generated a *pcare1*-deficient zebrafish line using CRISPR/Cas9 technology. Analysis of the morphology and physiology of embryonic and adult *pcare1*$^{rmc100/rmc100}$ zebrafish results in a clear retinal disease phenotype. We provide an additional excellent model organism to study retinal degeneration caused by *PCARE* mutations which will be useful to understand the disease mechanisms. Furthermore, our findings support the hypothesis of the involvement of PCARE in forming and/or maintaining photoreceptor outer segments and, thereby, proper vision.

4.5 Methods

4.5.1 Ethics statement

Animal experiments were conducted in accordance with the Dutch guidelines for the care and use of laboratory animals, with the approval of the local Animal Experimentation Committee (Dier Experimenten Commissie [DEC]) (Protocol #DEC 2016–0091).

4.5.2 Zebrafish maintenance

Experimental procedures were conducted in accordance with international and institutional guidelines. Wild-type adult Tupfel Long Fin (TLF) zebrafish were used. Zebrafish eggs were obtained from natural spawning of wild-type breeding fish. Larvae were maintained and raised by standard methods.[38] In brief, embryos were raised in E3 medium (5 mM NaCL, 0.17 mM KCL, 0.33 mM $CaCl_2$, 0.33 mM $MgSO_4$, supplemented with 0.1% methylene blue) in a 28°C incubator with the same day/night cycle (14 h light / 10 h dark). The medium was daily changed and during the process curved and dead larvae were discarded. Behavioral testing was carried out at 5 days post-fertilization (dpf).

4.5.3 Target site selection and gRNA synthesis

Sites for targeted genome editing were selected using the online software ZiFiT Targeter version 4.2 (http://zifit.partners.org/ZiFiT/).[39,40] Templates for gRNA transcription were generated by annealing gene-specific oligonucleotides containing the T7 (5'-TAATACGACTCACTATA-3') promoter sequence, the 20-base target sequence without the PAM (5'-GGGGGAGAACACTACTTCCA-3'), and a complementary region to a constant oligonucleotide encoding the reverse complement of the

tracrRNA tail. T4 DNA polymerase (New England Biolabs, Ipswich, Massachusetts, USA) was used to fill the ssDNA overhang and the template was purified using columns (Sigma, St. Louis, Missouri, USA). Transcription of the gRNAs was performed using the MEGAshortscript Kit (Ambion®, Thermo Fisher Scientific, Waltham, Massachusetts, USA).

4.5.4 Microinjections

Zebrafish embryos were collected and injected at single cell stage with 1 nl of a mix consisting of 4.5 µl gRNA (173,72 ng/ul), 2.5 µl Cas9 protein (2 µg/µl, PNA Bio Inc, Newbury Park, California, USA), 2 µl 1M KCl and 1 µl 0.5% phenol red dye. To screen for genomic lesions, genomic DNA was extracted from a pool of 15 embryos at 2.5 dpf.

4.5.5 Genotyping PCR

After injections, genomic DNA was extracted from 2.5 dpf larvae or caudal fin tissue of adult zebrafish. Tissue was incubated in 25 µl (larvae) or 75 µl (fin tissue) lysis buffer (40 mM NaOH, 0.2 mM EDTA) for 20 min at 95°C. The lysed samples were diluted 10 times after which 1 µl was incubated together with 0.5 µM of the forward and reverse primer, 100 µM dNTPs (Roche, Basel, Switzerland), 0.25 U Taq polymerase (Roche, Basel, Switzerland) and 10x PCR buffer + 15 mM MgCl2 (Roche, Basel, Switzerland) in a total volume of 25 µl. Samples were denatured at 94°C for 5 min followed by 35 cycles of amplification consisting of 30 seconds (sec) at 94°C, 30 sec at 58°C and 60 sec at 68°C, followed by a final primer extension of 10 min at 72°C. To screen for genomic lesions, PCR products were sequenced directly. Primer sequences are listed in Supplemental Table S1.

4.5.6 Establishment of a *pcare1*$^{rmc100/rmc100}$ zebrafish line

Mosaic fish were out-crossed with wild-type TLF fish to determine germline transmission and the exact introduced genomic lesion. Heterozygous mutants were mated to generate homozygous *pcare1* mutants, which were subsequently crossed for a number of generations. A *pcare1*$^{rmc100/rmc100}$ zebrafish line was established containing a 29-basepair deletion at the start of exon 1 of *pcare1* (c. 21_49del). This is predicted to lead to premature termination of translation after amino acid 16.

4.5.7 RT-PCR analysis

To analyze the expression of *pcare1* and *pcare2*, we performed RT-PCR using cDNA extracted from wild-type zebrafish eyes. One microgram of total RNA was incubated with 1 µl iScript Reverse Transcriptase (1708891, Bio-Rad, Hercules, California, USA) and 1x reaction mix in a total volume of 20 µl nuclease free water. For the RT-reaction, the mixture was incubated for 5 min at 25°C, 30 min

at 42°C and the reaction was stopped by heating at 85°C for 5 min. PCR analysis was performed as described above. The primers used are listed in Supplemental Table S1.

4.5.8 Preparation of zebrafish sections

Larvae (5 dpf) were collected in an eppendorf tube and sedated with 2-phenoxyethanol (1:500). After one wash with PBS, embryos or adult eyes (6 mpf) were fixed in 4% PFA overnight, brought gradually to 100% MetOH and stored overnight at -20°C. After the overnight incubation, samples were rehydrated (75% MetOH in 0.1% PBS-Tween20 (PBS-T), 50% MetOH in 0.1% PBS-Tween20, 25% MetOH in 0.1% PBS-Tween20 for 15 min each), followed by 15 min incubation in 0.1% PBS-Tween20. After this, 10% sucrose in 0.1% PBS-Tween20 was added, followed by an incubation step in 30% sucrose in 0.1% PBS-Tween20 for 1 h at room temperature (RT). Samples were embedded in O.C.T. compound (Tissue-Tek®, 25608-930, VWR, Radnor, Pennsylvania, USA) and snap frozen in isopentane cooled by liquid nitrogen. Cryosectioning was done following standard protocols (seven µm thickness along the lens/optic nerve axis).

4.5.9 Bodipy staining

To analyze outer segments morphology, cryostat sections of 5 dpf larvae were briefly washed with 1xPBS, permeabilized with 0.5% Triton X-100 in PBS, washed in PBS and incubated for 20 min with TR methyl ester (Bodipy, 1:5,000, Life Technologies, Carlsbad, Califoria, USA) and DAPI (1:8000, ITK Diagnostics, Uithoorn, The Netherlands). Sections were washed in PBS, followed by a brief wash with MilliQ and mounted with ProLong(R) Gold antifade reagent (P36930, Life Technologies, Carlsbad, California, USA).

4.5.10 Immunohistochemistry

Slides were incubated for 2 min in 0.1% PBS-T. Antigen retrieval was done by autoclaving the slides in 10 mM sodium citrate for 1 min at 121°C. After that, sections were washed three times in 0.1% PBS-T and blocked for 1 h in blocking solution (10% non-fat dry milk in 0.1% PBS-T). Primary antibody (Rhodopsin clone 4D2, mouse, 1:2000, Novus Biological NBP1-48334; GNAT2, rabbit, 1:500, MBL PM075) was incubated in blocking solution overnight at 4°C. After primary antibody incubation, sections were washed in 0.1% PBS-T, followed by secondary antibody (Alexa Fluor 568® phalloidin, 1:100, Molecular Probes A-12380; Goat IgG, Alexa Fluor 488, donkey, 1:500, Molecular Probes A11055; Mouse IgG, Alexa Fluor 488, donkey, 1:500, Life Technologies A21202) incubation for 45 min in blocking solution. Afterwards, sections were washed in PBS-T and mounted with anti-fade Prolong(R) Gold antifade reagent (P36930, Life technologies, Carlsbad, California, USA). To analyze

the thickness of ONL and INL in 6 mpf zebrafish, up to 10 different measurements were taken for each section. Two different sections were analyzed for one wild-type fish and one *pcare1* mutant fish (Supplemental Figure S2).

4.5.11 Optokinetic response (OKR) assay

All measurements were conducted between 10 am and 5 pm. The OKR was measured as described previously.[41-43] In brief, zebrafish larvae were mounted in an upright position in 3% methylcellulose in a small Petri dish placed on a platform surrounded by a rotating drum. A pattern of alternating black and white vertical stripes was displayed on the drum interior. Larvae (5 dpf) were visualized through a stereomicroscope positioned over the drum. Eye movements were recorded while larvae were optically stimulated by the rotating stripes. Larvae were subjected to a protocol of a 30 sec counterclockwise rotation, a 10 sec rest, and a 30 sec clockwise rotation. Measurements were recorded blinded. Graphs were generated and statistical analysis was done with Graphpad Prism6 software (La Jolla, CA, USA).

4.5.12 Visual motor response (VMR) assay (DanioVision)

Locomotor activity in response to light-dark conditions was analyzed using the DanioVision system (Noldus B.V., Wageningen, The Netherlands). Larvae were transferred to a 48-wells plate filled with 200 µl E3 medium without methylene blue. Each run consisted of 24 mutant larvae and 24 age-matched control wild-type zebrafish larvae using a 48-wells plate. During the experiment, the temperature was constant at 28°C using a heating/cooling system (Noldus B.V., Wageningen, The Netherlands). The protocol consisted of 20 min of acclimation (with lid of the system open; room light: 500-650 lux), closing of the lid followed by alternating periods of 10 min dark, 10 min bright light (about 3000 lux) and 10 min dark (in total 12 cycles).

Variables of interest were: *distance moved* (mm) for general activity under dark and light conditions; change in *maximum velocity* (mm·s-1), to measure the change from dark to light (*maximum velocity* first 30 sec with light minus maximum velocity last 30 sec without light); change in *distance moved* (mm), to measure the change from light to dark (*distance moved* first 30 seconds without light minus *distance moved* from last 30 sec with light).[44-46] Zebrafish tracks were analyzed using the analysis software (EthioVision). First, the missed subjects (<10%) were filtered out. Next, the heat maps of 5-minute interval were plotted, to check for general activity. Fish not moving were removed from the analysis. The distance moved (DM (mm)) per unit of time (1 min, 30 sec or 1 sec intervals) for each animal and group was used as a measure for locomotor activity. In addition, the speed of movement (Vmax (mm/s)) was measured in the dark-to-light transition. The values of 1-second interval were

used to study more precisely immediate effects of a sudden change from the dark to the light transition and from the light to dark transition. First, the distance moved was expressed by 30 sec/1 min intervals and compared between the different groups; Second, the more precise per 1 sec interval was used to analyze the direct effects of light/dark and dark/light transitions. EthioVision XT was used to quantify the experiments. Complementary to it, R programming language was used to generate plots, calculate mean values and SEM values, and perform statistical tests. The difference between wild-type and mutant was analyzed using two-tailed, unpaired Student's t-test, and p-values were corrected for multiple testing using Benjamini-Hochberg method. The means vs. standard errors of the mean are shown. Exact p-values can be found in Supplemental Table S2. The means vs. standard errors of the mean are shown.

4.5.13 Electroretinograms (ERG)

ERG was performed on isolated larval eyes (5 dpf) as previously described.[47] Larvae were dark-adapted for a minimum of 30 min prior to the measurements and subsequently handled under dim red illumination. The isolated eye was positioned to face the light source. Under visual control via a standard microscope equipped with red illumination (Stemi 2000C, Zeiss, Oberkochen, Germany), the recording electrode with an opening of approximately 20 μm at the tip was placed against the center of the cornea. This electrode was filled with E3 medium (5 mM NaCl, 0.17 mM KCl, 0.33 mM CaCl, and 0.33 mM MgSO4), the same in which the embryos were raised and held. The electrode was moved with a micromanipulator (M330R, World Precision Instruments Inc., Sarasota, USA). A custom-made stimulator was invoked to provide light pulses of 100 ms duration, with a light intensity of 6000 lux. It uses a ZEISS XBO 75W light source and a fast shutter (Uni-Blitz Model D122, Vincent Associates, Rochester, NY, USA) driven by a delay unit interfaced to the main ERG recording setup. Electronic signals were amplified 1000 times by a pre-amplifier (P55 A.C. Preamplifier, Astro-Med. Inc, Grass Technology) with a band pass between 0.1 and 100 Hz, digitized by DAQ Board NI PCI-6035E (National Instruments) via NI BNC-2090 accessories and displayed via self-developed NI Labview program.[48] All the experiments were performed at room temperature (22°C). Statistical analysis was performed using GraphPad Prism6 (La Jolla, CA, USA), and graphs were generated in R (Boston, USA) or GraphPad Prism6. For statistical analysis of b-wave amplitude (Figure 5B), two-tailed unpaired t-test with Welch's correction was performed; p-value = 0,0004; t=4.309, df=19.

4.6 References

1. Collin, R.W.J., Safieh, C., Littink, K.W., Shalev, S.A., Garzozi, H.J., Rizel, L., Abbasi, A.H., Cremers, F.P.M., den Hollander, A.I., Klevering, B.J., et al. (2010). Mutations in C2ORF71 cause autosomal-recessive retinitis pigmentosa. Am J Hum Genet 86, 783-788.
2. Nishimura, D.Y., Baye, L.M., Perveen, R., Searby, C.C., Avila-Fernandez, A., Pereiro, I., Ayuso, C., Valverde, D., Bishop, P.N., Manson, F.D., et al. (2010). Discovery and functional analysis of a retinitis pigmentosa gene, C2ORF71. Am J Hum Genet 86, 686-695.
3. Hebrard, M., Manes, G., Bocquet, B., Meunier, I., Coustes-Chazalette, D., Herald, E., Senechal, A., Bolland-Auge, A., Zelenika, D., and Hamel, C.P. (2011). Combining gene mapping and phenotype assessment for fast mutation finding in non-consanguineous autosomal recessive retinitis pigmentosa families. Eur J Hum Genet 19, 1256-1263.
4. Xu, Y., Guan, L., Shen, T., Zhang, J., Xiao, X., Jiang, H., Li, S., Yang, J., Jia, X., Yin, Y., et al. (2014). Mutations of 60 known causative genes in 157 families with retinitis pigmentosa based on exome sequencing. Hum Genet 133, 1255-1271.
5. Bocquet, B., Marzouka, N.A., Hebrard, M., Manes, G., Senechal, A., Meunier, I., and Hamel, C.P. (2013). Homozygosity mapping in autosomal recessive retinitis pigmentosa families detects novel mutations. Mol Vis 19, 2487-2500.
6. Sergouniotis, P.I., Li, Z., Mackay, D.S., Wright, G.A., Borman, A.D., Devery, S.R., Moore, A.T., and Webster, A.R. (2011). A survey of DNA variation of C2ORF71 in probands with progressive autosomal recessive retinal degeneration and controls. Invest Ophthalmol Vis Sci 52, 1880-1886.
7. Audo, I., Lancelot, M.E., Mohand-Said, S., Antonio, A., Germain, A., Sahel, J.A., Bhattacharya, S.S., and Zeitz, C. (2011). Novel C2orf71 mutations account for approximately 1% of cases in a large French arRP cohort. Hum Mutat 32, E2091-2103.
8. Liu, Y.P., Bosch, D.G., Siemiatkowska, A.M., Rendtorff, N.D., Boonstra, F.N., Moller, C., Tranebjaerg, L., Katsanis, N., and Cremers, F.P. (2017). Putative digenic inheritance of heterozygous RP1L1 and C2orf71 null mutations in syndromic retinal dystrophy. Ophthalmic Genet 38, 127-132.
9. Gerth-Kahlert, C., Tiwari, A., Hanson, J.V.M., Batmanabane, V., Traboulsi, E., Pennesi, M.E., Al-Qahtani, A.A., Lam, B.L., Heckenlively, J., Zweifel, S.A., et al. (2017). C2orf71 Mutations as a Frequent Cause of Autosomal-Recessive Retinitis Pigmentosa: Clinical Analysis and Presentation of 8 Novel Mutations. Invest Ophthalmol Vis Sci 58, 3840-3850.
10. Chaitin, M.H., Schneider, B.G., Hall, M.O., and Papermaster, D.S. (1984). Actin in the photoreceptor connecting cilium: immunocytochemical localization to the site of outer segment disk formation. J Cell Biol 99, 239-247.
11. Kevany, B.M., Zhang, N., Jastrzebska, B., and Palczewski, K. (2015). Animals deficient in C2Orf71, an autosomal recessive retinitis pigmentosa-associated locus, develop severe early-onset retinal degeneration. Hum Mol Genet 24, 2627-2640.
12. Lu, Z., Hu, X., Liu, F., Soares, D.C., Liu, X., Yu, S., Gao, M., Han, S., Qin, Y., Li, C., et al. (2017). Ablation of EYS in zebrafish causes mislocalisation of outer segment proteins, F-actin disruption and cone-rod dystrophy. Sci Rep 7, 46098.
13. Yu, M., Liu, Y., Li, J., Natale, B.N., Cao, S., Wang, D., Amack, J.D., and Hu, H. (2016). Eyes shut homolog is required for maintaining the ciliary pocket and survival of photoreceptors in zebrafish. Biol Open 5, 1662-1673.
14. Liu, F., Chen, J., Yu, S., Raghupathy, R.K., Liu, X., Qin, Y., Li, C., Huang, M., Liao, S., Wang, J., et al. (2015). Knockout of RP2 decreases GRK1 and rod transducin subunits and leads to photoreceptor degeneration in zebrafish. Hum Mol Genet 24, 4648-4659.
15. Slijkerman, R.W., Song, F., Astuti, G.D., Huynen, M.A., van Wijk, E., Stieger, K., and Collin, R.W. (2015). The pros and cons of vertebrate animal models for functional and therapeutic research on inherited retinal dystrophies. Prog Retin Eye Res 48, 137-159.
16. Bibliowicz, J., Tittle, R.K., and Gross, J.M. (2011). Toward a better understanding of human eye disease insights from the zebrafish, Danio rerio. Prog Mol Biol Transl Sci 100, 287-330.
17. Meyer, A., and Schartl, M. (1999). Gene and genome duplications in vertebrates: the one-to-four (-to-eight in fish) rule and the evolution of novel gene functions. Curr Opin Cell Biol 11, 699-704.
18. Howe, K., Clark, M.D., Torroja, C.F., Torrance, J., Berthelot, C., Muffato, M., Collins, J.E., Humphray, S., McLaren, K., Matthews, L., et al. (2013). The zebrafish reference genome sequence and its relationship to the human genome. Nature 496, 498-503.

19. Eisen, J.S., and Smith, J.C. (2008). Controlling morpholino experiments: don't stop making antisense. Development 135, 1735-1743.
20. Gentsch, G.E., Spruce, T., Monteiro, R.S., Owens, N.D.L., Martin, S.R., and Smith, J.C. (2018). Innate Immune Response and Off-Target Mis-splicing Are Common Morpholino-Induced Side Effects in Xenopus. Dev Cell 44, 597-610 e510.
21. Dowling, J.E. (2012). What can a zebrafish see with only an off-pathway and other fish stories? J Ophthalmic Vis Res 7, 97-99.
22. May-Simera, H., Nagel-Wolfrum, K., and Wolfrum, U. (2017). Cilia - The sensory antennae in the eye. Prog Retin Eye Res 60, 144-180.
23. Emran, F., Rihel, J., and Dowling, J.E. (2008). A behavioral assay to measure responsiveness of zebrafish to changes in light intensities. J Vis Exp.
24. Fernandes, A.M., Fero, K., Arrenberg, A.B., Bergeron, S.A., Driever, W., and Burgess, H.A. (2012). Deep brain photoreceptors control light-seeking behavior in zebrafish larvae. Curr Biol 22, 2042-2047.
25. Davies, W.I., Tamai, T.K., Zheng, L., Fu, J.K., Rihel, J., Foster, R.G., Whitmore, D., and Hankins, M.W. (2015). An extended family of novel vertebrate photopigments is widely expressed and displays a diversity of function. Genome Res 25, 1666-1679.
26. Branchek, T., and Bremiller, R. (1984). The development of photoreceptors in the zebrafish, Brachydanio rerio. I. Structure. J Comp Neurol 224, 107-115.
27. Morris, A.C., and Fadool, J.M. (2005). Studying rod photoreceptor development in zebrafish. Physiol Behav 86, 306-313.
28. Collins, J.E., White, S., Searle, S.M., and Stemple, D.L. (2012). Incorporating RNA-seq data into the zebrafish Ensembl genebuild. Genome Res 22, 2067-2078.
29. Collery, R., McLoughlin, S., Vendrell, V., Finnegan, J., Crabb, J.W., Saari, J.C., and Kennedy, B.N. (2008). Duplication and divergence of zebrafish CRALBP genes uncovers novel role for RPE- and Muller-CRALBP in cone vision. Invest Ophthalmol Vis Sci 49, 3812-3820.
30. Seiler, C., Finger-Baier, K.C., Rinner, O., Makhankov, Y.V., Schwarz, H., Neuhauss, S.C., and Nicolson, T. (2005). Duplicated genes with split functions: independent roles of protocadherin15 orthologues in zebrafish hearing and vision. Development 132, 615-623.
31. Morrow, J.M., Lazic, S., Dixon Fox, M., Kuo, C., Schott, R.K., de, A.G.E., Santini, F., Tropepe, V., and Chang, B.S. (2017). A second visual rhodopsin gene, rh1-2, is expressed in zebrafish photoreceptors and found in other ray-finned fishes. J Exp Biol 220, 294-303.
32. Trivedi, D., Colin, E., Louie, C.M., and Williams, D.S. (2012). Live-cell imaging evidence for the ciliary transport of rod photoreceptor opsin by heterotrimeric kinesin-2. J Neurosci 32, 10587-10593.
33. Sukumaran, S., and Perkins, B.D. (2009). Early defects in photoreceptor outer segment morphogenesis in zebrafish ift57, ift88 and ift172 Intraflagellar Transport mutants. Vision Res 49, 479-489.
34. Krock, B.L., and Perkins, B.D. (2008). The intraflagellar transport protein IFT57 is required for cilia maintenance and regulates IFT-particle-kinesin-II dissociation in vertebrate photoreceptors. J Cell Sci 121, 1907-1915.
35. Wan, J., and Goldman, D. (2016). Retina regeneration in zebrafish. Curr Opin Genet Dev 40, 41-47.
36. Bringmann, A., Iandiev, I., Pannicke, T., Wurm, A., Hollborn, M., Wiedemann, P., Osborne, N.N., and Reichenbach, A. (2009). Cellular signaling and factors involved in Muller cell gliosis: neuroprotective and detrimental effects. Prog Retin Eye Res 28, 423-451.
37. Goldman, D. (2014). Muller glial cell reprogramming and retina regeneration. Nat Rev Neurosci 15, 431-442.
38. Kimmel, C.B., Ballard, W.W., Kimmel, S.R., Ullmann, B., and Schilling, T.F. (1995). Stages of embryonic development of the zebrafish. Dev Dyn 203, 253-310.
39. Sander, J.D., Maeder, M.L., Reyon, D., Voytas, D.F., Joung, J.K., and Dobbs, D. (2010). ZiFiT (Zinc Finger Targeter): an updated zinc finger engineering tool. Nucleic Acids Res 38, W462-468.
40. Sander, J.D., Zaback, P., Joung, J.K., Voytas, D.F., and Dobbs, D. (2007). Zinc Finger Targeter (ZiFiT): an engineered zinc finger/target site design tool. Nucleic Acids Res 35, W599-605.
41. Phillips, J.B., Blanco-Sanchez, B., Lentz, J.J., Tallafuss, A., Khanobdee, K., Sampath, S., Jacobs, Z.G., Han, P.F., Mishra, M., Titus, T.A., et al. (2011). Harmonin (Ush1c) is required in zebrafish Muller glial cells for photoreceptor synaptic development and function. Dis Model Mech 4, 786-800.
42. Huber-Reggi, S.P., Mueller, K.P., and Neuhauss, S.C. (2013). Analysis of optokinetic response in zebrafish by computer-based eye tracking. Methods Mol Biol 935, 139-160.
43. Hodel, C., and Neuhauss, S.C. (2008). Computer-based analysis of the optokinetic response in zebrafish larvae. CSH Protoc 2008, pdb prot4961.

44. de Esch, C., van der Linde, H., Slieker, R., Willemsen, R., Wolterbeek, A., Woutersen, R., and De Groot, D. (2012). Locomotor activity assay in zebrafish larvae: influence of age, strain and ethanol. Neurotoxicol Teratol 34, 425-433.
45. Gao, Y., Zhang, G., Jelfs, B., Carmer, R., Venkatraman, P., Ghadami, M., Brown, S.A., Pang, C.P., Leung, Y.F., Chan, R.H., et al. (2016). Computational classification of different wild-type zebrafish strains based on their variation in light-induced locomotor response. Comput Biol Med 69, 1-9.
46. Liu, Y., Carmer, R., Zhang, G., Venkatraman, P., Brown, S.A., Pang, C.P., Zhang, M., Ma, P., and Leung, Y.F. (2015). Statistical Analysis of Zebrafish Locomotor Response. PLoS One 10, e0139521.
47. Sirisi, S., Folgueira, M., Lopez-Hernandez, T., Minieri, L., Perez-Rius, C., Gaitan-Penas, H., Zang, J., Martinez, A., Capdevila-Nortes, X., De La Villa, P., et al. (2014). Megalencephalic leukoencephalopathy with subcortical cysts protein 1 regulates glial surface localization of GLIALCAM from fish to humans. Hum Mol Genet 23, 5069-5086.
48. Rinner, O., Makhankov, Y.V., Biehlmaier, O., and Neuhauss, S.C. (2005). Knockdown of cone-specific kinase GRK7 in larval zebrafish leads to impaired cone response recovery and delayed dark adaptation. Neuron 47, 231-242.

4.7 Acknowledgements

We thank Tom Spanings, Antoon van der Horst, Max D. van Essen and Franziska Wagner for technical assistance, and Dyah Karjosukarso for assistance with OKR and DanioVision data analysis. This work was funded by the FP7-PEOPLE-2012-ITN programme EyeTN, Brussels, Belgium (grant agreement no.: 317472) to R.W.J.C.

4.8 Supplemental Data

Supplemental Figure S1. Sequence alignment of human PCARE protein with zebrafish pcare1, pcare2 and mutant pcare1$^{rmc100/rmc100}$ proteins. Identical residues in all sequences are white on a black background, whereas similar amino acids are white on a gray background. Residues that are common for two protein sequences are indicated in black on a light gray background.

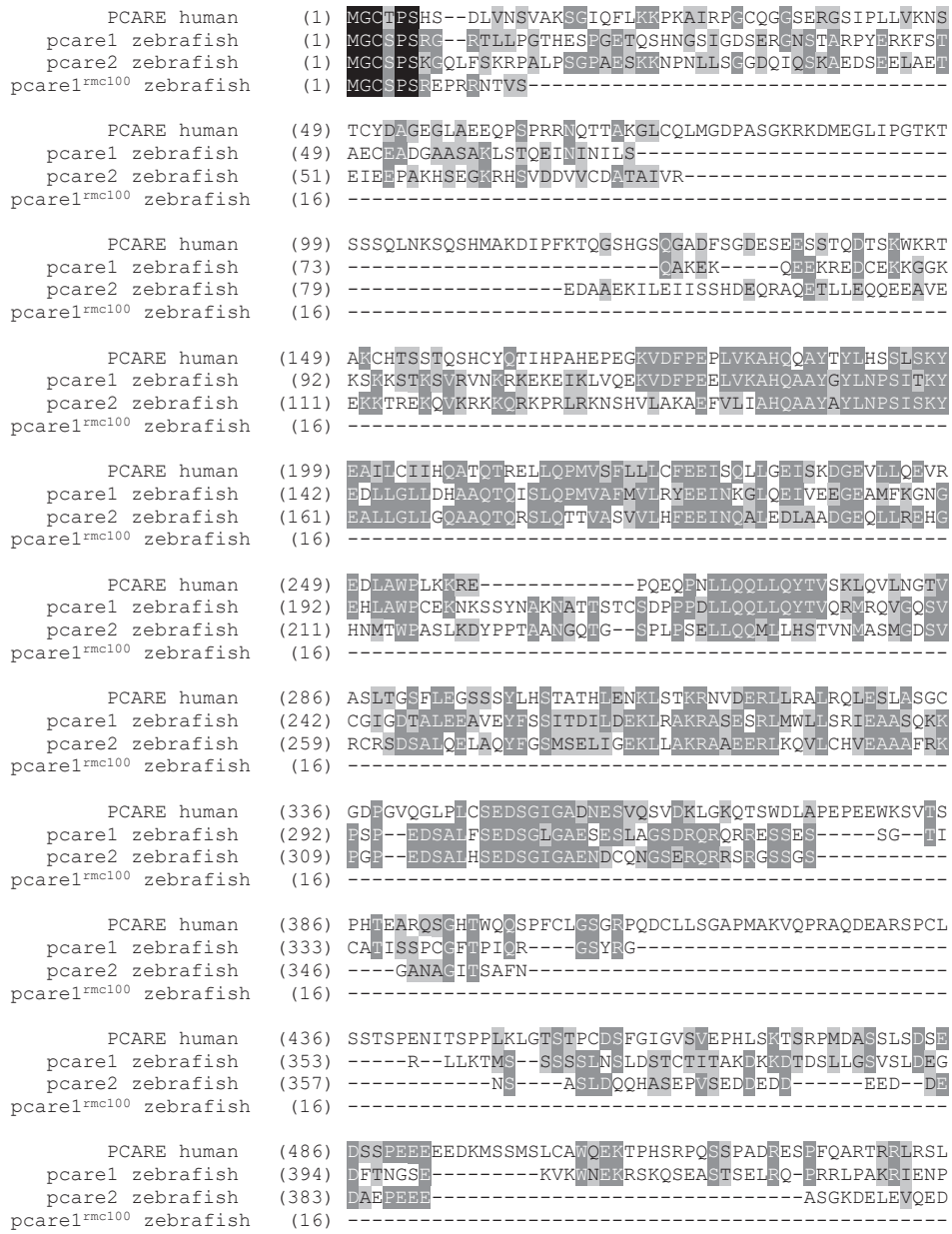

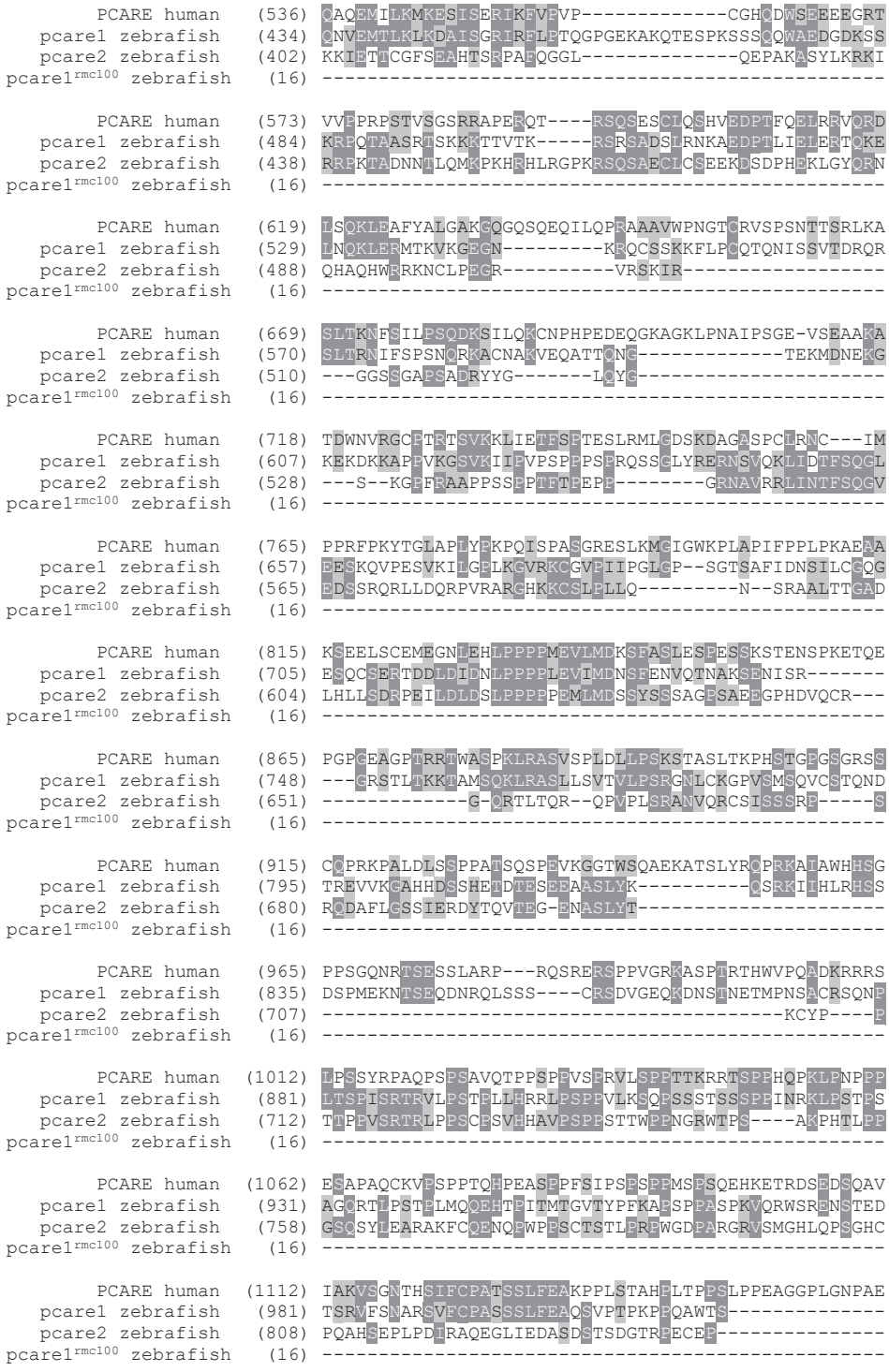
PCARE human (536) CAQEMILKMKESISERIKFVEVP----------CGHQDWSPEEEGRT
pcare1 zebrafish (434) CNVEMTLKLKDAISGRIRFLPTQGPGEKAKQTESPKSSSQQWAEDGDKSS
pcare2 zebrafish (402) KKIETTCGFSEAHTSSPAFQGGL----------QEPAKASYLKRKI
pcare1rmc100 zebrafish (16) ----------
PCARE human (573) VVEPRPSTVSGSSRRAPERQT----RSQSESCLQSHVEDPTFQEIRRVQRD
pcare1 zebrafish (484) KRPQTAASRTSKKKTTVTK-----RSRSADSLRNKAEDPTLIELERTQKE
pcare2 zebrafish (438) RREKTADNNTLQMKPKHRHLRGPKRSQSAECLCSEEKQSDPHELKLGYQRN
pcare1rmc100 zebrafish (16) ----------
PCARE human (619) LSQKLEAFYALGAKCQGQSQEQILQPRAAAVWPNGTGRVSPSNTTSRLKA
pcare1 zebrafish (529) LNQKLERMTKVKGECN----------KRQCSSKKFLPQQTQNISSVTDRQR
pcare2 zebrafish (488) QHAQHWRRKNCLPECR----------VRSKIR----------
pcare1rmc100 zebrafish (16) ----------
PCARE human (669) SLTKNFSILPSQDKSILQKCNPHPEDEQGKAGKLPNAIPSGE-VSEAAKA
pcare1 zebrafish (570) SLTRNIFSPSNQRKACNAKVEQATTQNG----------TEKMDNEKG
pcare2 zebrafish (510) ---GGSSGAPSADRYYG-------LQYG----------
pcare1rmc100 zebrafish (16) ----------
PCARE human (718) TDWNVRGCETRTSVKKLIETFSETESLRMLGDSKDAGASPCLRNC---IM
pcare1 zebrafish (607) KEKDKKAPEVKGSVKIIPVPSPESPSRQSSGLYRERNSVQKLIDTFSQGL
pcare2 zebrafish (528) ---S--KGEFRAAPPSSPPTFTEEPP--------GRNAVRRLINTFSQGV
pcare1rmc100 zebrafish (16) ----------
PCARE human (765) PPRFPKYTGLAPLYEKPQISPASGRESLKMGIGWKPLAPIFPPLPKAEAA
pcare1 zebrafish (657) EESKQVPESVKILGELKGVRKGGVPIIPGLGP--SGTSAFIDNSILCGQG
pcare2 zebrafish (565) EDSSRQRLLDQRPVRARGHKKCSLPLLQ---------N--SRAALTTGAD
pcare1rmc100 zebrafish (16) ----------
PCARE human (815) KSEELSCEMEGNLEHLPPPPMEVLMDKSFASLESPESSKSTENSPKETQE
pcare1 zebrafish (705) ESQCSERTDDLDIDNLPPPPLEVIMDNSFENVQTNAKSENISR-------
pcare2 zebrafish (604) LHLLSDRPEILDLDSLPPPPPEMLMDSSYSSSAGPSAEEGPHDVQCR---
pcare1rmc100 zebrafish (16) ----------
PCARE human (865) PGPGEAGPTRRTWASPKLRASVSPLDLLPSKSTASLTKPHSTGEGSGRSS
pcare1 zebrafish (748) ---GRSTLTKKTAMSQKLRASLLSVTVLPSRGNLCKGPVSMSQVCSTQND
pcare2 zebrafish (651) ----------G-QRTLTQR--QPVPLSRANVQRCSISSSRE-----S
pcare1rmc100 zebrafish (16) ----------
PCARE human (915) CQPRKPALDLSSPPAISQSPEVKGGTWSQAEKATSLYRQPRKAIAWHHSG
pcare1 zebrafish (795) TREVVKCAHHDSSHEIDTESEPAASLYK----------QSRKIEHLRHSS
pcare2 zebrafish (680) RQDAFLGSSIERDYTQVTEG-ENASLYT----------
pcare1rmc100 zebrafish (16) ----------
PCARE human (965) PPSGQNRTSESSLARP---RQSRERSPPVGRKASPIRTHWVPQADKRRRS
pcare1 zebrafish (835) DSPMEKNTSEQDNRQLSSS----CRSDVGEQKDNSINETMPNSACRSQNP
pcare2 zebrafish (707) ----------KCYP----P
pcare1rmc100 zebrafish (16) ----------
PCARE human (1012) LPSSYRPAQPSPSAVQTPPSPEVSPRVLSPETTKRRTSPPHQPKLPNPPP
pcare1 zebrafish (881) LTSPISRTRVLPSTELLHRRLPSPPVLKSQPSSSTSSSPPINRKLPSTPS
pcare2 zebrafish (712) TTPPVSRTRLPPSCESVHHAVPSPPSTTWPENGRWTPS----AKPHTLPP
pcare1rmc100 zebrafish (16) ----------
PCARE human (1062) ESAPAQCKVESPPTQHPEASPPFSIPSPSPEMSPSQEHKETRDSEDSQAV
pcare1 zebrafish (931) AQQRTLPSTELMQQEHTPITMTGVTYPFKAESPPASPKVQRWSREDNSTED
pcare2 zebrafish (758) GSQSYLEARAKFCQENQPWPESCTSTLPREWGDPARGRVSMGHLQPSGHC
pcare1rmc100 zebrafish (16) ----------
PCARE human (1112) IAKVSGNTHSIFCPATSSLFEAKPPLSTAHELTPPSLPPEAGGPLGNPAE
pcare1 zebrafish (981) TSRVFSNARSVFCPASSSLFEAQSVPTPKPEQAWTS----------
pcare2 zebrafish (808) PQAHSEPLPDIRAQEGLIEDASDSTSDGTREECEP----------
pcare1rmc100 zebrafish (16) ----------

```
          PCARE human  (1162) CWKNSSGPWLRADSQRFAALCAINPLPFLRRTASDFQFGGRPQPPTLDPT
     pcare1 zebrafish  (1017) --TGSNVLPRPWGERGRLPVSARGPQPFIRRSQSDERF--SLSMSSRVPV
     pcare2 zebrafish   (843) ------------EPADSHLNTLQPQQIAD--------------------
pcare1rmc100 zebrafish   (16) --------------------------------------------------

          PCARE human  (1212) STSYESQLGQNSS----SEESPKKDTEPGSSPCSPELQGG-TRRASPPEF
     pcare1 zebrafish  (1063) ISVAETCGSEPAICTHGLEEGPVREDKIRSEQ---TEIRSAVRSVSHPDL
     pcare2 zebrafish   (860) --------------------------------------------------
pcare1rmc100 zebrafish   (16) --------------------------------------------------

          PCARE human  (1257) CVLGHGLQPEPRTGHIQDKSQPEAQPQQEEVS
     pcare1 zebrafish  (1110) CIVGQGLQREWEK-------------------
     pcare2 zebrafish   (860) --------------------------------
pcare1rmc100 zebrafish   (16) --------------------------------
```

Supplemental Figure S2. Measurement of the thickness of outer and inner nuclear layers in *pcare1*$^{rmc100/rmc100}$ and wild-type zebrafish at 6mpf. A, Representative images of wild-type and *pcare1*$^{rmc100/rmc100}$ zebrafish retinas at 6 mpf. Nuclear layers were stained with DAPI and inverted in grey images. RPE: Retinal Pigment Epithelium; ONL: Outer Nuclear Layer; OPL: Outer Plexiform Layer; INL: Inner Nuclear Layer; IPL: Inner Plexiform Layer; GCL: Ganglion Cell Layer. Scale bars: 20 µm. **B**, Measurements in wild-type and *pcare1*$^{rmc100/rmc100}$ zebrafish at 6 mpf shows a significant reduction of both ONL and INL thickness in the *pcare1*$^{rmc100/rmc100}$ zebrafish. p-values < 0,01 using a Mann-Whitney U test.

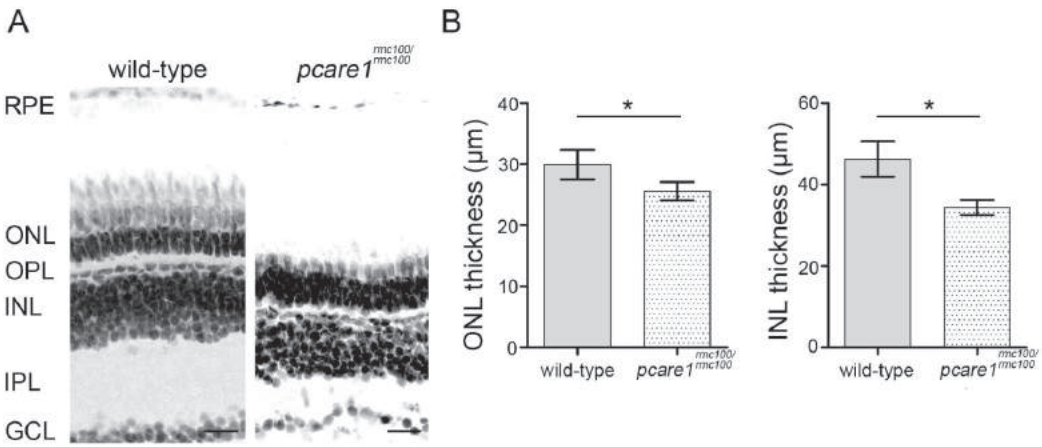

Supplemental Table S1. Primers used in this study.

Primer Name	Sequence (5'-3')
pcare1_zebrafish_genotyping_F	TCAATGTGTAACTACTGTGG
pcare1_zebrafish_genotyping_R	TTCTTTGACTTCTTTCCTCC
pcare1_zebrafish_F	TGGACCTCCACTGGTAGCAATG
pcare1_zebrafish_R	CAGCTATTTCATTCCCCAGCAG
pcare2_zebrafish_F	TCCAACCACTCCACCAGTCT
pcare2_zebrafish_R	GTTCAGGTGAGAGTCTGCCG

Supplemental Table S2. P-values of **A**, ΔDistance moved (mm) and **B**, ΔVmax (mm/s). R programming language was used to generate plots, calculate mean values and SEM values, and perform statistical tests. The difference between wild-type and mutant larvae was analyzed using two-tailed, unpaired Student's t-test, and p-values were corrected for multiple testing using Benjamini-Hochberg method.

A,

Time point (min.)	Experiment 1 – Average wild types	Experiment 2 – Average wild types	Experiment 3 – Average wild types	Experiment 1 – Average *pcare1*$^{rmc100/rmc100}$ mutants	Experiment 2 – Average *pcare1*$^{rmc100/rmc100}$ mutants	Experiment 3 – Average *pcare1*$^{rmc100/rmc100}$ mutants	p-value	Adjusted p-value
30	4.489031	3.417126	3.099486	2.977334	0.766855	1.027767	0.076637	0.084301
50	7.982758	5.421336	2.889139	2.966498	0.637896	0.951405	0.09942	0.09942
70	6.509943	4.097312	4.064718	2.596576	0.773006	1.246267	0.032556	0.05864
90	8.29358	6.715224	4.338462	2.303252	0.884807	1.39785	0.038115	0.05864
110	7.61268	5.575122	6.094735	2.01309	0.445177	2.39469	0.0049	0.017968
130	7.515253	5.567596	5.10233	2.183769	1.133339	1.964503	0.016343	0.035954
150	7.343226	6.447082	6.517712	1.394266	0.940354	2.536749	0.001805	0.017968
170	4.840743	7.028744	6.056858	2.460793	0.942638	1.85287	0.007478	0.020563
190	5.800346	5.243898	6.054689	2.121457	0.840032	2.275547	0.004418	0.017968
210	9.109013	6.809481	3.597526	1.60152	0.221808	2.653249	0.071066	0.084301
230	8.23621	4.533497	5.385639	1.619625	0.701135	1.9175	0.042647	0.05864

B,

Time point (min.)	Experiment 1 – Average wild types	Experiment 2 – Average wild types	Experiment 3 – Average wild types	Experiment 1 – Average *pcare1*$^{rmc100/rmc100}$ mutants	Experiment 2 – Average *pcare1*$^{rmc100/rmc100}$ mutants	Experiment 3 – Average *pcare1*$^{rmc100/rmc100}$ mutants	p-value	Adjusted p-value
30	32.90559	21.00921	23.42852	18.3454	6.149363	7.165309	0.04644	0.073936
50	48.34021	28.71532	21.14943	20.63709	7.536889	8.933083	0.111795	0.111795
70	39.96277	24.55223	27.03901	18.93714	5.513233	10.22137	0.03933	0.073936
90	46.33764	31.22294	21.29981	13.46355	8.134596	8.308291	0.080041	0.088046
110	45.24621	29.19242	25.68748	14.22291	4.724764	14.50949	0.046076	0.073936
130	46.59508	29.04535	26.0247	12.64319	9.390405	12.43636	0.069475	0.084914
150	41.43107	31.15287	26.87081	15.17567	10.33201	15.93244	0.03246	0.073936
170	26.16697	33.99695	26.01176	17.57142	6.420388	15.40455	0.024947	0.073936
190	39.15427	24.80746	30.02824	14.69152	3.367739	19.32694	0.041441	0.073936
210	43.72703	31.82563	21.26107	9.284293	3.57503	19.82126	0.06193	0.084914
230	43.39386	24.82262	27.74842	9.85108	5.58792	11.89881	0.04705	0.073936

Chapter 5

Generation and transcriptome analysis of *PCARE*-deficient iPSCs-derived photoreceptor-like cells

Generation and transcriptome analysis of *PCARE*-deficient iPSCs-derived photoreceptor-like cells

Julio C. Corral-Serrano[1,2], Alejandro Garanto[1,3], Thomas Piofczyk[4], Nele Nijs[4], Ramon van Huet[3,5], Frans P.M. Cremers[1,3], Silvia Albert[1,3], Jan Hellemans[4], Rob W.J. Collin[1,3]

[1]Department of Human Genetics, Radboud University Medical Center, Nijmegen, The Netherlands; [2]Radboud Institute for Molecular Life Sciences, Radboud University Medical Center, Nijmegen, The Netherlands; [3]Donders Institute for Brain, Cognition and Behaviour, Radboud University, Nijmegen, The Netherlands; [4]Biogazelle, Ghent, Belgium; [5]Department of Ophthalmology, Radboud University Medical Center, Nijmegen, The Netherlands.

5.1 Abstract

Retinitis Pigmentosa (RP) and cone-rod dystrophy (CRD) are a group of monogenic diseases characterized by progressive degeneration of the photoreceptor cells of the outer neural retina. Mutations in the ciliary gene *PCARE* (photoreceptor cilium actin regulator) are causative for autosomal recessive RP or CRD. Ciliation studies in fibroblast cells from an individual carrying a point mutation in *PCARE* (c.947del; p.Asn316Metfs*7) that is predicted to result in premature termination of protein synthesis, showed no defects in cilium length. This could be explained by the low expression levels of *PCARE* in fibroblasts compared to retinal cells, and it is in line with the hypothesis that the function of PCARE is restricted to the photoreceptor cells within the retina. To model the disease *in vitro*, we have generated patient-specific induced pluripotent stem cells (iPSCs) and followed a 90-day differentiation protocol to generate iPSCs-derived photoreceptor-like cells from patient-derived fibroblasts. Transcriptome analysis of the differentiated cells revealed that, while wild-type cells were able to differentiate into a neuronal cell fate, the majority of patient-derived iPSCs differentiate into a plasma cell fate. In addition, a relatively low number of reads for photoreceptor- and RPE-specific genes was detected, indicating that this population of cells is under-represented in the differentiated cultures. These data suggest a defect in the patient cells to differentiate into a neuronal fate, and an improved protocol of iPSCs differentiation will be needed to assess the pathophysiological mechanisms behind the disease.

5.2. Introduction

Inherited retinal diseases (IRDs) are a group of disorders that affect the cells from the retina. The prevalence of these diseases in the population is of 1:4,000 individuals worldwide.[1] Clinical features include night blindness, tunnel vision, and loss of central vision in advanced cases. As described in **chapter 2** of this thesis, we have identified that the protein PCARE, encoded by the gene *PCARE* (formerly known as *C2orf71*), mutated in autosomal recessive retinitis pigmentosa (arRP) or cone-rod dystrophy (CRD), is important for the morphogenesis of photoreceptor outer segments by the delivery and deployment of a ciliary actin assembly module. However, the process of photoreceptor cell morphogenesis when *PCARE* is mutated has not yet been studied.

PCARE is a ciliary protein presumed to be specifically active in photoreceptor cells.[2] Since it is not possible to obtain photoreceptor cells from a patient to study the defective protein without inflicting permanent damage to the retina, the best alternative model is the use of induced pluripotent stem cell (iPSC) technology to generate photoreceptor-like cells.[3] To this aim, e.g. fibroblasts are obtained from a skin biopsy of patients with mutations in the gene of interest and reprogrammed into iPSCs. Different studies have demonstrated that, under specific culture conditions, embryonic stem cells (ESCs) and iPSCs can be differentiated into a retinal fate, including photoreceptor precursor cells.[4-8]
In vivo, retinal cell differentiation takes place through several steps. It starts with the development of the eye field, a centrally-organized domain that contains anterior neuroepithelial cells that will become retinal progenitors.[9] The eye field is characterized by the expression of a group of transcription factors, mainly *PAX6*, *RX*, *LHX2* and *SIX6*.[9] Next, the eye field develops into the future neural retina (NR) and retinal pigment epithelium (RPE). Two transcription factors, *VSX2* and *MITF*, regulate this specification and they are expressed in the NR (*VSX2*) and RPE (*MITF*). After this, the neuroretina begins to differentiate to give rise to the different retinal layers.

Three-dimensional retinal organoids reproduce many aspects of embryonic retinal development, including the formation of a bi-layered optic cup and light-detecting photoreceptor cells.[8] However, until now, there has been little research about the transcriptome changes during the differentiation of iPSCs into photoreceptor cells. Such analyses are currently commonly performed by the direct sequencing of transcripts using high-throughput RNA Sequencing (RNA-Seq) technology. Compared to microarrays, RNA-Seq directly detects transcripts, avoiding hybridization biases and providing more precise information on transcript levels.[10]

In this study, we aimed to study *PCARE*-associated retinal disease in an *in vitro* context. We first show that *PCARE*-deficient fibroblasts do not present any ciliary defects. Subsequently, we have reprogrammed these fibroblasts into iPSCs and followed a 90-day protocol of differentiation into

photoreceptor-like cells. Finally, we have conducted RNA-Seq to study the transcriptional landscape of iPSCs-derived *PCARE*-deficient photoreceptor-like cells.

5.3 Results

5.3.1. Fibroblasts from a patient with a homozygous *PCARE* mutation do not show ciliary defects

Since PCARE is a ciliary protein, we first aimed to assess whether it has an important function in the primary cilium of fibroblasts. Therefore, we monitored ciliogenesis and cilium length in primary fibroblasts derived from a patient with a mutation in *PCARE* (c.947del) that is predicted to lead to a frame shift p.(Asn316Metfs*7), and compared them to cells derived from three age-matched healthy controls. Immunocytochemical analysis did not show any morphological defect in the cilium (Figure 1A).

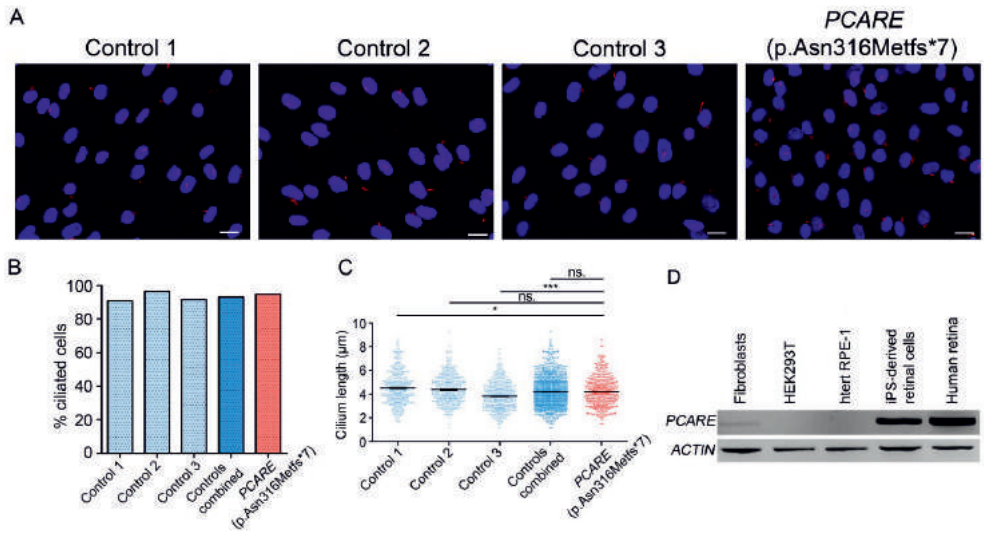

Figure 1. Patient-derived fibroblast cells carrying the *PCARE* (p.Asn316Metfs*7) mutation do not show ciliary defects. A, Fibroblasts from a patient with a homozygous *PCARE* mutation (c.947del) were serum-starved for cilium growth and compared with three different control fibroblasts in two different experiments. Cilia were stained with acetylated α-tubulin (red). Nuclei are marked in blue (DAPI). Scale bars = 20 µm. **B,** Percentage of ciliated cells for the three unrelated healthy controls, the average of all controls combined and the *PCARE* (c.947del) mutant fibroblasts is represented in the graph. At least 200 cells were counted per condition. **C,** Cilium length was measured by using ImageJ.[11] *PCARE* (p.Asn316Metfs*7) fibroblasts do not show a significant difference in cilium length compared with controls. P-value control 1 vs patient = 0,0157, *, two-tailed, t=2,429 df=339. P-value control 2 vs patient = 0,0794, ns, two-tailed, t=1,759, df =371. P-value control 3 vs. patient < 0,0001, ***, two-tailed, t=5,158, df=836. P-value controls combined vs. patient = 0.8025. **D,** RT-PCR analysis to detect *PCARE* expression in different ciliated cell types reveals low expression in fibroblasts compared with induced pluripotent stem cell-derived retinal cells and human retina. *PCARE* is not expressed in HEK293T cells and hTERT RPE-1 cells.

PCARE mutant fibroblasts developed over 90% of ciliated cells, similar to the healthy controls, indicating that ciliogenesis was not altered (Figure 1B). Similarly, the cilium length of the mutant cells did not differ significantly from all three controls (Figure 1C). Our results show no major ciliary defects, which could be explained by the very low gene expression of *PCARE* in fibroblast cells (Figure 1D).

5.3.2. Generation of iPSCs cells from fibroblasts

The absence of ciliary defects in patient fibroblasts strengthened our hypothesis of a more photoreceptor-specific function of PCARE. Therefore, we followed a protocol to reprogram the patient-derived fibroblasts into iPSCs, which can then be further used for differentiation into photoreceptor cells. In addition, fibroblasts from a control individual were taken along. Immunocytochemistry revealed that the iPSCs were positive for the pluripotency markers NANOG, SSEA4, OCT4 and TRA1-81 (Figure 2A). The positive expression of the pluripotency markers was validated by quantitative real-time polymerase chain reaction (qRT-PCR) (Figure 2B).

5.3.3. Differentiation of iPSCs into photoreceptor-like cells

To mimic the *in vivo* retinal differentiation process, we have followed a retinal differentiation protocol adapted from previous work (Figure 3A).[7,12] Morphological changes were tracked during the whole differentiation process. We observed that patient cells morphology was different from wild-type cells, showing a deficient aggregation process (Figure 3B). In wild-type cells, spheres formed a solid structure. Importantly, no evident neuroretinal vesicles were observed in either wild-type or patient-derived cultures (Figure 3C).

5.3.4. Transcriptome analysis of iPSCs-derived differentiated cells

To study the transcriptomic changes after differentiation, undifferentiated iPSCs at day 0 (D0) and iPSCs-derived differentiated cells at day 90 (D90), that underwent the differentiation protocol towards photoreceptor-like cells, were collected. Total RNA was extracted from 10 independent samples: 2 biological replicates of RNA at day 0 (one control, one patient), and 8 biological replicates of RNA at day 90 (4 biological replicates of the control line and 4 biological replicates of the patient line). Each biological replicate at day 0 was subdivided in 4 different samples (technical replicates).

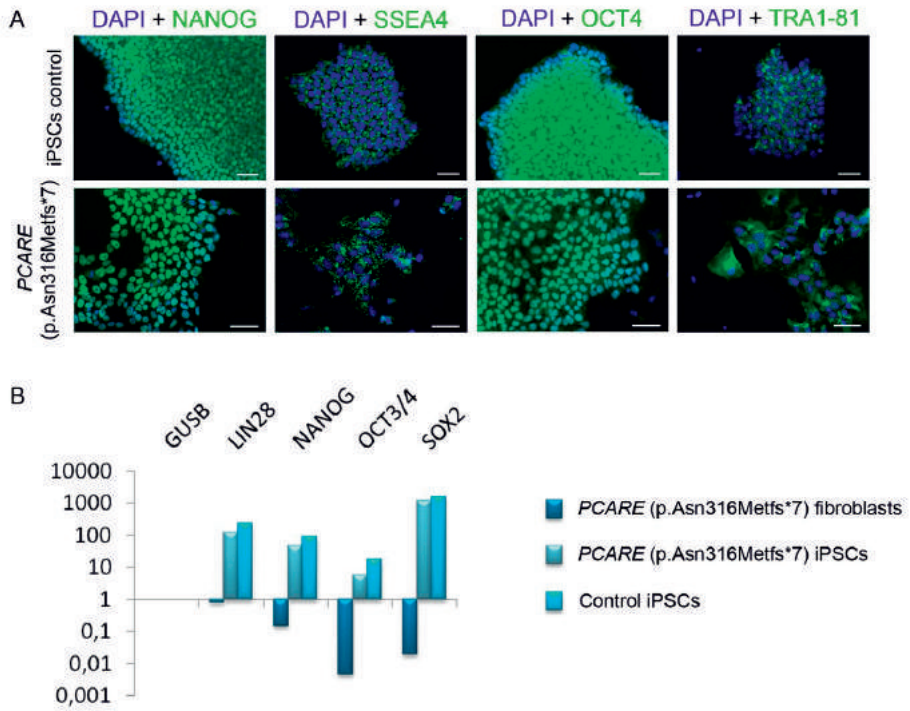

Figure 2. Characterization of iPSCs obtained from control and patient fibroblast cells. A, Both iPSC lines reprogrammed from control and patient fibroblasts express the pluripotency markers NANOG, SSEA4, OCT4 and TRA1-81, marked in green. DAPI is stained in blue. Scale bar is 50 µM (upper panels) and 20 µM (lower panels). **B,** qRT-PCR reveals the expression of pluripotency markers *LIN28*, *NANOG*, *OCT3/4* and *SOX2* in the control and patient iPSCs clones. Log expression values were normalized against the housekeeping gene *GUSB*.

Afterwards, deep sequencing of 16 samples was performed. On average, 23.3 million reads were generated per sample (Supplemental Figure S1), with a minimal read count of 15.7 million reads. For most samples, the majority of reads mapped to the transcriptome, highlighting efficient enrichment for poly-A+ RNA (Supplemental Figure S2). Sample-based clustering of the samples showed that there were no experimental artefacts and confirmed that the samples were grouped according to the known categories (mutant and wild-type) (Figure 4).

5.3.5. *PCARE*-deficient differentiated photoreceptor-like cells show reduced expression of extracellular matrix organization and cell adhesion genes

To study the differential gene expression analysis, we performed five different comparisons. In table 1, the compared conditions and the number of up- and down-regulated genes are listed. The results of each test are displayed as Volcano plots (Supplemental Figure S3).

We then performed analysis of the enriched terms associated with the expressed genes using DAVID Software v.8.[13,14] Genes with log2FoldChange>5 were taken into the analysis. When comparing the

enriched terms associated with the differentially expressed genes between control cells at day 0 vs patient day 0, we observed that the control cells have an enrichment in extracellular matrix organization and cell adhesion (Table 2), which could explain the differences between the morphology of the embryoid bodies of control and patient cell lines. At day 90, the control cells are also more enriched in synaptic transmission and neural tissue pathways (Table 3).

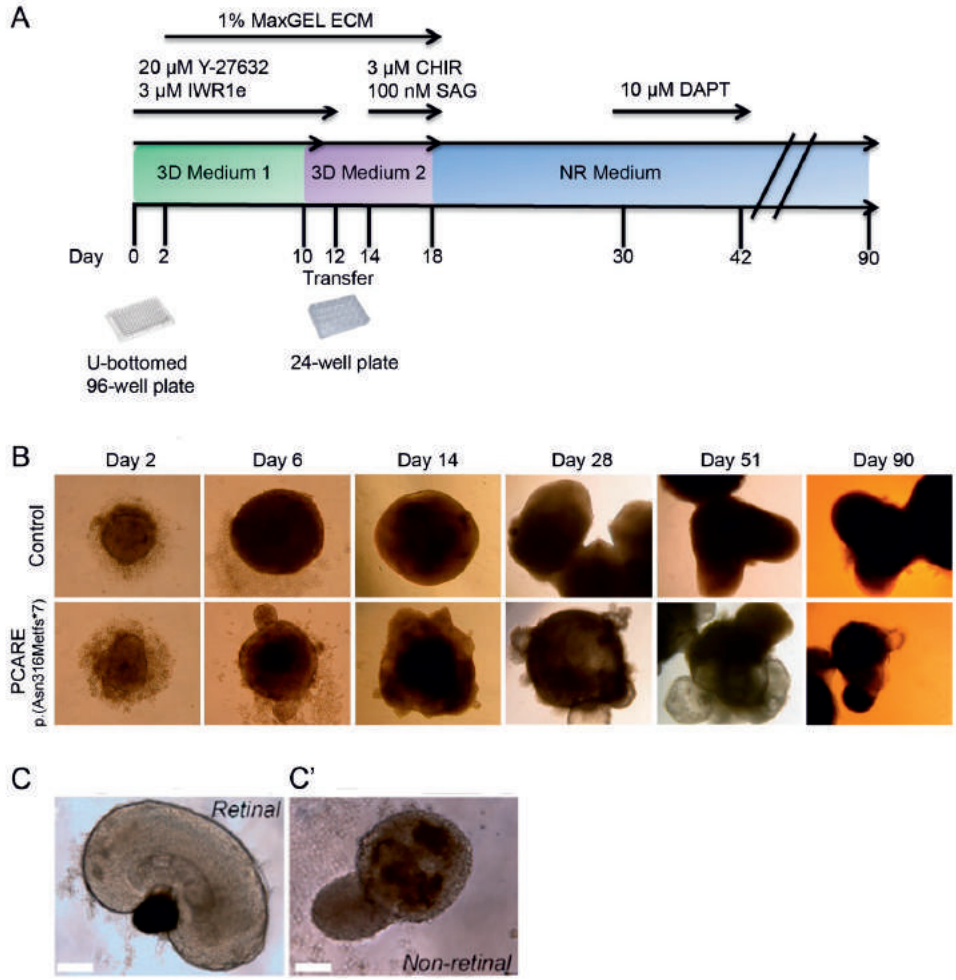

Figure 3. Photoreceptor differentiation in 3D cultures from iPSCs. A, Schematic of NR-selective culture of iPSCs to recapitulate retinogenesis *in vitro*. **B,** Bright-field view of the developing control and PCARE (p.Asn316Metfs*7) at different time points. **C,** Expected morphology of the retinal structures, and **C'**, morphology of non-retinal structures (image adapted from Gonzalez-Cordero et al.[15]).

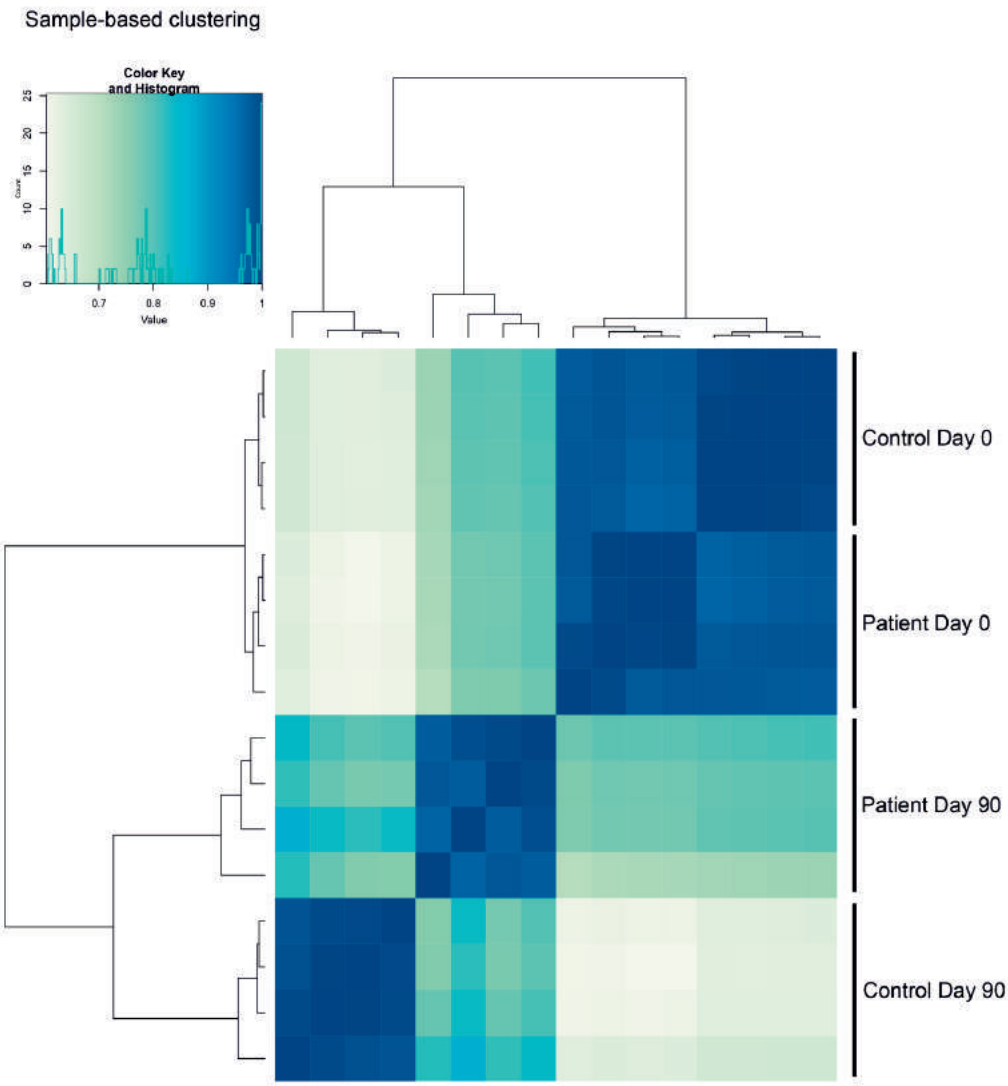

Figure 4. Sample-based clustering using normalized gene expression data. Pair-wise sample Pearson correlation coefficients were visualized in a heat map. The samples form two large groups, day 0 (D0) and day 90 (D90), with two subgroups based on the respective control and patient cell lines.

Table 1. Differential gene expression analysis. Five comparisons were performed. In each comparison, several thousand significantly differentially expressed genes were found. 22565 genes with non-zero total read count were included in the analysis; up: number of upregulated genes at FDR<0.05; down: number of downregulated genes at FDR<0.05. FDR: False discovery rate. D0: Day 0, pluripotent state. D90: Day 90, differentiated state.

	Comparison	Up	Down	Unique
A	Control_D90 vs. Control_D0	7790	6871	170
B	Patient_D90 vs. Patient_D0	8473	6624	176
C	Patient_D0 vs. Control_D0	4464	4243	181
D	Patient_D90 vs. Control_D90	6270	5737	315
E	D90 vs. D0	8261	6223	142

To confirm the pluripotency of the cells, the average of all the replicate samples was taken and the average reads per kilobase per million (RPKM) of pluripotency genes was calculated. For all pluripotency markers, *NANOG*, *TRA1-81*, *LIN28*, *OCT4* and *SOX2*, the number of reads was higher in the iPSCs than in the differentiated cells (Figure 5A). To study whether the differentiated cells expressed retina-specific genes, the average RPKM of retinal pigmented epithelium (RPE) specific genes (Figure 5B) and photoreceptor-specific genes (Figure 5C) was also calculated. Compared to the iPSCs, we detected an increase in the number of reads for the RPE-specific genes *RPE65*, *LGI1* and *BEST1*, while there was a similar number of reads for *RLBP1* between the two time points. Interestingly, the analysis detected more reads for the gene *LRAT* in the iPSCs compared to the differentiated cells. Finally, the expression of photoreceptor and neural markers was validated by qRT-PCR (Supplemental Figure 4). Interestingly, *PCARE* expression was detected by qRT-PCR with an ~80-fold increased comparing the iPSCs to the differentiated cells, indicating that *PCARE* is expressed in the differentiated cells. These results indicate that, although the differentiation did not yield an enrichment in cells with morphological photoreceptor-like characteristics, the cells do express several photoreceptor-specific genes.

Table 2. Enriched terms associated with the differentially expressed genes between control cells at day 0 vs patient cells at day 0 and control cells at day 90 vs patient cells at day 90. P-values are Bonferroni corrected. Displayed are the top enriched terms for each category.

Category	Control (D0) vs Patient (D0)	Gene count	%	P-value	Category	Control (D90) vs Patient (D90)	Gene Count	%	P-value
Gene Ontology	Extracellular matrix organization	57	3.1	8.1E-10	Gene Ontology	Synaptic transmission	127	6.5	1.8E-41
	Cell adhesion	66	3.6	1.8E-8		Transmembrane transport	116	6.0	6.2E-16
	Learning	20	1.1	2.4E-8		Ion transmembrane transport	58	3.0	1.4E-13
Tissue	Plasma	57	3.1	8.2E-11	Tissue	Brain	935	48.2	2.7E-43
	Brain	670	36.4	1.3E-3		Hippocampus	82	4.2	7.0E-11
						Amygdala	96	4.9	1.1E-9
						Fetal brain	99	5.1	2.2E-5
Kegg Pathway	Cell adhesion molecules (CAMs)	31	1.7	8.0E-8	Kegg Pathway	Neuroactive ligand-receptor interaction	78	4.0	9.7E-26
	Neuroactive ligand-receptor interaction	45	2.4	5.8E-7		Calcium signaling pathway	47	2.4	1.4E-14
	Hippo signaling pathway	27	1.5	2.7E-5		Nicotine addiction	21	1.1	6.8E-11

Table 3. Enriched terms associated with the differentially expressed genes between control cells at day 90 vs day 0 and patient cells at day 90 vs day 0. P-values are Bonferroni corrected. Displayed are the top enriched terms for each category.

Category	Control (D90 vs D0)	Gene count	%	P-value	Category	Patient (D90 vs D0)	Gene Count	%	P-value
Gene Ontology	Anterior/posterior pattern formation	30	3.8	2.0E-21	Gene Ontology	Anterior/posterior pattern specification	35	3.2	2.4E-18
	Synaptic transmission	54	6.9	7.7E-17		Embryonic skeletal system morphogenesis	18	1.6	1.1E-8
	Embryonic skeletal system morphogenesis	17	2.2	1.9E-13		Negative regulation of endopeptidase activity	27	2.4	6.6E-6
Tissue	Nervous system development	30	3.8	6.5E-8	Tissue	Embryonic forelimb morphogenesis	14	1.3	5.5E-6
	Brain	373	47.6	2.2E-9		Plasma	63	5.7	3.7E-22
	Amygdala	46	5.9	2.6E-4		Liver	175	15.9	1.2E-9
	Hippocampus	38	4.9	2.3E-4		Skeletal muscle	62	5.6	5.9E-8
Kegg Pathway	Brain cortex	15	1.9	7.6E-3	Kegg Pathway	Intestine	11	1.0	3.4E-5
	Neuroactive ligand-receptor interaction	35	4.5	8.0E-13		Complement and coagulation cascades	20	1.8	5.6E-10
	Calcium signaling pathway	25	3.2	2.5E-10		Retinol metabolism	18	1.6	1.1E-8

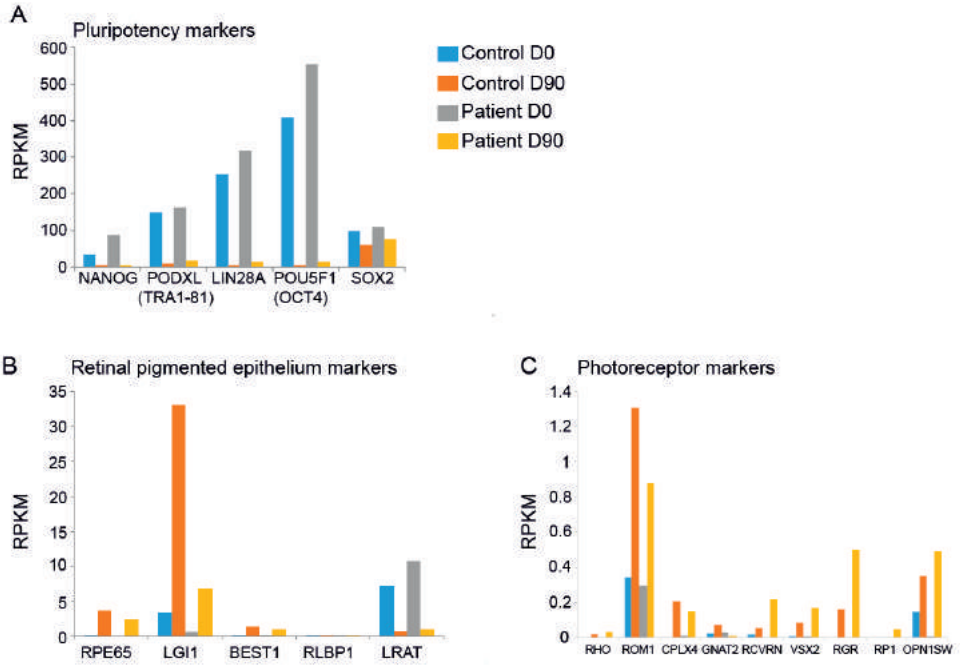

Figure 5. Analysis of the transcriptome reads for RPE markers and photoreceptor markers confirms the expression of these genes in the differentiated cultures. Reads per kilobase per million (RPKM, Y-axis) were calculated for **A,** pluripotency genes *NANOG*, *PDXL*, *LIN28A*, *POU5F1* and *SOX2*, **B,** retinal pigmented epithelium genes *RPE65*, *LGI1*, *BEST1*, *RLBP1* and *LRAT* and **C,** photoreceptor specific genes *RHO*, *ROM1*, *CPLX4*, *GNAT2*, *RCVRN*, *VSX2*, *RGR*, *RP1* and *OPN1SW*.

5.4. Discussion

The retina is a tissue of difficult access that cannot be sampled directly from patients. Because PCARE is a ciliary protein, we first wanted to assess whether its function could be studied by using a ciliated cell type. Consequently, we obtained fibroblasts from a patient with the c.947del (p.Asn316Metfs*7) mutation in *PCARE* to study potential ciliary defects. We did not observe any ciliary defects in the fibroblasts, likely due to the low expression of *PCARE* in this cell type. The observed high variation in cilia length within the same sample can be explained by the imaging of 2D projections,[16] but also due to the variability that can be found in the population. In addition, other genetic variants in ciliary genes could potentially act as modifiers, and this may increase the variability among samples. Although RPE cells can be more easily obtained than photoreceptors (the RPE differentiation protocol only takes up to 30 days),[17-19] *PCARE* expression is restricted to photoreceptors.[20] To date, protocols for photoreceptor generation from iPSCs require long and expensive cultures,[7,8,12,15,21,22] but some of those show a relatively high success rate, with expression of photoreceptor markers

appearing as early as 12 weeks post-differentiation.[12,15] For that reason, and to study the PCARE function, we tested a 90-day 3D differentiation protocol to generate photoreceptor-like cells from iPSCs of the *PCARE* c.947del patient, and cells from a non-affected individual as a control.

Morphological changes were observed during the differentiation, indicating its progression. However, using our differentiation protocol, we did not observe evident neuroretinal vesicle formation in either wild-type or mutant cell lines. Recent studies showed that the percentage of cultures that achieve a good differentiation into neuroretinal vesicles is usually quite low.[15,21] On top of that, in our 3D protocol, some neuroretinal structures might be hidden inside the conglomerate of cells, which would make them difficult to be observed through the microscope. Importantly, we did detect formation of pigmented cells in the cultures (data not shown), suggesting that there might have been RPE formation, which motivated us to continue with the differentiation. Alternatively, melanocytes are also pigmented, and given the heterogeneity of the culture, those cells could be the source of the observed pigmentation.

After 90 days of differentiation, we did not detect any cells clearly positive for different neuroretinal markers (e.g., CRX, NRL or OPN1SW) at immunocytochemistry (ICC) level (data not shown). This may be because the selected conglomerate of cells for immunostaining from the wild-type cells was not neuroretinally differentiated. Additionally, these markers were upregulated in the differentiated cells compared to iPSCs (Supplemental Figure S4), although the gene expression levels were perhaps too low to be detected at the protein level by ICC.

Analysis of the transcriptome of the iPSCs at day 0 revealed that the patient cell line presents a downregulation of extracellular matrix genes, which could explain the problems in aggregation observed in Figure 3. We know that PCARE has a relation with the actin cytoskeleton through its interaction with the Wiskott-Aldrich Syndrome protein WASF3, therefore a cytoskeletal problem might be taking place in the patient cells at the iPSCs level. Importantly, aggregation is known to be crucial for consequent differentiation into a neural fate.[7,8]

Both control and patient cells grouped in different independent clusters (Figure 4). Although the NR tissues were not enriched in retinal cells, we detected low expression of the photoreceptor-specific genes *VSX2*, *RGR*, *RHO*, *OPN1SW* in the transcriptome, and RPE-specific genes (*RPE65*, *BEST1*, *RLBP1*, *LGI1, LRAT*). Interestingly, for *LRAT*, the number of transcripts detected in the transcriptome was higher in the iPSCs than in the RPE, suggesting that it may have a role in iPSCs in addition to its known role in RPE cells (Figure 5B). The low number of reads in the transcriptome for retinal genes indicates that, although there may have been some photoreceptor-like cells in our culture, the photoreceptor cell population is under-represented in the complete sample. To enrich this

photoreceptor population, a selection process such as fluorescence-activated cells sorting (FACS) will be needed in future experiments.

Several factors can be playing a role in the success of differentiation. The first factor is the cell type choice. Our protocol is mainly an adaptation of that of Yoshiki Sasai,[7] in which they use human embryonic stem cells (hESCs) for the differentiation into photoreceptors. In our protocol, we used iPSCs derived from fibroblasts, as they did in the groups of Canto-Soler[8] and Ali.[15] The transcription profiles of iPS and ES cells are almost identical, with a small group of genes differentially expressed between several iPS and ES cells lines.[23] However, there are differences in individual reprogramming experiments between iPSC and ESC lines. First, the iPSCs do not efficiently silence the expression pattern of the somatic cells from which they are derived. Second, because of the epigenetic memory, the iPSCs fail to induce some ESC specific genes to the level of expression in ESCs.[23-26]

The second factor playing a role in a successful differentiation is the composition of the medium used in the protocol. One important compound is the supplement chosen to allow neural survival. Meyer et al.[21] and Zhong et al.[8] used B27 supplement, in comparison to N2 supplement that was used by Nakano et al.[7] and Reichman et al.[22] Since the type of neural survival supplement does not seem to be a limiting factor, N2 supplement was finally chosen for this study. The use of extracellular matrix also does not seem to be restrictive for the growth of neuroretinal vesicles. In Gonzalez-Cordero et al.,[15] they were able to grow neuroretinas in suspension, while the protocol of Zhong and colleagues used Matrigel (growth-factor-reduced; BD Biosciences) for maintaining the neuroretinas.[8] Another important component of the differentiation medium is fetal bovine serum (FBS). FBS has been shown to induce the reprogramming into iPSCs in a concentration-dependent manner.[27] The concentration of FBS also plays an important role in neuroretinal differentiation *in vitro*. Treatment with low levels of FBS favors differentiation of rhodopsin-positive photoreceptors, interneurons and retinal ganglion cells, while high FBS concentrations preferentially induce differentiation of glia cells.[28] In this protocol we used 10% FBS, a concentration previously reported.[7,8,15] The addition of DAPT, which is thought to increase cone differentiation,[29] and retinoic acid, which suppresses cone maturation,[29] also vary between protocols. Moreover, an increase in addition of compounds does not automatically mean better differentiation, since the absence of other supplements during the final stage of differentiation helps the maturation of photoreceptor cells.[30]

The third factor is the time. Although the majority of protocols report expression of photoreceptor markers after 80-100 days, some take up to 120 or 150 days to obtain mature photoreceptors. Important in this aspect is the capacity to assess the progression at intermediate states of differentiation to analyse the expression of early neural markers and early photoreceptor markers.

Because of the restricted yield of the cellular material in this experiment, we did not include these evaluations.

Another important factor is the iPSCs generation using lentivirus. Lentivirus is an integrative virus, implicating that rearrangement of the cell genome may occur and there is a chance of random viral insertion. An alternative to lentivirus are other non-integrative methods, e.g. Sendai virus, Epstein-Barr virus-derived sequences that facilitate episomal plasmid DNA replication, or mRNA transfection.[31]

Current knowledge suggests that a combination of 2D/3D protocols is the best approach for a good differentiation. Sometimes it is suggested to excise the neural retinas once they are formed in a monolayer, around the third and fourth weeks.[8,15] At that time, it is possible to already assess and select the neuroretinal vesicles and continue to grow them in 3D suspension. At the same time, it is possible to also analyse the expression of neural markers in those cultures. Similarly to what happens in the fetal development *in vivo*, by 15 weeks of differentiation it is possible to observe a defined ONL-like layer at the apical edge of the developing neuroepithelium.[32] The CRX neural marker appears as early as week 6, while RCV1 appears at week 10. NRL and RHO are also abundant after 15 weeks, indicating the presence of rod photoreceptors.[15] The human cone S OPSIN and L/M OPSIN proteins appear in the fovea around fetal weeks 11 and 15 respectively,[33] while *in vitro* they are observed at week 12 and 17 of differentiation, respectively.[15]

Our study used fibroblasts cells from one patient and one control, with the limitations that these numbers implicate. To increase the significance of the study, analysis of at least one more control and patient cell line would be needed. Alternatively, the use of isogenic lines would reduce some of the variation. In this case, the desired *PCARE* mutation could be introduced by CRISPR/Cas9 technology in a population of wild-type cells, leaving the non-targeted population as isogenic control.

In conclusion, we showed that iPSCs derived from a patient with the *PCARE* c.947del mutation present a different gene expression pattern than iPSCs derived from a healthy control. To study the potential of these iPSCs to generate photoreceptor cells, we have tested a 90-day differentiation protocol into a retinal fate. Transcriptome analysis of the iPSCs at day 0 showed downregulation of expression of genes coding for actin cytoskeletal proteins in *PCARE*-deficient iPSCs, pointing towards a defect in the actin cytoskeleton pathway. Analysis of the gene expression of the differentiated cells at day 90 revealed that, while wild-type cells showed tendency to differentiate into a neuronal cell fate, the majority of patient-derived iPSCs tend to differentiate into a plasma cell fate. However, only a low number of reads of photoreceptor-specific genes was detected, indicating that the culture was not significantly enriched in photoreceptor cells. Therefore, an improved protocol that allows more

enrichment of photoreceptor cells will be needed to specifically assess the potential morphological defects due to *PCARE* mutation.

5.5. Methods

5.5.1. Isolation of fibroblast cells

Our research was conducted according to the tenets of the Declaration of Helsinki. The procedures for obtaining human skin biopsies to establish primary fibroblasts cell lines were approved by the Ethical Committee of the Radboud University Medical Centre (Commissie Mensgebonden Onderzoek Arnhem-Nijmegen, file number 2015-1543). Written informed consent was gathered from all participating individuals. All procedures were carried out in the Netherlands.

5.5.2. Immunostaining and cilium length measurements

Patient and control fibroblasts were cultured in DMEM medium (20% fetal calf serum (FCS), 1% sodium pyruvate and 1% Pen/Strep). Cells were seeded in a 24-well plate with a coverslip. To allow cilium generation, fibroblasts were serum starved with 0.2% FCS for 48 h before immunostaining. For immunocytochemistry, cells were fixed in 2% Paraformaldehyde (PFA) (18501, Ted Pella Inc, Redding, California, USA) 20 min, permeabilized in ultra-pure grade phosphate-buffered saline (PBS) (J373-4L, VWR, Radnor, Pennsylvania, USA) with 1% Triton® X-100 (cat. # 108643, Merck Millipore, Billerica, Massachusetts, United States) 5 min and blocked 30 min with 2% bovine serum albumin (A7906-100G, Sigma-Aldrich, St. Louis, Missouri, USA) in PBS at room temperature (RT). A mouse anti-acetylated tubulin antibody (1:1,000, T6793-100ul, Sigma-Aldrich, St. Louis, Missouri, USA) was used to detect the cilium axoneme. Cells were incubated with the primary antibody 60 min, followed by 3 washes of 5 min in PBS. Subsequently, cells were incubated with a 1:500 dilution of the corresponding Alexa Fluor-conjugated antibody. Cells were washed 3 x 5 min in PBS, rinsed in MQ and mounted in VECTASHIELD® antifade mounting medium with DAPI (VECTH-1200, VWR, Radnor, Pennsylvania, USA). Images were taken with a Carl Zeiss Axio Observer Z1 Microscope (Carl Zeiss Microscopy GmbH, Oberkochen, Germany). Cells presenting cilia were counted and the cilium length was measured using ImageJ.[11]

5.5.3. RT-PCR

To analyse the gene expression of *PCARE*, we performed RT-PCR of cDNA extracted from ciliated fibroblasts, HEK293T and hTERT RPE-1 cells. As positive controls, cDNA from iPS-derived retinal cells and human retina were taken along. For cDNA synthesis, 1 µg of total RNA was incubated with 1 µl iScript Reverse Transcriptase (1708891, Bio-Rad, Hercules, California, USA) and 1x reaction mix in a final volume of 20 µl. For the RT-reaction, the mixture was incubated 5 min at 25°C, 30 min at 42°C and the reaction was stopped by heating it 5 min at 85°C. PCR analysis was performed with Taq DNA polymerase (18038042, Life Technologies, Carlsbad, California, USA), the primers: *PCARE* forward 5'GCTAAACCGCCACTCTCAAC-3', *PCARE* reverse 5'ACAGAACTCTGGGGGAGATG-3', and the following program: 94°C for 3 minutes, followed by 35 cycles of denaturation at 94°C for 20 seconds, annealing for 20 seconds at 58°C and extension of 30 sec at 72°C, with a final extension for 6 minutes at 72°C.

5.5.4. iPSCs generation and characterization

Before reprogramming, fibroblasts were seeded (200,000 cell/well in a 6-well plate) and grown until 70% confluence 24 h before infection. Cells were refreshed with DMEM containing 4 µg/ml Polybrene. 50 µL of virus (home-made) was added to the well and incubated 24 h at 37°C, 5% CO_2. Cells were then washed three times with 1xPBS and cultured in hES medium. MEFs were seeded onto 0.1% (w/v) gelatin. 48 h post infection, fibroblasts were transferred into the MEFs-coated dishes and let adhere for 24 h. After that, cells were maintained in hES medium containing 1 mM Valproic acid sodium salt (VPA). VPA was removed after 6 days. Twenty-eight days post-transduction, iPSC colonies were picked, passaged and clonally expanded.

5.5.5. 3D Retinal Differentiation from iPSCs

For retinal differentiation, iPSCs were dissociated to single cells in TrypLE Express (12604013, Invitrogen, Carlsbad, California, USA) and quickly re-aggregated in ultra-low attachment 96-well plates with U-bottomed conical wells (444-1020 (corn7007), VWR, Radnor, Pennsylvania, USA). Cells were counted with Scepter™ 2.0 cell counter and sensors (Merck Millipore, Billerica, Massachusetts, USA). To each well, 10,000 cells were seeded in 3D medium (DMEM, cat. # D0819, 10% heat-inactivated fetal calf serum, 20% knockout serum replacement (KSR) (cat. # 10828-028, Invitrogen, Carlsbad, California, USA), 0.1 mM MEM non-essential amino acids (cat. # M7145, Sigma-Aldrich, St. Louis, Missouri, USA), 1mM sodium pyruvate (cat. # S8636, Sigma-Aldrich, St. Louis, Missouri, USA), 0.1 mM 2-Mercaptoethanol (cat. # 31350-010, Thermo Fisher Scientific, Waltham, Massachusetts, USA), 1 mL primocin (cat. # ant-pm-2, Bio-Connect, San Diego, California, USA) supplemented with 20 µM ROCKi Y-27632 (cat. # Y0503, Sigma-Aldrich, St. Louis, Missouri, USA) and 3 nM IWR-1 endo (cat.

681669, Merck Millipore, Billerica, Massachusetts, USA). The Wnt inhibitor IWR1-1 endo was added to counteract the caudalization effect of the KSR serum. The ROCK inhibitor Y-27632 was added to avoid dissociation-induced apoptosis, as previously reported.[7,34] On day 2, medium was refreshed and 1% MaxGel™ ECM mixture (cat # E0282, Sigma-Aldrich, St. Louis, Missouri, USA) was added. ROCKi and IWR1e were used from days 0 to 10, and removed on day 12 for optic cup formation. On day 12, spheres were transferred to ultra-low-attachment 24 well plates (cat. # 734-1584 (corn3473), VWR, Radnor, Pennsylvania, USA). On day 14, the medium was supplemented with 3 µM CHIR99021 (cat # 4423/10, Bio-Techne, Abingdon, United Kingdom) and 100 nM SAG (cat # ALX-270-426-M001, Enzo Life Sciences, New York, USA) until day 18. From day 18 onwards, the culture was sustained with neuroretinal (NR) medium composed by DMEM/F12 (cat. # 51448C, Sigma-Aldrich, St. Louis, Missouri, USA) 2 mM GlutaMAX Supplement, (cat. # 35050061, Thermo Fisher Scientific, Waltham, Massachusetts, USA), N2 supplement, (cat. # 17502048, Thermo Fisher Scientific, Waltham, Massachusetts, USA), 1 mL primocin, DAPT supplement (cat. # D5942, Sigma-Aldrich, St. Louis, Missouri, USA) was added between day 30 and 40 to enhance the number of photoreceptor cells.[7] After that period, spheres were grown in NR medium until day 90 refreshing the medium every other day.

5.5.6. RNA Extraction, quantification and quality control

Cell pellets were harvested, immediately frozen in liquid nitrogen and stored at -80 °C until RNA extraction. Total RNA, including miRNA, was extracted from cells at day 0 and 90 with QIAGEN RNeasy kit (cat. # 12943, Qiagen, Hilden, Germany) according to the manufacturer´s instructions. RNA was quantified with Qubit fluorometer 2.0 (Thermo Fisher Scientific) and quality was measured with Bioanalyzer (Agilent Technologies, Santa Clara, California, USA). Samples with an RNA Integrity Number >8.0 were used for complementary DNA (cDNA) library preparation.

5.5.7. PolyA+ RNA sequencing and data processing

Libraries for mRNA sequencing were prepared with the TruSeq stranded mRNA sample prep kit (Illumina, San Diego, CA, USA). One-hundred nanograms of total RNA was mRNA enriched by using the oligodT bead system (Illumina). The isolated mRNA was subsequently subjected to enzymatic fragmentation. Then, first and second strand synthesis were performed and the double stranded cDNA was purified (Agencourt AMPure XP, Beckman Coulter). The cDNA was end repaired, 3'-adenylated and ligated onto the fragments ends with sequencing adaptors. Then, the library was purified and the polyA+ RNA stranded libraries were pre-amplified with PCR and purified (Agencourt AMPure XP). The library size distribution was validated and the quality inspected on the 2100 Bioanalyzer with a high sensitivity DNA chip (Agilent Technologies). High quality libraries were

quantified with the Qubit fluorometer (Life Technologies), the concentration was normalized and the samples pooled according to the project specification (number of reads). Single-end sequencing was performed on NextSeq500 instrument according to the manufacturer instructions (Illumina).

5.5.8. RNA-Seq alignment with TopHat 2 and Bowtie 2 within the Basespace environment

Data analysis was performed by using the RNA-Seq Aignment tool v1.0.0 with TopHat 2 and Bowtie 2 within the Basespace environment.[35] TopHat2 is a fast splice junction mapper for RNA-Seq reads. It aligns the sequencing reads to the reference genome by using the sequence aligner Bowtie 2. The reads were counted and reported and then used for downstream analysis. Annotation of the obtained sequences was performed by using the reference annotation "*Homo sapiens* UCSC hg38 (RefSeq & Genecode gene annotations)".

5.5.9. Transcriptome data analysis

Sample-sample clustering (Euclidean distance, complete agglomeration) was performed on pair-wise Pearson correlation coefficients based on normalized gene expression values for each sample. Differential gene expression analysis was performed separately for each condition. Therefore, a total of 5 separate analyses were performed. Differential gene expression analysis was performed with the DEseq2 package v1.8.2 in R. All visualizations were performed with R.

5.5.10. qRT-PCR

Twenty-five nanograms cDNA was used for each reaction in a 96-well plate (Applied Biosystems) together with 2x GoTaq master mix (Promega), 3 µM gene-specific forward and reverse primers, dissolved in DNase and RNase free water up to 20 µl. Each cDNA sample was run in triplicate. The reactions were then run on an ABI Prism 7900HT Fast Real-time Sequence Detection System (Applied Biosystems Ltd., UK) equipped with SDS 2.4 software for amplification results analysis. From amplification curves, Ct values were obtained for each sample. Expression levels were normalized to *GUSB* gene to assess the relative expression of the genes in different experimental conditions. Cycling conditions were as follows: 2 min at 50°C, 10 min at 95°C, 40 cycles of 15 sec at 95°C and 1 min at 60°C. Supplemental Table 1 contains the list of gene-specific primer sequences used.

5.6. References

1. Hartong, D.T., Berson, E.L., and Dryja, T.P. (2006). Retinitis pigmentosa. Lancet 368, 1795-1809.
2. Collin, R.W.J., Safieh, C., Littink, K.W., Shalev, S.A., Garzozi, H.J., Rizel, L., Abbasi, A.H., Cremers, F.P.M., den Hollander, A.I., Klevering, B.J., et al. (2010). Mutations in C2ORF71 cause autosomal-recessive retinitis pigmentosa. Am J Hum Genet 86, 783-788.
3. Takahashi, K., and Yamanaka, S. (2006). Induction of pluripotent stem cells from mouse embryonic and adult fibroblast cultures by defined factors. Cell 126, 663-676.
4. Ikeda, H., Osakada, F., Watanabe, K., Mizuseki, K., Haraguchi, T., Miyoshi, H., Kamiya, D., Honda, Y., Sasai, N., Yoshimura, N., et al. (2005). Generation of Rx+/Pax6+ neural retinal precursors from embryonic stem cells. Proc Natl Acad Sci U S A 102, 11331-11336.
5. Lamba, D.A., Karl, M.O., Ware, C.B., and Reh, T.A. (2006). Efficient generation of retinal progenitor cells from human embryonic stem cells. Proc Natl Acad Sci U S A 103, 12769-12774.
6. Osakada, F., Ikeda, H., Mandai, M., Wataya, T., Watanabe, K., Yoshimura, N., Akaike, A., Sasai, Y., and Takahashi, M. (2008). Toward the generation of rod and cone photoreceptors from mouse, monkey and human embryonic stem cells. Nat Biotechnol 26, 215-224.
7. Nakano, T., Ando, S., Takata, N., Kawada, M., Muguruma, K., Sekiguchi, K., Saito, K., Yonemura, S., Eiraku, M., and Sasai, Y. (2012). Self-formation of optic cups and storable stratified neural retina from human ESCs. Cell Stem Cell 10, 771-785.
8. Zhong, X., Gutierrez, C., Xue, T., Hampton, C., Vergara, M.N., Cao, L.H., Peters, A., Park, T.S., Zambidis, E.T., Meyer, J.S., et al. (2014). Generation of three-dimensional retinal tissue with functional photoreceptors from human iPSCs. Nat Commun 5, 4047.
9. Zuber, M.E., Gestri, G., Viczian, A.S., Barsacchi, G., and Harris, W.A. (2003). Specification of the vertebrate eye by a network of eye field transcription factors. Development 130, 5155-5167.
10. de Klerk, E., and t Hoen, P.A. (2015). Alternative mRNA transcription, processing, and translation: insights from RNA sequencing. Trends Genet 31, 128-139.
11. Schindelin, J., Arganda-Carreras, I., Frise, E., Kaynig, V., Longair, M., Pietzsch, T., Preibisch, S., Rueden, C., Saalfeld, S., Schmid, B., et al. (2012). Fiji: an open-source platform for biological-image analysis. Nat Methods 9, 676-682.
12. Tucker, B.A., Anfinson, K.R., Mullins, R.F., Stone, E.M., and Young, M.J. (2013). Use of a synthetic xeno-free culture substrate for induced pluripotent stem cell induction and retinal differentiation. Stem Cells Transl Med 2, 16-24.
13. Huang da, W., Sherman, B.T., and Lempicki, R.A. (2009). Systematic and integrative analysis of large gene lists using DAVID bioinformatics resources. Nat Protoc 4, 44-57.
14. Huang da, W., Sherman, B.T., and Lempicki, R.A. (2009). Bioinformatics enrichment tools: paths toward the comprehensive functional analysis of large gene lists. Nucleic Acids Res 37, 1-13.
15. Gonzalez-Cordero, A., Kruczek, K., Naeem, A., Fernando, M., Kloc, M., Ribeiro, J., Goh, D., Duran, Y., Blackford, S.J.I., Abelleira-Hervas, L., et al. (2017). Recapitulation of Human Retinal Development from Human Pluripotent Stem Cells Generates Transplantable Populations of Cone Photoreceptors. Stem Cell Reports 9, 820-837.
16. Saggese, T., Young, A.A., Huang, C., Braeckmans, K., and McGlashan, S.R. (2012). Development of a method for the measurement of primary cilia length in 3D. Cilia 1, 11.
17. Cho, M.S., Kim, S.J., Ku, S.Y., Park, J.H., Lee, H., Yoo, D.H., Park, U.C., Song, S.A., Choi, Y.M., and Yu, H.G. (2012). Generation of retinal pigment epithelial cells from human embryonic stem cell-derived spherical neural masses. Stem Cell Res 9, 101-109.
18. Iwasaki, Y., Sugita, S., Mandai, M., Yonemura, S., Onishi, A., Ito, S., Mochizuki, M., Ohno-Matsui, K., and Takahashi, M. (2016). Differentiation/Purification Protocol for Retinal Pigment Epithelium from Mouse Induced Pluripotent Stem Cells as a Research Tool. PLoS One 11, e0158282.
19. Hazim, R.A., Karumbayaram, S., Jiang, M., Dimashkie, A., Lopes, V.S., Li, D., Burgess, B.L., Vijayaraj, P., Alva-Ornelas, J.A., Zack, J.A., et al. (2017). Differentiation of RPE cells from integration-free iPS cells and their cell biological characterization. Stem Cell Res Ther 8, 217.
20. Kevany, B.M., Zhang, N., Jastrzebska, B., and Palczewski, K. (2015). Animals deficient in C2Orf71, an autosomal recessive retinitis pigmentosa-associated locus, develop severe early-onset retinal degeneration. Hum Mol Genet 24, 2627-2640.
21. Meyer, J.S., Shearer, R.L., Capowski, E.E., Wright, L.S., Wallace, K.A., McMillan, E.L., Zhang, S.C., and Gamm, D.M. (2009). Modeling early retinal development with human embryonic and induced pluripotent stem cells. Proc Natl Acad Sci U S A 106, 16698-16703.

22. Reichman, S., Terray, A., Slembrouck, A., Nanteau, C., Orieux, G., Habeler, W., Nandrot, E.F., Sahel, J.A., Monville, C., and Goureau, O. (2014). From confluent human iPS cells to self-forming neural retina and retinal pigmented epithelium. Proc Natl Acad Sci U S A 111, 8518-8523.
23. Chin, M.H., Mason, M.J., Xie, W., Volinia, S., Singer, M., Peterson, C., Ambartsumyan, G., Aimiuwu, O., Richter, L., Zhang, J., et al. (2009). Induced pluripotent stem cells and embryonic stem cells are distinguished by gene expression signatures. Cell Stem Cell 5, 111-123.
24. Bilic, J., and Izpisua Belmonte, J.C. (2012). Concise review: Induced pluripotent stem cells versus embryonic stem cells: close enough or yet too far apart? Stem Cells 30, 33-41.
25. Marchetto, M.C., Yeo, G.W., Kainohana, O., Marsala, M., Gage, F.H., and Muotri, A.R. (2009). Transcriptional signature and memory retention of human-induced pluripotent stem cells. PLoS One 4, e7076.
26. Ghosh, Z., Wilson, K.D., Wu, Y., Hu, S., Quertermous, T., and Wu, J.C. (2010). Persistent donor cell gene expression among human induced pluripotent stem cells contributes to differences with human embryonic stem cells. PLoS One 5, e8975.
27. Kwon, D., Kim, J.S., Cha, B.H., Park, K.S., Han, I., Park, K.S., Bae, H., Han, M.K., Kim, K.S., and Lee, S.H. (2016). The Effect of Fetal Bovine Serum (FBS) on Efficacy of Cellular Reprogramming for Induced Pluripotent Stem Cell (iPSC) Generation. Cell Transplant 25, 1025-1042.
28. Hu, Y., Ji, J., Xia, J., Zhao, P., Fan, X., Wang, Z., Zhou, X., Luo, M., and Gu, P. (2013). An in vitro comparison study: the effects of fetal bovine serum concentration on retinal progenitor cell multipotentiality. Neurosci Lett 534, 90-95.
29. Kruczek, K., Gonzalez-Cordero, A., Goh, D., Naeem, A., Jonikas, M., Blackford, S.J.I., Kloc, M., Duran, Y., Georgiadis, A., Sampson, R.D., et al. (2017). Differentiation and Transplantation of Embryonic Stem Cell-Derived Cone Photoreceptors into a Mouse Model of End-Stage Retinal Degeneration. Stem Cell Reports 8, 1659-1674.
30. Mellough, C.B., Sernagor, E., Moreno-Gimeno, I., Steel, D.H., and Lako, M. (2012). Efficient stage-specific differentiation of human pluripotent stem cells toward retinal photoreceptor cells. Stem Cells 30, 673-686.
31. Schlaeger, T.M., Daheron, L., Brickler, T.R., Entwisle, S., Chan, K., Cianci, A., DeVine, A., Ettenger, A., Fitzgerald, K., Godfrey, M., et al. (2015). A comparison of non-integrating reprogramming methods. Nat Biotechnol 33, 58-63.
32. O'Brien, K.M., Schulte, D., and Hendrickson, A.E. (2003). Expression of photoreceptor-associated molecules during human fetal eye development. Mol Vis 9, 401-409.
33. Xiao, M., and Hendrickson, A. (2000). Spatial and temporal expression of short, long/medium, or both opsins in human fetal cones. J Comp Neurol 425, 545-559.
34. Watanabe, K., Ueno, M., Kamiya, D., Nishiyama, A., Matsumura, M., Wataya, T., Takahashi, J.B., Nishikawa, S., Nishikawa, S., Muguruma, K., et al. (2007). A ROCK inhibitor permits survival of dissociated human embryonic stem cells. Nat Biotechnol 25, 681-686.
35. Kim, D., Pertea, G., Trapnell, C., Pimentel, H., Kelley, R., and Salzberg, S.L. (2013). TopHat2: accurate alignment of transcriptomes in the presence of insertions, deletions and gene fusions. Genome Biol 14, R36.

5.7. Acknowledgements

This work was funded by the FP7-PEOPLE-2012-ITN programme EyeTN, Brussels, Belgium (grant agreement no.: 317472) to RWJC

5.8. Supplemental data

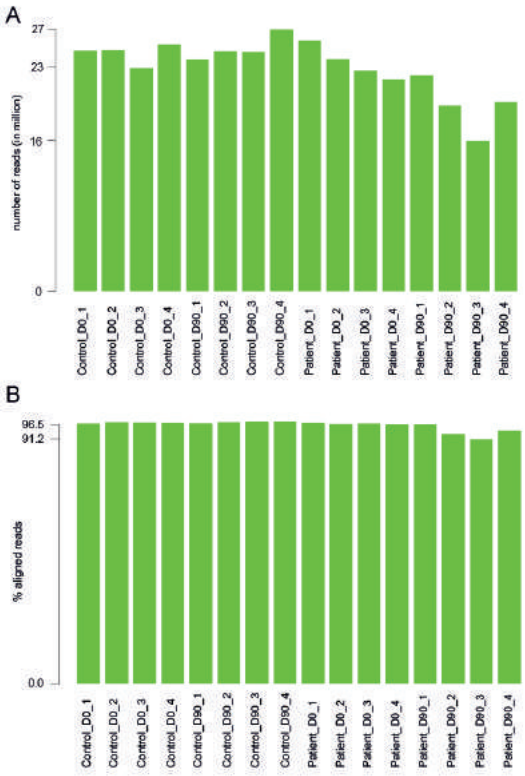

Supplemental Figure S1. Data quality control. A, Number of reads per sample. **B,** Fraction of reads mapping to the transcriptome. For most samples, the majority of reads map to the transcriptome, highlighting efficient enrichment for polyA+ RNA.

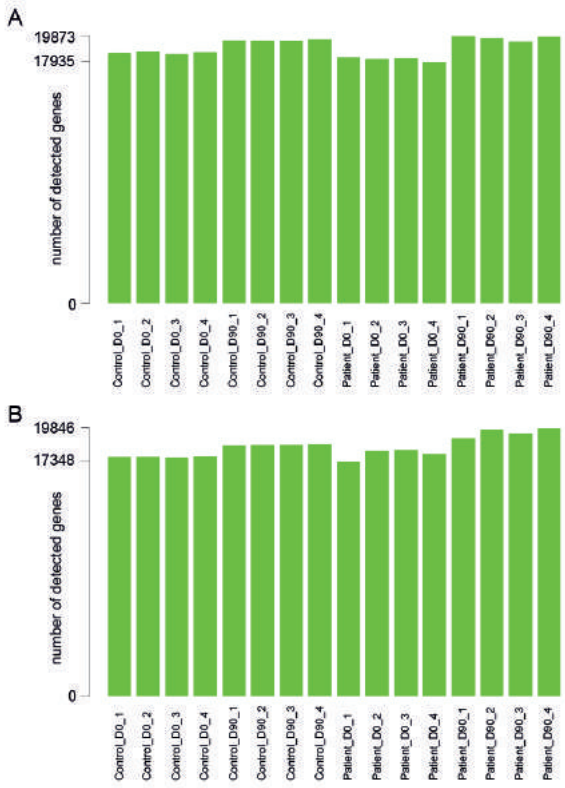

Supplemental Figure S2. Number of detected genes in each sample. A, A gene was considered to be expressed when it contained at least 1 raw read or **B,** at least 1 read after normalization with DEseq2. Differences between D0 and D90 samples are significant (average D0 = 17,813; average D90 = 19,054; Mann-Whitney-U-test, p-value = 0.0001554).

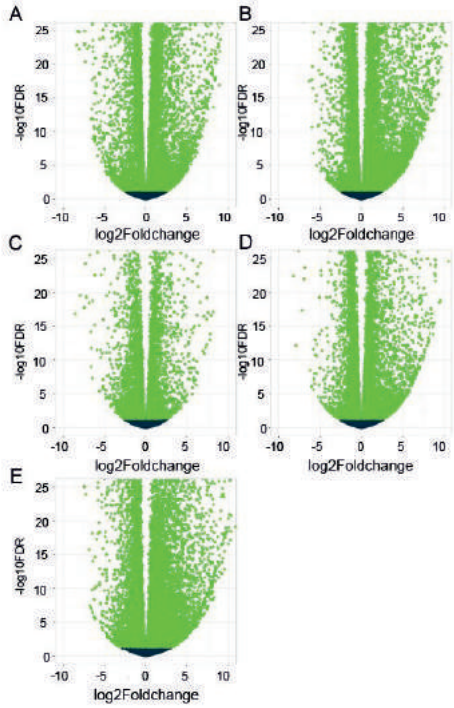

Supplemental Figure S3. Volcano plot showing –log10 FDR in function of the log2 for the five comparisons (A-E). Green points indicate significantly differential expressed genes at FDR < 0.05. FDR: False discovery rate.

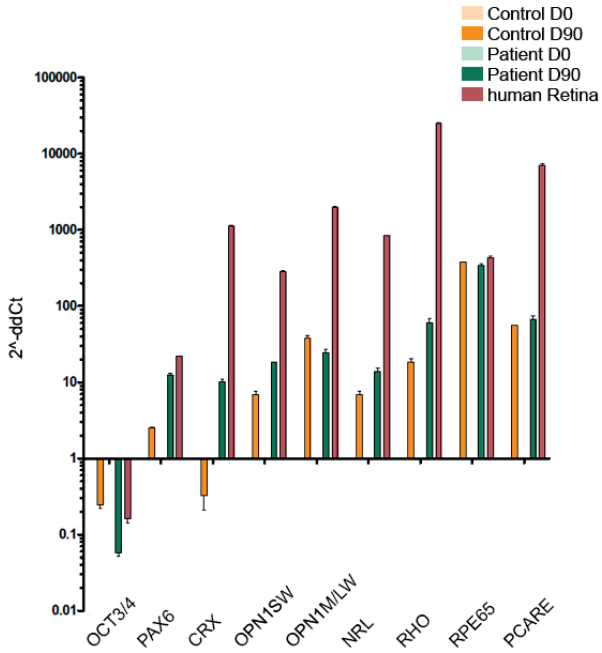

Supplemental Figure S4. Validation of the expression of neural and photoreceptor markers by qRT-PCR. Values were normalized to the expression of the gene *GUSB*.

Supplemental Table 1. Primers used for qRT-PCR

Gene	Forward Primer (5'-3')	Reverse Primer (5'-3')
OCT3/4	GTTCTTCATTCACTAAGGAAGG	CAAGAGCATCATTGAACTTCAC
PAX6	TCTAATCGAAGGGCCAAATG	TGTGAGGGCTGTGTCTGTTC
CRX	ATGATGGCGTATATGAACCC	TCTTGAACCAAACCTGAACC
OPN1SW	GCGCTACATTGTCATCTGTAAGCC	GAAGGAATGGTGACAAGCCGTAAG
OPN1ML/LW	GTGCAGTCTTACATGATTGTCCTC	AGATAACGGGGTTGTAGATAGTGG
NRL	GCCTTCAGTCTCCTGGGAAG	GGAGGCACTGAGCTGTAAGG
RHO	CAACTACATCCTGCTCAACCTAGC	GTGTAGTAGTCGATTCCACACGAG
RPE65	GCCCTCCTGCACAAGTTTGACTTT	AGTTGGTCTCTGTGCAAGCGTAGT
C2ORF71/PCARE	GCTGTGAAATGGAGGGGAAC	GTTCTCTGTGGACTTGCTGC
GUSB	CTGTACACGACACCCACCAC	TACAGATAGGCAGGGCGTTC
NANOG	TTCTTCCACCAGTCCCAAAG	TTGCTCCACATTGGAAGGTT
SOX2	GCTAGTCTCCAAGCGACGAA	GCAAGAAGCCTCTCCTTGAA
LIN28	TTGTCTTCTACCCTGCCCTCT	GAACAAGGGATGGAGGGTTTT

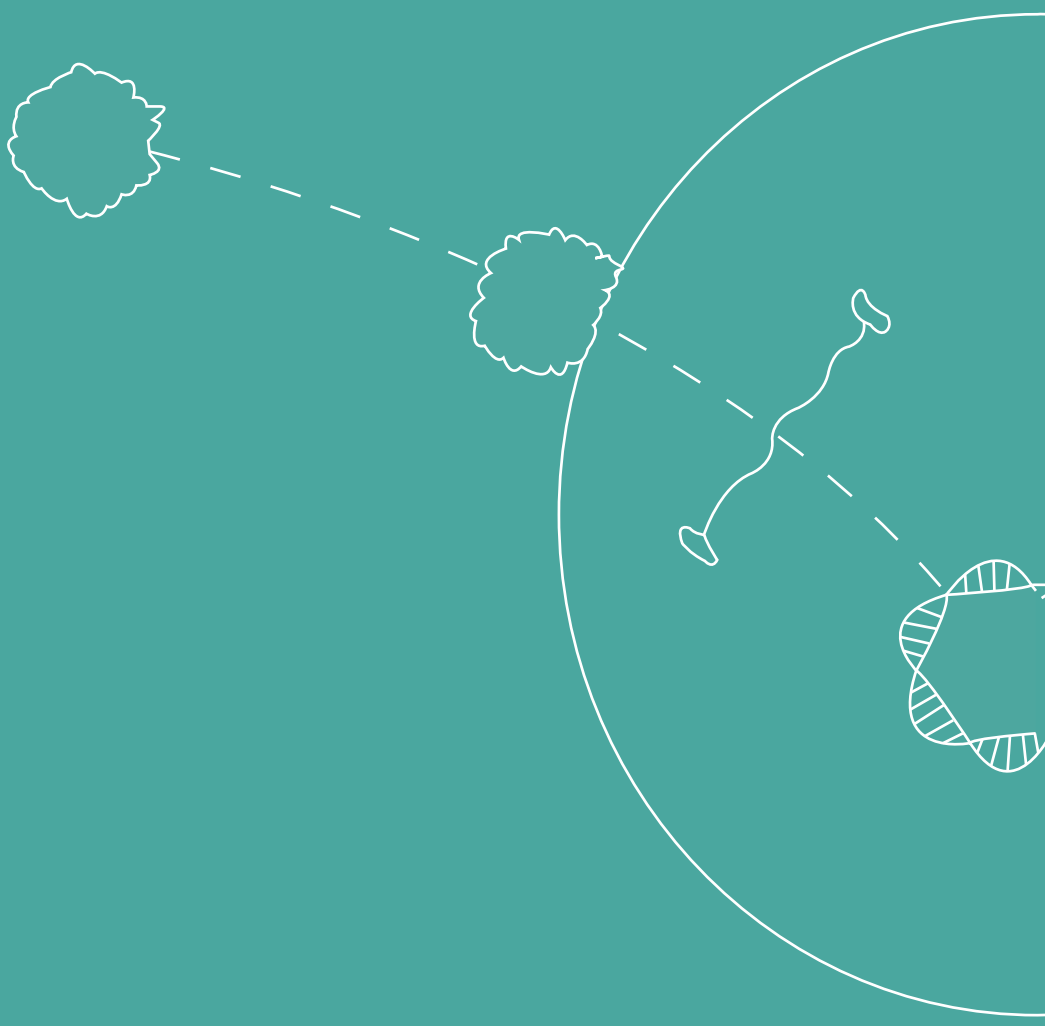

Chapter 6

Generation and characterization of an adeno-associated virus (AAV) vector containing full-length *PCARE* cDNA

Generation and characterization of an adeno-associated virus (AAV) vector containing full-length *PCARE* cDNA

Julio C. Corral-Serrano[1,2], Lonneke Duijkers[1], Max D. Van Essen[1], Ru Xiao[3], Alejandro Garanto[1,4], Luk Vandenberghe[3], Rob W.J. Collin[1,4]

[1]Department of Human Genetics, Radboud University Medical Center, Nijmegen, The Netherlands; [2]Radboud Institute for Molecular Life Sciences, Radboud University Medical Center, Nijmegen, The Netherlands; [3]Schepens Eye Research Institute, Grousbeck Gene Therapy Center, Boston, Massachusetts, United States; [4]Donders Institute for Brain, Cognition and Behaviour, Radboud University, Nijmegen, The Netherlands.

6.1 Abstract

Patients with mutations in *PCARE* suffer from retinitis pigmentosa subtype 54, an inherited retinal disease (IRD) for which no treatment is available. Retinal gene therapy using adeno-associated viruses (AAVs) holds a great promise for the treatment of some subtypes of IRD. By introducing the cDNA encoding the functional protein into the patient retina before degeneration of the retinal cells occurs, gene therapy aims at slowing the progression of the disease, and/or improving visual function. A disadvantage of AAVs is their limited cargo capacity of ~4.8 kb. As the cDNA sequence of *PCARE* is 3.8 kb in size, and a therapeutic vector also needs several regulatory elements, we have generated an expression cassette with minimal spacer sequences such that all elements necessary to drive *PCARE* expression would fit into a single AAV. Expression analysis in hTERT RPE-1 cells of the expression cassette containing *PCARE* cDNA in a plasmid vector, either with or without the spacer sequences, showed correct expression of the PCARE protein in the primary cilium, albeit at very low expression levels. Following the generation of AAV particles containing the minimal *PCARE* expression cassette, and subsequent transduction of the resulting AAVs in hTERT RPE-1 cells, no detectable expression of *PCARE* could be observed. Analysis by droplet digital PCR and RT-PCR analysis showed that the expression cassette was fully packaged into the AAV vector. Immunofluorescence and western blot analysis pointed to a problem of expression levels of the transgene in the selected cell type (hTERT RPE-1 cells). This suggests that alternative *in vitro* solutions or *in vivo* injections in mice are required to assess the functionality of this vector.

6.2 Introduction

Inherited retinal diseases (IRDs) are a major cause of visual impairment, affecting more than 2 million individuals worldwide.[1] In the last years, the identification of many IRD-associated genes has paved the way for the development of novel therapies. The eye is considered a model organ for the development of new therapeutic strategies, in particular for the anatomical accessibility of the retinal tissue and its immune-privileged nature. Gene augmentation therapy is currently the most advanced possibility for treating some subtypes of IRDs, supported by the successful proof-of-principle in animal models and data from human clinical trials.[2]

The first subtype of IRD targeted for gene augmentation therapy was Leber congenital amaurosis type 2 (LCA2) which is caused by bi-allelic mutations in the *RPE65* gene. Following proof-of-concept in animal models and a successful outcome of clinical trials, [3-7] this treatment was recently approved by the FDA (U.S. Food and Drug Administration) under the name Luxturna.[8,9] Luxturna consists in the delivery of a normal copy of the *RPE65* cDNA directly to the RPE cells, using an adeno-associated virus (AAV) as a vector. Recombinant AAVs are attractive therapeutic vectors for a wide variety of medical applications, as they have no known role in disease, are unable to replicate without a helper virus, do not integrate into the host genome and elicit a negligible immune-response.[10] The most significant drawback is the restricted cargo capacity of this virus, with ~4.8 kb being the maximum size of the therapeutic construct that can be incorporated and enveloped.[11,12] Pre-clinical safety and efficacy studies using AAVs are ongoing for an increasing number of IRD-causing genes, some of which have already entered the phase of clinical testing in humans. Known examples include *CHM*, mutated in choroideremia,[13] *MERTK*, mutated in retinitis pigmentosa type 38,[14] and several others (https://www.clinicaltrials.gov/). The long-term effects of AAV-based gene augmentation therapy in humans are still unknown.[15]

PCARE, previously known as *C2ORF71*, is mutated in patients with retinitis pigmentosa (RP) type 54,[16,17] and there is no treatment available yet. *PCARE* mutations are believed to result in loss-of-function of the encoded protein, and patients with bi-allelic *PCARE* mutations are thought to lack sufficient levels of functional PCARE protein. As described in **chapter 2**, the PCARE protein appears to recruit an actin assembly module into the connecting cilium of the photoreceptors. We propose that this module is involved in evagination of the photoreceptor ciliary membrane to initiate the formation of new outer segment discs. Mutant PCARE is unable to activate this process, thereby impeding proper outer segment disc morphogenesis (**chapter 2**). Since the size of *PCARE* cDNA is 3.8 kb, *PCARE*-associated retinal disease could be a potential candidate for AAV-driven gene augmentation therapy, although also when other elements required to drive the expression of a

therapeutic gene (e.g. promoter, poly-adenylation signal) are incorporated, the resulting length will be close to the maximum (4.8 kb) AAV cargo capacity. Our aim here is to develop an expression cassette harboring human *PCARE* cDNA that can be incorporated into a functional AAV vector for future therapeutic purposes.

6.3 Results

6.3.1 Generation of a Gateway-adapted pDEST-AAV plasmid containing *PCARE* cDNA

A wild-type AAV contains a *rep* gene, necessary for genome replication and packaging proteins, and c*ap* and *aap* genes, that encode capsid and assembly proteins, respectively.[18-20] These genes are flanked by two Inverted Terminal Repeats (ITRs) which are sophisticated double hairpin-structures vital for *in vivo* genome replication and, if rep-proteins are present, the integration into the host genome.[21] In recombinant AAVs (rAAV), the ITRs are still required, but the endogenous viral genome can be replaced with a (tissue-specific) promoter sequence, the transgene of interest, and a poly-adenylation site (Figure 1A). The resulting AAV genome can be used to produce transgenic virions that are capable of infecting a cell and exploiting its endogenous nuclear systems. The ITR-flanked transgenes encoded within the rAAV can form circular concatemers that are episomal in the nucleus of transduced cells,[22] and can result in stable transcription of the therapeutic transgene (Figure 1B), without integrating into the host cell.

In order to simplify future cloning of photoreceptor-specific genes of interest into an AAV plasmid, we designed a gateway-compatible destination vector (pDEST) using the DNA of an AAV plasmid as a backbone with a rhodopsin kinase (RK) promoter and an EGFP-insert (Supplemental Figure 1A). Following vector linearization, a standard pDEST cassette was inserted, containing recombination sites (attR), a chloramphenicol-resistance gene (*CamR*), and a *ccdB*-selection gene. Transformation of the assembled product into *E.coli* yielded a cloning efficiency of 100%, and Sanger sequencing of a selected clone confirmed the presence of the complete insert. To assess the functionality of the pDEST-AAV, an LR-reaction reaction was performed, thereby transferring *PCARE* from an entry vector (pENTR) into a destination vector (pDEST). Presence of the insert was verified by restriction digest with *Bam*HI (Supplemental Figure 1B), and Sanger sequencing confirmed that *PCARE* was successfully cloned into the pDEST-AAV. These results confirm the creation of a functional pDEST-AAV, and the cloning of *PCARE* into this vector, now coined pAAV-RK-PCARE.

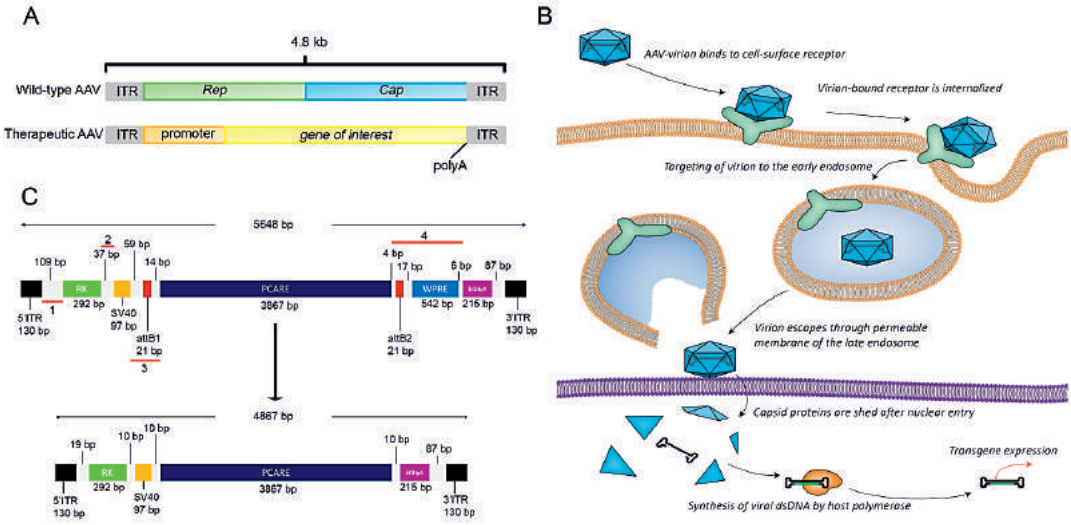

Figure 1. Design and administration of therapeutic adeno-associated virus (AAV). A, The genome of a typical therapeutic AAV contains a tissue-specific promoter, a transgene of interest, and a poly-adenylation site to facilitate eukaryotic transcription. **B**, Following exposure of the virus to a target cell, a viral capsid binds to a cellular receptor, thereby initiating the internalization of the virion and the receptor. Active proton-pumps gradually decrease the pH of the resulting endosome, allowing the virus to dissociate from the receptor and escape through the permeabilized membrane. The capsid can then translocate to the nucleus and use host DNA polymerases to synthesize double-stranded DNA, which can subsequently be used as a transcription-template for transgene expression. Rep: replication gene; Cap: capsid gene; polyA: polyadenylation signal. **C**, Strategy to reduce the ITRs-flanked plasmid sequence. The upper part shows a scheme of the insert between ITRs and the four-steps PCR strategy (marked 1 to 4) to remove all presumably non-essential sequences from the plasmid used for AAV generation containing *PCARE* cDNA. The lower part shows a scheme of the final insert including ITRs after removal of presumably non-essential sequences. RK: Rhodopsin Kinase promoter; SV40 intron: simian vacuolating virus 40 intron; ITR: inverted terminal repeat; WPRE: WHP Post-transcriptional Response Element; bGHpA: Bovine Growth Hormone Polyadenylation Signal.

6.3.2 Reduction of the size of the pAAV-RK-PCARE

In the pAAV-RK-PCARE plasmid that was generated, the size of the region between the two ITRs including *PCARE* cDNA was 5648 bp (ITRs included). Because the maximum capacity of an AAV is ~4.8 kb, we made an effort to reduce the insert size by several rounds of site-directed mutagenesis PCR. First, we removed the WPRE (WHP Post-transcriptional Response Element), a regulatory element (542 bp) that is known to enhance the transgene transcription.[23] Since the SV40 intron is also present in the plasmid insert and has a similar function compared to the WPRE, this sequence was left in. Next, we removed 90 bp in between the 5'-ITR and the start of the RK promoter sequence, as well as 27 bp between the RK promoter and the SV40 region. Finally, we removed the sequences between the SV40 intron and *PCARE* cDNA (84 bp), and between *PCARE* cDNA and the bGHpA polyadenylation signal (580 bp) (Figure 1C).

With a final size of 4867 bp, the size of the insert was at the limit to be packaged into an AAV, so we pursued to generate an AAV vector. Prior to AAV generation, we analyzed whether the plasmid allowed correct expression of PCARE after removal of the non-essential sequences. To this aim, we serum starved hTERT RPE-1 cells to allow for cilia growth and transfected both the regular construct pAAV-RK-PCARE (~5.6 kb) and the shortened version of the plasmid pAAV-RK-PCARE-S (~4.8 kb). In both cases, we observed typical localization of PCARE in the cilium (Figure 2), in general however, we detected low transfection efficiency in both regular and the short expression constructs.

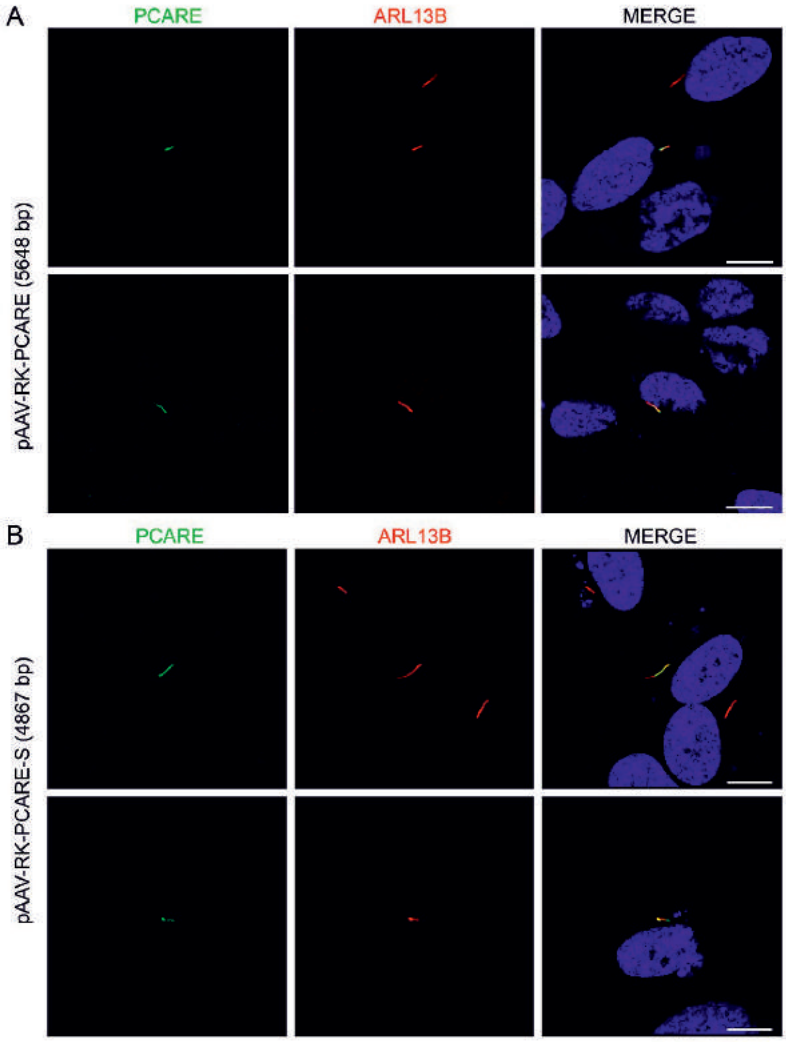

Figure 2. Immunofluorescence to test the expression of PCARE. hTERT RPE-1 cells were serum starved to allow cilium formation and subsequently transfected with **A**, pAAV-RK-PCARE (5648 bp) or **B**, pAAV-RK-PCARE-S (4867 bp). An antibody directed against PCARE (green) was used to detect the PCARE protein. ARL13B (red) was used as ciliary marker. DAPI (blue) marks the nucleus. Size bars = 5 µm.

6.3.3 Generation and assessment of expression of the AAV2/9.RK.PCARE.S vector

Because the pAAV-RK-PCARE-S (4867 bp) expression construct in some cells did show proper ciliary PCARE expression, we next aimed to analyze whether this construct could be packaged into an AAV to express *PCARE*. To this aim, we chose an AAV2 vector, which is widely used in gene therapy for the retina,[24] and the capsid 9, which has high tropism for all retinal layers except for bipolar and Müller glia cells.[25] Analysis by RT-PCR and Droplet Digital PCR showed that *PCARE* could be fully packaged into the AAV2/9 vector (Figure 3). Next, we compared the expression levels of the generated virus with the generated plasmid (Figure 4A). As shown by immunofluorescence (Figure 4B), there was no detectable expression of the AAV2/9.RK.PCARE.S vector in hTERT RPE-1 cells, but the AAV2/9.GFP vector, under a CMV promoter, was clearly expressed. In addition, the levels of PCARE were also not sufficient to detect the PCARE protein on western blot under control of the RK promoter, but GFP, expressed under control of a CMV promoter, was detectable (Figure 4C).

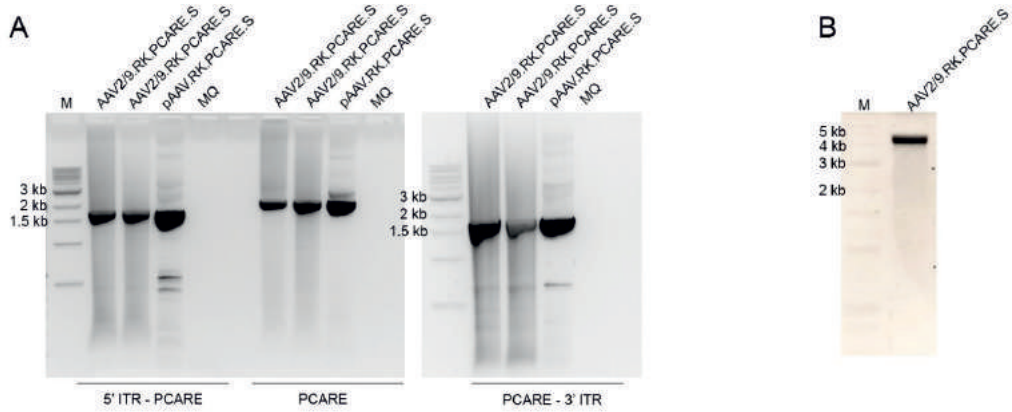

Figure 3. Analysis of the AAV2/9.RK.PCARE.S packaging. **A**, To verify correct packaging of the insertion cassette in the AAV2/9 vector, we performed RT-PCR analysis covering the region between the 5' ITR and 3' ITR. Expected sizes: 5' ITR to *PCARE* cDNA, 1717 bp; within *PCARE* cDNA, 2165bp; *PCARE* cDNA to 3' ITR, 1793bp. **B**, Droplet Digital PCR shows proper packaging of the insertion cassette into the AAV2/9 vector. Expected band size: 4.86 kB.

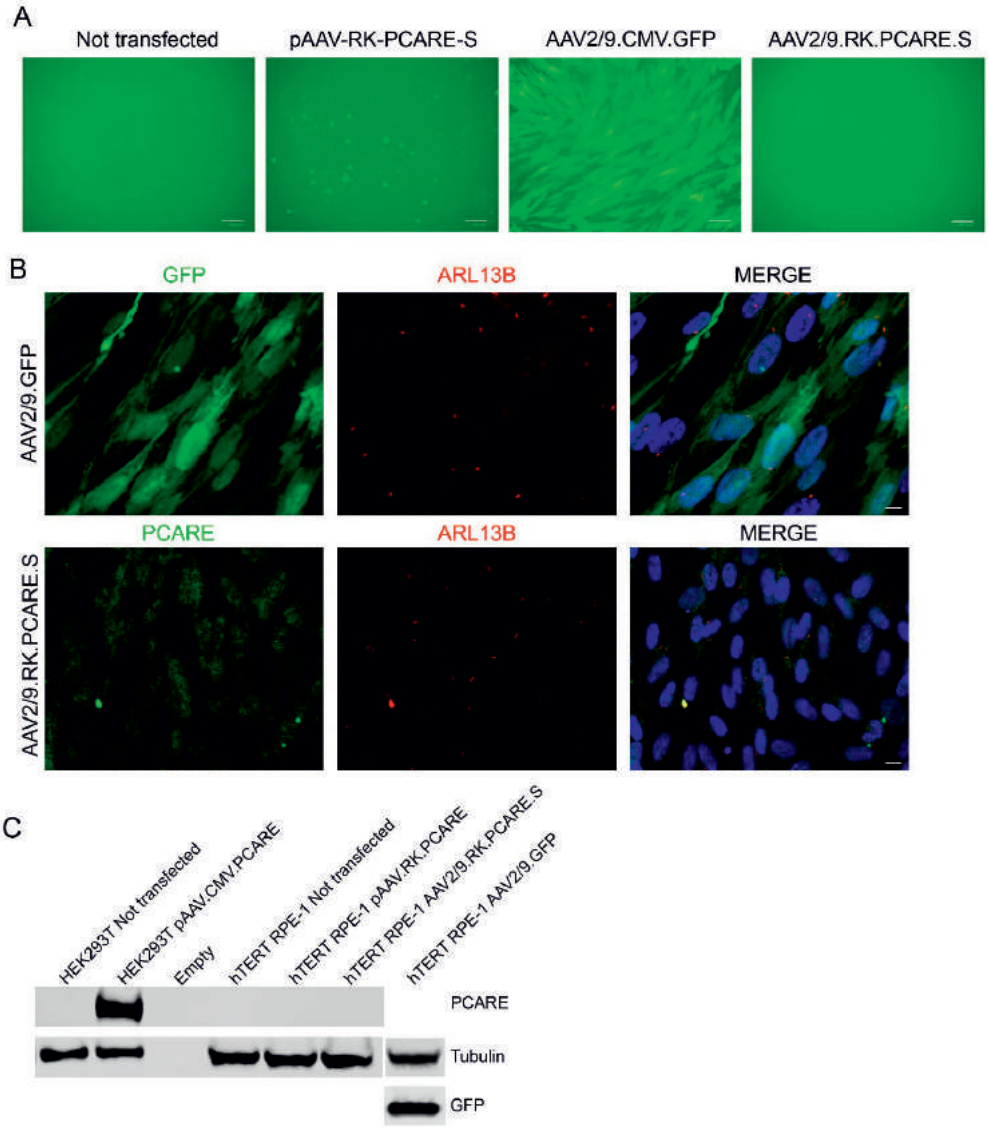

Figure 4. Evaluation of the expression of the generated AAV2/9.RK.PCARE.S vector in hTERT RPE-1 cells. **A**, comparison of the expression levels after transfection or transduction of hTERT RPE-1 cells with either the plasmid pAAV-RK-PCARE-S or the viral vectors AAV2/9.CMV.GFP and AAV2/9.RK.PCARE.S. Scale = 100 µm. **B**, hTERT RPE-1 cells were transduced with AAV2/9.RK.PCARE.S or the control vector AAV2/9.CMV.GFP. Cells express GFP under the CMV promoter but not PCARE under the RK promoter. The blob observed in the lower panels is due to an staining artefact. Scale = 5 µm. **C**, Western blot analysis of the expression of the different vectors. PCARE levels are detectable in HEK293T cells under the CMV promoter but not in hTERT RPE-1 cells under the RK promoter.

6.4 Discussion

Gene therapy for inherited retinal dystrophies is coming of age. Currently, there are over 70 different AAV-mediated gene therapy clinical trials ongoing for autosomal recessive diseases (https://clinicaltrials.gov), including 18 for retinal disease.

The gene *C2ORF71*/*PCARE* was first identified in 2010 by the group of Graeme C.M. Black[17] and our group.[16] Thereafter, different studies have reported *PCARE* to be mutated in ~1% of all arRP cases.[26-28] Additionally, *PCARE* was found mutated in one patient with cone-rod dystrophy (CRD)[29] and in an atypical form of Usher syndrome.[30] Prior to selecting the most suitable therapeutic approach, one first needs to understand the function of the corresponding protein. Recently, we have demonstrated that PCARE could play a role in the morphogenesis of outer segment discs by its interaction with an actin network (**chapter 2**). In this study, we aimed at obtaining a functionally active recombinant AAV vector that contains *PCARE* cDNA for future therapeutic purposes.

First, we adapted an AAV plasmid into the gateway system to facilitate the insertion of therapeutic genes for the generation of AAV vectors. Next, we inserted *PCARE* cDNA into the generated gateway-adapted AAV plasmid to use as template for the generation of a therapeutic AAV vector. A point of concern was the possible interference of plasmid attR sites with the ITR regions of the AAV, as both DNA sequences are capable of recombination. Such deleterious recombination is unlikely to occur, as a different group has already successfully generated virions from pDEST-AAVs.[31]

After transduction of the generated AAV2/9.RK.PCARE.S, we did not detect expression of the PCARE protein by immunofluorescence or by western blot. This may be due to several factors. One factor is the limited cargo capacity of an AAV, which is a really restrictive virus when it comes to its maximum packaging size. Unsuccessful packaging of the AAV may also cause lack of expression of the transgene. Fragments of DNA from the helper plasmids or the cell genome can be packaged inside the vectors during production. Though these impurities are generally considered innocuous for research-grade vectors, they should be preferably at a very low concentration. However, we show here that the packaging of the AAV was successful (Figure 3), ruling out this option. Another factor causing lack of transgene expression is the titer of the virus. The titer of the virus depends on the method and cells used for titration. The cells used must be readily permissive to all steps from viral entry to integration of the viral DNA. Measured titers can vary with the conditions used for titration, like the volume of sample during vector-cell incubation, time of vector-cell incubation or the number of cells used. We therefore tested different virus titers, ranging from 10 vg/mL up to 100000 vg/mL, but none of these gave positive expression of *PCARE* (data not shown). There are different types of recombinant AAV2 vectors that can be used. Different serotypes and capsids show different

efficiency in mediating gene delivery to photoreceptor cells.[32-34] Since the GFP was able to be detected in hTERT RPE-1 cells, we can also rule out a problem of viral capsid affinity.

To be able to fit *PCARE* cDNA into an AAV, we aimed to remove "non-essential" sequences between the different coding elements (Figure 3). These "non-essential" sequences however may as well be "essential", working as spacer sequences between the coding elements to allow better transcriptional activity. Lack of the woodchuck hepatitis post-transcriptional regulatory element (WPRE) in the short 4.8 kb version of the plasmid may also explain why *PCARE* is not properly expressed, since this element has been shown to improve the expression of the transgene.[35] An important element of the cassette is the promoter. Different promoters show variable success in driving expression of transgenes in photoreceptors.[36-39] The rhodopsin kinase promoter allows to drive robust transgene expression in rod and cone cells.[40] We chose this promoter first because of its specificity to both photoreceptor cells, and secondly because of its compact size (of only 292 bp). A drawback to study the effects of this promoter *in vitro* is the lack of established photoreceptor cell cultures. Therefore, we first aimed to test the expression of the AAV vector in hTERT RPE-1 cell cultures. As shown, the generated AAV2/9 containing the RK promoter does not drive *PCARE* transgene expression in hTERT RPE-1 cells to robust leves. To further analyze whether the AAV2/9 is able to drive transgene expression, we could test the vector in a different cell type, such as the retinoblastoma 661W cells, or retinal-differentiated iPSCs. Another plausible alternative is to test the vector directly *in vivo* in mice, which would give a more direct outcome.

If the transgene expression problem persists, other options to engineer the vector are possible. For example, we could use a more potent promoter such as the CMV, or strong enhancer sequences.[41] The problem of this is the lack of specificity of these elements for a determined cell type which could be very relevant in our study.

Another alternative to tackle low expression is to fragment the gene in different parts, and reconstitute it by homologous recombination for functional protein expression inside a cell.[11] Packaged AAV genomes never exceed 5.2 kb in length, independently of the capsid or vector, and overpackaging can result in genome fragmentation.[12] Transduction of larger genomes can be enhanced by addition of proteasome inhibitors, given that proteasomes in the cytoplasm act as barriers to AAV infection.[42] Regulatory elements required to drive gene expression also add to the final size and may render genes too large for AAV packaging, as is the case for *PCARE*. In these cases, dual AAV vectors are an option to consider. There are three strategies to construct a dual AAV vector. First, the overlapping strategy, where the two halves of the transgene expression cassette contain homologous overlapping sequences, which will produce the reconstitution of the transgene

by homologous recombination.[43] Second, the trans-splicing strategy, where the 5'-half vector carries a splice donor (SD) signal at the 3' end, while the 3'-half vector has a splice acceptor (SA) signal at the 5' end. This allows trans-splicing of a single mRNA molecule following tail-to-head concatemerization of the two AAV.[44] Third, the hybrid approach is the combination of the trans-splicing and overlapping approaches. The hybrid approach adds a recombinogenic region to the trans-splicing vectors, in order to increase the recombination efficiency.[45] Dual trans-splicing and hybrid vectors have been shown to efficiently transduce mouse and pig photoreceptors and significantly improve the retinal phenotype in models of Stargardt Disease (STGD) and Usher syndrome type 1B (USH1B).[46-50]

A different choice is to use different viral vectors, like lentivirus, which have a packaging capacity of around 10 kb and allow for delivery of bigger transgenes. Lentiviruses can integrate in the chromosome of the target cell, which allows for more permanent expression of the transgene. The drawback however is that they do not effectively transduce non-dividing cells, and variability of transgene expression because of epigenetic modifications or silencing can occur.[51] Nonetheless, successful rescue of the *Abca4*$^{-/-}$ mouse model of Stardargt macular dystrophy by an equine infectious anemia virus (EIAV) vector has been reported,[52] and the vector is currently being used in Phase I/II clinical trials (Clinical trials.gov identifier NCT01367444).

Instead of viral vectors, genome targeted editing could be used as an alternative to treat *PCARE*-associated retinal disease. The drawback is that these techniques rely on homology-directed repair pathway, which is active during DNA replication, to be effective. Homology-independent targeted integration (HITI) combines CRISPR/Cas9 system and non-homologous end-joining repair to allow for DNA knock-in in dividing and non-dividing cells. Recently, HITI has proven successful in a rat model of retinitis pigmentosa.[53] Although successful, the authors draw attention to the fact that visual function was not fully restored, since it was applied in three weeks old rats, therefore it would not be useful when retinal degeneration has already happened.[53]

Together, we have generated an AAV2/9 vector containing full-length *PCARE* cDNA and the necessary elements to allow transgene expression. Future *in vitro* and *in vivo* analysis of this vector will determine its efficacy to express *PCARE* in photoreceptor cells and its validity for future therapeutic approaches.

6.5 Methods

6.5.1 Generation of pDEST-AAV

Original AAV plasmid containing EGFP insert was linearized by a double digestion with HindIII and NotI (New England Biolabs, NEB) at 37°C for 2 h. Linear plasmid backbone was purified on column using a DNA clean-up kit. The Gateway-insert was generated by PCR with a Q5 High Fidelity DNA Polymerase (NEB) on a standard destination vector template p3xFLAG-CMV-9 (Sigma-Aldrich) containing a chloramphenicol-resistance cassette. Primers were designed to have 30 bp overhang with the AAV backbone (Supplemental Table 1). Cloning was performed with a Gibson Assembly Cloning kit (New England Biolabs), using 50 ng of linear backbone and 400 ng of insert DNA. The assembly mixture was incubated for 1 h at 50°C, after which 5 µl of assembled product was transformed into Oneshot-*ccdB*-survival competent *E. coli* cells (ThermoFisher Scientific), according to the manufacturer's protocol. LR reactions were performed with a Gateway LR Clonase II kit (ThermoFisher Scientific) overnight at 25°C, using 150 ng of entry vector (pENTR with PCARE or EGFP) and destination vector (pDEST-AAV with an RK promoter or CMV promoter) as input. From the assembled expression vectors, 5 µl were transformed in DH5-α cells. Transformed cells were grown on LB-Agarose plates with corresponding antibiotics (e.g. ampicillin) overnight at 37°C. Inoculated colonies were grown overnight in 3 mL LB-medium (10 g/L Tryptone, 5 g/L Yeast Extract, 5 g/L NaCl) with 1:1000 chloramphenicol at 37°C, after which plasmid isolation was performed using a Nucleospin Plasmid Easypure kit (Macherey-Nagel). Clones were verified using an EcoRI-digest (NEB) and subsequent Sanger sequencing.

6.5.2 Removal of sequences from pAAV-RK-PCARE

We performed mutagenesis on the pAAV-RK-PCARE plasmid to remove non-essential sequences and reduce the size of the insert between the ITR's, from 5648 bp to 4867 bp. A minimum distance of 10 bp was left between the different elements. Mutagenesis primers of 30 to 40 bp were designed to remove the non-essential sequences. The first part of the primer consisted of the sequence to be removed, and the last part of the primer being the sequence after the first part. To remove parts 1, 2 and 3 (Figure 3), we performed PCR using Phusion® High-Fidelity DNA Polymerase (NEB) and GC buffer with the following program: 94°C for 5 min, followed by 10 cycles of denaturation at 94°C for 30 sec, annealing for 30 sec at 50°C or 55°C, final extension for 11 minutes at 72°C and final step of 15 min at 94°C. Subsequent PCR products were run on agarose gels. To remove part 4 (Figure 3), we used the Q5® Site-Directed Mutagenesis Kit (NEB) kit with the following program: initial denaturation at 98°C for 3 min, followed by 20 cycles of 98°C for 10 sec, 50°C for 30 sec and extension at 72°C for 9

min, and a final extension at 72°C for 10 min. Primer sequences can be found in Supplemental Table 1.

After DpnI treatment for 4.5 h at 37°C, the enzyme was heat-inactivated, and 5 µl of the PCR product were transformed in DH5a cells. Removal of the sequence was confirmed by restriction enzyme digestion, and Sanger sequencing was used to verify the deletion. Primers used are listed in Supplemental Table 1.

6.5.3 Generation of AAV2/9.RK.PCARE.S vector

pAAV-RK-PCARE-S plasmid DNA was purified using the Megaprep kit (Qiagen) following manufacturers instruction. The pAAV-RK-PCARE-S construct was packaged into an AAV by transfection of three plasmids (pAAV-RK-PCARE-S plasmid containing PCARE cDNA, AAV package plasmid encoding AAV Rep and Cap proteins from serotype 9 and adenovirus helper plasmid) in HEK293 cells. Three days after transfection, cells and culture medium were collected and enzymatically treated with Benzonase at high salt concentration (650 mM NaCl). The cell debris was removed by high speed centrifugation and regular filtration. The supernatant went through a tangential flow filter which concentrated the viral solution. Recombinant AAV vector particles were isolated and extracted by running the concentrated supernatant through the iodixanol density gradient. The purified supernatant was then further concentrated by running through an Amicon filter with a 100,000 molecular weight cut off. The AAV titer was determined by real-time PCR and the purity was verified by SDS–PAGE.

6.5.4 Transduction

hTERT RPE-1 cells were seeded ($5.90x10^5$ cells per well of a 6-well plate). The next day, viral particles were thawed and added to the cells at a multiplicity of infection (MOI) of 100,000. Cells were incubated for 96 h at 37°C before immunocytochemistry or western blot analysis.

6.5.5 Immunocytochemistry

hTERT RPE-1 cells were grown on 12-well plates until reaching 90% confluency. To induce cilia growth, cells were fed with serum starvation medium (DMEM/F12, 0.2% FCS + 1% Pen/Strep + 1% NaPy). Twenty-four hours post-starvation, cells were transfected with DNA plasmids using Lipofectamine® 2000 (Thermo Fisher Scientific) in a 1:2.5 ratio following manufacturer's instructions. Twenty hours post-transfection, cultured cells were fixed in PFA 2% for 20 min at RT, followed by 1% Triton-X-100 treatment for 3 min and blocking in 2% BSA for 20 min. Subsequently, cells were incubated with primary antibodies (PCARE, rabbit, home-made; ARL13B, mouse, NeuroMab, cat.# 75-

287) diluted in blocking solution for 1 h. After incubation, cells were washed three times in PBS and incubated with the corresponding Alexa Fluor conjugated secondary antibody. Finally, slides were washed three times in PBS for 5 min and mounted in ProLong(R) Gold antifade reagent (P36930, Life Technologies).

6.5.6 Western blot analysis

HEK293T or hTERT RPE-1 cell pellets were resuspended in 150 µl RIPA buffer (50 mM Tris pH 7.5, 1 mM EDTA, 150 mM NaCl, 0.5% Na-Deoxycholate, 1% NP-40 plus protease inhibitors) rotating for 30 min at 4°C. Cells were sonicated for 15 seconds and centrifuged for 5 min at 12,000 *g*, 4°C. The supernatant was mixed with loading buffer supplemented with 0.1 M DTT and proteins were separated on a 3-8% NuPAGE Tris-Acetate Gel. Proteins were transferred onto a nitrocellulose membrane (Amersham Protran 0.45 NC, GE Healthcare Life Sciences) overnight at 4°C. After transfer, membranes were briefly washed in PBS and blocked for 1 h at RT in 5% Blotting-Grade Blocker (Bio-Rad) in PBS. Primary antibodies were incubated overnight in 2.5% blocker (Blotting Grade Blocker Non-Fat Dry Milk, Bio-Rad) in PBS. Subsequently, the membrane was washed three times in PBS-Tween 0.2% at RT and incubated with secondary antibodies in 2.5% blocking milk for 45 min. After secondary antibody incubation, the membrane was washed three times for 10 min in PBS-Tween 0.2% followed by a finally wash in 1xPBS. Fluorescence was analyzed on a Li-Cor Odyssey 2.1 infrared scanner using Image Studio 4.0 software.

6.5.7 PCR on viral DNA

To analyze correct packaging of AAV2/9.RK.PCARE.S, samples were treated with DNAse I for 30 min at 37°C. Then, we performed RT-PCR using the following program: 98°C for 30 sec, followed by 35 cycles of denaturation at 98°C for 10 seconds, annealing for 30 seconds at 60°C and extension of 6 min at 72°C, with a final extension for 10 min at 72°C. Primers are listed on Supplemental Table 1.

6.6 References

1. Hafler, B.P. (2017). Clinical Progress in Inherited Retinal Degenerations: Gene Therapy Clinical Trials and Advances in Genetic Sequencing. Retina 37, 417-423.
2. Trapani, I., Banfi, S., Simonelli, F., Surace, E.M., and Auricchio, A. (2015). Gene therapy of inherited retinal degenerations: prospects and challenges. Human gene therapy 26, 193-200.
3. Bainbridge, J.W., Smith, A.J., Barker, S.S., Robbie, S., Henderson, R., Balaggan, K., Viswanathan, A., Holder, G.E., Stockman, A., Tyler, N., et al. (2008). Effect of gene therapy on visual function in Leber's congenital amaurosis. N Engl J Med 358, 2231-2239.
4. Maguire, A.M., Simonelli, F., Pierce, E.A., Pugh, E.N., Jr., Mingozzi, F., Bennicelli, J., Banfi, S., Marshall, K.A., Testa, F., Surace, E.M., et al. (2008). Safety and efficacy of gene transfer for Leber's congenital amaurosis. N Engl J Med 358, 2240-2248.
5. Jacobson, S.G., Cideciyan, A.V., Ratnakaram, R., Heon, E., Schwartz, S.B., Roman, A.J., Peden, M.C., Aleman, T.S., Boye, S.L., Sumaroka, A., et al. (2012). Gene therapy for leber congenital amaurosis caused by RPE65 mutations: safety and efficacy in 15 children and adults followed up to 3 years. Arch Ophthalmol 130, 9-24.
6. Hauswirth, W.W., Aleman, T.S., Kaushal, S., Cideciyan, A.V., Schwartz, S.B., Wang, L., Conlon, T.J., Boye, S.L., Flotte, T.R., Byrne, B.J., et al. (2008). Treatment of leber congenital amaurosis due to RPE65 mutations by ocular subretinal injection of adeno-associated virus gene vector: short-term results of a phase I trial. Hum Gene Ther 19, 979-990.
7. Cideciyan, A.V., Aleman, T.S., Boye, S.L., Schwartz, S.B., Kaushal, S., Roman, A.J., Pang, J.J., Sumaroka, A., Windsor, E.A., Wilson, J.M., et al. (2008). Human gene therapy for RPE65 isomerase deficiency activates the retinoid cycle of vision but with slow rod kinetics. Proc Natl Acad Sci U S A 105, 15112-15117.
8. Russell, S., Bennett, J., Wellman, J.A., Chung, D.C., Yu, Z.F., Tillman, A., Wittes, J., Pappas, J., Elci, O., McCague, S., et al. (2017). Efficacy and safety of voretigene neparvovec (AAV2-hRPE65v2) in patients with RPE65-mediated inherited retinal dystrophy: a randomised, controlled, open-label, phase 3 trial. Lancet 390, 849-860.
9. Pierce, E.A., and Bennett, J. (2015). The Status of RPE65 Gene Therapy Trials: Safety and Efficacy. Cold Spring Harb Perspect Med 5, a017285.
10. Giacca, M., and Zacchigna, S. (2012). Virus-mediated gene delivery for human gene therapy. Journal of controlled release : official journal of the Controlled Release Society 161, 377-388.
11. Dong, B., Nakai, H., and Xiao, W. (2010). Characterization of genome integrity for oversized recombinant AAV vector. Mol Ther 18, 87-92.
12. Wu, Z., Yang, H., and Colosi, P. (2010). Effect of genome size on AAV vector packaging. Mol Ther 18, 80-86.
13. MacLaren, R.E., Groppe, M., Barnard, A.R., Cottriall, C.L., Tolmachova, T., Seymour, L., Clark, K.R., During, M.J., Cremers, F.P., Black, G.C., et al. (2014). Retinal gene therapy in patients with choroideremia: initial findings from a phase 1/2 clinical trial. Lancet 383, 1129-1137.
14. Conlon, T.J., Deng, W.T., Erger, K., Cossette, T., Pang, J.J., Ryals, R., Clement, N., Cleaver, B., McDoom, I., Boye, S.E., et al. (2013). Preclinical potency and safety studies of an AAV2-mediated gene therapy vector for the treatment of MERTK associated retinitis pigmentosa. Hum Gene Ther Clin Dev 24, 23-28.
15. Wright, A.F. (2015). Long-term effects of retinal gene therapy in childhood blindness. N Engl J Med 372, 1954-1955.
16. Collin, R.W.J., Safieh, C., Littink, K.W., Shalev, S.A., Garzozi, H.J., Rizel, L., Abbasi, A.H., Cremers, F.P.M., den Hollander, A.I., Klevering, B.J., et al. (2010). Mutations in C2ORF71 cause autosomal-recessive retinitis pigmentosa. Am J Hum Genet 86, 783-788.
17. Nishimura, D.Y., Baye, L.M., Perveen, R., Searby, C.C., Avila-Fernandez, A., Pereiro, I., Ayuso, C., Valverde, D., Bishop, P.N., Manson, F.D., et al. (2010). Discovery and functional analysis of a retinitis pigmentosa gene, C2ORF71. Am J Hum Genet 86, 686-695.
18. Naumer, M., Sonntag, F., Schmidt, K., Nieto, K., Panke, C., Davey, N.E., Popa-Wagner, R., and Kleinschmidt, J.A. (2012). Properties of the adeno-associated virus assembly-activating protein. J Virol 86, 13038-13048.
19. Samulski, R.J., and Muzyczka, N. (2014). AAV-Mediated Gene Therapy for Research and Therapeutic Purposes. Annu Rev Virol 1, 427-451.
20. Naso, M.F., Tomkowicz, B., Perry, W.L., 3rd, and Strohl, W.R. (2017). Adeno-Associated Virus (AAV) as a Vector for Gene Therapy. BioDrugs 31, 317-334.

21. Weitzman, M.D., Kyostio, S.R., Kotin, R.M., and Owens, R.A. (1994). Adeno-associated virus (AAV) Rep proteins mediate complex formation between AAV DNA and its integration site in human DNA. Proceedings of the National Academy of Sciences of the United States of America 91, 5808-5812.
22. Choi, V.W., McCarty, D.M., and Samulski, R.J. (2006). Host cell DNA repair pathways in adeno-associated viral genome processing. J Virol 80, 10346-10356.
23. Zufferey, R., Donello, J.E., Trono, D., and Hope, T.J. (1999). Woodchuck hepatitis virus posttranscriptional regulatory element enhances expression of transgenes delivered by retroviral vectors. J Virol 73, 2886-2892.
24. Zhang, J.X., Wang, N.L., and Lu, Q.J. (2015). Development of gene and stem cell therapy for ocular neurodegeneration. Int J Ophthalmol 8, 622-630.
25. Watanabe, S., Sanuki, R., Ueno, S., Koyasu, T., Hasegawa, T., and Furukawa, T. (2013). Tropisms of AAV for subretinal delivery to the neonatal mouse retina and its application for in vivo rescue of developmental photoreceptor disorders. PLoS One 8, e54146.
26. Audo, I., Lancelot, M.E., Mohand-Said, S., Antonio, A., Germain, A., Sahel, J.A., Bhattacharya, S.S., and Zeitz, C. (2011). Novel C2orf71 mutations account for approximately 1% of cases in a large French arRP cohort. Hum Mutat 32, E2091-2103.
27. Sergouniotis, P.I., Li, Z., Mackay, D.S., Wright, G.A., Borman, A.D., Devery, S.R., Moore, A.T., and Webster, A.R. (2011). A survey of DNA variation of C2ORF71 in probands with progressive autosomal recessive retinal degeneration and controls. Invest Ophthalmol Vis Sci 52, 1880-1886.
28. Gerth-Kahlert, C., Tiwari, A., Hanson, J.V.M., Batmanabane, V., Traboulsi, E., Pennesi, M.E., Al-Qahtani, A.A., Lam, B.L., Heckenlively, J., Zweifel, S.A., et al. (2017). C2orf71 Mutations as a Frequent Cause of Autosomal-Recessive Retinitis Pigmentosa: Clinical Analysis and Presentation of 8 Novel Mutations. Invest Ophthalmol Vis Sci 58, 3840-3850.
29. Mendonca, L.S.M., Avila, M.P., Silva, I.M.B.M., Lavigne, L.C., Oliveira, T., Chiang, J., Jordão, A., Rassi, A.T., Chaves, L.F.O.B., and Gabriel, L.A.R. (2014). Novel nonsense mutation in C2orf71 gene in a brazilian patient with autosomal recessive cone-rod dystrophy. Investigative Ophthalmology & Visual Science 55, 3275-3275.
30. Khateb, S., Zelinger, L., Mizrahi-Meissonnier, L., Ayuso, C., Koenekoop, R.K., Laxer, U., Gross, M., Banin, E., and Sharon, D. (2014). A homozygous nonsense CEP250 mutation combined with a heterozygous nonsense C2orf71 mutation is associated with atypical Usher syndrome. J Med Genet 51, 460-469.
31. White, M.D., Milne, R.V., and Nolan, M.F. (2011). A Molecular Toolbox for Rapid Generation of Viral Vectors to Up- or Down-Regulate Neuronal Gene Expression in vivo. Frontiers in molecular neuroscience 4, 8.
32. Rabinowitz, J.E., Rolling, F., Li, C., Conrath, H., Xiao, W., Xiao, X., and Samulski, R.J. (2002). Cross-packaging of a single adeno-associated virus (AAV) type 2 vector genome into multiple AAV serotypes enables transduction with broad specificity. J Virol 76, 791-801.
33. Ali, R.R., Reichel, M.B., Thrasher, A.J., Levinsky, R.J., Kinnon, C., Kanuga, N., Hunt, D.M., and Bhattacharya, S.S. (1996). Gene transfer into the mouse retina mediated by an adeno-associated viral vector. Hum Mol Genet 5, 591-594.
34. Bennett, J., Maguire, A.M., Cideciyan, A.V., Schnell, M., Glover, E., Anand, V., Aleman, T.S., Chirmule, N., Gupta, A.R., Huang, Y., et al. (1999). Stable transgene expression in rod photoreceptors after recombinant adeno-associated virus-mediated gene transfer to monkey retina. Proc Natl Acad Sci U S A 96, 9920-9925.
35. Klein, R., Ruttkowski, B., Knapp, E., Salmons, B., Gunzburg, W.H., and Hohenadl, C. (2006). WPRE-mediated enhancement of gene expression is promoter and cell line specific. Gene 372, 153-161.
36. Le Meur, G., Stieger, K., Smith, A.J., Weber, M., Deschamps, J.Y., Nivard, D., Mendes-Madeira, A., Provost, N., Pereon, Y., Cherel, Y., et al. (2007). Restoration of vision in RPE65-deficient Briard dogs using an AAV serotype 4 vector that specifically targets the retinal pigmented epithelium. Gene Ther 14, 292-303.
37. Lem, J., Flannery, J.G., Li, T., Applebury, M.L., Farber, D.B., and Simon, M.I. (1992). Retinal degeneration is rescued in transgenic rd mice by expression of the cGMP phosphodiesterase beta subunit. Proc Natl Acad Sci U S A 89, 4422-4426.
38. Chen, J., Tucker, C.L., Woodford, B., Szel, A., Lem, J., Gianella-Borradori, A., Simon, M.I., and Bogenmann, E. (1994). The human blue opsin promoter directs transgene expression in short-wave cones and bipolar cells in the mouse retina. Proc Natl Acad Sci U S A 91, 2611-2615.
39. Glushakova, L.G., Timmers, A.M., Issa, T.M., Cortez, N.G., Pang, J., Teusner, J.T., and Hauswirth, W.W. (2006). Does recombinant adeno-associated virus-vectored proximal region of mouse rhodopsin promoter support only rod-type specific expression in vivo? Mol Vis 12, 298-309.

40. Khani, S.C., Pawlyk, B.S., Bulgakov, O.V., Kasperek, E., Young, J.E., Adamian, M., Sun, X., Smith, A.J., Ali, R.R., and Li, T. (2007). AAV-mediated expression targeting of rod and cone photoreceptors with a human rhodopsin kinase promoter. Invest Ophthalmol Vis Sci 48, 3954-3961.
41. Schlabach, M.R., Hu, J.K., Li, M., and Elledge, S.J. (2010). Synthetic design of strong promoters. Proc Natl Acad Sci U S A 107, 2538-2543.
42. Grieger, J.C., and Samulski, R.J. (2005). Packaging capacity of adeno-associated virus serotypes: impact of larger genomes on infectivity and postentry steps. J Virol 79, 9933-9944.
43. Duan, D., Yue, Y., and Engelhardt, J.F. (2001). Expanding AAV packaging capacity with trans-splicing or overlapping vectors: a quantitative comparison. Mol Ther 4, 383-391.
44. Yan, Z., Zhang, Y., Duan, D., and Engelhardt, J.F. (2000). Trans-splicing vectors expand the utility of adeno-associated virus for gene therapy. Proc Natl Acad Sci U S A 97, 6716-6721.
45. Ghosh, A., Yue, Y., Lai, Y., and Duan, D. (2008). A hybrid vector system expands adeno-associated viral vector packaging capacity in a transgene-independent manner. Mol Ther 16, 124-130.
46. Trapani, I., Colella, P., Sommella, A., Iodice, C., Cesi, G., de Simone, S., Marrocco, E., Rossi, S., Giunti, M., Palfi, A., et al. (2014). Effective delivery of large genes to the retina by dual AAV vectors. EMBO Mol Med 6, 194-211.
47. Carvalho, L.S., Turunen, H.T., Wassmer, S.J., Luna-Velez, M.V., Xiao, R., Bennett, J., and Vandenberghe, L.H. (2017). Evaluating Efficiencies of Dual AAV Approaches for Retinal Targeting. Front Neurosci 11, 503.
48. Trapani, I., Toriello, E., de Simone, S., Colella, P., Iodice, C., Polishchuk, E.V., Sommella, A., Colecchi, L., Rossi, S., Simonelli, F., et al. (2015). Improved dual AAV vectors with reduced expression of truncated proteins are safe and effective in the retina of a mouse model of Stargardt disease. Hum Mol Genet 24, 6811-6825.
49. Colella, P., Trapani, I., Cesi, G., Sommella, A., Manfredi, A., Puppo, A., Iodice, C., Rossi, S., Simonelli, F., Giunti, M., et al. (2014). Efficient gene delivery to the cone-enriched pig retina by dual AAV vectors. Gene Ther 21, 450-456.
50. Dyka, F.M., Boye, S.L., Chiodo, V.A., Hauswirth, W.W., and Boye, S.E. (2014). Dual adeno-associated virus vectors result in efficient in vitro and in vivo expression of an oversized gene, MYO7A. Hum Gene Ther Methods 25, 166-177.
51. Park, F. (2007). Lentiviral vectors: are they the future of animal transgenesis? Physiol Genomics 31, 159-173.
52. Kong, J., Kim, S.R., Binley, K., Pata, I., Doi, K., Mannik, J., Zernant-Rajang, J., Kan, O., Iqball, S., Naylor, S., et al. (2008). Correction of the disease phenotype in the mouse model of Stargardt disease by lentiviral gene therapy. Gene Ther 15, 1311-1320.
53. Suzuki, K., Tsunekawa, Y., Hernandez-Benitez, R., Wu, J., Zhu, J., Kim, E.J., Hatanaka, F., Yamamoto, M., Araoka, T., Li, Z., et al. (2016). In vivo genome editing via CRISPR/Cas9 mediated homology-independent targeted integration. Nature 540, 144-149.

6.7 Acknowledgements

This work was funded by the FP7-PEOPLE-2012-ITN programme EyeTN, Brussels, Belgium (grant agreement no.: 317472) to RWJC.

6.8 Supplemental data

Supplemental Table 1. Primers used in this study.

Primer name	Sequence Forward (5'-3')	Sequence Reverse (3'-5')
pAAV-attR	aaaagctgcggaattgtacccgcggccgccacaagtt tgtacaaaaaagctgaacgagaa	tgtaatccagaggttgattggatccaagctaccactttgta caagaaagctgaacgagaa
pAAV-RK-PCARE-mutagenesis-1	gtagttaatgattaacccggggccccagaagcctgg	ccaccaggcttctggggccccgggttaatcattaactac
pAAV-RK-PCARE-mutagenesis-2	ggccaagggccctcgatcgagtaagtttagtctttttg	gacaaaaagactaaacttactcgatcgagggcccttgg
pAAV-RK-PCARE-mutagenesis-3-F	gatgttgcctttacttctagcgccgccaccatggggtg	gtacaccccatggtggcggcgctagaagtaaaggcaac
pAAV-RK-PCARE-mutagenesis-4-F	ggtgtcctgacacccagcttgcctcgactgtgccttc	ctagaaggcacagtcgaggcaagctgggtgtcaggac
pAAV-RK-PCARE-mutagenesis-seq-1-F	gagtggccaactccatcac	aaagacaatcccctgagctg
pAAV-RK-PCARE-mutagenesis-seq-2-F	ttagcctggtgctgtgtcag	aggcaacatccactgaggag
pAAV-RK-PCARE-mutagenesis-seq-3-F	ggtggtggtgcaaatcaaag	ttgctttgggctttttcaag
pAAV-RK-PCARE-mutagenesis-seq-4-F	aggacaaatcccagccagag	aggggcaaacaacagatgg
AAV-5'ITR-PCARE-Seq	ggttccttgtagttaatgattaacccggggccccagaa gcc	ctgtgctcgtggctgaac
AAV-PCARE-Seq	ttggcctttgaagaaaagagag	ctgaggtcctgttttgtccag
AAV-PCARE-3´ITR	gcccttagcacctatctttcc	ggttccttgtagttaatgattaacccgccatgctacttatc

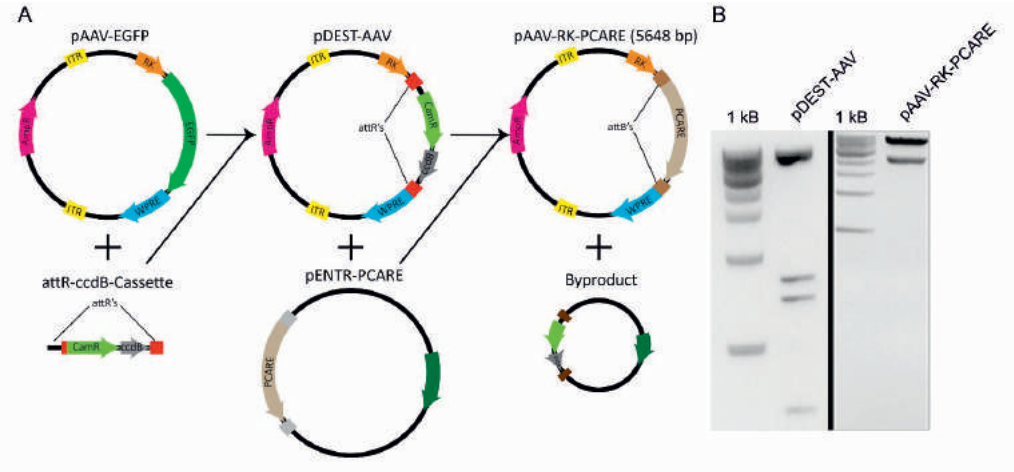

Supplemental Figure 1. Strategy to obtain a Gateway-adapted AAV plasmid and Gateway cloning to introduce *PCARE* cDNA. A, Cloning strategy describing the insertion of a standard attR-*ccdB*-Cassette into an AAV. The resulting pDEST-AAV was then used to clone *PCARE* cDNA from a pENTR, resulting in an expression vector with an AAV backbone and a *PCARE*-insert (pAAV-RK-PCARE). **B,** Restriction enzyme digestion with a correct pattern for pDEST-AAV (BamHI; 4401 bp, 816 bp, 703 bp, 315 bp) and pAAV-RK-PCARE (XhoI; 6229 bp and 2171 bp), each displaying a correct restriction pattern. attR/B: R/B-integration sequence, *ccdB*: *ccdB*-toxin encoding gene, RK: Rhodopsin Kinase promoter, WPRE: WHP Post-transcriptional Response Element, ITR: Inverted Terminal Repeat, *AmpR*: Ampicilline-resistance gene, *CamR*: Chloramphenicol-resistance gene, 1 kb: 1 kb Ladder.

Chapter 7

General discussion

The understanding of the biology of the eye has remained an exciting quest ever since Charles Darwin could not help but wonder "that natural selection could produce… an organ so wonderful as the eye" (Darwin, Origin of Species, 1859).[1]

7.1 Development of the ciliary photoreceptor cell outer segment

Photoreceptor cells within the retina need particularly high amounts of membranes that allow accommodating a large number of proteins required for photoreception and -transduction. In the animal kingdom, we can distinguish two types of photoreceptor cells based on the process that drives the formation of the unit that contains the opsin-loaded membrane stacks: formation of a microvilli-based unit (rhabdomeric photoreceptors), or formation of a modified cilium (ciliary photoreceptors). Rhabdomeric and ciliary photoreceptors probably evolved from a single precursor, and are present in all metazoans.[2] The rhabdomeric photoreceptor cells fold the apical cell surface, while the ciliary photoreceptor cells fold the ciliary membrane.[3] In invertebrates, microvillar photoreceptors are preferred, since they support vision in dim light with large responses to single photons, but also in bright light with fast visual response.[4] In vertebrates, ciliary rod photoreceptors account for high-sensitivity detection of low light, and cone photoreceptors allow low-sensitivity detection in bright light. Though slower than microvillar photoreceptors, ciliary photoreceptors can cover a broad range of intensities.

Ciliary photoreceptor cells have been well characterized over the last two decades, since this cell type degenerates in inherited retinal diseases (IRDs). Genetic studies enabled the discovery of many genes encoding ciliary proteins that are mutated in IRD, which improved our understanding of their ciliary function and their role in photoreceptor cell biology and development. These proteins localize to the photoreceptor sensory cilium, encompassing the photoreceptor outer segment, its proximally adjacent connecting cilium or ciliary transition zone, and the ciliary basal body. The first major breakthrough in our knowledge of the biogenesis and homeostasis of the sensory cilium however dates back to 1967, when Richard Young reported the exciting finding that rod and cone outer segments are continually rebuilt.[5] This new insight raised the question of how the disc membranes are initially formed. Until recently, two main hypotheses explained this phenomenon. The original work from Steinberg and colleagues in 1980 supports that new discs generate by evagination of the ciliary plasma membrane at the base of the outer segments.[6] An alternative hypothesis supports that disc biogenesis occurs by fusion of intracellular vesicles transported to the outer segments.[7-9] However, it was not until 2015 that the work of different groups confirmed the validity of the classical evagination hypothesis. Ding et al. observed that membranes of newly formed discs were

exposed to the extracellular space.[10] Burgoyne et al. showed by electron microscopy that rhodopsin traffics to the OS via the ciliary plasma membrane, and that new discs form extracellularly, making novel contacts with the IS.[11] Both articles showed, using different fixation experiments, that what were interpreted as vesicles at the proximity of the outer segments, were in fact tissue fixation artifacts, indicating the alternative vesicular fusion hypothesis to be false.

At early stages, before OS discs are formed, the photoreceptor cilium has a distinct transition zone and its distal domain is enriched in its main membrane proteins, rhodopsin[12] and peripherin-2.[13] Proteins and membranes accumulate at the tip of the cilium and eventually organize to give rise to nascent outer segment disks. Volland et al. used electron microscope tomography to show that the membrane of nascent discs first bulges and invaginates, and it is continuous with the ciliary plasma membrane.[14] This initial invagination may be important to reshape the membrane and form a flattened structure that can later evaginate, and it is also needed to properly anchor the incipient rim of the nascent disc. In the end, the disc matures once the lamellae (central portion of disc) reaches full diameter.[14]

7.2 Role of actin in outer segment discs morphogenesis

The involvement of actin in this evagination process has been long suggested, because of evidence for the presence of actin at the base of the outer segments.[15-17] Actin is one of the most highly-conserved proteins known. Six actin-encoding genes are found in mammals (*ACTA1*, *ACTA2*, *ACTB*, *ACTG1*, *ACTG2*, *ACTC1*), and defects in muscle actins cause different myopathies in humans.[18] Since knockout of cytoplasmic actins causes embryonic lethality in mice, the effect of their absence in photoreceptor cells has not been well studied. In the photoreceptor cell, actin has been shown to interact with α-actinin,[19] fascin2[20] and TULP1.[21] The functions of α-actinin and fascin2 have been linked to actin assembly; however, the role of TULP1 is not yet clear. Filamentous (F) actin is assembled from monomeric (G) actin subunits that are added to the barbed ends of the filaments and dissociate from the pointed ends. On one hand, inhibition of actin polymerization by cytochalasin D causes disruption of the ciliary plasma membrane evagination, preventing initiation of new disc membranes and discs.[22] On the other hand, the evaginations leading to disc membrane biogenesis have a depth of 11 nm, compared to the 100 nm depth of lamellipodia. Lammelipodia are flat membrane protrusions filled with actin that form at the periphery of moving cells,[23] and contain multiple layers of actin filaments of ~10 nm in diameter, as well as a large number of cytoskeletal and signaling proteins.[24] For this reason, some authors do not support the idea that outer segment biogenesis is driven by an actin-mediated mechanism, and they suggest that the outward growth of the lamellae may be more similar to a blebbing protrusion without actin involvement.[11]

Recent studies, however, place actin back at the center of OS disc morphogenesis. Nager et al.[25] described actin-driven ectocytosis as a mechanism of ciliary membrane release. Their work shows that F-actin, myosin VI and drebrin mediate ectosome scission from ciliary tips, and cytochalasin D treatment results in accumulation of multiple tip buds. Next to this, the work of Megaw et al. proposes that peripherin-2, which localizes to both open and closed discs at the rims but not at the disc edges,[10,26] is an inhibitor of ectosomal release from the photoreceptor cilium, setting this mechanism as the first step in OS disc formation.[27] Another recent study shows that the X-linked RP-associated protein RPGR interacts with and activates the actin-severing protein gelsolin in the connecting cilium, and facilitates rhodopsin transport to the outer segments.[28] More specifically, RPGR would facilitate OS disc budding or completion of disc formation by regulation of actin disassembly through gelsolin.

The link between actin and other proteins involved in OS disc morphogenesis is not as well known. Rom-1, homologous to peripherin-2, is thought to function as a modulator of peripherin-2.[29] Contrary to peripherin-2, which locates at the disc edges, rom-1 is confined to the disc rim, to help maintaining the curvature of the rim.[29,30] The rim of a disc is the hairpin-shaped boundary of the disc, while disc edges refer to U-shaped boundaries between two adjacent discs. Prominin-1 is a protein present in microvilli and the tip of primary cilia where it is implicated in stabilization of curved membrane protrusions.[31,32] In photoreceptors, it localizes to the base of the OS, and interacts with β-actin.[33] Knockout of prominin-1 alters disc morphogenesis and causes photoreceptor degeneration.[33-35] Neuroepithelial cells of the neurocortex present prominin-1 at the ciliary tip.[36] Interestingly, extracellular membrane particles enriched in prominin-1 are released from the primary cilium of these neuroepithelial cells. These particles contain anillin, an actin-binding protein associated with the contractile ring.[37] Protocadherin 21 is present at the linking edges of nascent discs with the IS,[38] and it is thought to work as a connector between these discs, however this is solely based on co-localization data.[11] Protocadherin 21 interacts physically with prominin-1,[33] but the relevance of this interaction in OS disc morphogenesis also remains to be elucidated.

The role of phototransduction cascade proteins in outer segment disc formation has also been described. For instance, rhodopsin is essential for OS formation and occupies disc surfaces.[39,40] In rhodopsin mutant mice, the photoreceptor ciliary tip membrane expansion is formed, but disc assembly and elongation are disrupted.[13,41] Also, the ATP-binding cassette protein ABCA4 is present within the disc membranes at the rim.[42] Although knockout of guanylyl cyclases[43] or *Abca4*[44] does not impair OS formation, the discs are abnormal and eventually degenerate. Despite these observations, it is unknown if there is a link to actin assembly.

7.3 PCARE association to actin in the photoreceptor cilium

In **chapter 2** of this thesis, we investigated the function of the uncharacterized protein C2ORF71/PCARE (photoreceptor cilium actin regulator), associated with inherited retinal dystrophy subtype RP54. This work provided novel understanding of the molecular mechanisms involved in modification of the photoreceptor ciliary plasma membrane, deciphering the missing molecular link between the mechanisms of outer segment discs biogenesis and actin-linked ciliary ectocytosis (as indicated above), an exciting new topic in the field of retinal ciliopathies in the recent years. In **chapter 2**, we showed that PCARE interacts with and recruits the Arp2/3 activator WASF3 to the primary cilium. During the first experiments with hTERT RPE-1 cells, we analyzed the interaction of these two proteins in primary cilia using a conventional fluorescence microscope. As we focused on spotting cilia with a typical antenna-like morphology, we initially excluded structures from the analysis that, although they were PCARE and/or WASF3 positive, were not antenna-shaped thus considered artifacts. After taking a closer look at these structures, we noticed that they were in fact cilia, as they also expressed the ciliary marker ARL13B, but they had a peculiar rounded morphology. Analysis by confocal microscope of these “reshaped” cilia showed that the primary cilium acquires a circular shape when PCARE and WASF3 are overexpressed in hTERT RPE-1 and also in mIMCD-3 cells, recruiting F-actin and other actin components to the cilium. This finding was striking, since polymerized actin has not yet been observed in the ciliary axoneme by conventional microscopy.[25] Actin has been previously observed at the ciliary pocket,[45] and at the ciliary tip prior to ectocytosis[25] or decapitation.[46] We named these rounded ciliary structures evaginations, because the bulged tip of these cilia seems to form a disc-like structure. Similar to the lamellipodium,[24] outer segments discs are flattened,[47] and our first impression was that the bulged cilia were also flattened. The evagination at the ciliary tip could be mistaken with a "tipping" phenomenon that has been described for the motor protein KIF17.[48] However, the ciliary bulges formed by PCARE/WASF3 were significantly different from those generated by KIF17 (see **chapter 2**, figure 3, and reference 48). The bulged cilia however could still be swelling artifacts caused by accumulation of proteins in the cilium. To discard this possibility, and to study whether the cilium flattens upon evagination, we are currently performing experiments to analyze these structures under scanning and transmission electron microscopy. Nonetheless, we observed that these bulged cilia or evaginations were disrupted by latrunculin B, a stronger actin poison than cytochalasin D, suggesting implication of actin in this process. Also, a missense mutation in *PCARE* associated with RP54 strongly affected the evagination process, which supports our model of active regulation of actin dynamics by PCARE.

Proteomic analysis of the photoreceptor outer segments shows that several actin-related proteins involved in membrane protrusion that interact directly or indirectly with PCARE are also present in

these outer segments.[49,50] These proteins include the WASF proteins 1 and 3, several subunits of the Arp2/3 complex, profilin, filamin, actinins, spectrins, RAC1 (but not RAC2), and huntingtin associated proteins (related to IFT57 and KALRN). Some of these proteins, like WASF3, KALRN and RAC1, translocate to the primary cilium in hTERT RPE-1 cells only when PCARE is present, supporting the idea that PCARE may as well be responsible for their transport to the OS.

The strongest interactor of PCARE appears to be the Wiskott-Aldrich syndrome protein WASF3 (also known as WAVE3). This protein seems to bind to the N-terminal region of PCARE (**chapter 2**, page 85). PCARE and WASF3 share a proline-rich region at the C-terminus and a predicted verprolin homology domain (also known as WASP homology 2, WH2) with actin-binding properties.[51,52] Proline-rich domains alone can have actin polymerase activity in the presence of profilin-actin, and the tandem of proline-rich domains and WH2 domains cooperate to enhance polymerase activity.[53] While PCARE contains a WH2 domain, it does not contain a central/acidic (CA) domain as WASF3 does, which binds and activates the Arp2/3 complex.[52,54]

In N-WASP, the proline-rich region assists in the interaction with the SH3 domains of EFC (extended Fer-CIP4 homology) and F-BAR (FCH-Bin/Amphiphysin/Rvs) domain-containing proteins, which are thought to induce curvature of the membrane.[55] In WASF2, the proline-rich region binds to the SH3 domain of IRSp53, a RCB (Rac binding)/IMD (IRSp53-MIM homology domain) domain-containing protein similar to the EFC/F-BAR proteins.[56] WASF2 is ubiquitously expressed, while WASF1 and WASF3 are brain-specific. A few studies describe the role of WASF3 in cancer,[57,58] but the interaction of WASF3 with other proteins is not well described. WASF proteins localize to the leading edge of lamellipodia.[23] The branched actin network forming lamellipodia is produced by the small GTPase Rac (Rac1). Rac1 is known to activate the WAVE regulatory complex (WRC) to drive actin polymerization by the Arp2/3 complex.[59] The interaction of PCARE with WASF3 and their ability to bulge the primary cilium (as demonstrated in **chapter 2**), the presence of previously mentioned actin-binding proteins in the ciliary bulges, and the defective bulging observed in the PCARE mutant p.Ile201Phe, supports the hypothesis of actin-driven ciliary membrane evagination as the mechanism underlying OS disc formation and unveils novel potential molecules involved in this process.

7.4 The role of retinal ciliopathy proteins in actin-driven formation of outer segment discs

As shown in **chapter 2**, PCARE and WASF3 overexpression in hTERT RPE-1 not only causes recruitment of an actin module to the primary cilium, but retinal ciliopathy proteins also modify this process. The proteins encoded by *CEP290* and *OFD1*, both found mutated in various retinal ciliopathies,[60-64] do not translocate to the cilium by PCARE alone, but they do when WASF3 is present at ciliary evaginations (**chapter 2**). CEP290 is an interesting protein, since it has high similarity to

myosin and it plays a role in ciliogenesis and ciliary trafficking.[65] It interacts with PCM1, also a PCARE interactor, which is required for organizing the cytoplasmic microtubule network.[66] CEP290 recruits the small GTPase Rab8a, important for elongation of the ciliary membrane, and knockdown of *CEP290* causes mislocalization of Rab8.[66] Vesicle trafficking through Rab8 is driven along microtubules and may be also actin-dependent.[67,68] Inhibition of Rab8 activation causes disruption of rhodopsin transport and mislocalization from OS.[68,69] RPGR is another putative CEP290 interactor,[66,70] and as mentioned before, RPGR interacts with the actin-regulator gelsolin.[28] A truncated CEP290 mutant associates and retains RPGR in the inner segments.[71] Because of this, RPGR cannot exert its function at the base of the OS, which may be an indirect cause of OS disc malformation. Both MKS3 and CC2D2A, important proteins for photoreceptor outer segment development,[72] interact with CEP290 and are involved in retinal disease.[73-76] CC2D2A has been proposed, similar to CEP290, as a gate-keeper at the transition zone, restricting the entry of proteins to the cilium. Interestingly, Rab8 is also mislocalized in CC2D2A mutant zebrafish photoreceptors,[77] suggesting a role in vesicle transport of CC2D2A to the basal body. In **chapter 2**, figure 2, electron microscopy analysis shows a high accumulation of PCARE at the daughter centriole. This finding, together with the connection of PCARE with CEP290, could indicate that PCARE may also play a role at the centriole, possibly participating in the sorting of proteins at the basal body of photoreceptors.

OFD1 localizes to the centrosome of the primary cilium and is a component of the centriolar satellites. OFD1 was found as direct interactor of PCARE (**chapter 2**). OFD1 physically interacts with lebercilin, the protein encoded by *LCA5*.[64] Lebercillin interacts with the IFT machinery and disruption in mice of IFT causes displacement of opsins from the OS.[78] *RPGR* knockout mice show reduced abundance of OFD1 at the photoreceptor cilium, and the authors postulate that it may share functions with RPGR.[79] In rat degeneration models, OFD1 has a neuroprotective function of the photoreceptor cell.[80] Additionally, the phenotypes of *Ofd1* and *Rpgrip1l* knock-out mice overlap, again indicating that these proteins play a similar role.[81] Although the function of OFD1 has been mostly restricted to the ciliary basal body, we hint towards an additional putative role in the neogenesis of outer segments, and a link to actin should not be discarded. Interestingly, loss of Rpgrip1l results in defective glioma-associated oncogene (Gli) processing and Sonic hedgehog (Shh) signaling in mice.[82] Although not described in this thesis, the evaluation of ciliary signaling cascades such as Shh signaling, would allow to analyze whether PCARE plays a role in these pathways.[83]

The microtubule and actin crosslinking factor 1, MACF1, is a giant protein that mediates interactions between microtubule and actin networks for proper ciliogenesis and photoreceptor differentiation, indicating an interconnection between these two networks.[84] SPATA7 is a microtubule-associated protein that interacts with RPGRIP1, and it is important to maintain its localization at the connecting

cilium.[85] RPGRIP1 is a structural protein of the photoreceptor ciliary axoneme and it is thought to play a role in discs formation.[86] *Rpgrip1* ko mice produce overgrown disc membranes, and it is thought that RPGRIP1 mediates actin cytoskeletal dynamics.[86] RPGRIP1 interacts with RPGR and NPHP4, and it is also involved in ciliary protein trafficking.[87-89] Similar to RPGRIP1L, RPGRIP1 could also have an actin-related function in the photoreceptor, but this needs to be further studied.

As described in **chapter 1**, the photoreceptor ciliary axoneme is mainly microtubule-based, with less microtubular content as we enter the OS base and tip.[90] The protein RP1 is a connector between nascent discs and the photoreceptor ciliary axoneme, helping the discs to form in the correct orientation and stack up into outer segments.[91] Mutations in RP1 cause autosomal dominant retinitis pigmentosa.[92] Interestingly, digenic inheritance of *RP1L1* and *PCARE* truncating mutations has been reported in one patient with syndromic retinitis pigmentosa.[93] In the protein-protein interaction dataset of PCARE in **chapter 2**, microtubule-based kinesin motors and dynein-linked proteins are identified. This may indicate a possible link to the transport of PCARE across the connecting cilium through IFT motors. Given that IFT74 and IFT57 were found as well in the dataset, they might mediate the connection with PCARE for trafficking as IFT cargo along the cilium. As mentioned in **chapter 4**, the phenotypes between *Pcare1*- and *Ift57*-deficient zebrafish mutants are similar, indicating a possible connection between these two proteins.[94]

Actin is also found at the periciliary membrane complex, a place where post-Golgi vesicles dock and sort their cargoes closely connected to the basal body.[95,96] Usherin and other proteins from the periciliary membrane are linked to actin and genes encoding for these proteins are found mutated in Usher syndrome.[95] RPGR interacts with whirlin, a protein present in hair cells and photoreceptors.[97] Whirlin interacts with the actin cross-linking protein espin to regulate the actin network at the periciliary membrane complex of photoreceptors, and disruption of whirlin can cause both vision and hearing loss.[98,99]

In the PCARE interactome we also detected myosin-linked proteins. Myosins are motor proteins that use ATP to travel along actin filaments.[100] Mutations in *MYO7A* cause Usher syndrome type 1B.[101] MYO7A is a motor protein that acts in actin-related opsin transport through the connecting cilium.[102,103] Mutations in another five genes, coding for protocadherin-15, cadherin-23, harmonin, sans, and CIB2, cause other subtypes of Usher syndrome type 1.[101,104-106] These proteins all localize to the calyceal processes of photoreceptor cells.[107] Cadherin-23 is anchored by marshalin to the microtubules of the outer segments and regulates microtubule networks.[108] The common affection of both vision and hearing in Usher syndrome may be due to a similar role of these proteins in stereocilia and the calyceal processes of photoreceptor cells. When calyceal processes are missing,

the OS discs overgrow, indicating that they are important to limit the growth of the OS beyond its basal region.[109] MYO7A is well-described in stereocilia, and functions to keep the ciliary tip-links under tension at rest.[110] Defects in other myosins, myosin 1a, myosin IIIa, myosin VI, and myosin XVa cause hearing loss in humans and/or mice,[111,112] and produce abnormal hair bundles of auditory and vestibular hair cells. The hair bundle is composed of actin-filled stiff microvilli, called the stereocilia. Stereocilia are arranged in different rows of increasing height.[113] In brush border microvilli, the composition of actin is of about 20 polarized actin filaments with the barbed end facing the plasma membrane at the tip of the microvillus. The content of actin in stereocilia is high, of over 3,000 filaments.[114] The number of filaments in other microvilli is not known, but this number reflects the physical forces that it has to support from the surrounding plasma membrane and the environment. In the photoreceptor cell, the outer segments do not need to support many forces, so we may expect a lower number of actin filaments needed to maintain its structure. The microvilli from RPE cells extend to and surround the entire outer segment of photoreceptor cells, reaching the inner segment in mouse photoreceptors, thus providing also mechanical support to the outer segment morphogenesis, and their role may be more critical in species lacking well-developed calyceal processes.[109]

7.5 *PCARE*-associated retinal disease and disease models

In **chapter 3**, we collected all reported patients with disease-causing mutations in *PCARE* until April 2018. *PCARE* mutations are distributed along the entire *PCARE* coding sequence; however, there was no observable correlation between the position of the mutation and the age at onset of retinal disease. As pointed out in **chapter 3**, the small number of patients with mutations in *PCARE* makes it difficult to establish a clear genotype-phenotype correlation. At the protein level, we were able to detect differences between the PCARE wild-type protein and five different mutants (data not shown). The PCARE missense mutant p.Ile201Phe is able to expand the ciliary membrane, but in a lesser extent than wild-type PCARE (**chapter 2**). Truncating PCARE mutants p.Glu135*, p.Trp650*, p.Lys919Thrfs*2 and p.Trp1001* lose the ability to locate to the axoneme of the primary cilium in hTERT RPE-1 cells (**chapter 3, data in preparation**). Therefore, proper localization of PCARE to the axoneme of the cilium seems important to properly execute its function as actin regulator. If the truncating mutants are produced *in vivo*, their ability to localize to the basal bodies might indicate that some PCARE function is still retained, while aberrant mislocalized PCARE may additionally have malignant effects. Besides a different residual function of the protein depending of the position and type of mutation, the clinical variability observed may be due to different genetic backgrounds, where other genes can act as modifiers. Whole genome sequencing of patients with mutations in

PCARE would allow studying the presence of such modifiers and explaining the clinical variability. At the same time, it would also be helpful for a better selection of patients for potential therapies.

In vivo models of *PCARE*-associated retinal disease will also help to better understand the function of PCARE. In **chapter 4**, we generated a *pcare1* mutant fish using CRISPR/Cas9 technology. We show that *pcare1*$^{-/-}$ larvae and adult fish generate highly disorganized outer segments, while the larvae also present visual dysfunction. This phenotype resembles the phenotype observed in *Pcare*$^{-/-}$ mice, which also show a high disorganization of outer segments.[115] To better understand the defects leading to dysmorphic outer segments in these models, a more detailed study by electron microscopy in early stages before the first discs are formed (between P4 and P15 in mice, and between 2 dpf and 5 dpf in zebrafish) would be of interest to analyze whether any discs form prior to the onset of degeneration and cell death. Additionally, superresolution microscopy of living rods stained with lipophilic dyes or fluorescent antibodies against PCARE in wild-type animals could give further insights of the evagination model of disc formation.

Defects in photoreceptor formation due to *PCARE* mutations can be also assessed in cultured cells. Downregulation of expression of genes coding for actin cytoskeletal proteins in iPSCs derived from a patient with a protein-truncating *PCARE* mutation (**chapter 5**) already hints to a defect in the actin cytoskeleton pathway, although further studies are needed to have a better understanding of this process. In our study, validation of the expression of neural and photoreceptor markers by qRT-PCR showed an increase in the expression of these markers in the differentiated cells compared to the original iPS cells, suggesting that some cells were able to differentiate towards a retinal fate. However, the transcriptome analysis revealed an under-representation of photoreceptor cell population, as shown by the low number of transcripts obtained from photoreceptor-specific genes like *RHO* or *PCARE*. Lessons from this and previously published protocols will help us to achieve a more successful differentiation in the future. Some elements that may aid to this end are the selection of differentiation factors that allow better specification into retinal cells, the prolongation of the culturing time until the obtention of mature photoreceptors, or the use of non-integrative vectors to avoid genomic alteration in the iPSCs. Additionally, comparison of CRISPR/Cas9 engineered wild-type and mutant isogenic lines would help to reduce variability present between different individuals. Use of desired CRISPR/Cas9 technology would facilitate the insertion of the *PCARE* mutation in a population of wild-type cells, leaving the non-targeted population as isogenic control.

The generation of the iPSCs technology by the group of Yamanaka in 2006[116] marked a breakthrough that allowed the expansion of cells from donor individuals *in vitro* and the possibility to differentiate them into any cell type. The retinal organoid model has the advantage to better replicate the retinal

developmental environment *in vivo* than 2D culture techniques.[117,118] Organoid culturing also allows for drug screening and, combined with gene editing, also disease modeling and repair. However, the retinal organoid model has certain drawbacks, such as the high heterogeneity between different pluripotent stem cell lines.[119,120] Also, the generation of invaginated optic cups as described by the group of Sasai[119] has been rarely observed,[121-123] and the laborious manual separation of optic cups from 3D aggregates is an additional challenge for this method. To overcome this, some groups are starting to use cyst cultures that can acquire neuroepithelial identity after five days.[124] Still, the long culturing times and the lack of techniques to isolate different retinal sub-types limits the immediate translation of retinal organoids into the clinic, though once these challenges are overcomed, stem-cell-derived organoid technology may hold great promise for future treatment of retinal diseases.[125]

7.6 Potential therapies for the treatment of *PCARE*-associated retinal disease

Actin polymerization inhibitors are known drugs used in therapeutics for the treatment of diseases such as cancer.[126,127] Inhibition of myosin II is used for the treatment of methamphetamine use.[128] However, in the case of *PCARE*-associated retinal disease, actin is already defective in the cell and these therapies would not be of use, since the aim is not to inhibit the actin cytoskeleton but to restore its function. The structure and function of the actin cytoskeleton is regulated by actin associated proteins, thus, restoration of the pathway working upstream PCARE and/or enhancement of actin polymerization at the base of photoreceptor OS could be one of the therapeutic targets.

Gene augmentation therapy can be a safe option to treat *PCARE*-associated retinal disease, as many gene augmentation therapy studies show, both in animal models and human clinical trials.[129-132] In addition, the US Food and Drug Administration (FDA) recently approved the first gene therapy for a retinal disease caused by mutations in *RPE65*, under the name Luxturna™. Together, these examples demonstrate the potential of gene augmentation therapy to treat some specific subtypes of IRD. Therefore, as described in **chapter 6,** we generated an AAV vector containing full length *PCARE* cDNA that can later on be used for therapeutic purposes. Many different aspects still need to be tested in order to assess whether this vector is valid for therapeutic intervention. For example, while we observe that the pAAV-PCARE plasmid is able to transfect RPE cells, AAV-PCARE did not produce detectable PCARE protein expression by immunofluorescence in hTERT RPE-1 cells. It is important to note that the expression of an AAV can vary *in vitro* and *in vivo*, and per cell type.[133] Depending on the AAV serotype, the efficiency to transduce cultured stem cell-derived mouse and human retinal cells varies.[134] These findings highlight the importance of selecting the appropriate AAV serotype for efficient cell transduction for *in vitro* studies. In addition, the developmental stage of the organoid may also affect the transduction efficiency and transcript expression levels. Therefore, the AAV-

PCARE should be first tested in mammalian retinas to evaluate whether PCARE is properly produced in photoreceptor cells. If AAV-PCARE does not yield good *PCARE* expression because of size constrains, an alternative to tackle this problem is to test a reduced transgene. Given that the PCARE C-terminal part is not crucial for proper PCARE function (based on our functional studies), exon 2 of *PCARE* could be removed (aa 1223-1288) to be able to accommodate PCARE into an AAV. An alternative is to use other types of viral vectors like lentivirus,[135] helper-dependent adenoviral vectors[136] or non-viral vectors like nanoparticles that allow for expression of transgenes of bigger size (as reviewed in **chapter 1**).[137,138] Dual AAVs are an attractive option for gene therapy of retinal diseases, thanks to the ability of the AAVs to concatemerize, and large retinal genes have been effectively delivered to mouse and pig photoreceptors using this method.[139,140] Additionally, nanoparticles can deliver genes into retinal cells and have been shown to partially rescue retinitis pigmentosa in *rds* (retinal degeneration slow) mice.[141]

An unpredictable variable of delivery of vectors to the subretinal space is the surgical procedure. To minimize trauma, nanoengineering of AAV capsids may facilitate gene therapy to target photoreceptors by using an intravitreal delivery instead of subretinal delivery, which has already been tested in dogs with some success.[142]

The zebrafish is a good animal model to understand the disease, but the efficiency of AAV transduction in zebrafish is not extensively reported.[143] Therefore, mutant *Pcare*$^{-/-}$ mice would be the first option to test the therapeutic vector. Alternatively, naturally occurring *Pcare* mutations in the dog are known,[144] making it an additional excellent model to test therapeutic vectors.

When the disease is diagnosed at a late stage, vision is generally absent due to loss of photoreceptor cells. In these cases, retinal prostheses, stem cell transplants and optogenetic therapies are plausible alternatives (as summarized in **chapter 1**). Stem cells can be obtained from different sources such as bone marrow,[145] or ESCs. To avoid allogenic transplantation, fibroblasts can be obtained through a skin biopsy of the patient, reprogrammed into iPSCs, corrected via genome editing engineering, and transplanted into the retina of the same patient.

In this thesis, we aimed to shed light on the molecular role of *PCARE* in health as well as in retinal disease. We have found that PCARE is an actin-associated protein that interacts with the actin nucleator WASF3 to promote the evagination of the ciliary plasma membrane. We thereby uncovered new molecular players in the long-known process of actin-driven outer segments discs neogenesis in the photoreceptor connecting cilium. The deficiency in expression of extracellular matrix genes in *PCARE*-deficient patient-derived iPSCs suggests a defect in actin-related pathways, supporting this hypothesis. We have also generated a *pcare1* mutant zebrafish that recapitulates the retinal phenotype observed in human and mice, and can serve as an excellent model to further investigate the function of *pcare* in a non-mammalian system. Finally, we have begun a route for gene augmentation therapy for *PCARE*-associated retinal disease with the generation of an AAV vector containing full length wild-type *PCARE* cDNA. Future research will elucidate the exact mechanisms and molecules responsible for the dynamic and interesting process that is actin-driven photoreceptor outer segment formation.

7.7 Concluding remarks

Major progress has been made in the last half century to understand photoreceptor cell biology and mechanisms that lead to disease, but many questions still remain unanswered. In this thesis, we have contributed to the broad field of the retinal ciliopathies by studying the function of the photoreceptor-specific protein PCARE. Learning about this protein has showed us that there is still a lot to uncover in this field, specifically from the molecular composition and regulation of outer segment morphogenesis and homeostasis at the photoreceptor ciliary membrane. Further studies of the function of PCARE and other microtubule and actin-associated ciliary proteins that play a role in this process may lead to a better understanding of retinal diseases associated with photoreceptor degeneration and fuel the development of novel therapies. In the future, retinal gene therapy will most likely be adapted to each patient to optimally target the specific genetic defect. Monogenic defects will benefit from therapies aiming at correcting or ablating the defective gene. Yet, the low frequency of these diseases poses challenges to generate cost-effective therapies. These challenges will lead towards the need of generation of therapies that target a broader range of genetic defects.

7.8 References

1. Darwin, C. (1859). On the origin of species by means of natural selection.(London,: J. Murray).
2. Arendt, D. (2003). Evolution of eyes and photoreceptor cell types. Int J Dev Biol 47, 563-571.
3. Eakin, R.M. (1965). Evolution of photoreceptors. Cold Spring Harb Symp Quant Biol 30, 363-370.
4. Fain, G.L., Hardie, R., and Laughlin, S.B. (2010). Phototransduction and the evolution of photoreceptors. Curr Biol 20, R114-124.
5. Young, R.W. (1967). The renewal of photoreceptor cell outer segments. J Cell Biol 33, 61-72.
6. Steinberg, R.H., Fisher, S.K., and Anderson, D.H. (1980). Disc morphogenesis in vertebrate photoreceptors. J Comp Neurol 190, 501-508.
7. Chuang, J.Z., Zhao, Y., and Sung, C.H. (2007). SARA-regulated vesicular targeting underlies formation of the light-sensing organelle in mammalian rods. Cell 130, 535-547.
8. Chuang, J.Z., Hsu, Y.C., and Sung, C.H. (2015). Ultrastructural visualization of trans-ciliary rhodopsin cargoes in mammalian rods. Cilia 4, 4.
9. Obata, S., and Usukura, J. (1992). Morphogenesis of the photoreceptor outer segment during postnatal development in the mouse (BALB/c) retina. Cell Tissue Res 269, 39-48.
10. Ding, J.D., Salinas, R.Y., and Arshavsky, V.Y. (2015). Discs of mammalian rod photoreceptors form through the membrane evagination mechanism. J Cell Biol 211, 495-502.
11. Burgoyne, T., Meschede, I.P., Burden, J.J., Bailly, M., Seabra, M.C., and Futter, C.E. (2015). Rod disc renewal occurs by evagination of the ciliary plasma membrane that makes cadherin-based contacts with the inner segment. Proc Natl Acad Sci U S A 112, 15922-15927.
12. Insinna, C., and Besharse, J.C. (2008). Intraflagellar transport and the sensory outer segment of vertebrate photoreceptors. Dev Dyn 237, 1982-1992.
13. Lee, E.S., Burnside, B., and Flannery, J.G. (2006). Characterization of peripherin/rds and rom-1 transport in rod photoreceptors of transgenic and knockout animals. Invest Ophthalmol Vis Sci 47, 2150-2160.
14. Volland, S., Hughes, L.C., Kong, C., Burgess, B.L., Linberg, K.A., Luna, G., Zhou, Z.H., Fisher, S.K., and Williams, D.S. (2015). Three-dimensional organization of nascent rod outer segment disk membranes. Proc Natl Acad Sci U S A 112, 14870-14875.
15. Chaitin, M.H., Schneider, B.G., Hall, M.O., and Papermaster, D.S. (1984). Actin in the photoreceptor connecting cilium: immunocytochemical localization to the site of outer segment disk formation. J Cell Biol 99, 239-247.
16. Chaitin, M.H., and Burnside, B. (1989). Actin filament polarity at the site of rod outer segment disk morphogenesis. Invest Ophthalmol Vis Sci 30, 2461-2469.
17. Chaitin, M.H. (1989). Immunogold localization of actin and opsin in rds mouse photoreceptors. Prog Clin Biol Res 314, 265-274.
18. Tubridy, N., Fontaine, B., and Eymard, B. (2001). Congenital myopathies and congenital muscular dystrophies. Curr Opin Neurol 14, 575-582.
19. Arikawa, K., and Williams, D.S. (1989). Organization of actin filaments and immunocolocalization of alpha-actinin in the connecting cilium of rat photoreceptors. J Comp Neurol 288, 640-646.
20. Saishin, Y., Ishikawa, R., Ugawa, S., Guo, W., Ueda, T., Morimura, H., Kohama, K., Shimizu, H., Tano, Y., and Shimada, S. (2000). Retinal fascin: functional nature, subcellular distribution, and chromosomal localization. Invest Ophthalmol Vis Sci 41, 2087-2095.
21. Xi, Q., Pauer, G.J., Marmorstein, A.D., Crabb, J.W., and Hagstrom, S.A. (2005). Tubby-like protein 1 (TULP1) interacts with F-actin in photoreceptor cells. Invest Ophthalmol Vis Sci 46, 4754-4761.
22. Williams, D.S., Linberg, K.A., Vaughan, D.K., Fariss, R.N., and Fisher, S.K. (1988). Disruption of microfilament organization and deregulation of disk membrane morphogenesis by cytochalasin D in rod and cone photoreceptors. J Comp Neurol 272, 161-176.
23. Nozumi, M., Nakagawa, H., Miki, H., Takenawa, T., and Miyamoto, S. (2003). Differential localization of WAVE isoforms in filopodia and lamellipodia of the neuronal growth cone. J Cell Sci 116, 239-246.
24. Atilgan, E., Wirtz, D., and Sun, S.X. (2005). Morphology of the lamellipodium and organization of actin filaments at the leading edge of crawling cells. Biophys J 89, 3589-3602.
25. Nager, A.R., Goldstein, J.S., Herranz-Perez, V., Portran, D., Ye, F., Garcia-Verdugo, J.M., and Nachury, M.V. (2017). An Actin Network Dispatches Ciliary GPCRs into Extracellular Vesicles to Modulate Signaling. Cell 168, 252-263 e214.
26. Arikawa, K., Molday, L.L., Molday, R.S., and Williams, D.S. (1992). Localization of peripherin/rds in the disk membranes of cone and rod photoreceptors: relationship to disk membrane morphogenesis and retinal degeneration. J Cell Biol 116, 659-667.

27. Salinas, R.Y., Pearring, J.N., Ding, J.D., Spencer, W.J., Hao, Y., and Arshavsky, V.Y. (2017). Photoreceptor discs form through peripherin-dependent suppression of ciliary ectosome release. J Cell Biol 216, 1489-1499.
28. Megaw, R., Abu-Arafeh, H., Jungnickel, M., Mellough, C., Gurniak, C., Witke, W., Zhang, W., Khanna, H., Mill, P., Dhillon, B., et al. (2017). Gelsolin dysfunction causes photoreceptor loss in induced pluripotent cell and animal retinitis pigmentosa models. Nat Commun 8, 271.
29. Clarke, G., Goldberg, A.F., Vidgen, D., Collins, L., Ploder, L., Schwarz, L., Molday, L.L., Rossant, J., Szel, A., Molday, R.S., et al. (2000). Rom-1 is required for rod photoreceptor viability and the regulation of disk morphogenesis. Nat Genet 25, 67-73.
30. Moritz, O.L., and Molday, R.S. (1996). Molecular cloning, membrane topology, and localization of bovine rom-1 in rod and cone photoreceptor cells. Invest Ophthalmol Vis Sci 37, 352-362.
31. Huttner, W.B., and Zimmerberg, J. (2001). Implications of lipid microdomains for membrane curvature, budding and fission. Curr Opin Cell Biol 13, 478-484.
32. Iglic, A., Hagerstrand, H., Veranic, P., Plemenitas, A., and Kralj-Iglic, V. (2006). Curvature-induced accumulation of anisotropic membrane components and raft formation in cylindrical membrane protrusions. J Theor Biol 240, 368-373.
33. Yang, Z., Chen, Y., Lillo, C., Chien, J., Yu, Z., Michaelides, M., Klein, M., Howes, K.A., Li, Y., Kaminoh, Y., et al. (2008). Mutant prominin 1 found in patients with macular degeneration disrupts photoreceptor disk morphogenesis in mice. J Clin Invest 118, 2908-2916.
34. Zacchigna, S., Oh, H., Wilsch-Brauninger, M., Missol-Kolka, E., Jaszai, J., Jansen, S., Tanimoto, N., Tonagel, F., Seeliger, M., Huttner, W.B., et al. (2009). Loss of the cholesterol-binding protein prominin-1/CD133 causes disk dysmorphogenesis and photoreceptor degeneration. J Neurosci 29, 2297-2308.
35. Han, Z., Anderson, D.W., and Papermaster, D.S. (2012). Prominin-1 localizes to the open rims of outer segment lamellae in Xenopus laevis rod and cone photoreceptors. Invest Ophthalmol Vis Sci 53, 361-373.
36. Dubreuil, V., Marzesco, A.M., Corbeil, D., Huttner, W.B., and Wilsch-Brauninger, M. (2007). Midbody and primary cilium of neural progenitors release extracellular membrane particles enriched in the stem cell marker prominin-1. J Cell Biol 176, 483-495.
37. Field, C.M., and Alberts, B.M. (1995). Anillin, a contractile ring protein that cycles from the nucleus to the cell cortex. J Cell Biol 131, 165-178.
38. Rattner, A., Smallwood, P.M., Williams, J., Cooke, C., Savchenko, A., Lyubarsky, A., Pugh, E.N., and Nathans, J. (2001). A photoreceptor-specific cadherin is essential for the structural integrity of the outer segment and for photoreceptor survival. Neuron 32, 775-786.
39. Humphries, M.M., Rancourt, D., Farrar, G.J., Kenna, P., Hazel, M., Bush, R.A., Sieving, P.A., Sheils, D.M., McNally, N., Creighton, P., et al. (1997). Retinopathy induced in mice by targeted disruption of the rhodopsin gene. Nat Genet 15, 216-219.
40. Lem, J., Krasnoperova, N.V., Calvert, P.D., Kosaras, B., Cameron, D.A., Nicolo, M., Makino, C.L., and Sidman, R.L. (1999). Morphological, physiological, and biochemical changes in rhodopsin knockout mice. Proc Natl Acad Sci U S A 96, 736-741.
41. Lee, E.S., and Flannery, J.G. (2007). Transport of truncated rhodopsin and its effects on rod function and degeneration. Invest Ophthalmol Vis Sci 48, 2868-2876.
42. Illing, M., Molday, L.L., and Molday, R.S. (1997). The 220-kDa rim protein of retinal rod outer segments is a member of the ABC transporter superfamily. J Biol Chem 272, 10303-10310.
43. Baehr, W., Karan, S., Maeda, T., Luo, D.G., Li, S., Bronson, J.D., Watt, C.B., Yau, K.W., Frederick, J.M., and Palczewski, K. (2007). The function of guanylate cyclase 1 and guanylate cyclase 2 in rod and cone photoreceptors. J Biol Chem 282, 8837-8847.
44. Weng, J., Mata, N.L., Azarian, S.M., Tzekov, R.T., Birch, D.G., and Travis, G.H. (1999). Insights into the function of Rim protein in photoreceptors and etiology of Stargardt's disease from the phenotype in abcr knockout mice. Cell 98, 13-23.
45. Molla-Herman, A., Ghossoub, R., Blisnick, T., Meunier, A., Serres, C., Silbermann, F., Emmerson, C., Romeo, K., Bourdoncle, P., Schmitt, A., et al. (2010). The ciliary pocket: an endocytic membrane domain at the base of primary and motile cilia. J Cell Sci 123, 1785-1795.
46. Phua, S.C., Chiba, S., Suzuki, M., Su, E., Roberson, E.C., Pusapati, G.V., Setou, M., Rohatgi, R., Reiter, J.F., Ikegami, K., et al. (2017). Dynamic Remodeling of Membrane Composition Drives Cell Cycle through Primary Cilia Excision. Cell 168, 264-279 e215.

47. Skiba, N.P., Spencer, W.J., Salinas, R.Y., Lieu, E.C., Thompson, J.W., and Arshavsky, V.Y. (2013). Proteomic identification of unique photoreceptor disc components reveals the presence of PRCD, a protein linked to retinal degeneration. J Proteome Res 12, 3010-3018.
48. Funabashi, T., Katoh, Y., Michisaka, S., Terada, M., Sugawa, M., and Nakayama, K. (2017). Ciliary entry of KIF17 is dependent on its binding to the IFT-B complex via IFT46-IFT56 as well as on its nuclear localization signal. Mol Biol Cell 28, 624-633.
49. Liu, Q., Tan, G., Levenkova, N., Li, T., Pugh, E.N., Jr., Rux, J.J., Speicher, D.W., and Pierce, E.A. (2007). The proteome of the mouse photoreceptor sensory cilium complex. Mol Cell Proteomics 6, 1299-1317.
50. Kwok, M.C., Holopainen, J.M., Molday, L.L., Foster, L.J., and Molday, R.S. (2008). Proteomics of photoreceptor outer segments identifies a subset of SNARE and Rab proteins implicated in membrane vesicle trafficking and fusion. Mol Cell Proteomics 7, 1053-1066.
51. Dominguez, R. (2016). The WH2 Domain and Actin Nucleation: Necessary but Insufficient. Trends Biochem Sci 41, 478-490.
52. Marchand, J.B., Kaiser, D.A., Pollard, T.D., and Higgs, H.N. (2001). Interaction of WASP/Scar proteins with actin and vertebrate Arp2/3 complex. Nat Cell Biol 3, 76-82.
53. Bieling, P., Hansen, S.D., Akin, O., Li, T.D., Hayden, C.C., Fletcher, D.A., and Mullins, R.D. (2018). WH2 and proline-rich domains of WASP-family proteins collaborate to accelerate actin filament elongation. EMBO J 37, 102-121.
54. Panchal, S.C., Kaiser, D.A., Torres, E., Pollard, T.D., and Rosen, M.K. (2003). A conserved amphipathic helix in WASP/Scar proteins is essential for activation of Arp2/3 complex. Nat Struct Biol 10, 591-598.
55. Itoh, T., and Takenawa, T. (2009). Mechanisms of membrane deformation by lipid-binding domains. Prog Lipid Res 48, 298-305.
56. Miki, H., Yamaguchi, H., Suetsugu, S., and Takenawa, T. (2000). IRSp53 is an essential intermediate between Rac and WAVE in the regulation of membrane ruffling. Nature 408, 732-735.
57. Sossey-Alaoui, K., Downs-Kelly, E., Das, M., Izem, L., Tubbs, R., and Plow, E.F. (2011). WAVE3, an actin remodeling protein, is regulated by the metastasis suppressor microRNA, miR-31, during the invasion-metastasis cascade. Int J Cancer 129, 1331-1343.
58. Teng, Y., Pi, W., Wang, Y., and Cowell, J.K. (2016). WASF3 provides the conduit to facilitate invasion and metastasis in breast cancer cells through HER2/HER3 signaling. Oncogene 35, 4633-4640.
59. Chen, B., Chou, H.T., Brautigam, C.A., Xing, W., Yang, S., Henry, L., Doolittle, L.K., Walz, T., and Rosen, M.K. (2017). Rac1 GTPase activates the WAVE regulatory complex through two distinct binding sites. Elife 6.
60. den Hollander, A.I., Koenekoop, R.K., Yzer, S., Lopez, I., Arends, M.L., Voesenek, K.E., Zonneveld, M.N., Strom, T.M., Meitinger, T., Brunner, H.G., et al. (2006). Mutations in the CEP290 (NPHP6) gene are a frequent cause of Leber congenital amaurosis. Am J Hum Genet 79, 556-561.
61. Helou, J., Otto, E.A., Attanasio, M., Allen, S.J., Parisi, M.A., Glass, I., Utsch, B., Hashmi, S., Fazzi, E., Omran, H., et al. (2007). Mutation analysis of NPHP6/CEP290 in patients with Joubert syndrome and Senior-Loken syndrome. J Med Genet 44, 657-663.
62. Frank, V., den Hollander, A.I., Bruchle, N.O., Zonneveld, M.N., Nurnberg, G., Becker, C., Du, B.G., Kendziorra, H., Roosing, S., Senderek, J., et al. (2008). Mutations of the CEP290 gene encoding a centrosomal protein cause Meckel-Gruber syndrome. Hum Mutat 29, 45-52.
63. Valente, E.M., Silhavy, J.L., Brancati, F., Barrano, G., Krishnaswami, S.R., Castori, M., Lancaster, M.A., Boltshauser, E., Boccone, L., Al-Gazali, L., et al. (2006). Mutations in CEP290, which encodes a centrosomal protein, cause pleiotropic forms of Joubert syndrome. Nat Genet 38, 623-625.
64. Coene, K.L., Roepman, R., Doherty, D., Afroze, B., Kroes, H.Y., Letteboer, S.J., Ngu, L.H., Budny, B., van Wijk, E., Gorden, N.T., et al. (2009). OFD1 is mutated in X-linked Joubert syndrome and interacts with LCA5-encoded lebercilin. Am J Hum Genet 85, 465-481.
65. Betleja, E., and Cole, D.G. (2010). Ciliary trafficking: CEP290 guards a gated community. Curr Biol 20, R928-931.
66. Kim, J., Krishnaswami, S.R., and Gleeson, J.G. (2008). CEP290 interacts with the centriolar satellite component PCM-1 and is required for Rab8 localization to the primary cilium. Hum Mol Genet 17, 3796-3805.
67. Hattula, K., Furuhjelm, J., Tikkanen, J., Tanhuanpaa, K., Laakkonen, P., and Peranen, J. (2006). Characterization of the Rab8-specific membrane traffic route linked to protrusion formation. J Cell Sci 119, 4866-4877.
68. Deretic, D., Huber, L.A., Ransom, N., Mancini, M., Simons, K., and Papermaster, D.S. (1995). rab8 in retinal photoreceptors may participate in rhodopsin transport and in rod outer segment disk morphogenesis. J Cell Sci 108 (Pt 1), 215-224.

69. Moritz, O.L., Tam, B.M., Hurd, L.L., Peranen, J., Deretic, D., and Papermaster, D.S. (2001). Mutant rab8 Impairs docking and fusion of rhodopsin-bearing post-Golgi membranes and causes cell death of transgenic Xenopus rods. Mol Biol Cell 12, 2341-2351.
70. Tsang, W.Y., Bossard, C., Khanna, H., Peranen, J., Swaroop, A., Malhotra, V., and Dynlacht, B.D. (2008). CP110 suppresses primary cilia formation through its interaction with CEP290, a protein deficient in human ciliary disease. Dev Cell 15, 187-197.
71. Chang, B., Khanna, H., Hawes, N., Jimeno, D., He, S., Lillo, C., Parapuram, S.K., Cheng, H., Scott, A., Hurd, R.E., et al. (2006). In-frame deletion in a novel centrosomal/ciliary protein CEP290/NPHP6 perturbs its interaction with RPGR and results in early-onset retinal degeneration in the rd16 mouse. Hum Mol Genet 15, 1847-1857.
72. Tiwari, S., Hudson, S., Gattone, V.H., 2nd, Miller, C., Chernoff, E.A., and Belecky-Adams, T.L. (2013). Meckelin 3 is necessary for photoreceptor outer segment development in rat Meckel syndrome. PLoS One 8, e59306.
73. Baala, L., Romano, S., Khaddour, R., Saunier, S., Smith, U.M., Audollent, S., Ozilou, C., Faivre, L., Laurent, N., Foliguet, B., et al. (2007). The Meckel-Gruber syndrome gene, MKS3, is mutated in Joubert syndrome. Am J Hum Genet 80, 186-194.
74. Smith, U.M., Consugar, M., Tee, L.J., McKee, B.M., Maina, E.N., Whelan, S., Morgan, N.V., Goranson, E., Gissen, P., Lilliquist, S., et al. (2006). The transmembrane protein meckelin (MKS3) is mutated in Meckel-Gruber syndrome and the wpk rat. Nat Genet 38, 191-196.
75. Gorden, N.T., Arts, H.H., Parisi, M.A., Coene, K.L., Letteboer, S.J., van Beersum, S.E., Mans, D.A., Hikida, A., Eckert, M., Knutzen, D., et al. (2008). CC2D2A is mutated in Joubert syndrome and interacts with the ciliopathy-associated basal body protein CEP290. Am J Hum Genet 83, 559-571.
76. Leitch, C.C., Zaghloul, N.A., Davis, E.E., Stoetzel, C., Diaz-Font, A., Rix, S., Alfadhel, M., Lewis, R.A., Eyaid, W., Banin, E., et al. (2008). Hypomorphic mutations in syndromic encephalocele genes are associated with Bardet-Biedl syndrome. Nat Genet 40, 443-448.
77. Bachmann-Gagescu, R., Dona, M., Hetterschijt, L., Tonnaer, E., Peters, T., de Vrieze, E., Mans, D.A., van Beersum, S.E., Phelps, I.G., Arts, H.H., et al. (2015). The Ciliopathy Protein CC2D2A Associates with NINL and Functions in RAB8-MICAL3-Regulated Vesicle Trafficking. PLoS Genet 11, e1005575.
78. Boldt, K., Mans, D.A., Won, J., van Reeuwijk, J., Vogt, A., Kinkl, N., Letteboer, S.J., Hicks, W.L., Hurd, R.E., Naggert, J.K., et al. (2011). Disruption of intraflagellar protein transport in photoreceptor cilia causes Leber congenital amaurosis in humans and mice. J Clin Invest 121, 2169-2180.
79. Rao, K.N., Li, L., Anand, M., and Khanna, H. (2015). Ablation of retinal ciliopathy protein RPGR results in altered photoreceptor ciliary composition. Sci Rep 5, 11137.
80. Wang, J., Chen, X., Wang, F., Zhang, J., Li, P., Li, Z., Xu, J., Gao, F., Jin, C., Tian, H., et al. (2016). OFD1, as a Ciliary Protein, Exhibits Neuroprotective Function in Photoreceptor Degeneration Models. PLoS One 11, e0155860.
81. Delous, M., Baala, L., Salomon, R., Laclef, C., Vierkotten, J., Tory, K., Golzio, C., Lacoste, T., Besse, L., Ozilou, C., et al. (2007). The ciliary gene RPGRIP1L is mutated in cerebello-oculo-renal syndrome (Joubert syndrome type B) and Meckel syndrome. Nat Genet 39, 875-881.
82. Vierkotten, J., Dildrop, R., Peters, T., Wang, B., and Ruther, U. (2007). Ftm is a novel basal body protein of cilia involved in Shh signalling. Development 134, 2569-2577.
83. Yildiz, O., and Khanna, H. (2012). Ciliary signaling cascades in photoreceptors. Vision Res 75, 112-116.
84. May-Simera, H.L., Gumerson, J.D., Gao, C., Campos, M., Cologna, S.M., Beyer, T., Boldt, K., Kaya, K.D., Patel, N., Kretschmer, F., et al. (2016). Loss of MACF1 Abolishes Ciliogenesis and Disrupts Apicobasal Polarity Establishment in the Retina. Cell Rep 17, 1399-1413.
85. Eblimit, A., Nguyen, T.M., Chen, Y., Esteve-Rudd, J., Zhong, H., Letteboer, S., Van Reeuwijk, J., Simons, D.L., Ding, Q., Wu, K.M., et al. (2015). Spata7 is a retinal ciliopathy gene critical for correct RPGRIP1 localization and protein trafficking in the retina. Hum Mol Genet 24, 1584-1601.
86. Zhao, Y., Hong, D.H., Pawlyk, B., Yue, G., Adamian, M., Grynberg, M., Godzik, A., and Li, T. (2003). The retinitis pigmentosa GTPase regulator (RPGR)- interacting protein: subserving RPGR function and participating in disk morphogenesis. Proc Natl Acad Sci U S A 100, 3965-3970.
87. Roepman, R., Bernoud-Hubac, N., Schick, D.E., Maugeri, A., Berger, W., Ropers, H.H., Cremers, F.P., and Ferreira, P.A. (2000). The retinitis pigmentosa GTPase regulator (RPGR) interacts with novel transport-like proteins in the outer segments of rod photoreceptors. Hum Mol Genet 9, 2095-2105.
88. Boylan, J.P., and Wright, A.F. (2000). Identification of a novel protein interacting with RPGR. Hum Mol Genet 9, 2085-2093.

89. Patil, H., Tserentsoodol, N., Saha, A., Hao, Y., Webb, M., and Ferreira, P.A. (2012). Selective loss of RPGRIP1-dependent ciliary targeting of NPHP4, RPGR and SDCCAG8 underlies the degeneration of photoreceptor neurons. Cell Death Dis 3, e355.
90. Eckmiller, M.S. (2000). Microtubules in a rod-specific cytoskeleton associated with outer segment incisures. Vis Neurosci 17, 711-722.
91. Liu, Q., Zhou, J., Daiger, S.P., Farber, D.B., Heckenlively, J.R., Smith, J.E., Sullivan, L.S., Zuo, J., Milam, A.H., and Pierce, E.A. (2002). Identification and subcellular localization of the RP1 protein in human and mouse photoreceptors. Invest Ophthalmol Vis Sci 43, 22-32.
92. Bowne, S.J., Daiger, S.P., Hims, M.M., Sohocki, M.M., Malone, K.A., McKie, A.B., Heckenlively, J.R., Birch, D.G., Inglehearn, C.F., Bhattacharya, S.S., et al. (1999). Mutations in the RP1 gene causing autosomal dominant retinitis pigmentosa. Hum Mol Genet 8, 2121-2128.
93. Liu, Y.P., Bosch, D.G., Siemiatkowska, A.M., Rendtorff, N.D., Boonstra, F.N., Moller, C., Tranebjaerg, L., Katsanis, N., and Cremers, F.P. (2017). Putative digenic inheritance of heterozygous RP1L1 and C2orf71 null mutations in syndromic retinal dystrophy. Ophthalmic Genet 38, 127-132.
94. Sukumaran, S., and Perkins, B.D. (2009). Early defects in photoreceptor outer segment morphogenesis in zebrafish ift57, ift88 and ift172 Intraflagellar Transport mutants. Vision Res 49, 479-489.
95. Kremer, H., van Wijk, E., Marker, T., Wolfrum, U., and Roepman, R. (2006). Usher syndrome: molecular links of pathogenesis, proteins and pathways. Hum Mol Genet 15 Spec No 2, R262-270.
96. Maerker, T., van Wijk, E., Overlack, N., Kersten, F.F., McGee, J., Goldmann, T., Sehn, E., Roepman, R., Walsh, E.J., Kremer, H., et al. (2008). A novel Usher protein network at the periciliary reloading point between molecular transport machineries in vertebrate photoreceptor cells. Hum Mol Genet 17, 71-86.
97. Wright, R.N., Hong, D.H., and Perkins, B. (2012). RpgrORF15 connects to the usher protein network through direct interactions with multiple whirlin isoforms. Invest Ophthalmol Vis Sci 53, 1519-1529.
98. Peters, K.R., Palade, G.E., Schneider, B.G., and Papermaster, D.S. (1983). Fine structure of a periciliary ridge complex of frog retinal rod cells revealed by ultrahigh resolution scanning electron microscopy. J Cell Biol 96, 265-276.
99. Yang, J., Liu, X., Zhao, Y., Adamian, M., Pawlyk, B., Sun, X., McMillan, D.R., Liberman, M.C., and Li, T. (2010). Ablation of whirlin long isoform disrupts the USH2 protein complex and causes vision and hearing loss. PLoS Genet 6, e1000955.
100. Cope, M.J., Whisstock, J., Rayment, I., and Kendrick-Jones, J. (1996). Conservation within the myosin motor domain: implications for structure and function. Structure 4, 969-987.
101. Weil, D., Blanchard, S., Kaplan, J., Guilford, P., Gibson, F., Walsh, J., Mburu, P., Varela, A., Levilliers, J., Weston, M.D., et al. (1995). Defective myosin VIIA gene responsible for Usher syndrome type 1B. Nature 374, 60-61.
102. Liu, X., Udovichenko, I.P., Brown, S.D., Steel, K.P., and Williams, D.S. (1999). Myosin VIIa participates in opsin transport through the photoreceptor cilium. J Neurosci 19, 6267-6274.
103. Liu, X., Vansant, G., Udovichenko, I.P., Wolfrum, U., and Williams, D.S. (1997). Myosin VIIa, the product of the Usher 1B syndrome gene, is concentrated in the connecting cilia of photoreceptor cells. Cell Motil Cytoskeleton 37, 240-252.
104. Bitner-Glindzicz, M., Lindley, K.J., Rutland, P., Blaydon, D., Smith, V.V., Milla, P.J., Hussain, K., Furth-Lavi, J., Cosgrove, K.E., Shepherd, R.M., et al. (2000). A recessive contiguous gene deletion causing infantile hyperinsulinism, enteropathy and deafness identifies the Usher type 1C gene. Nat Genet 26, 56-60.
105. Verpy, E., Leibovici, M., Zwaenepoel, I., Liu, X.Z., Gal, A., Salem, N., Mansour, A., Blanchard, S., Kobayashi, I., Keats, B.J., et al. (2000). A defect in harmonin, a PDZ domain-containing protein expressed in the inner ear sensory hair cells, underlies Usher syndrome type 1C. Nat Genet 26, 51-55.
106. Ahmed, Z.M., Riazuddin, S., Bernstein, S.L., Ahmed, Z., Khan, S., Griffith, A.J., Morell, R.J., Friedman, T.B., Riazuddin, S., and Wilcox, E.R. (2001). Mutations of the protocadherin gene PCDH15 cause Usher syndrome type 1F. Am J Hum Genet 69, 25-34.
107. Sahly, I., Dufour, E., Schietroma, C., Michel, V., Bahloul, A., Perfettini, I., Pepermans, E., Estivalet, A., Carette, D., Aghaie, A., et al. (2012). Localization of Usher 1 proteins to the photoreceptor calyceal processes, which are absent from mice. J Cell Biol 199, 381-399.
108. Takahashi, S., Mui, V.J., Rosenberg, S.K., Homma, K., Cheatham, M.A., and Zheng, J. (2016). Cadherin 23-C Regulates Microtubule Networks by Modifying CAMSAP3's Function. Sci Rep 6, 28706.
109. Schietroma, C., Parain, K., Estivalet, A., Aghaie, A., Boutet de Monvel, J., Picaud, S., Sahel, J.A., Perron, M., El-Amraoui, A., and Petit, C. (2017). Usher syndrome type 1-associated cadherins shape the photoreceptor outer segment. J Cell Biol 216, 1849-1864.

110. Grati, M., and Kachar, B. (2011). Myosin VIIa and sans localization at stereocilia upper tip-link density implicates these Usher syndrome proteins in mechanotransduction. Proc Natl Acad Sci U S A 108, 11476-11481.
111. Petit, C., Levilliers, J., and Hardelin, J.P. (2001). Molecular genetics of hearing loss. Annu Rev Genet 35, 589-646.
112. Frolenkov, G.I., Belyantseva, I.A., Friedman, T.B., and Griffith, A.J. (2004). Genetic insights into the morphogenesis of inner ear hair cells. Nat Rev Genet 5, 489-498.
113. Nam, J.H., Cotton, J.R., Peterson, E.H., and Grant, W. (2006). Mechanical properties and consequences of stereocilia and extracellular links in vestibular hair bundles. Biophys J 90, 2786-2795.
114. Tilney, L.G., Derosier, D.J., and Mulroy, M.J. (1980). The organization of actin filaments in the stereocilia of cochlear hair cells. J Cell Biol 86, 244-259.
115. Kevany, B.M., Zhang, N., Jastrzebska, B., and Palczewski, K. (2015). Animals deficient in C2Orf71, an autosomal recessive retinitis pigmentosa-associated locus, develop severe early-onset retinal degeneration. Hum Mol Genet 24, 2627-2640.
116. Takahashi, K., and Yamanaka, S. (2006). Induction of pluripotent stem cells from mouse embryonic and adult fibroblast cultures by defined factors. Cell 126, 663-676.
117. Lamba, D.A., Karl, M.O., Ware, C.B., and Reh, T.A. (2006). Efficient generation of retinal progenitor cells from human embryonic stem cells. Proc Natl Acad Sci U S A 103, 12769-12774.
118. Osakada, F., Ikeda, H., Mandai, M., Wataya, T., Watanabe, K., Yoshimura, N., Akaike, A., Sasai, Y., and Takahashi, M. (2008). Toward the generation of rod and cone photoreceptors from mouse, monkey and human embryonic stem cells. Nat Biotechnol 26, 215-224.
119. Eiraku, M., Takata, N., Ishibashi, H., Kawada, M., Sakakura, E., Okuda, S., Sekiguchi, K., Adachi, T., and Sasai, Y. (2011). Self-organizing optic-cup morphogenesis in three-dimensional culture. Nature 472, 51-56.
120. Hiler, D., Chen, X., Hazen, J., Kupriyanov, S., Carroll, P.A., Qu, C., Xu, B., Johnson, D., Griffiths, L., Frase, S., et al. (2015). Quantification of Retinogenesis in 3D Cultures Reveals Epigenetic Memory and Higher Efficiency in iPSCs Derived from Rod Photoreceptors. Cell Stem Cell 17, 101-115.
121. Gonzalez-Cordero, A., West, E.L., Pearson, R.A., Duran, Y., Carvalho, L.S., Chu, C.J., Naeem, A., Blackford, S.J.I., Georgiadis, A., Lakowski, J., et al. (2013). Photoreceptor precursors derived from three-dimensional embryonic stem cell cultures integrate and mature within adult degenerate retina. Nat Biotechnol 31, 741-747.
122. Decembrini, S., Koch, U., Radtke, F., Moulin, A., and Arsenijevic, Y. (2014). Derivation of traceable and transplantable photoreceptors from mouse embryonic stem cells. Stem Cell Reports 2, 853-865.
123. Santos-Ferreira, T., Völkner, M., Borsch, O., Haas, J., Cimalla, P., Vasudevan, P., Carmeliet, P., Corbeil, D., Michalakis, S., Koch, E., et al. (2016). Stem Cell–Derived Photoreceptor Transplants Differentially Integrate Into Mouse Models of Cone-Rod Dystrophy. Investigative Ophthalmology & Visual Science 57, 3509-3520.
124. Zhu, Y., Carido, M., Meinhardt, A., Kurth, T., Karl, M.O., Ader, M., and Tanaka, E.M. (2013). Three-dimensional neuroepithelial culture from human embryonic stem cells and its use for quantitative conversion to retinal pigment epithelium. PLoS One 8, e54552.
125. Llonch, S., Carido, M., and Ader, M. (2018). Organoid technology for retinal repair. Dev Biol 433, 132-143.
126. Yu, Q., Zhang, B., Li, J., and Li, M. (2017). The design of peptide-grafted graphene oxide targeting the actin cytoskeleton for efficient cancer therapy. Chem Commun (Camb) 53, 11433-11436.
127. Foerster, F., Braig, S., Moser, C., Kubisch, R., Busse, J., Wagner, E., Schmoeckel, E., Mayr, D., Schmitt, S., Huettel, S., et al. (2014). Targeting the actin cytoskeleton: selective antitumor action via trapping PKCvarepsilon. Cell Death Dis 5, e1398.
128. Young, E.J., Briggs, S.B., and Miller, C.A. (2015). The Actin Cytoskeleton as a Therapeutic Target for the Prevention of Relapse to Methamphetamine Use. CNS Neurol Disord Drug Targets 14, 731-737.
129. Acland, G.M., Aguirre, G.D., Ray, J., Zhang, Q., Aleman, T.S., Cideciyan, A.V., Pearce-Kelling, S.E., Anand, V., Zeng, Y., Maguire, A.M., et al. (2001). Gene therapy restores vision in a canine model of childhood blindness. Nat Genet 28, 92-95.
130. Bennett, J., Wellman, J., Marshall, K.A., McCague, S., Ashtari, M., DiStefano-Pappas, J., Elci, O.U., Chung, D.C., Sun, J., Wright, J.F., et al. (2016). Safety and durability of effect of contralateral-eye administration of AAV2 gene therapy in patients with childhood-onset blindness caused by RPE65 mutations: a follow-on phase 1 trial. Lancet 388, 661-672.

131. MacLaren, R.E., Groppe, M., Barnard, A.R., Cottriall, C.L., Tolmachova, T., Seymour, L., Clark, K.R., During, M.J., Cremers, F.P., Black, G.C., et al. (2014). Retinal gene therapy in patients with choroideremia: initial findings from a phase 1/2 clinical trial. Lancet 383, 1129-1137.
132. Pierce, E.A., and Bennett, J. (2015). The Status of RPE65 Gene Therapy Trials: Safety and Efficacy. Cold Spring Harb Perspect Med 5, a017285.
133. Pang, J.J., Lauramore, A., Deng, W.T., Li, Q., Doyle, T.J., Chiodo, V., Li, J., and Hauswirth, W.W. (2008). Comparative analysis of in vivo and in vitro AAV vector transduction in the neonatal mouse retina: effects of serotype and site of administration. Vision Res 48, 377-385.
134. Gonzalez-Cordero, A., Goh, D., Kruczek, K., Naeem, A., Fernando, M., Kleine Holthaus, S.M., Takaaki, M., Blackford, S.J.I., Kloc, M., Agundez, L., et al. (2018). Assessment of AAV Vector Tropisms for Mouse and Human Pluripotent Stem Cell-Derived RPE and Photoreceptor Cells. Hum Gene Ther.
135. Greenberg, K.P., Lee, E.S., Schaffer, D.V., and Flannery, J.G. (2006). Gene delivery to the retina using lentiviral vectors. Adv Exp Med Biol 572, 255-266.
136. Lam, S., Cao, H., Wu, J., Duan, R., and Hu, J. (2014). Highly efficient retinal gene delivery with helper-dependent adenoviral vectors. Genes Dis 1, 227-237.
137. Adijanto, J., and Naash, M.I. (2015). Nanoparticle-based technologies for retinal gene therapy. Eur J Pharm Biopharm 95, 353-367.
138. Al-Halafi, A.M. (2014). Nanocarriers of nanotechnology in retinal diseases. Saudi J Ophthalmol 28, 304-309.
139. Trapani, I., Colella, P., Sommella, A., Iodice, C., Cesi, G., de Simone, S., Marrocco, E., Rossi, S., Giunti, M., Palfi, A., et al. (2014). Effective delivery of large genes to the retina by dual AAV vectors. EMBO Mol Med 6, 194-211.
140. Trapani, I., Toriello, E., de Simone, S., Colella, P., Iodice, C., Polishchuk, E.V., Sommella, A., Colecchi, L., Rossi, S., Simonelli, F., et al. (2015). Improved dual AAV vectors with reduced expression of truncated proteins are safe and effective in the retina of a mouse model of Stargardt disease. Hum Mol Genet 24, 6811-6825.
141. Cai, X., Nash, Z., Conley, S.M., Fliesler, S.J., Cooper, M.J., and Naash, M.I. (2009). A partial structural and functional rescue of a retinitis pigmentosa model with compacted DNA nanoparticles. PLoS One 4, e5290.
142. Mowat, F.M., Gornik, K.R., Dinculescu, A., Boye, S.L., Hauswirth, W.W., Petersen-Jones, S.M., and Bartoe, J.T. (2014). Tyrosine capsid-mutant AAV vectors for gene delivery to the canine retina from a subretinal or intravitreal approach. Gene Ther 21, 96-105.
143. Kawasaki, T., Saito, K., Mitsui, K., Ikawa, M., Yamashita, M., Taniguchi, Y., Takeda, S., Mitani, K., and Sakai, N. (2009). Introduction of a foreign gene into zebrafish and medaka cells using adenoviral vectors. Zebrafish 6, 253-258.
144. Downs, L.M., Bell, J.S., Freeman, J., Hartley, C., Hayward, L.J., and Mellersh, C.S. (2013). Late-onset progressive retinal atrophy in the Gordon and Irish Setter breeds is associated with a frameshift mutation in C2orf71. Anim Genet 44, 169-177.
145. Park, S.S., Moisseiev, E., Bauer, G., Anderson, J.D., Grant, M.B., Zam, A., Zawadzki, R.J., Werner, J.S., and Nolta, J.A. (2017). Advances in bone marrow stem cell therapy for retinal dysfunction. Prog Retin Eye Res 56, 148-165.

Summary

The outer segment of retinal photoreceptor cells is a highly modified and specialized sensory cilium important for phototransduction, and thus for vision (**chapter 1.3**). Inherited retinal diseases (IRDs) in which photoreceptor cells degenerate due to a dysfunction of the photoreceptor cilium are named retinal ciliopathies. These diseases are phenotypically and genetically highly variable, challenging molecular genetic diagnostics for the patients (**chapter 1.4**). Mutations in the *C2ORF71* gene were identified in 2010 to be responsible for the condition Retinitis Pigmentosa (RP), a subtype of IRD characterized by progressive vision loss. *C2ORF71* was initially suggested to play a role in the photoreceptor cilium, as exogenous expression in cells revealed localization of C2ORF71 to the primary cilium. In the last eight years, various novel *C2ORF71* mutations have been found in patients with Retinitis Pigmentosa or cone-rod dystrophy, but there is a lack of studies that address the function of this gene and the protein it encodes. In this thesis, we aimed at gaining insights on the molecular role of C2ORF71 in photoreceptor homeostasis and retinal disease.

Chapter 2 focuses on the elucidation of the function of C2ORF71, which is now officially renamed to PCARE (photoreceptor cilium actin regulator) based on our results. Protein-protein interaction studies, employing a combination of yeast two-hybrid systems and tandem affinity purifications, revealed that PCARE interacts with modules of microtubule-, centrosome-, and actin-associated proteins. Localization studies in mouse retinae showed that PCARE co-localizes with an actin module at the base of the outer segments of photoreceptors, while in *Pcare*$^{-/-}$ mice, this actin module is mislocalized. Old, damaged outer segment discs are shed at the photoreceptor apex and phagocytized by the adjacent retinal pigment epithelium. Daily, the ciliary plasma membrane evaginates at the base of the outer segments to initiate renewal of the phototransductive discs. While actin has been proposed to play a role in this process, the exact molecular mechanism behind it remains unknown. We show that PCARE recruits one of their actin-associated interactors, the Wiskott-Aldrich syndrome family protein WASF3, from the perinuclear membrane to the primary cilium in hTERT RPE-1 cells. The presence of both PCARE and WASF3 in the primary cilium recruits actin polymerization components to the primary cilium, inducing the evagination of the ciliary plasma membrane. The RP-associated PCARE missense mutant p.Ile201Phe generates ciliary membrane evaginations less frequently, and these are smaller compared to wild-type PCARE. These data point to disturbance of actin-dynamics driven ciliary membrane evagination as the pathogenetic mechanism behind *PCARE*-associated retinal disease. In addition, these findings unveil novel potential molecules involved in the process of ciliary membrane evagination.

The clinical and genetic information of all reported patients with *PCARE*-associated retinal disease is presented in **chapter 3**. *PCARE*-associated retinal disease is very rare, with just over 40 patients reported. Some patients show symptoms at an early age, while others are reported late in adulthood, the median age at first visit to the clinic being 31.5 years. For the majority of patients, night blindness is reported. Retinal thinning and loss of retinal lamination is characteristic for all patients, while reduced or non-recordable full-field electroretinography is also common. Homozygous *PCARE* mutations are mostly truncating, with only two homozygous missense mutations reported. The majority of patients present truncating or missense mutations at the N-terminus of the PCARE protein. Analysis of the position of the mutation in the PCARE protein and age of onset revealed no clear correlation between the age of disease onset and the position of the *PCARE* mutation in patients with *PCARE*-associated retinal disease.

Chapter 4 reports the duplication of the gene *pcare* in zebrafish and the generation of a novel mutant *pcare1* zebrafish model using CRISPR/Cas9 technology, termed *pcare1*$^{rmc100/rmc100}$. In zebrafish, *pcare1*, the true orthologue of human *PCARE*, is located on chromosome 17 and codes for a protein of 1122 amino acids, while *pcare2* locates to chromosome 20 and encodes a protein of 859 amino acids. The specific generated mutation by CRISPR/Cas9 is a 29-basepair deletion in exon 1 of *pcare1* (c. 21_49del), predicted to result in the premature termination of translation after amino acid 16 of pcare1 (p.Gly8Glufs*9). *Pcare1* mutant zebrafish show defects in photoreceptor outer segments morphology, both in the embryonic (5 days post fertilization) and adult (6 months post fertilization) states. Analysis of visual function using optokinetic and visual motor response measurements indicate visual impairment of *pcare1*$^{rmc100/rmc100}$ mutant zebrafish. *Pcare1*$^{rmc100/rmc100}$ zebrafish show reduced ERG responses, indicating a defect in the transretinal current. Thus, *pcare1*$^{rmc100/rmc100}$ zebrafish are an additional animal model to study *PCARE*-associated retinal disease. Moreover, these findings further support the involvement of PCARE in forming and/or maintaining photoreceptor outer segments.

Fibroblast cells derived from a patient with a homozygous point mutation (c.947del; p.Asn316Metfs*7) in *PCARE* do not show ciliary defects, probably explained by the low *PCARE* expression in this cell type compared to the retina. This is also in line with the photoreceptor-specific function of PCARE. Therefore, to study *PCARE*-associated retinal disease *in vitro*, we took advantage of induced pluripotent stem cell (iPSC) technology in **chapter 5**. To model the disease *in vitro*, *PCARE*-deficient fibroblasts were reprogrammed into iPSCs and differentiated during 90 days into a neuroretinal fate. To study the transcriptome of these cells, RNA sequencing was performed. Transcriptome data analysis revealed downregulation of expression of genes coding for actin cytoskeletal proteins in *PCARE*-deficient iPSCs compared to wild-type cells. Additionally, while wild-

type cells differentiated into a neuronal cell fate, the patient-derived iPSCs differentiated into a plasma cell fate. The low number of reads of photoreceptor-specific genes detected indicates that the culture was not significantly enriched in photoreceptor cells in either wild-type or mutant cells. Therefore, an improved protocol that optimizes the enrichment of photoreceptor precursor cells will be necessary to specifically assess the potential morphological defects due to *PCARE* mutations.

Chapter 6 describes the generation of an adeno-associated virus (AAV) vector containing full-length *PCARE* cDNA, with the aim to use it for future therapeutic purposes. An AAV plasmid was adapted to the Gateway cloning system to facilitate the insertion of full length *PCARE* cDNA. Because AAV vectors are restrictive in size, the insertion cassette between the AAV plasmid´s ITRs was reduced from 5.6 kb to 4.8 kb, the limit of what an AAV can accommodate. Next, an AAV2/9 vector was generated containing the minimal elements to allow transgene expression: a photoreceptor-specific rhodopsin kinase promoter, an SV40 intron, *PCARE* cDNA, and a bovine Growth Hormone polyAdenylation signal (bGHpA). Analysis by RT-PCR and droplet digital PCR showed that the insertion cassette was properly packaged in the AAV vector. However, *PCARE* expression was not detected either by immunofluorescence or western blot after transduction of hTERT RPE-1 cells using different multiplicity of infections. These results suggested a problem of the AAV vector to drive transgene expression in hTERT RPE-1 cells. *In vivo* assessment of the efficacy of the AAV2/9.RK.PCARE.S vector in mice is needed to assess the validity of the vector to transduce photoreceptor cells.

The main topics of this thesis are discussed in **chapter 7**. An introductory discussion based on previous knowledge about the development of the ciliary photoreceptor cell outer segment, from the findings of Richard Young in 1967 that outer segments are constantly rebuilt, to recent reports that confirm that outer segments discs form through an evagination mechanism of the ciliary plasma membrane (**chapter 7.1**). Previous literature on the involvement of actin and actin-associated proteins in the process of outer segment disc formation is reviewed in **chapter 7.2**. The role of the PCARE protein and its association to the Arp2/3 complex activator WASF3 protein, as well as the formation of ciliary membrane evaginations are discussed in **chapter 7.3**. The role of retinal ciliopathy proteins in the actin-dependent formation of outer segment discs is examined in **chapter 7.4**. In **chapter 7.5**, we analyze *PCARE*-associated retinal disease and discuss the animal and cellular models currently available to further study the disease features. Finally, potential therapies to treat this disease such as AAV-based gene augmentation therapy are discussed in **chapter 7.6**.

Samenvatting

Het buitenste segment van de fotoreceptorcellen in het netvlies is een gemodificeerd en zeer gespecialiseerd sensorisch cilium dat belangrijk is voor de fototransductie, en dus ook voor het zien (**hoofdstuk 1.3**). Erfelijke netvliesaandoeningen (inherited retinal diseases; IRDs) waarin de fotoreceptorcellen afsterven vanwege een niet-functionerend cilium, worden ook wel retinale ciliopathieën genoemd. Deze ziekten zijn zowel klinisch als genetisch zeer variabel, waardoor moleculair genetische diagnostiek voor de patiënten niet eenvoudig is (**hoofdstuk 1.4**). Mutaties in het *C2ORF71*-gen werden in 2010 voor het eerst geïdentificeerd als zijnde verantwoordelijk voor de aandoening Retinitis Pigmentosa (RP), een IRD subtype dat gekenmerkt wordt door een progressief verlies van het gezichtsvermogen. Gezien de localisatie van exogeen tot expressie gebracht C2orf71 eiwit, werd verondersteld dat dit eiwit een rol speelt binnen het cilium in de fotoreceptorcellen. In de afgelopen acht jaar zijn er verschillende nieuwe *C2ORF71*-mutaties gevonden bij patiënten met Retinitis Pigmentosa of met kegel-staaf-dystrofie, een verwante vorm van IRD. Studies die de exacte functie van dit gen en het gecodeerde eiwit hebben onderzocht bleven helaas achter. In dit proefschrift hebben we ons gericht op het verkrijgen van inzichten in de moleculaire rol van C2ORF71 in fotoreceptorhomeostase alsook in netvliesaandoeningen.

Hoofdstuk 2 richt zich op de opheldering van de functie van C2ORF71 dat, op basis van onze resultaten, nu officieel is omgedoopt tot **PCARE** (photoreceptor cilium actin regulator). Eiwit-eiwit interactiestudies, waarbij gebruik werd gemaakt van een combinatie van het yeast-two-hybrid systeem alsook van tandem affinity purification, wezen uit dat PCARE een interactie aangaat met microtubule-, centrosoom- en actine-geassocieerde eiwitten. Lokalisatiestudies in het netvlies van muizen toonden aan dat PCARE co-lokaliseert met een actine-module aan de basis van de buitenste segmenten van fotoreceptoren, terwijl deze actinemodule in mutante *Pcare* knock-out muizen verkeerd was gelokaliseerd. Oude, beschadigde stukjes (*discs*) van het buitenste segment worden afgestoten aan de apicale zijde van de fotoreceptorcel, en vervolgens 'opgegeten' door het aangrenzende retinale pigmentepitheel. Dagelijks evolueert het ciliaire plasmamembraan aan de basis van de buitenste segmenten om de vernieuwing van de fototransductie *discs* te initiëren. Hoewel al lang geleden is gepostuleerd dat actine een rol speelt binnen dit proces, blijft het precieze moleculaire mechanisme hierachter onbekend. Wij hebben aangetoond dat PCARE in staat is om één van de actine-geassocieerde interactoren, het Wiskott-Aldrich-syndroom-familie-eiwit WASF3, van het perinucleaire membraan naar het primaire cilium in hTERT RPE-1-cellen te rekruteren. De aanwezigheid van zowel PCARE als WASF3 in het primaire cilium zorgt ervoor dat andere componenten die betrokken zijn bij de polymerisatie van actine, ook naar het primaire cilium

worden verplaatst. Daardoor wordt een soort evaginatie van het ciliaire plasmamembraan geïnduceerd. Verder bleek dat mutant PCARE eiwit (met de p.Ile201Phe mutatie die in RP patiënten is gevonden) minder vaak deze ciliary membraan-evaginaties induceert, en dat de evaginaties die gevormd worden ook kleiner zijn in vergelijking met wild-type PCARE. Deze data wijzen op een verstoring van actine-aangedreven ciliaire membraan-evaginatie als het pathogene mechanisme achter *PCARE*-geassocieerde netvliesziekte. Bovendien onthullen onze bevindingen nieuwe moleculen die potentieel betrokken zijn bij het proces van ciliaire membraan-evaginatie.

De klinische en genetische informatie van alle tot dusver gepubliceerde patiënten met *PCARE*-geassocieerde IRD is weergegeven in **hoofdstuk 3**. *PCAR*E-geassocieerde IRD is zeer zeldzaam, met iets meer dan 40 patiënten die tot dusver in de literatuur zijn beschreven. Sommige patiënten vertonen de eerste symptomen op jonge leeftijd, terwijl bij anderen de eerste klachten pas als volwassene optreden. De gemiddelde leeftijd van een patiënt bij het eerste bezoek aan de kliniek was 31,5 jaar. Bij de meerderheid van de patiënten werd nachtblindheid als eerste gerapporteerd. Het dunner worden van het netvlies, en verlies van de juiste gelaagdheid van het netvlies, zijn kenmerkend voor alle patiënten, terwijl verminderde of niet-aanwezige full-field elektroretinografie ook gebruikelijk is. *PCARE*-mutaties zijn meestal eiwit-truncerend, terwijl slechts twee homozygote missense mutaties zijn gerapporteerd. De meerderheid van de patiënten vertoont truncerende of missense mutaties aan de N-terminus van het PCARE-eiwit. Een analyse van de positie van de mutatie in het PCARE-eiwit ten opzichte van de beginleeftijd van de visuele klachten bracht geen duidelijke correlatie naar voren tussen de leeftijd waarop de ziekte begint en de positie van de PCARE-mutatie bij patiënten met *PCARE*-geassocieerde IRD.

In **hoofdstuk 4** beschrijven we de duplicatie van het *pcare* gen in de zebravis, en de generatie van een nieuw mutant *pcare1* zebravismodel, genaamd *pcare*$^{rmc100/rmc100}$, middels CRISPR/Cas9 technologie. In de zebravis bevindt *pcare1*, het gen dat het meeste lijkt op het humane *PCARE* gen, zich op chromosoom 17 en codeert het voor een eiwit van 1122 aminozuren, terwijl *pcare2* zich op chromosoom 20 bevindt en codeert voor een eiwit van 859 aminozuren. De specifiek gegenereerde mutatie zorgt ervoor dat 29 basenparen in exon 1 van *pcare1* (c.221_49del) uit het gen zijn verwijderd, waarvan wordt voorspeld dat deze zal resulteren in de voortijdige beëindiging van pcare1 eiwitsynthese na aminozuur 16 (p.Gly8Glufs*9). *Pcare1* mutante zebravissen vertonen afwijkingen in de morfologie van de buitenste segmenten van de fotoreceptorcellen, zowel in het embryonale (5 dagen na bevruchting) als het volwassen (6 maanden na bevruchting) stadium. Analyse van de visuele functie met behulp van optokinetische en visueel motorische reactiemetingen duiden op een visuele beperking van pcare1$^{rmc100/rmc100}$ mutante zebravissen. De mutante zebravissen vertonen ook verminderde ERG-reacties, iets dat wijst op een defect in de

transretinale signaalprocessing. Daarmee hebben we aangetoond dat *pcare1*$^{rmc100/rmc100}$ zebravissen een aanvullend diermodel zijn om *PCARE*-geassocieerde IRD te bestuderen. Bovendien ondersteunen onze bevindingen de eerder gevonden betrokkenheid van PCARE bij het vormen en/of behouden van de buitenste segmenten in de fotoreceptorcel.

Fibroblast (huid) cellen, verkregen van een patiënt met een homozygote *PCARE* mutatie (c.947del; p.Asn316Metfs*7) vertonen geen ciliaire defecten, waarschijnlijk verklaard door de lage PCARE-expressie in dit celtype in vergelijking met die in het netvlies. Dit komt ook overeen met de veronderstelde fotoreceptor-specifieke functie van PCARE. Om *PCARE*-geassocieerde IRD *in vitro* te kunnen bestuderen, hebben we daarom gebruik gemaakt van geïnduceerde pluripotente stamcel (iPSC)-technologie, zoals beschreven in **hoofdstuk 5**. Om de ziekte *in vitro* na te bootsen, werden *PCARE*-deficiënte fibroblasten geherprogrammeerd naar iPSCs, en vervolgens gedurende 90 dagen gedifferentieerd tot neuroretinale voorlopercellen. Om het transcriptoom van deze cellen te bestuderen, werd RNA sequencing uitgevoerd. Transcriptoom data-analyse toonde een downregulatie van expressie van genen die coderen voor actine cytoskeletale eiwitten aan in de *PCARE*-deficiënte iPSCs, in vergelijking met wild-type cellen. Daarnaast, terwijl cellen van het wilde type differentieerden tot neuronaal-achtige cellen, leken de patiënt-afgeleide iPSC's meer tot een soort van plasmacel te zijn gedifferentieerd. De lage expressie van fotoreceptor-specifieke genen gaf aan dat de celkweek niet significant verrijkt was in fotoreceptorcellen, zowel in wild-type als in de *PCARE*-mutante cellen. Daarom zal een verbeterd protocol dat de verrijking van fotoreceptor precursorcellen mogelijk maakt, noodzakelijk zijn om in de toekomst specifiek de potentiële morfologische defecten als gevolg van *PCARE*-mutaties te beoordelen.

Hoofdstuk 6 beschrijft de generatie van een adeno-geassocieerde virus (AAV) vector met het volledige *PCARE* cDNA, met als doel deze te gebruiken voor toekomstige therapeutische behandelingen. Een AAV-plasmide werd aangepast aan het Gateway-kloneringssysteem om de insertie van het volledige *PCARE*-cDNA te vergemakkelijken. Omdat AAV-vectoren een beperkte hoeveelheid DNA kunnen opnemen, werd de insertiecassette tussen de ITR's van het AAV-*PCARE*-plasmide verlaagd van 5,6 kb tot 4,8 kb, de maximale hoeveelheid DNA die een AAV kan verpakken. Vervolgens werd een AAV2/9-vector gegenereerd die de minimale elementen bevatte om transgen-expressie mogelijk te maken: een fotoreceptor-specifieke rhodopsine kinase promoter, een SV40-intron, *PCARE*-cDNA en een runder-groei-hormoon-polyadenyleringssignaal (bGHpA). Analyse door RT-PCR en *digital droplet* PCR toonde aan dat de verkorte insertiecassette op de juiste wijze was verpakt in de AAV-vector. Helaas werd PCARE-expressie echter niet gedetecteerd middels immunofluorescentie of Western blot na transductie van hTERT-RPE-1-cellen. Deze resultaten suggereren dat de gemaakte AAV-vector niet goed genoeg in staat is om transgene *PCARE* expressie

in hTERT RPE-1-cellen te realiseren. *In vivo* beoordeling van de werkzaamheid van de AAV2/9.RK.PCARE.S-vector in het netvlies van muizen is dus nodig om de therapeutische potentie van deze vector voor de transductie van fotoreceptorcellen te beoordelen.

De belangrijkste onderwerpen van dit proefschrift worden nog eens bediscussieerd in **hoofdstuk 7**. Een inleidende discussie is gebaseerd op eerdere kennis over de ontwikkeling van het ciliaire buitenste segment van de fotoreceptorcel, van de bevindingen van Richard Young in 1967 dat de buitenste segmenten constant worden herbouwd, tot aan recente publicaties die bevestigen dat de buitenste segmenten units (*discs*) vormen middels evaginatie van het ciliaire plasmamembraan (**hoofdstuk 7.1**). Eerdere literatuur over de betrokkenheid van actine en actine-geassocieerde eiwitten in dit proces wordt besproken in **hoofdstuk 7.2**. De rol van het PCARE-eiwit, haar associatie met het WASF3-eiwit dat behoort tot het Arp2/3-complex, alsook de vorming van de membraan-evaginaties, worden besproken in **hoofdstuk 7.3**. De rol van retinale ciliopathie-eiwitten in de actine-afhankelijke vorming van buitenste segment *discs* wordt beschreven in **hoofdstuk 7.4**. In hoofdstuk 7.5 bediscussiëren we *PCARE*-geassocieerde IRD, alsook de cellulaire- en dier-modellen die momenteel beschikbaar zijn om de ziektekenmerken verder te bestuderen. Ten slotte worden mogelijke therapieën voor de behandeling van deze ziekte, zoals op AAV gebaseerde gentherapie nog eens uitvoerig besproken.

Resumen

Los fotorreceptores de la retina, conos y bastones, son las células encargadas de capturar y transformar la luz en impulsos eléctricos, en un proceso llamado fototransducción (**capítulo 1.3**). El segmento externo de los fotorreceptores es un cilio especialmente modificado compuesto de cientos de discos membranosos importantes para el proceso de fototransducción, y por tanto para una correcta visión. Las enfermedades hereditarias de retina causadas por un mal funcionamiento del cilio de los fotorreceptores se denominan ciliopatías de la retina. Estas enfermedades son raras y muy variables desde el punto de vista genético y fenotípico, lo que complica el diagnóstico molecular de los pacientes (**capítulo 1.4**). En 2010, se identificaron por primera vez mutaciones causantes de la enfermedad Retinosis Pigmentaria en el gen *C2ORF71*, un subtipo de distrofia de retina caracterizada por la pérdida progresiva de la visión. Inicialmente, se asoció la función del gen *C2ORF71* con el cilio de los fotorreceptores, ya que al expresar exógenamente el gen en células epiteliales se observó que la proteína C2ORF71 localizaba en el cilio primario, una especie de antena que permite a la célula intercambiar información con el exterior. En los últimos ocho años, se han encontrado nuevas mutaciones en *C2ORF71* en pacientes con Retinosis Pigmentaria o Distrofia de conos y bastones. Sin embargo, hasta ahora no hay estudios que describan la función de este gen y la proteína que codifica. El objetivo de esta tesis ha sido el de estudiar la función a nivel molecular de C2ORF71 en la homeostasis de los fotorreceptores y su contribución a las distrofias de retina.

El **capítulo 2** se centra en el estudio de la función del gen *C2ORF71*, ahora oficialmente reconocido como *PCARE* (por sus siglas en inglés "photoreceptor cilium actin regulator", y en castellano "regulador de actina en el cilio de fotorreceptores") basado en nuestros resultados. Estudios de interacciones proteína-proteína basados en las técnicas del doble híbrido en levadura y purificación por afinidad en tándem, revelaron que PCARE interactúa con módulos de proteínas asociadas a microtúbulos, centrosoma y actina. Posteriormente, estudios de localización en retinas de ratón mostraron que PCARE co-localiza con un módulo de actina en la parte basal de los segmentos externos de los fotorreceptores, mientras que en ratones *Pcare*$^{-/-}$ (ratones carentes del gen *Pcare*) este módulo de actina está deslocalizado. La fotorrecepción provoca que los discos del segmento externo de fotorreceptores se dañen tras su uso. Los discos dañados se vierten en el ápice del fotorreceptor y son fagocitados por el epitelio pigmentado de la retina adyacente a los fotorreceptores. Diariamente, la membrana plasmática del cilio en la base de los segmentos externos se pliega hacia el exterior (evaginación) para iniciar la renovación de los discos de los fotorreceptores. Desde hace décadas se ha propuesto que la actina tiene un papel importante en este proceso, sin embargo, el mecanismo molecular exacto detrás de la formación de nuevos discos

de los fotorreceptores es aún desconocido. En esta tesis mostramos que PCARE interactúa con la proteína de la familia del síndrome Wiskott-Aldrich, WASF3. Nuestras observaciones indican que PCARE transporta a WASF3 desde la membrana perinuclear al cilio primario en células hTERT RPE-1. La presencia de PCARE y WASF3 en el cilio primario recluta a otros componentes asociados con la actina hacia el cilio primario, induciendo la evaginación de la membrana plasmática del cilio. Tras insertar la mutación de cambio de sentido p.Ile201Phe en *PCARE*, previamente encontrada en pacientes con Retinosis Pigmentaria, observamos que la evaginación de la membrana del cilio es menos frecuente, y cuando se encuentra, las evaginaciones son más pequeñas en comparación con las que produce la proteína PCARE correcta. Estos resultados indican que el mecanismo detrás de la distrofia de retina asociada al gen *PCARE* es la alteración de la evaginación de la membrana plasmática del cilio promovida por las dinámicas de la actina. Además, nuestros resultados revelan nuevas moléculas que pueden estar implicadas en el proceso de evaginación de la membrana plasmática del cilio.

En el **capítulo 3** se recoge la información clínica y genética de todos los pacientes descritos con distrofia de retina asociada a *PCARE*, cuya frecuencia es muy rara. Hasta la fecha sólo 40 pacientes han sido reportados. Algunos pacientes muestran síntomas a edad temprana, mientras otros los muestran en la edad adulta. La edad media de la primera visita a la clínica es de 31.5 años. La mayoría de los pacientes experimenta ceguera nocturna. Otras características clínicas comunes presentes en todos los pacientes son la presencia de una retina más fina y la pérdida de la laminación de ésta. Las electrorretinografías suelen ser reducidas o imposibles de medir dada la pérdida de los fotorreceptores. Las mutaciones homocigotas en *PCARE* son en su mayoría de terminación, es decir, no permiten la síntesis de la proteína completa, y tan solo dos mutaciones de cambio de sentido han sido descritas. La mayoría de los pacientes presentan las mutaciones en la posición N-terminal de la proteína PCARE. Sin embargo, nuestros estudios muestran que no existe correlación entre la posición de la mutación en la proteína PCARE y la edad de aparición de la enfermedad.

El **capítulo 4** describe la duplicación del gen *pcare* en pez cebra, y la generación de un modelo mutante de *pcare1* en este modelo animal usando la tecnología de CRISPR/Cas9, denominado *pcare1*$^{rmc100/rmc100}$. En pez cebra, *pcare1*, el verdadero ortólogo del gen humano *PCARE*, está localizado en el cromosoma 17 y codifica una proteína de 1122 aminoácidos, mientras *pcare2* está situado en el cromosoma 20 y codifica una proteína de 859 aminoácidos. La mutación específica generada mediante CRISPR/Cas9 es una deleción de 29 pares de bases en el exón 1 de *pcare1* (c. 21_49del), que se predice que forme una terminación prematura de la traducción tras el aminoácido 16 de pcare1 (p.Gly8Glufs*9). Los peces cebra mutantes *pcare1*$^{rmc100/rmc100}$ muestran irregularidades

en la morfología del segmento externo de los fotorreceptores, tanto en el estado embrionario (5 días después de la fertilización), como en el adulto (6 meses después de la fertilización). Los análisis de la función visual de los peces cebra usando mediciones de la respuesta optocinética y visomotora indican que la visión de los peces cebra mutantes *pcare1*$^{rmc100/rmc100}$ está deteriorada. Estos peces presentan también electrorretinografías reducidas, lo que indica un fallo en la corriente eléctrica que atraviesa la retina. Los peces cebra mutantes *pcare1*$^{rmc100/rmc100}$ son por lo tanto un excelente modelo animal que permite estudiar la distrofia de retina asociada a *PCARE*. Además, estos resultados apoyan la hipótesis que sugiere que PCARE es importante para formar y/o mantener los segmentos externos de los fotorreceptores.

Debido a que no existen líneas celulares de fotorreceptores que se puedan mantener en cultivo, un método común para estudiar ciliopatías de retina es utilizar células derivadas del paciente para analizar los efectos de las mutaciones genéticas en el cilio primario. Los fibroblastos son células de tejido conectivo que se pueden obtener a través de una biopsia de la piel de un paciente. En el **capítulo 5**, se muestra que los fibroblastos derivados de un paciente con una mutación puntual homocigótica en *PCARE* (c.947del; p.Asn316Metfs*7) no tienen defectos en el cilio, lo que se puede explicar por la baja expresión de *PCARE* en fibroblastos en comparación con la expresión en retina. Esto también está en línea con la función específica de PCARE en fotorreceptores. Por ello, para estudiar la enfermedad de retina asociada a *PCARE in vitro*, se utilizó la tecnología de células madre pluripotentes inducidas (iPSCs) con el objetivo de obtener fotorreceptores en cultivo. Para modelar la enfermedad *in vitro*, se reprogramaron los fibroblastos con la mutación en *PCARE* a iPSCs, y se siguió un protocolo de diferenciación de 90 días para obtener neuroretinas. Para estudiar el transcriptoma de estas células, se utilizó la técnica de secuenciación del ARN. El análisis de los datos del transcriptoma reveló que había menor expresión de genes codificantes para proteínas citoesqueléticas relacionadas con actina en las iPSCs derivadas del paciente con la mutación en *PCARE*. Además, mientras las células derivadas de un individuo control fueron capaces de diferenciarse en células neuronales, las iPSCs derivadas del paciente se diferenciaron en células de plasma. El transcriptoma también reveló que había una baja expresión de genes específicos de fotorreceptores, indicando que el cultivo celular no estaba enriquecido en células fotorreceptoras tanto en la línea control como en la del paciente. Por ello, futuros experimentos que permitan enriquecer el cultivo en células fotorreceptoras son necesarios para poder determinar el potencial de defectos morfológicos en este tipo celular debido a mutaciones en *PCARE*.

El **capítulo 6** describe la generación de un virus adeno-asociado (AAV) que incluye el ADN complementario (ADNc) completo de *PCARE*, con el objetivo de ser usado como vector terapéutico. Primeramente, un plásmido con la secuencia del AAV se adaptó al sistema de clonaje Gateway para

facilitar la inserción del ADNc completo de *PCARE*. Debido a que los vectores AAV son restrictivos en cuanto a tamaño, el casete de inserción entre las repeticiones terminales invertidas (ITRs) del plásmido AAV se redujo de 5.6 kb a 4.8 kb, en el límite de lo que un AAV puede acomodar. Posteriormente, un vector AAV2/9 fue generado compuesto por los elementos mínimos que permiten la expresión del transgén: un promotor, en este caso el de la rodopsina quinasa, específico de fotorreceptores; un intrón SV40; el ADNc de *PCARE*, y una señal de poliadenilación de la hormona de crecimiento bovina. Este vector se denominó AAV2/9.RK.PCARE.S. El ánálisis por RT-PCR y PCR digital a gotas mostraron que el casete de inserción estaba correctamente empaquetado en el vector AAV. Sin embargo, la expresión de *PCARE* no se detectó ni por inmunofluorescencia ni western blot tras transducir células hTERT RPE-1 usando diferentes multiplicidades de infección. Estos resultados sugieren un problema del vector AAV para producir la expresión del transgén en células hTERT RPE-1. La evaluación *in vivo* de la eficacia del vector AAV2/9.RK.PCARE.S en ratones sería necesaria para comprobar la validez del vector para transducir células fotorreceptoras.

Los temas principales de esta tesis son discutidos en el **capítulo 7**. Una discusión introductoria basada en el conocimiento previo sobre el desarrollo del segmento externo ciliar de la célula fotorreceptora, desde los descubrimientos de Richard Young en 1967 que indican que los segmentos externos se renuevan continuamente, hasta publicaciones actuales que confirman que los discos de los segmentos externos se forman mediante un mecanismo de evaginación de la membrana plasmática del cilio (**capítulo 7.1**). La literatura previa sobre la implicación de la actina y proteínas asociadas a la actina en el proceso de formación de los discos del segmento externo es revisada en el **capítulo 7.2**. El papel de la proteína PCARE y su asociación con la proteína WASF3, así como la formación de evaginaciones de la membrana del cilio son discutidas en el **capítulo 7.3**. El papel de proteínas causantes de ciliopatías en la formación dependiente de actina de los discos del segmento externo es examinado en el **capítulo 7.4**. En el **capítulo 7.5**, se analiza la distrofia de retina asociada a *PCARE*, y se discuten los modelos animales y celulares disponibles actualmente que permiten estudiar los rasgos distintivos de la enfermedad. Finalmente, en el **capítulo 7.6** se discuten potenciales terapias que permitan tratar esta enfermedad, tales como la terapia de reemplazamiento mediante AAV.

Data management

Type of data	Subject to privacy (Yes/No)	Way of anonymization	Storage
Patient-derived cell lines	Yes	All patients received an untraceable number, the identity of the patients is only known to the treating physician.	Cell lines were frozen in liquid nitrogen and stored on an assigned freezer at -80˚C at the Department of Human Genetics. Each cell line received a traceable number and was registered at the cell culture facility. The number of the cell lines used for the experiments can be found on the lab journal of Julio Cesar Corral Serrano, stored in the Department of Human Genetics, or in the Labguru account of the project under the name C2ORF71: https://radboudumc.labguru.com/knowledge/projects/691. Contact person to find the cell lines in the assigned freezer: Saskia van der Velde-Visser, saskia.vandervelde-visser@radboudumc.nl
Other cell lines	No	N.a.	A traceable number was given to all cell lines at the cell culture facility of the Department of Human Genetics. Cells were stored and grown according to the manufacturer's instructions. The number of the cell lines used for the experiments can be found on the lab journal of Julio Cesar Corral Serrano, stored in the Department of Human Genetics, or in the Labguru account of the project under the name C2ORF71https://radboudumc.labguru.com/knowledge/projects/691. Contact person to find them in the assigned freezer: Saskia van der Velde-Visser, saskia.vandervelde-visser@radboudumc.nl
Fluorescence images	No	N.a.	Fluorescence imaging data were stored by date on the private network of the group at the Department of Human Genetics, Radboudumc: T:\PIgroup-Rob-Collin\02 Microscopy images\03 Julio Corral
Plasmids	No	N.a.	Plasmids were stored in an assigned freezer at -80˚C at the Department of Human Genetics with a traceable number. All plasmids and their specifications are listed in the Gene Therapy database file with a pGT code: H:\GR Theme groups\10 PI Group Rob Collin\05 Vector_AAV_AON Database Contact person to find them in the assigned freezer: Lonneke Duijkers, Lonneke.Duijkers@radboudumc.nl
Transcriptomic data	Yes	RNA was isolated from patient-derived cells, which were previously anonymized (see patient-derived cells). For the samples subjected to transcriptome analysis, a project number was assigned and kept confidential at the company Biogazelle, Gent, Belgium.	Transcriptomic data were stored in the BaseSpace Sequence Hub server from Illumina protected with a password, under the project JCR. The bam files from the RNA Seq can be found in this folder: T:\PIgroup-Rob-Collin\16 RNA Seq Data\Julio\C2orf71 iPSCs Contact person at Radboudumc: Rob Collin, rob.collin@radboudumc.nl Contact person at Biogazelle: Gaëlle Van Severen, gaelle.vanseveren@biogazelle.com

Type of data	Subject to privacy (Yes/No)	Way of anonymization	Storage
Proteomic data	No	N.a.	Proteomic data were stored on a private network at the Radboudumc, Department of Human Genetics, under this link: H:\GR Theme groups\10 PI Group Rob Collin\01 Personal folders\Corral, Julio\Protein-protein interaction (Y2H, TAP) Contact person at Radboudumc: Ideke Lamers, Ideke.Lamers@radboudumc.nl
Viruses (AAVs)	No	N.a.	Viruses were stored on an assigned freezer at -80˚C at the Department of Human Genetics with a traceable number. All viruses and their specifications are listed in the Gene Therapy database file with an AAV-GT code: H:\GR Theme groups\10 PI Group Rob Collin\05 Vector_AAV_AON Database Contact person to find them in the assigned freezer: Lonneke Duijkers, Lonneke.Duijkers@radboudumc.nl
Antibodies	No	N.a.	Antibodies were stored with a traceable number in an assigned fridge/freezer at the Department of Human Genetics, according to manufacturer's instructions. Antibodies were registered in the Antibody database from the Department of Human Genetics in Labguru: https://radboudumc.labguru.com/biocollections/antibodies Contact person to retrieve them in the assigned fridge/freezer: Ideke Lamers, Ideke.Lamers@radboudumc.nl

N.a. = not applicable

Acknowledgements

What defines a place where you have lived is not the place itself, but the people you have shared moments with. Nijmegen felt like home to me thanks to the people I met along the way. My stay of four and a half years at the Radboud hospital and the completion of this thesis would not have been possible without the help and support from many people, friends and colleagues, whom I here have the opportunity to show my gratitude.

To my supervisors. **Rob**, thank you for your guidance from the beginning until the end. I value your positivity and optimism at all times, with me and everyone in your group. A group which grew until the point that it became a challenge to make a Spanish tortilla that could feed everyone. You taught me the importance of being *precis* on time, and always gave me good advices. You are diligent and an excellent mentor, a great chaperone! I've grown a lot personally and professionally during my PhD, and that is also thanks to you. **Ronald**, I joined your group to work on a "side project", which in the end turned out to be the main chapter of my thesis. I admire your creativity and appreciate your closeness. I was lucky to be part of the discussions in your group, I always felt welcomed and part of it. This project introduced me to the exciting field of ciliopathies, and I'm thrilled to remain in this research line, looking forward to future collaborations! **Alex**, thank you very much for your support throughout my whole PhD. I value your readiness to always help and give counselling. Your commitment with science is something to revere, always making the deadlines. It has been great working with you.

To the members of the **BGT lab**, present and past: Lonneke, Muriël, Dyah, Galuh, Manon, Matthijs, Simon, Alex, Anita, Tamara, Tess. **Lonneke**, you have been the perfect right-hand support in the lab, always there to help me with a smile. **Dyah** and **Muriël**, zebrafish buddies, thank you also for your help with my project, it has been great to share the PhD experience with you!

To my students **Renata**, **Max** and **Anita**. I was lucky to supervise three different but all bright people, from whom I also learnt a lot. I wish you all the best in your careers.

The ciliary protein-protein interaction work was accomplished together with many people from the **protein lab**: Ideke, Machteld, Jeroen, Stef, Sylvia, Minh, Edgar, Simone, Cenna, Miriam, Ka Man, Zeineb. **Ideke**, aka Mega Mindy, I'm so happy that you are continuing the PCARE project. It has been so much fun working and discussing science with you! **Brooke**, my Airyscan buddy, I'm going to miss our restorative conversations behind the microscope. **Mariam**, thank you for your constant good advices, you are going to be such a great mum. **Ka Man** and **Sylvia**, thank you for your technical help, it was always nice to come to the lab to pick up an antibody and hear you cheerfully say "Julio!".

To the **ZAT-lab** members: Erik, Erwin, Hannie, Lisette, Margo, Ralph, Sanne, Theo. Thank you all for your help and advice, it was great to share the lab with you. Not forgetting the excellent hand of Tom in the Huygensgebouw, thank you for taking good care of our zebrafish.

To everyone in the departments of **Human Genetics** and **Ophthalmology**, especially to Anneke, Dyon, Roos, Maartje, Björn, Frans, Imran, Anke, Susanne, Silvia, Ellen, Zeinab, Saskia, Marlie, Michael, Remco, Sarah, Mireia, Anna, Jordi, Brechtje, Rosanne, Richarda, Alex Hoischen, Ineke, Domenique, Dennis, Miranda, Bas, Christian, Arjen, Gido, Sabrina, Mubeen, Raquel, Laura. Each of you have helped me in some way over these years.

To the **Marie Curie EyeTN** family: Giulia, Elfride, Miriam, Sandro, Raji, Elena, Pablo, Bernd, Susanne, Frans, Rob, Anneke, Laura, Riccardo, Patricia, Chris, Carla, Carmel, Evi, Prasoon, Simona, Vasiliki, Vincent. To all those meetings and training we had, but also to all those great (and funny) team-building activities. To the people in **Biogazelle, Gent** and **TIGEM, Naples**, thank you for making my EyeTN secondments an unforgettable experience.

To my **friends in Nijmegen**: Blanca, Carla, Laura, Daniel, Marc, Riccardo, Kaniye, Ellie, Pim, Ester, Brecht, Roque, Merce, Darío, Romi, Mía, Ivan, Alejandra, Bekalu, Lavinia, Giuliana, Simone, Celia, Quique, Silvia, María, Edu, Alberto, Anna, Omar, Antonio. Thank you for making Nijmegen feel like home.

Carla, Blanca, Daniel, Ellie, **Mireia**, **Sarah**, **Brooke**, thank you for the music! **Carla**, gracias por tantos Muntthee. Tenemos pendiente un viajecito a algún destino soleado. **Kaniye**, thank you for the memes!

Ester, los astros se alinearon para nuestro encuentro, gracias (en parte a tu prima) por descubrirme a alguien tan especial como tú. **Alba**, mi Petunia de toda la vida, aunque el destino nos haya separado siempre nos quedarán nuestros encuentros, de una vez al año como mucho, y las fotos del anuario.

Roque, **Darío**, gracias por hospedarme en vuestra casa tantas veces, y por muchas más cosas. Sois lo mejor y os deseo todo lo mejor también.

Ale, eres tan bonita por fuera como por dentro. Espero que la vida te sonría siempre, no cambies nunca.

Merce, por muchas cañas más (bueno la mía sin alcohol) en el barrio! Eres un ejemplo a seguir, te tengo mucho cariño y te admiro mogollón.

A mis paraninfos:

Daniel, nunca imaginei que um dos meus melhores amigos que fiz na Holanda seria de tão longe. Muito obrigado por todos os momentos que compartilhamos, que foram muitos! Não se esqueça que aqui você tem um amigo para sempre.

Laurita, te admiro mucho como persona y como amiga. Ha sido maravilloso compartir esta aventura contigo. Te quiero un montón.

Marquitos, αγαπημένε μου Έλληνα, ξέρεις ότι μου αρέσει να συζητώ οποιοδήποτε θέμα μαζί σου. Είσαι ένας υπέροχος άνθρωπος. Καλή όρεξη!

Riccardo, genio y figura hasta la sepultura, senza di te le ore in lab sarebbero state molto più tranquille... ma anche molto più noiose. Sei unico!

A mis amigos **orondos** del barrio: Alex, Carla, Celia, Diego, Miriam, Sandra, a los allegados Antía, Julia y Miguel. A Alexis, Juan Pablo, Miguel Ángel, Sergio, Silke, Kris, Yaiza y Salva. Gracias por estar siempre ahí y alegrar mis visitas a Madrid.

A mis padres, **Rosa** y **Julio**, por darme la libertad para cumplir mi sueño y respaldarme siempre.

Alexis, gracias por acompañarme en este viaje. Por apoyarme en los momentos buenos, y en los no tan buenos. Por venir a Nijmegen mil y una veces a verme. Por enseñarme tantísimas cosas. Gracias por todo.

List of publications

Corral-Serrano JC[*], Valkenburg D[*], Lamers IJC[*], Iwata T, Black GCM, Ben-Yosef T, Hoyng CB, Garanto A, Roepman R, Collin RWJ. Genotype-phenotype correlation study in *PCARE*-associated retinal disease.
Manuscript in preparation.

Corral-Serrano JC, van Reeuwijk J, Hoogendoorn ADM, Ruigrok RAA, Yildirim A, Duijkers L, Lamers IJC, Letteboer SFJ, van Essen MD, Sakami S, van Beersum SEC, Palczewski K, Boldt K, Wolfrum U, Ueffing M, Garanto A, Roepman R[#], Collin RWJ[#]. The photoreceptor-specific protein PCARE interacts with WASF3 to deploy a ciliary actin dynamics module.
Revised version in preparation.

Messchaert M, Dona M, Broekman S, Peters T, **Corral-Serrano JC**, Slijkerman RWN, van Wijk E, Collin RWJ. Eyes shut homolog is important for the maintenance of photoreceptor morphology and visual function in zebrafish.
PLoS One, 2018; ***13****: e0200789.*

Corral-Serrano JC, Messchaert M, Dona M, Peters T, Kamminga L, van Wijk E, Collin RWJ. *C2orf71a/pcare1* is important for photoreceptor outer segment morphogenesis and visual function in zebrafish.
Scientific Reports, 2018; ***8****: 9675.*

Garanto A, Chung DC, Duijkers L, **Corral-Serrano JC**, Messchaert M, Xiao R, Bennett J, Vandenberghe LH, Collin RWJ. In vitro and in vivo rescue of aberrant splicing in CEP290-associated LCA by antisense oligonucleotide delivery.
Human Molecular Genetics, 2016; ***25****: 2552-2563.*

[*],[#] these authors contributed equally.

Curriculum vitae

Julio César Corral Serrano was born on October 17, 1989 in Madrid, Spain. After finishing high school, in 2007 he started his bachelor studies in Biology at the Autonomous University of Madrid (UAM). In 2010, he moved to Germany with a scholarship from the Erasmus Program by the European Union, to carry out research at the Albert Ludwig University of Freiburg. He did his bachelor's internship at the Spanish National Cancer Research Centre (CNIO), studying biomarkers as predictors of a complete molecular response to Nilotinib, under the supervision of Dr. Luís Lombardía. In 2013, he completed his master's degree in Molecular Biomedicine at the UAM. During his master's internship, he worked on understanding the molecular role of the LOXL2 protein in cancer at the "Alberto Sols" Institute for Biomedical Research.

In October 2013, he joined the group of Dr. Rob W.J. Collin at the Radboud University Medical Centre (Radboudumc), Nijmegen, The Netherlands, as Early Stage Researcher part of the Marie Curie Initial Training Network EyeTN. His PhD work was focused on the functional characterization of the retinal ciliopathy protein PCARE, to understand *PCARE*-associated retinal disease using relevant cell and animal models. To achieve this, he worked as well under the supervision of Prof. dr. Ronald Roepman, head of the molecular biology of ciliopathies group, and Dr. Alejandro Garanto, assistant professor working on modulation therapies for inherited retinal diseases.

In October 2018, he was appointed post-doctoral fellow in the group of Prof. dr. Michael Cheetham at the Institute of Ophthalmology, University College London (UCL), to continue investigating the molecular mechanisms behind inherited retinal diseases.

PhD Portfolio

Name PhD candidate:	***Julio César Corral Serrano***	**PhD period:**	***01-10-2013 – 31-12-2017***
Department:	***Human Genetics***	**Supervisors:**	***Dr. R.W.J. Collin,***
Graduate School:	***Radboud Institute for Molecular Life Sciences***		***Prof. dr. R. Roepman***
		Co-supervisor:	***Dr. A. Garanto***

		Year(s)	ECTS
	TRAINING ACTIVITIES		
a)	**Courses & Workshops**		
	- ***Graduate Course (RIMLS)***	2014	2.0
	- ***Complementary Skills (EyeTN)***	2013-2015	4.9
	- ***Research Skills (EyeTN)***	2013-2015	4.9
	- ***Scientific Writing Course (Radboud University)***	2016	1.75
	- ***Laboratory Animal Science Course (CDL, Radboud University)***	2014	3.5
b)	**Seminars & lectures**		
	- ***Seminars and Lectures (RIMLS)***	2014	0.4
	- ***Radboud Research Rounds (Sensory Disorders, Donders Institute)***	2014-2017	0.5
	- ***Seminars (EyeTN)***	2013	0.2
c)	**Symposia & congresses**		
	- ***New Frontiers (RIMLS)****	2013-2015	2.25
	- ***PhD Retreat (RIMLS)****#***	2014-2017	3.25
	- ***Association for Research in Vision and Ophthalmology (ARVO, USA)*****	2015,2017	3.5
	- ***Alpbach Symposium on Affinity Proteomics (EyeTN)****	2015	1.25
	- ***Perception Day (Donders Institute)****	2016	0.5
	- ***Final Conference (EyeTN)#***	2016	1.5
	- ***Retinal dystrophies symposia (EyeTN)***	2014	0.8
d)	**Other**		
	- ***Literature discussion department of Human Genetics (4#)***	2013-2016	4.0
	- ***Theme discussion department of Human Genetics (2#)***	2013-2017	4.0
	- ***Sensory disorders division progress meetings (6#)***	2013-2017	4.0
	- ***Organizing Technical Forum in Statistics (RIMLS)***	2016	0.5
	TEACHING ACTIVITIES		
e)	**Lecturing**		
	- ***Lecture on Gene Augmentation Therapy and practical course, BSc and MSc students (Radboud Summer School)***	2015	1.0
	- ***DNA International Day, elementary children (EyeTN)***	2016	1.0
f)	**Supervision of internships / other**		
	- ***Supervision internship BSc (R.A.A. Ruigrok)***	2015	1.0
	- ***Supervision internship MSc (M.D. van Essen)***	2016	1.0
	- ***Supervision internship BSc (A.D.M. Hoogendoorn)***	2017	1.0
TOTAL			**48.7**

#Oral presentation
*Poster presentation

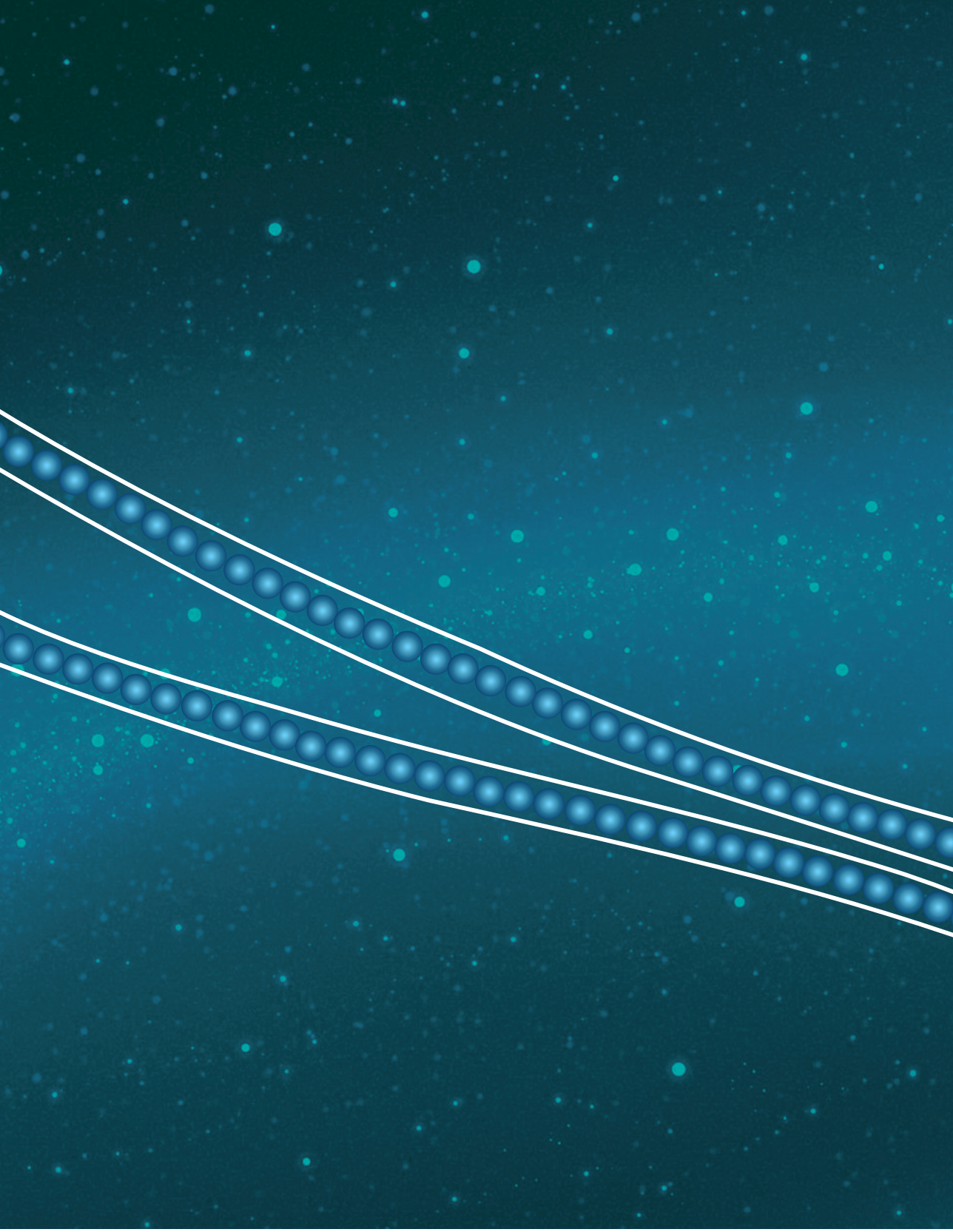

Institute for Molecular Life Sciences
Radboudumc